Synthesis and Material Properties of Aromatic Cation-Centred Compounds

JACK MARTIN WILLIAMSON

Durham University
Department of Chemistry

Synthesis and Material Properties of Aromatic Cation-Centred Compounds

Jack Martin Williamson

A Thesis Submitted for the Degree of Doctor of Philosophy

March 2022

Table of Contents

Abstract

Aromatic cations, such as cyclopropenium and tropylium, have access to delocalised electrons that spread the charge across their rings, enabling them to form stable ionic molecules.[1] They are readily accessible species which makes them of interest for integration as part of functional materials.

In the field of ionic liquid crystals, while aromatic species such as imidazoliums have been widely investigated as part of molecular design of mesogens,[2] the investigation of cyclopropeniums as part of liquid crystals has only just been undertaken.[3] However, their molecular structure lends themselves to being the symmetrical core part of a discotic liquid crystal, while integrating a charged character to the material to give them potential as functional materials for electronic devices.

This thesis will discuss the synthesis of a range of cyclopropenium centred liquid crystals, which possess columnar liquid crystal phases and show a conductive character. The electron study revealed the preservation of a liquid-like conductivity of these materials into the liquid crystal and solid phases, and no conductive anisotropy in the liquid crystal phase. The initial synthesis and characterisation of a new series of aminocyclopropenium liquid crystals with greater thermal stability was also undertaken. In addition, attempts to adapt the procedures used for the tropylium species are discussed, including the challenges of applying this chemistry to the larger cation.

1. D. Lyons, R. Crocker, M. Blümel, T. Nguyen, *Angwe. Chem. Int. Ed.*, 2017, **56**, 6, 1466.
2. A. Fernandez, P. Kouwer, *Int. J. Mol. Sci.*, 2016, **17**, 731.
3. J. Litterscheidt, J. Bandar, M. Ebert, R. Forschner, K. Bader, T. Lambert, W. Frey, A. Bühlmeyer, M. Brändle, F. Schluz, S. Laschat, *Angwe. Chem. Int. Ed.*, 2020, **59**, 26, 10557.

Declaration

The scientific work described in this Thesis was carried out in the Chemistry Department at Durham University between September 2017 and March 2022. Unless otherwise stated, it is the work of the author and has not been submitted in whole or in support of an application for another degree or qualification at this or any other University or institute of learning.

Signed:

Date:

Conferences Attended and Presentations Given

1. **Birmingham Soft Matter Inter-CDT Forum**, University of Birmingham, UK, June 2018.

2. **Soft Matter Showcase**, University of Edinburgh, UK, July 2018.

3. **Macrocyclic and Supramolecular Chemistry Early Career**, University of Manchester, UK, July 2018.

4. **SupraLyon**, University of Lyon, France, December 2018.

5. **Royal Society of Chemistry North East Organic Division Meeting**, University of York, UK, March 2019.
   Poster Presented: The Synthesis and Material Properties of Aromatic Cation Liquid Crystals

6. **International Soft Matter Conference**, University of Edinburgh, UK, June 2019.
   Poster Presented: The Synthesis and Material Properties of Aromatic Cation Liquid Crystals

7. **SOFI Industrial Showcase 2019**, University of Leeds, UK, June 2019.
   Poster Presented: The Synthesis and Material Properties of Aromatic Cation Liquid Crystals

8. **Macrocyclic and Supramolecular Chemistry Early Career**, University of Lincoln, UK, July 2019.
   Poster Presented: The Synthesis, Assembly and Material Properties of Aromatic Cation Liquid Crystals

9. **Inter-CDT Student Conference**, University of Durham, UK, December 2019.
   Oral Presentation: The Synthesis and Material Properties of Aromatic Cation Liquid Crystals

10. **SOFI Showcase 2020**, virtual conference, July 2020.
    Oral Presentation: Retention of Charge Transport Properties from Liquid Crystals to Solid Phases: Cyclopropenium Columnar Materials

11. **ChiralMat 2021**, virtual conference, March 2021.

12. **SOFI Showcase 2022**, virtual conference, July 2021.
    Oral Presentation: Isotropic Anisotropic Conductivity Materials

Acknowledgements

Paul McGonigal. Thank you for all the great guidance you have given me over the years. In particular, thank you for the support you have provided during the lockdown and later restrictions that have made continuing research difficult. I'm also grateful for all the efforts you made to help keep us motivated and connected as a group. I'm extremely grateful for all the incredible advice and support throughout my PhD, I've been very lucky to have had you as my supervisor.

Durham University, SOFI CDT and EPSCR. I am grateful to Durham University for providing me with considerable resources, and to the SOFI CDT and EPSRC for providing training and for funding my research over the past four years.

Harry Litt. Thank you for all the knowledge and assistance over the last few years, both while hosting me in Leeds and meeting by email and Teams. The work you have done for this project, from coding to dielectric experiments to educating me on the fundamental physics has been really helpful, and I am grateful for the all efforts you've put in.

Collaborators. Thank you to Professor Cliff Jones and Dr Michal Kohout for working with me throughout my PhD. I'm grateful to have been able to visit your research groups, and my trip to Prague was a highlight of my PhD. I would also like to thank Dr Silvio Poppe for the work he has done to bring valuable insight to the investigation of these materials.

Academic and Technical Staff. Certain staff members deserve a mention for their contribution to my PhD and they include: Dr Alyssa Avestro and Dr James Walton. I would also like to thank William D. Carswell for all his work on thermal analysis throughout my PhD.

CG235. I would like to thank everyone who has been a part of CG235 during my PhD, it really is a welcoming group and I am glad to have been here. Specific thanks to Dr Aisha Bismillah, Dr Andew Turley, Burhan Hussein, Dr Senthil Kumar and Dr Yulong Sun for the insight they have given me throughout the years, I feel you have really helped me become a better chemist.

Friends and Family. Thank you to all my family and friends for helping me through the years of this pandemic, it's been a tough time but your support has really helped me through it.

Abbreviations

5CB	4-Cyano-4'-pentylbiphenyl
Ac	Acetyl
ASAP	Atmospheric Solids Analysis Probe
Bu	Butyl
Col_{hex}	Hexagonal Columnar
Col_{obl}	Oblique Columnar
Col_{rec}	Rectangular Columnar
Col_{squ}	Square Columnar
COSY	Correlation Spectroscopy
CV	Cyclic Voltammetry
d	Doublet
DBDMH	1,3-Dibromo-5,5-dimethylhydantoin
DTCB	*Trans*-2-[3-(4-tert-butyl-phenyl)-2-methyl-2-propenylidene]malononitrile
DFT	Density Functional Theory
DSC	Differential Scanning Calorimetry
DTG	Derivative Thermogravimetry
equiv.	Equivalents
ESI	Electrospray Ionisation
ESP	Electrostatic Potential
Et	Ethyl
FTIR	Fourier Transformed Infrared
HAT	Heptaaminotropylium
HMBC	Heteronuclear Multiple Bond Correlation
HOMO	Highest Occupied Molecular Orbital
HR	High Resolution
HSQC	Heteronuclear Single Quantum Coherence
ICP	Inductively Coupled Plasma
^{i}Pr	Iso-Propyl
ITO	Indium Tin Oxide
LC	Liquid Crystal
LUMO	Lowest Unoccupied Molecular Orbital
m	Multiplet
MALDI	Matrix Assisted Laser Desorption/Ionisation

Me	Methyl
M.P.	Melting Point
MS	Mass Spectroscopy
NMR	Nuclear Magnetic Resonance
NOESY	Nuclear Overhauser Effect Spectroscopy
OFET	Organic Field-Effect Transistors
OLED	Organic Light Emitting Diodes
POM	Polarised Optical Microscopy
QtoF	Quadrupole Time of Flight
RT	Room Temperature
s	Singlet
SAXD	Small Angle X-ray Diffraction
t	Triplet
TAC	Triaminocyclopropenium
Tf	Trifluoromethanesulfonyl
TFSI	Bis(trifluoromethanesulfonyl)imide
TGA	Thermogravimetric Analysis
THF	Tetrahydrofuran
TLC	Thin Layer Chromatography
UV	Ultraviolet
V_{RMS}	Root Mean Square Voltage
WAXD	Wide Angle X-ray Diffraction
XPS	X-Ray Photoelectron Spectroscopy
XRD	X-Ray Diffraction

General Experimental Methods

Materials: All reagents, where not stated otherwise, were purchased from commercial suppliers (Sigma-Aldrich, Acros Organics, Fluorochem or Alfa Aesar) and used without further purification.

Instrumentation and Analytical Techniques: Reactions under anhydrous conditions were carried out using Schlenk line techniques under nitrogen. Flash column chromatography was carried out using a Teledyne Isco Combiflash Rf+ system, with pre-packed SiO_2 columns as a stationary phase. Analytical TLC was performed using aluminium-backed sheet silica gel plates (Fluka, 60778-25EA) and visualised under UV irradiation (254 nm). ^{1}H and ^{13}C NMR spectra were recorded in commercially available deuterated solvents on either a Bruker Advance-400 (^{1}H 400.130 MHz and ^{13}C 100.613 MHz), a Varian VNMRS-600 (^{1}H 600.130 MHz and ^{13}C 150.903 MHz), or a Varian VNMRS-700 spectrometer (^{1}H 700.130 MHz and ^{13}C 176.048 MHz), at a constant temperature of 298 K. All chemical shifts are given in their parts per million (ppm) and are referenced to a residual solvent signal (7.26 ppm for $CHCl_3$ in ^{1}H spectra and 77.16 ppm in ^{13}C spectra). All coupling constant (*J*) are reported in hertz (Hz). All ^{13}C spectra are reported as proton uncoupled. Assignment of the ^{1}H and ^{13}C spectra of synthesised compounds was achieved by two-dimensional NMR spectroscopy (COSY, NOESY, HSQC, HMBC). NMR spectra were processed using MestReNova version 11.00-17609. Data reported as follows: chemical shift, integration, multiplicity, coupling constants and assignment. MS-ASAP (Atmospheric Solids Analysis Probe - Mass Spectroscopy) was performed with a LCT Premier XE (Waters) high resolution spectrometer. MS-MALDI (Mass Spectroscopy - Matrix Assisted Laser Desorption/Ionisation) was performed with an Autoflex II ToF/ToF mass spectrometer. HRMS-ASAP (High Resolution Mass Spectroscopy - Atmospheric Solids Analysis Probe) were performed using a LCT Premier XE (Waters) high resolution spectrometer. ESI-QtoF (Electrospray Ionisation Quadrupole Time of Flight) was performed using a QtoF Premier mass spectrometer. Melting points were recorded using a Gallenkamp (Sanyo) apparatus or by DSC and are uncorrected and reported as a range. CV (Cyclic Voltammetry) was performed on an EmStat3 potentiostat. UV-Vis absorbance spectra of solution samples were recorded using an Agilent Technologies Cary Series UV-vis-NIR spectrophotometer at RT.

Thesis Layout

Chapter 1 provides an introduction to the chemistry of aromatic carbocations, focusing on cyclopropenium and tropyliums species, discussing their properties, synthesis and applications. Liquid crystal phase forming compounds are also discussed, including the varieties of liquid crystal phases that form and their applications, in particular their potential role as part of electronic devices. Chapter 2 focuses on a series of cyclopropenium centred compounds, and those compounds that form liquid crystal phases. A study of the electronic and material properties of the mesogenic materials is also fully documented. Chapter 3 focuses on the synthesis of aminocyclopropenium compounds based on the compounds discussed in Chapter 2, and initial study of their material properties. Chapter 4 focuses on the adaption of chemistry used in the synthesis of cyclopropenium for the tropylium compounds, and the difficulties encountered in this synthesis. Chapter 5 summarises the advances in aromatic cationic materials discussed in this thesis.

CHAPTER 1

INTRODUCTION TO AROMATIC IONS AND LIQUID CRYSTAL PHASES

Synopsis

This Chapter focuses first on a series of aromatic cations, looking at cyclopropenium, aminocyclopropenium, and tropylium. An overview of the synthetic methods of the formation of aromatic cations is given, as well as their properties and potential applications. The second section of this Chapter explores mesogenic compounds, with a focus upon discotic liquid crystals. An overview of the different varieties of liquid crystal phases, including nematic and columnar phases, is followed by a discussion of the applications of mesogens. The dielectric and anisotropic properties are discussed, along with the electronic applications of liquid crystal phases, in particular their role as ion conductive materials with a focus on lithium-ion batteries. The importance of alignment within the differing liquid crystal phases, including the methods to control the alignment, are addressed, as are the importance of conductivity and routes to enhance it. Finally, electron-transporting liquid crystal materials that make use of the overlap of stacked π-systems for conductivity are discussed.

1.1 Aromatic Ionic Species

Aromatic ring systems are normally formed when a ring is consistent with Hückel's rule, possessing 4n+2 delocalised π electrons. The delocalised electrons minimise the energy of the ring, and therefore increase the stability of the ring system. The number of aromatic systems that can form is increased by altering the ring systems such as by the addition of heteroatoms, like nitrogen, which can contribute two electrons from a lone pair to form a five-membered aromatic ring in a pyrrole, or the addition of an oxygen atom to make a five-membered aromatic furan.[1]

The range of aromatic rings that can be formed can be further expanded by the addition of charged species. The charged ring gains stability from the aromatic character which is generated by the charge (by making the ring's delocalised electrons obey Hückel's rule), with the charge distributed across the ring. A number of stable aromatic ionic species can be isolated, both as anions such as the cyclopentadiene anion, and as cations such as the cyclopropenium cation[2] and tropylium cation (Scheme 1.1, represented by unsubstituted cyclopropenium, **1**, and unsubstituted tropylium, **2**).[3]

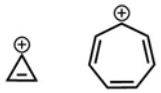

1 **2**

Scheme 1.1: The two simplest aromatic hydrocarbon cations, cyclopropenium (**1**) and tropylium (**2**).

1.1.1 Cyclopropenium

The smallest possible aromatic ring system is the cyclopropenium cation, with only three carbon atoms in a planar ring, possessing two delocalised π-electrons and a single positive charge distributed across the ring between the three carbon atoms.[4] The cyclopropenium cation was first synthesised by Breslow in 1957, in the form of triphenylcyclopropenium (a cyclopropenium substituted with three phenyl groups).[5] Although the cyclopropenium ring has a very high ring strain due to the constrained 60° bond angles between the carbon atoms, the additional stability obtained from the aromatic character of the ring means that molecules containing cyclopropenium rings can be readily synthesised and isolated as a stable carbocation.[2]

Cyclopropenium cations can be readily synthesised from a cyclopropene species, by the removal of a sufficiently labile leaving group. The cyclopropene precursor can be synthesised by a ring-forming reaction of an alkyne with a carbene species. In the first synthesis of cyclopropenium by Breslow, the cyclopropene precursor was made by the reaction of diphenylacetylene and phenyldiazoacetonitrile. Boron trifluoride was required to remove the nitrile leaving group to form the cyclopropenium.[5]

The use of a nitrile leaving group was restricted by the limited compatibility with the reagents that the procedure could be used for;[6] therefore an improved route was developed using a halide leaving group, which is readily accessible as a precursor from reagents such as tetrachlorocyclopropene (**3**).[2] The halide can be removed in the presence of a strong Lewis acid,[7] in turn generating the cyclopropenium. A chlorinated cyclopropene precursor can be made by formation of a carbene from a dichlorinated carbon. Breslow *et al* performed a reaction with a carbene derived from phenyldichloromethane (**4**) and an alkyne (diphenylethyne, **5**) to form a triphenylchlorocyclopropene intermediate (**6**) that was converted by potassium tert-butoxide to the tert-butoxylate cyclopropene (**7**). Addition of hydrogen bromide then generates triphenylcyclopropenium (**8**) (Scheme 1.2.a).[6] Removal of a chloride directly can be performed from chlorocyclopropene (**9**) using aluminium trichloride or other Lewis acids (Scheme 1.2.b).[7] The removal of a labile species from a cyclopropene enables the formation of substituted cyclopropenium species, by modifying the reagents used for making the cyclopropene.

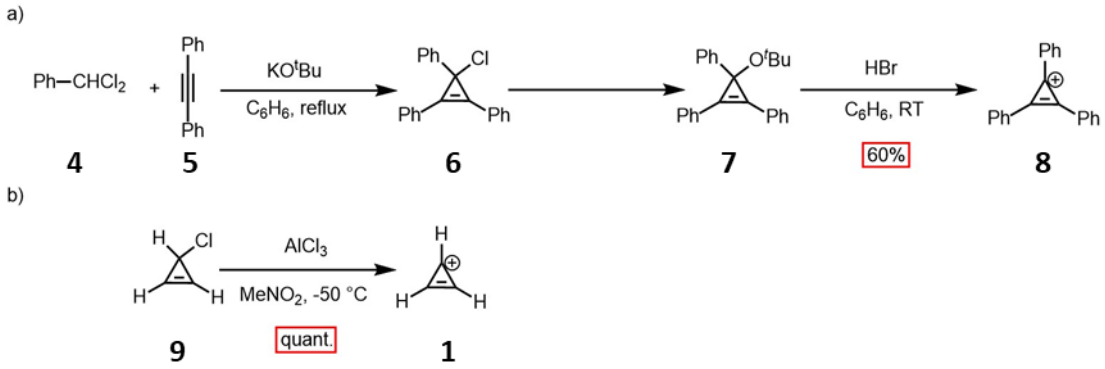

Scheme 1.2: Two reactions of the formation of cyclopropenium, showing a) a cycloaddition reaction followed by exchange and removal of a leaving group,[6] and b) direct removal of a chloride leaving group using a Lewis acid.[7]

The cyclopropenium cation can be reconverted into a cyclopropene by addition of a nucleophilic species onto the cationic ring; therefore breaking the aromaticity.[8] The cyclopropenium can be regenerated by the subsequent removal of the nucleophilic species.[9] This can be used to study their stability by the reaction of a cyclopropenium (such as cyclopropyldiphenylcyclopropenium, **10**) with water and so demonstrate the tendency to form a hydroxide (**11**, Scheme 1.3.a), giving the pK_R as the measure of stability.[8] Chlorinated cyclopropeniums can be used as an intermediate for the synthesis of cyclopropenones, such as by White *et al* showing that *in-situ* formed chlorodipropylcyclopropenium (**12**) can react with a base to form a hydroxide (**13**) which can then be oxidised to a ketone (**14**) on the ring (Scheme 1.3.b).[10]

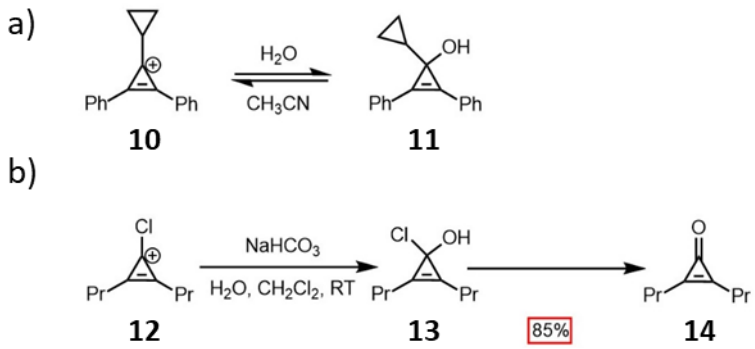

Scheme 1.3: Reactions of cyclopropeniums, showing a) the reversible removal of a cyclopropenium cation by nucleophilic addition,[8] and b) the generation of a cyclopropenone from a chlorinated cyclopropenium cation.[10]

The unsubstituted cyclopropenium cation can be stabilised through the addition of aromatic groups around the ring that can resonance stabilise the positive charge. The cyclopropenium forms a planar structure with the surrounding phenyl groups, allowing them to conjugate to the central cationic ring.[6] West *et al* showed that the use of Friedel-Crafts reactions of anisole (**15**) with trichlorocyclopropenium (made by reacting with $AlCl_3$) produces a fully phenyl-substituted cyclopropenium compound (**16**), with the cyclopropenium acting as the electrophile (Scheme 1.4).[11] However, cyclopropeniums gain more stability from alkyl group substituents than from phenyl group substituents, and the conjugative effects are less significant for the cation stability than the presence of inductively donating groups around the cyclopropenium.[8]

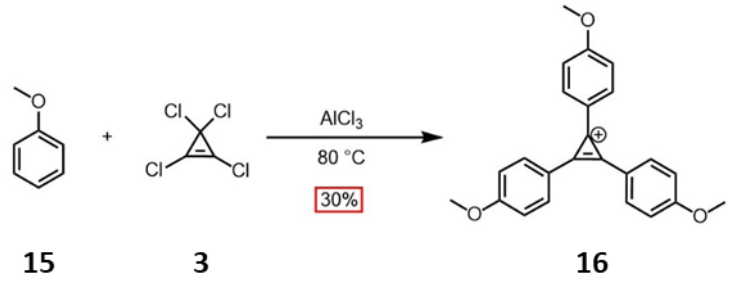

Scheme 1.4: Example of a Friedel-Crafts reaction of tetrarchlorocyclopropene with anisole in order to form a triphenylcyclopropenium.[11]

Cyclopropenium cations can be used as an intermediate as part of a dehydration reaction. Cyclopropene is attacked by an alcohol group to form a cyclopropenium intermediate, which upon dehydration becomes a cyclopropenone by-product.[12] Cyclopropenium-activated reactions have been successfully used in synthesises such as the formation of cyclic ethers,[13] and of alkyl chloride formation from alcohols, with dichlorodiphenylcyclopropene (**17**) being shown by Kelly *et al* to react with an alcohol (**18**) to form a cyclopropenium intermediate (**19**), which then forms the alkyl chloride product (**20**) with a cyclopropenone side-product (**21**, Scheme 1.5).[14]

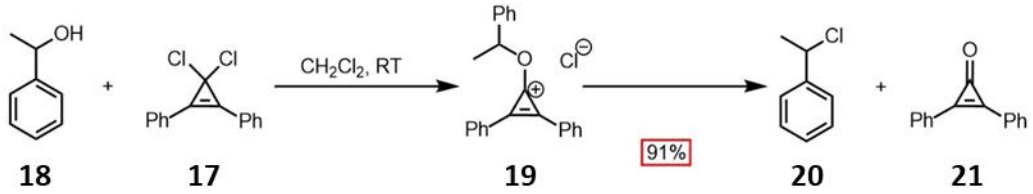

Scheme 1.5: Procedure for a cyclopropenium-activated alkyl chloride synthesis from an alcohol precursor (showing a yield for **20**).[14]

Cyclopropenium compounds can also be used as reagents for ring expansion reactions. These can occur by the nucleophilic attack of a species onto a cyclopropenium ring, breaking the three-membered ring. The broken ring can then recombine to give an expanded ring structure.[2] This procedure was used by Yoshida *et al* for the reaction of diphenylthiomethylcyclopropenium (**22**) with 2,4-pentadieone (**23**) to give a five-membered ring product (**24**, Scheme 1.6.a).[15] Yoneda *et al* used tris(thiomethyl)cyclopropenium (**25**) to make a quinoline product, with **25** undergoing

electrophilic addition to a phenyl amine species (**26**), leading to a ring opening followed by an electrophilic addition to give the product (**27**, Scheme 1.6.b).[16]

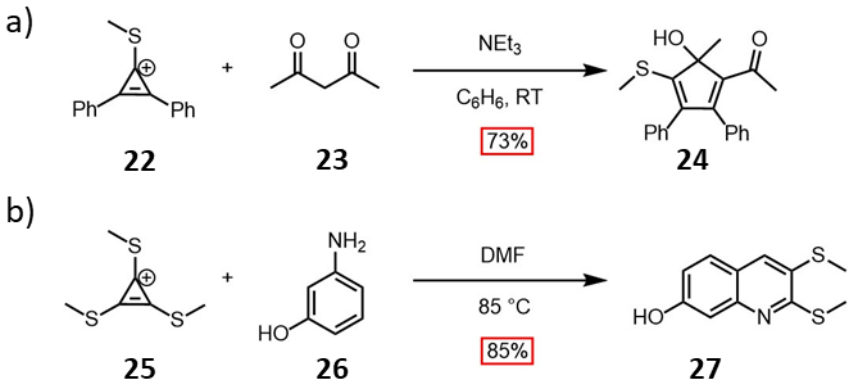

Scheme 1.6: Ring expansion reactions of cyclopropenium compounds, giving a) five-membered product[15], and b) six-membered quinoline product.[16]

1.1.2 Aminocyclopropenium

Aminocyclopropenium is a cyclopropenium species that contains amine substituents. These systems are most frequently formed fully substituted with three amine groups, as triaminocyclopropeniums,[17] but diaminocyclopropenium species can also be isolated.[18] Aminocyclopropenium compounds were first synthesised by Yoshide *et al* in 1974 with tri(diethyl)aminocyclopropenium (**28**, Scheme 1.7) and its diaminocyclopropenium equivalent.[19]

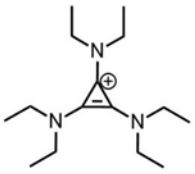

28

Scheme 1.7: Structure of the first synthesised triaminocyclopropenium cation, tri(diethyl)aminocyclopropenium.[19]

The amine groups substituted on the cyclopropenium makes the aromatic ring a more stable carbocation, due to the presence of lone pairs on the nitrogen atoms which reduce the energy of the central cation by donating electrons into the cyclopropenium ring. The stability of the cyclopropenium species increases with the number of amine groups

present on the ring, making aminocyclopropeniums more resilient to nucleophilic attack in comparison to other cyclopropenium cations, with high pK_R values.[20]

The presence of amine groups on the cyclopropenium lowers the oxidation potentials, due to a high energy of the highest occupied molecular orbital (HOMO) of the triaminocyclopropenium cation. Therefore, triaminocyclopropenium cations can be oxidised to form dication species.[20] These dications can be isolated and are slow to decay, lasting in air for hours but decaying over the course of a few weeks.[21] The stability and electrochemical activity of aminocyclopropenium cations makes them suitable as functional species, and they have been used within ionic liquids[17] and transition metal ligands.[20]

As with other cyclopropenium compounds, aminocyclopropeniums can be readily synthesised starting from compound **3**,[21] by nucleophilic substitution with secondary amines. Pentachlorocyclopropane (**29**) was used by Taylor *et al* as an alternative building block to synthesise aminocyclopropenium, with **29** being converted *in-situ* to **3** in the presence of excess base; **3** then undergoes the same reaction with diethyl amine to form **28** (Scheme 1.8.a). **29** is often favoured over **3** as it is a cheaper reagent,[22] and can be readily prepared from trichloroethene and sodium trichloroacetate.[23]

On the synthesis of aminocyclopropeniums by nucleophilic substitution with amines containing bulkier substituents, such as di(cyclohexyl)amine, the reaction can halt after the formation of a diaminocyclopropenium cation (**30**), rather than convert fully to the triaminocyclopropenium. However, on the addition of a second less sterically hindered amine (such as diethylamine) they become fully substituted to a triaminocyclopropenium, with a third separate substituent (**31**, Scheme 1.8.b).[24]

Aminocyclcopropeniums can also form by nucleophilic substitution by silyated amines, without needing an excess of base. This reaction allows for the addition of non-tertiary amine groups to cyclopropenium, such as for tri(phenylamino)cyclopropenium (**32**), which was used by Weiss *et al* to form a cyclopropenimine (**33**) through deprotonation of one secondary amine (Scheme 1.8.c).[25]

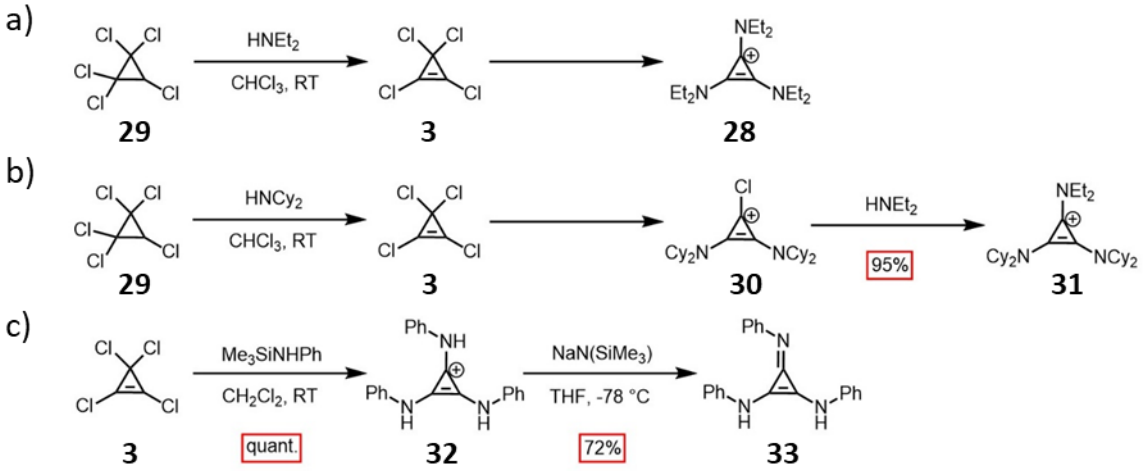

Scheme 1.8: Synthetic methods to form aminocyclopropeniums with: a) an excess of a secondary amine (no yield recorded),[22] b) sequential addition of two different amines in excess,[24] and c) a silylamine, followed by deprotonation of the amine to form a cyclopropenimine.[25]

Aminocyclopropenium cations show weak interactions with their counter anions, due to a high-lying non-bonding HOMO,[26] and the diffuse positive charge from the donation of nitrogen lone pairs into the cyclopropenium. An ion pair strain exists between aminocyclopropeniums and their counter anion, with the negative charges of the surrounding amine groups repelling the counter anion. The effect of the ion pair strain can be seen in tris(dimethyl)aminocyclopropenium chloride, with the cation and anion having the same $E_{1/2}$ value (+1.4 V vs Ag/AgCl).[27] Chloride counter ions can form dichloride hydrate cubes discrete from the cyclopropenium in the solid state.[28]

The donor-donor system of aminocyclopropeniums results in aminocyclopropenium halide counter anions being a ready source of reactive halide ions. This increase in reactivity is significant even for softer anions, as it enables the formation of hypervalent iodate salts from triaminocyclopropenium iodides.[29] The ion pair strain effect also enables aminocyclopropenium salts to solubilise carboxylic acids in organic solvents, by disrupting the carboxylic acids hydrogen bonding with chloride counter anions.[23] When mixed with donors such as a carboxylic acid and a phenol, the system results in the formation of hydrogen bonding complexes, with hydrogen bonding occurring between the chloride ions and the oxygen atoms within the donor species.[27]

On the removal of a solvent, small aminocyclopropenium cations with halide counter anions have been shown to coordinate with each other in dimeric species instead of the counter anions. Short π-π stacking distances (between 3 and 4 Å) connect the two cation species together, which can be seen in their crystal structure (Figure 1.1). The counter anions then coordinate surrounding the dimer to stabilise the charge.[30]

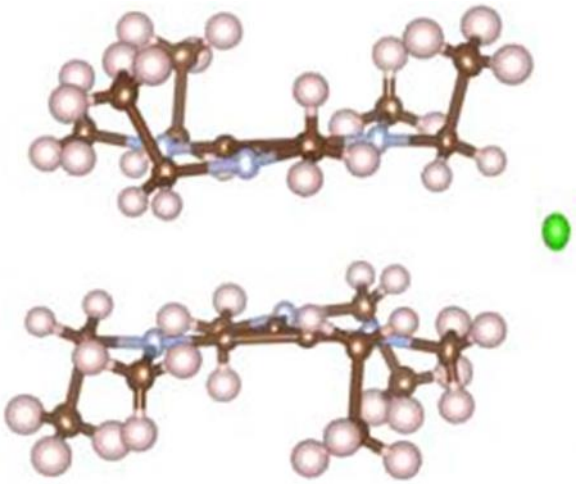

Figure 1.1: Side view of a dimer of tris(diethylamino)cyclopropenium iodide (CDCC number 1062302, ellipsoid probability 50%).[30]

1.1.3 Applications of Aminocyclopropenium

Due to being highly stabile carbocations, aminocyclopropeniums have been designed for use in the molecular structure of ionic liquids,[31] metal complexes,[20] and as ionic liquid crystals headgroups.[32] Aminocyclopropenium species have also been integrated into polymer backbones of polystyrene[33] and polyester[34] to make polyelectrolytes, with the aminocyclopropenium groups giving the polymers good ionic conductivity. This makes the polymers suitable as ion carrier membranes. Aminocyclopropeniums can also grant polymers antimicrobial properties, as the resulting positive charge along the polymer backbone enables the polymer to absorb negatively charged bacterial cell surfaces, so disrupting the cell membranes and thereby causing cell death.[34]

The stable radical dication species of aminocyclopropeniums makes them suitable as catalysts for electrochemical reactions, with activation occurring by oxidisation at low electron potentials. Overoxidation to form unwanted by-products can occur for

reactions at higher electron potentials, so performing a reaction at lower electron potentials with an aminocyclopropenium catalyst removes the risk of overoxidation. Aminocyclopropenium catalysts have been successfully deployed in olefin dioxygenation by Huang *et al* for the reaction of 1-phenylcycloheptene (**34**) to a hydroxyacetate (**35**, Scheme 1.9.a) as a single enantiomer by employing triaminocyclopropenium (**36**) as an electrocatalyst.[35] The same compound also showed catalytic ability in C–C bond formation by C–H activation, with the same trisaminocyclopropenium species **36** coupling THF and 4-bromoisoquinoline (**37**) to make a coupled product (**38**, Scheme 1.9.b).[36]

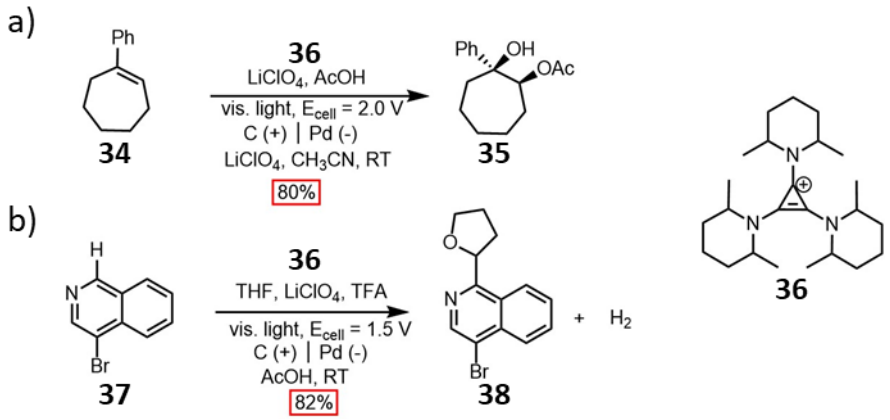

Scheme 1.9: Aminocyclopropenium catalysed electrochemical reactions of a) olefin dioxygenation,[35] and b) C–C bond formation.[36]

Aminocyclopropenium species are also of interest as materials for use within electronic devices. Diaminocyclopropenium species have been developed as catholytes in redox flow batteries,[18] and as redox shuttle additives to enhance the stability and safety of ion batteries.[37] Integrating triaminocyclopropeniums into polymer chains results in the formation of mechanically robust conductive polymers.[38]

1.1.4 Tropylium

The tropylium cation is the next in the series of aromatic hydrocarbon cationic systems after cyclopropenium. It is made of a seven-membered ring of carbon atoms with a single positive charge, giving six delocalised π-electrons spread across the ring. The tropylium cation was first synthesised in the form of unsubstituted tropylium in 1891

(**2**).[1] However, tropylium's structure was not correctly identified until over 60 years later, with the synthesis by Doering *et al* in 1954.[39] The unsubstituted cation has a D_{7h} symmetry,[40] and has a planar structure, although the addition of substituents around the ring can distort it into forming a boat configuration.[41]

A number of methods exist for the synthesis of tropylium cations. Cycloheptatriene (**39**) can be used as a starting material to generate the tropylium cation, which was used by Doering *et al* to synthesise tropylium using a direct oxidation with bromine. A dibromocycloheptatriene (**40**) intermediate was isolated, and then formed tropylium bromide by pyrolysis (Scheme 1.10.a).[39] A route for synthesis by hydride exchange from **39** was achieved by Duaben *et al*, through hydride extraction (Scheme 1.10.b).[42] Geske showed that tropylium could also be formed from cycloheptatriene by an electro-oxidation process, also releasing a proton (Scheme 1.10.c).[43]

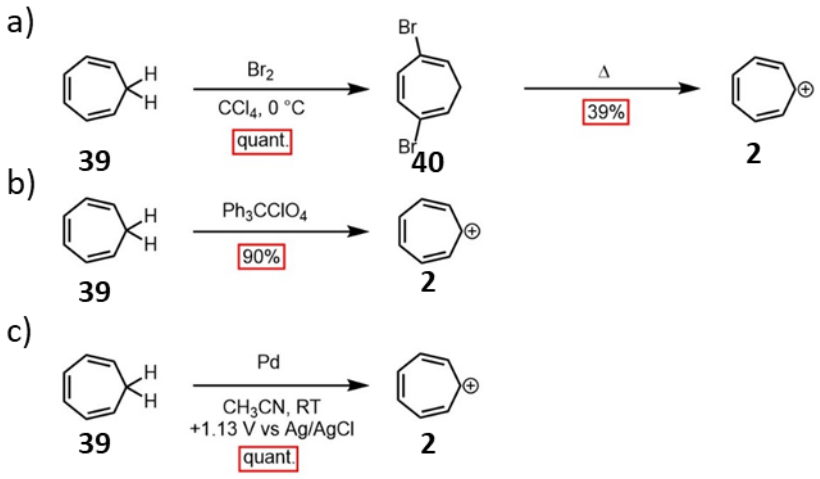

Scheme 1.10: Tropylium synthesis from cycloheptatriene by: a) directed oxidation and pyrolysis,[39] b) hydride extraction,[42] and c) electro-oxidation.[43]

The precursors to tropylium ions can be synthesised through from five-membered start materials. Octachlorobicyclo[3.2.0]hepta-2,6-diene (**41**) can be prepared by a reaction of pentachlorocyclopentadiene (**42**) with trichloroethene, giving nonachlorobicyclo[3.2.0]hepta-2-ene (**43**) as an intermediate which can then undergo an elimination reaction to form **41**.[44] **41** was used as a reagent in the formation of an octachlorocyclohepatriene (**44**) tropylium precursor by West *et al*, *via* the formation of

a tropylium itself as an intermediate with $AlCl_3$ (Scheme 1.11.a). A tropylium is formed from **44** by the removal of a chloride with a Lewis acid such as $AlCl_3$.[45]

A fully substituted tropylium precursor can be made through a Diels–Alder cycloaddition reaction between a three-membered alkene and a five-membered diene. This was reported by Battiste showing the formation of heptaphenylcycloheptatriene (**45**) by the reaction of triphenylcyclopropene (**46**) and tetraphenylcyclopentadienone (**47**), forming a bicyclic compound (**48**) that can then undergo a rearrangement to release carbon monoxide, leaving the desired substituted cycloheptatriene species (Scheme 1.11.b).[46] Making use of a Diels–Alder reaction of substituted species allows for control of the substituents on the tropylium species formed.

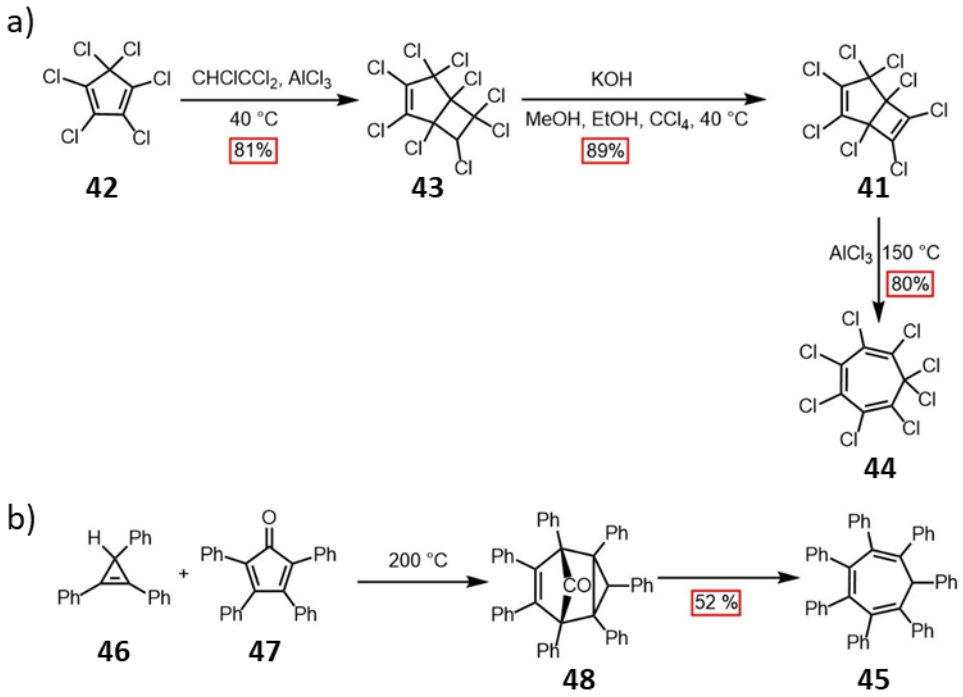

Scheme 1.11: Synthesis of tropylium precursors by: a) a [2+2] cycloaddition followed by elimination and ring expansion,[44, 45] and b) a Diels–Alder cycloaddition followed by elimination and ring opening.[46]

Similar to cyclopropenium cations forming cyclopropenones, tropylium species can be readily oxidised to form tropones with a strong acid.[45] The tropone and tropylium remain in equilibrium, with a negative charge on the oxygen atom of the tropylium species, due to the stability of the aromatic cation. This leads to tropone species being highly basic, as the tropone is able to readily uptake a proton to reform the tropylium.[47]

Like cyclopropenium cations, tropylium species can be used to activate reactions, and tropylium has been used as a catalyst for C–C bond forming reactions. Tran *et al* used **2** as a catalyst for carbonyl-olefin metathesis reactions. The weak Lewis acid tropylium catalyses the reaction by binding to the ketone (**49**), assisting in forming a four-membered intermediate by releasing the tropylium. The tropylium bonds again to the oxygen atom to release a ketone, generating the alkene product (**50**, Scheme 1.12).[48] Tropylium cations are also of interest as the basis of the chromophore of stable dyes as part of dye-sensitised solar cells. The absorbance of the dye can be readily tuned by changing the surrounding substituents on the tropylium.[49]

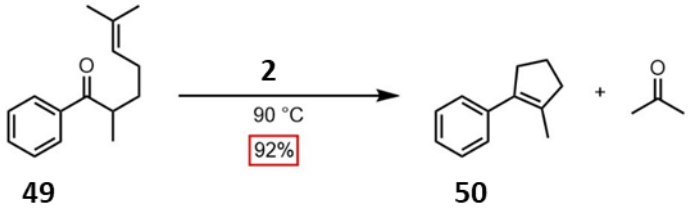

Scheme 1.12: Tropylium catalysed reaction of an intermolecular carbonyl-olefin metathesis reaction.[48]

1.2 Liquid Crystals

Mesogens are materials that possess at least one liquid crystal phase, which are a series of phases of matter that exists between the isotropic liquid and solid phases. Liquid crystals combine both a crystalline structure and long-ranged order with properties of liquid such as fluidity and short-ranged disorder. There are many different liquid crystal phases that can form, and they are defined by being anisotropic materials, which impacts their electronic, magnetic and optical properties.[50]

Liquid crystal phases were first discovered by Reinitzer in 1888 by extraction from natural sources in the form of a cholesterol benzoate (**51**, Scheme 1.13.a),[51] but it was not until much later in the second half of the 20th century that liquid crystals became of industrial interest for their use as part of display applications,[52] working with small rod-like liquid crystals such as 5CB (**52**, Scheme 1.13.b).[53]

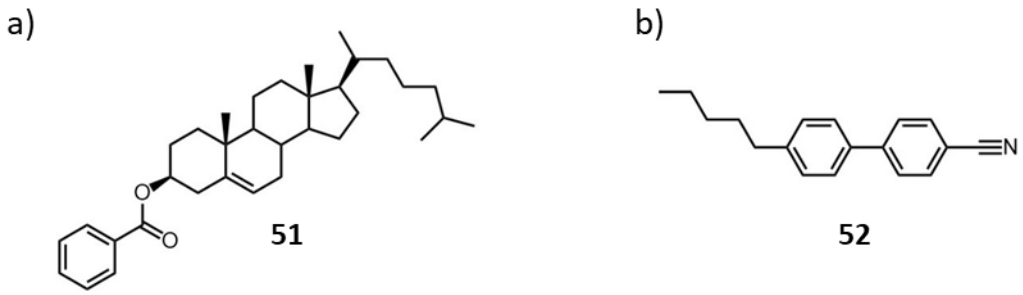

Scheme 1.13: A pair of liquid crystals, showing a) cholesterol benzoate, the first liquid crystal identified from natural sources,[51] and b) 5CB (4-cyano-4'-pentylbiphenyl), a widely used calamitic liquid crystal.[53]

Liquid crystals have primarily been prized for their optoelectronic properties. Liquid crystals characteristically are birefringent, with the direction of polarised light passing through a liquid crystal phase being redirected along the axis of the director of the liquid crystal (the vector upon which the phase is aligned). The birefringence of liquid crystal phases can be used to identify them under polarised microscopy. In addition, many liquid crystal phases have their director changed on the application of an electric field in the alignment of the desired director. These two optoelectronic properties are exploited to create the liquid crystal devices which are widely used in screen technologies, by controlling light passing through a polariser by rotating it with an aligned liquid crystal.[53] However, liquid crystals are also increasingly of interest for their electronic and material properties for many new applications.[54] Liquid crystals also show elasticity resulting from their fluidic nature, and possess dielectric anisotropy, meaning they have great potential for use as functional materials.[53]

Liquid crystals can be primarily divided into thermotropic liquid crystals, which change their phase with changes in temperature, and lyotropic liquid crystals, which change their phase with changes in their concentration within a solvent environment. Liquid crystals exist in a wide variety of distinct phases, with differences in order and symmetry, the makeup of which is determined by the structure of the mesogen molecules.[50] The formation of liquid crystal phases is driven by the nanosegregation of different sections of the liquid crystal molecules.[55]

Calamitic liquid crystal was the variety of liquid crystal which was first identified, and is currently the most used in industry. These mesogens are made of rod-shaped

molecules, such as *N*-(4-methoxybenzylidene)-4-butylaniline (**53**, Scheme 1.14.a), and are widely used in liquid crystal devices for display screens. Another major variety of mesogens are discotic liquid crystals, such as triphenylene derivatives (**54**, Scheme 1.14.b).[50] Discotic liquid crystals are made of disc-shaped molecules and favour the formation of stacked structures.[55]

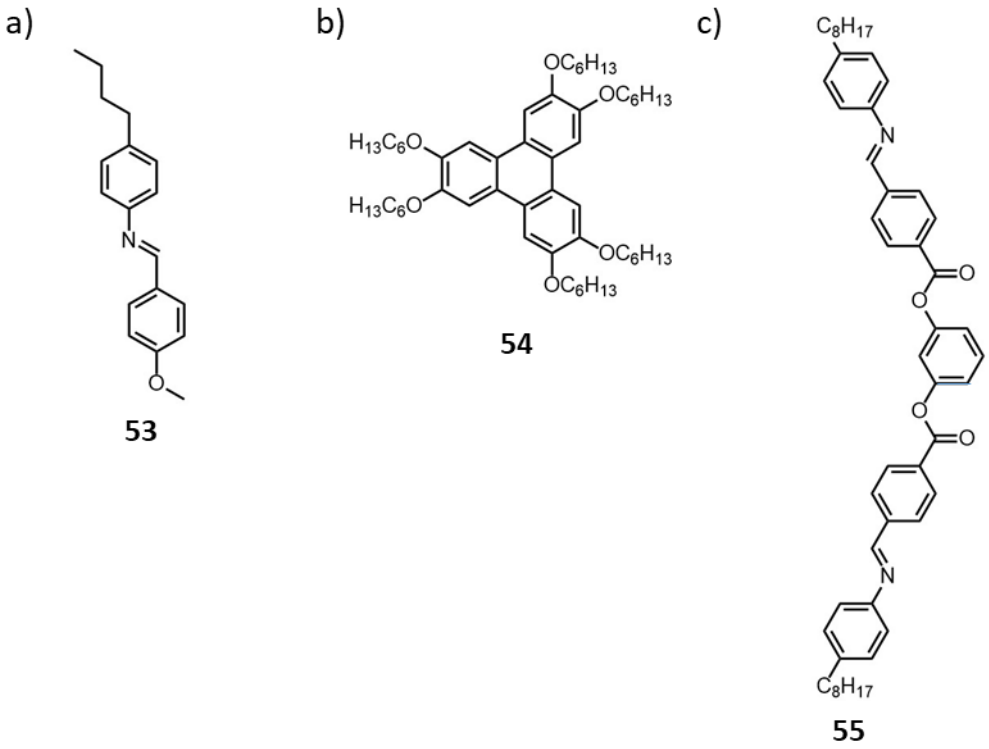

Scheme 1.14: Examples of molecules that form three common types of liquid crystal phases: a) calamitic, b) discotic,[50] c) and bent-core.[56]

A third variety is bent-core liquid crystals, which possess a molecular structure with a bent angle at the centre of a rod system that disrupts a straight shaped molecular structure. The bent angle results in these mesogens forming distinct chiral phases, even for molecules without chirality. The packing of smectic layers results in polar order arising within the smectic liquid crystal phases. Depending on the direction of polar structures within the smectic phases, the phases can show either ferroelectric or antiferroelectric properties (with layers either all aligned in the same direction or aligned in opposite directions respectively),[57] such as phenylene-bis[4-(4-octylphenylimino)methyl]benzoate (**55**, Scheme 1.14.c).[56, 58, 59]

The structure of the molecule determines the liquid crystal phases that can form. Calamitic mesogens form primarily either nematic phases, in which the molecules show only orientational order in the average alignment with the director and random arrangement between the differing mesogens molecules, or smectic phases, whereby the molecules form more ordered layered structures. However, discotic liquid crystals primarily show the formation of column structures through the stacking of molecules.[60] The various liquid crystal phases possess different characteristic textures that can be identified by imaging under polarised microscopy.[50]

1.2.1 Discotic Liquid Crystals

Discotic liquid crystal phases were first identified by Chandrasekhar *et al* in 1977 in benzene-hexa-*n*-alkonates.[61] Discotic liquid crystals are formed from disc-shaped molecules which stack together to form columnar structures.[55] Columnar liquid crystals are commonly formed from a planar molecular structure that possesses a flat core which is surrounded by long alkyl chains. The core is commonly formed of aromatic centres, such as a triphenylene (**56**, Scheme 1.15.a) or a polyaromatic group such as hexabenzocoronene (**57**, Scheme 1.15.b).[62] However, a range of other structures can be deployed for the molecular core, including metal ion centres such as phthalocyanine[63] and porphyrins (**58**, Scheme 1.15.c),[64] or crown rings.[65]

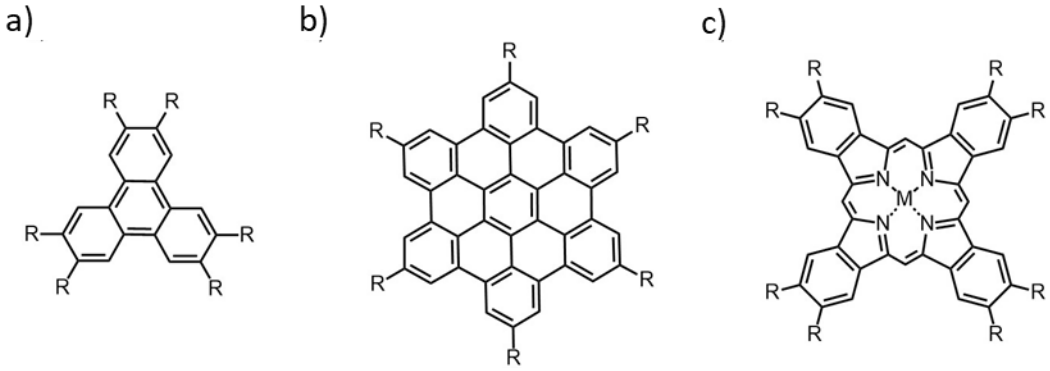

56 **57** **58**

Scheme 1.15: A selection of well-studied discotic molecular cores: a) triphenylene, b) hexabenzocoronene and c) porphyrin.[62, 63, 64]

The most distinctive phases formed by discotic liquid crystals are the columnar phases (Figure 1.2), where the discotic molecules stack into large column structures all aligned in the same direction. Columnar phases can be characterised as ordered, disordered or

tilted, with ordered phases showing regular packing with equidistant cores, disordered phases having irregularly stacked cores, and tilted phases having the cores aligned at an angle with respect to the axis of the columns. In all cases the alkyl chains remain disordered in a columnar phase.[66] Columnar phases can also be formed by the self-assembly of non-disc shaped molecules into a stacked system.[67]

Discotic liquid crystals can also form other phases besides the columnar phase, such as the nematic discotic phase (Figure 1.2). Similar to the nematic phase of calamitic molecules, the molecules possess full translational freedom, but the long axes of the discotic molecules are aligned roughly perpendicular to a director. A mesophase that combines the nematic and columnar phases is the nematic columnar phase (Figure 1.2), in which small stacked columns form, acting as individual units within a nematic phase.[55] Discotic liquid crystals also form a number of other phases, such as helical nematic phases, where the non-stacked molecules align into a helix structure, and cholesteric nematic phases, where a twisted nematic structure arises from chiral molecules or the addition of chiral dopants. Discotic mesogens are even able to show lamellar mesophases, where molecules are ordered in layers similar to a smectic phase formed for calamitic liquid crystals.[55]

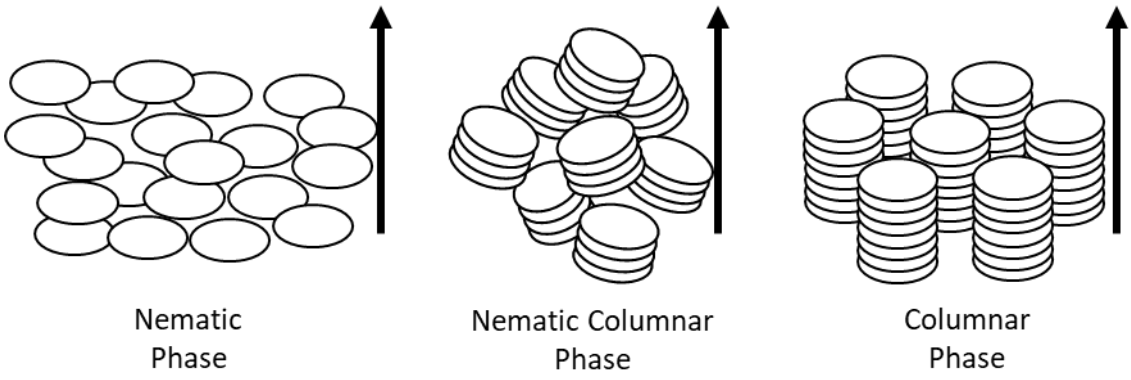

Figure 1.2: Diagrams of discotic liquid crystal phases, with an arrow showing the director of the phase in each case: nematic discotic phase, nematic columnar phase, and columnar phase.

Columnar mesophases can possess a range of symmetries in the packing of the substituent columns, with different mesophases forming hexagonal columnar (Col_{hex}), rectangular columnar (Col_{rec}), square columnar (Col_{squ}) or oblique columnar (Col_{obl})

phases (Figure 1.3). Within these mesophases, a variety of different symmetries of the packing of columns can be seen, defined by the planar space groups.[66]

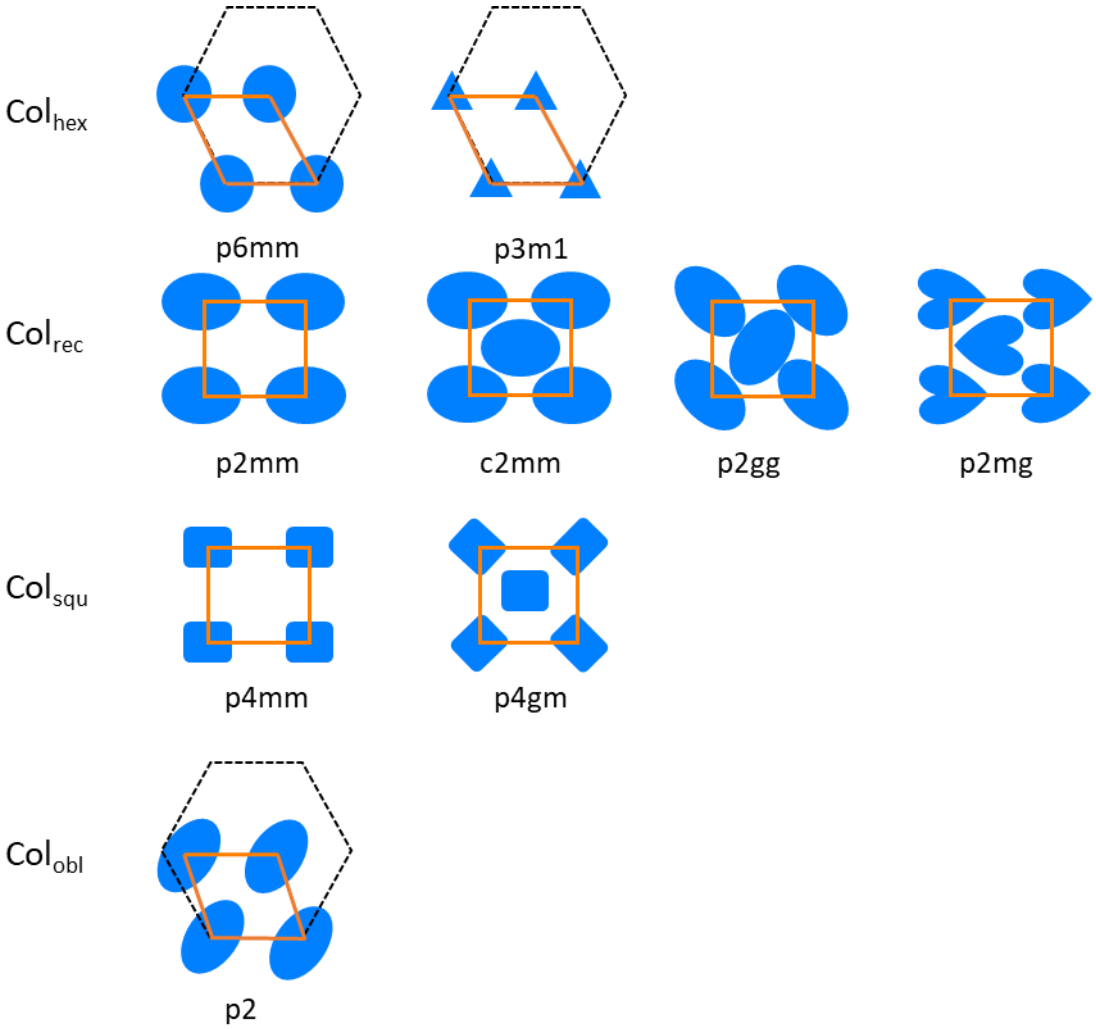

Figure 1.3: The symmetries of different columnar phases, giving the unit cells and planar space group for each example.[55] Representative molecular shapes chosen to allow the relevant symmetries while showing other symmetries are not viable.

The formation of columnar phases can be driven by face-to-face interactions of the aromatic cores of the discotic molecules, but they can also be influenced by hydrogen bonding and dipole-dipole interactions. Long alkyl side chains are required to form liquid crystal phases, as they create insulating regions that induce separation between the molecular cores and side groups. The insulating region stops the cores from aggregating, encouraging the formation of a liquid crystal phase.[68] These alkyl chains can be functionalised with heteroatomic groups,[69] or fluorinated side chains.[70]

Unlike calamitic liquid crystals, discotic liquid crystals are generally difficult to orientate with an electric field, as discotic mesogens tend to lack a central dipole moment that can cause rotation. Discotic liquid crystals also tend to have much greater viscosity than calamitic liquid crystals of the same weight. Therefore, discotic liquid crystals cannot be used for switching agents in liquid crystal devices in the manner of calamitic liquid crystals.[66]

1.2.2 Liquid Crystal Applications

The first major application of liquid crystals was in display technologies, as part of liquid crystal devices for screens. However, continued research into new liquid crystal phases and new mesogen materials has opened up opportunities for liquid crystals to be used for other applications, making use of a combined fluid and ordered structure.[71] Liquid crystals can form a variety of nanostructured phases, which can be adapted by adding new materials to the phases to enhance their properties.[72]

Liquid crystals can be used as the basis for many functional polymers, by performing *in-situ* polymerisation of the liquid crystal phase into a polymer. The polymerisation preserves the liquid crystal structure, allowing it to act as a template for the polymer.[73] *In-situ* polymerisation can be used for creating polymers suitable for the separation of materials in solution by turning liquid crystal phases into porous polymer films.[74] These polymer films are able to control the separation through the size of their pores. Unlike conventional membranes, the pore sizes of liquid crystal materials are well organised and of regular size, making them suitable materials for water treatment.[67]

Liquid crystals have also been designed as sensors, by the impact on optical properties that comes from reorientation of a liquid crystal phase. The analyte binds to the liquid crystal phase and changes the alignment, resulting in visible structural change occurring in the liquid crystal phase, and so enabling it to act as a sensor.[75]

One key area of research into liquid crystals is their use as materials for electronic applications, particularly as ion and electron conducting materials. The ability of liquid crystals to bridge the properties of solids and liquids makes them suitable alternatives

to liquids in electronic devices, and conductive liquid crystals have shown their potential as electrolytes and other useful conductive materials.[67]

1.2.3 Dielectrics of Liquid Crystals

The dielectric properties of a material is the degree to which it can be polarised by the application of an electric current, which results in a shift from an insulating material to a conductive material at a certain voltage.[76] The polarisation is dependent on the permittivity of the material, ε, which is a measure of the material's ability to be polarised by the application of an external electric field. The change in the permittivity is time dependent, with there being a delay in the change of permittivity after the application of the electric field. This delay means that the permittivity is expressed as a complex expression, with ε' as the real component of the permittivity, and ε'' as the imaginary component of the permittivity, forming the equation:[77]

$$\varepsilon = \varepsilon' + i\varepsilon''$$

Equation 1.1: Equation defining the components of complex permittivity.

The real ε' represents the ability of the material to store electrical energy, while the imaginary ε'' represents the loss of energy in the material *via* various relaxation processes that can occur.[76]

ε is made of contributions from a number of different mechanisms. The mechanisms that occur depend upon the frequency of the applied electronic field. Each mechanism possesses a particular cut off frequency, where there a drop in ε' and a peak of ε'' can be seen. Therefore, both ε' and ε'' are dependent on the frequency, with faster mechanisms dominating as the frequency increases. At low frequencies, ionic transit dominates, with the relaxation occurring by the movement of ions. As the frequency increases, dipole reorientation starts to influence the permittivity, with the electrical field placing a torque upon permanent and induced dipoles that causes the molecules to reorientate with the electrical field. At further higher frequencies, atomistic and electronic polarisation mechanisms appear, in which adjacent positive and negative ions stretch with an applied electric field, and the nucleus is displaced by the electric field relative to the surrounding electrons respectively (Figure 1.4).[76]

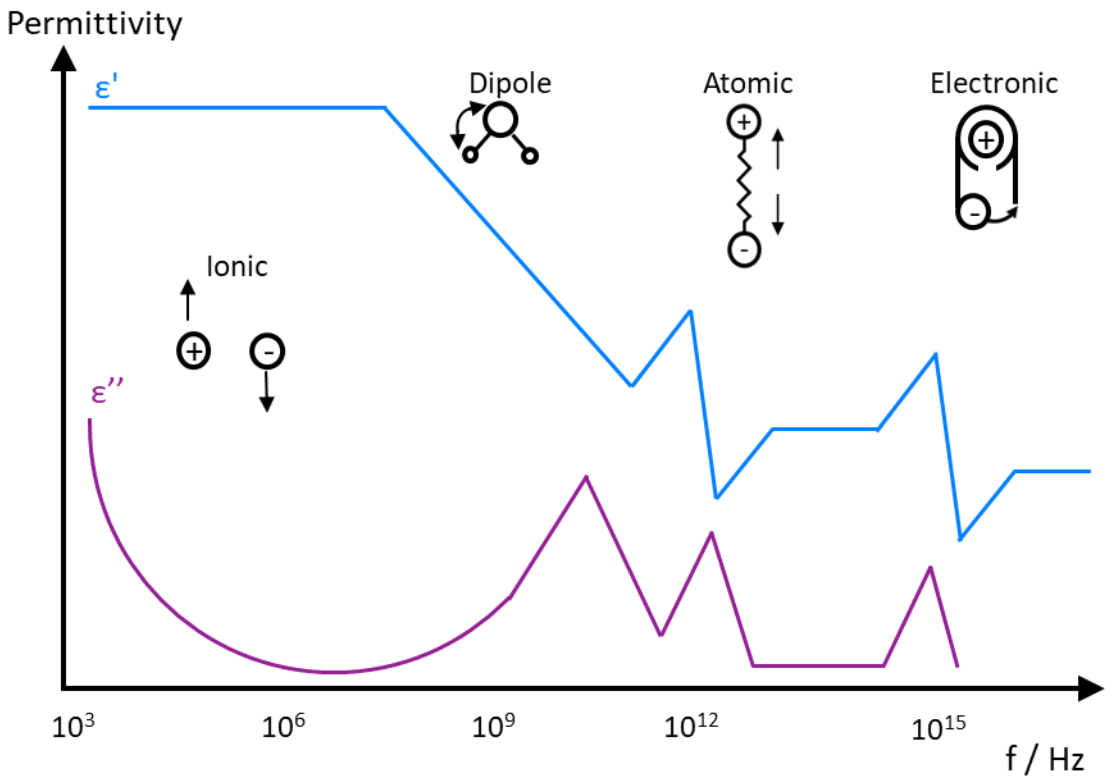

Figure 1.4: Diagram showing the responses of dielectric materials at different frequencies, showing both trends in ε' and ε''.[76]

Due to being anisotropic, the dielectric constant for a liquid crystal phase is made up of two different components - $\varepsilon_{\parallel}$ and $\varepsilon_{\perp}$, which represent the dielectric constant parallel to the director of the liquid crystal phase, and the dielectric constant perpendicular to the director of the liquid crystal phase, respectively. The two components come together to make the dielectric anisotropy, $\Delta\varepsilon$, the difference in permittivity with or against the alignment of the material, relative to the director of the liquid crystal. $\Delta\varepsilon$ is defined by the equation:[78]

$$\Delta\varepsilon = \varepsilon_{\parallel} - \varepsilon_{\perp}$$

Equation 1.2: Equation defining the components of dielectric anisotropy.

The presence of dielectric anisotropy means that the direction of the alignment of liquid crystals is of great importance in determining their properties, as the magnetic and conductive properties are also anisotropic in liquid crystal phases. However, in an isotropic phase, such as the liquid phase, the value of $\Delta\varepsilon$ is 0. When the material rises

above the melting point and transitions from a liquid crystal to the liquid phase, the dielectric anisotropy disappears (Figure 1.5) and a single ε value returns to the material.[78] The electrical anisotropy of a material can also be impacted by transitions between different liquid crystal phases.[79]

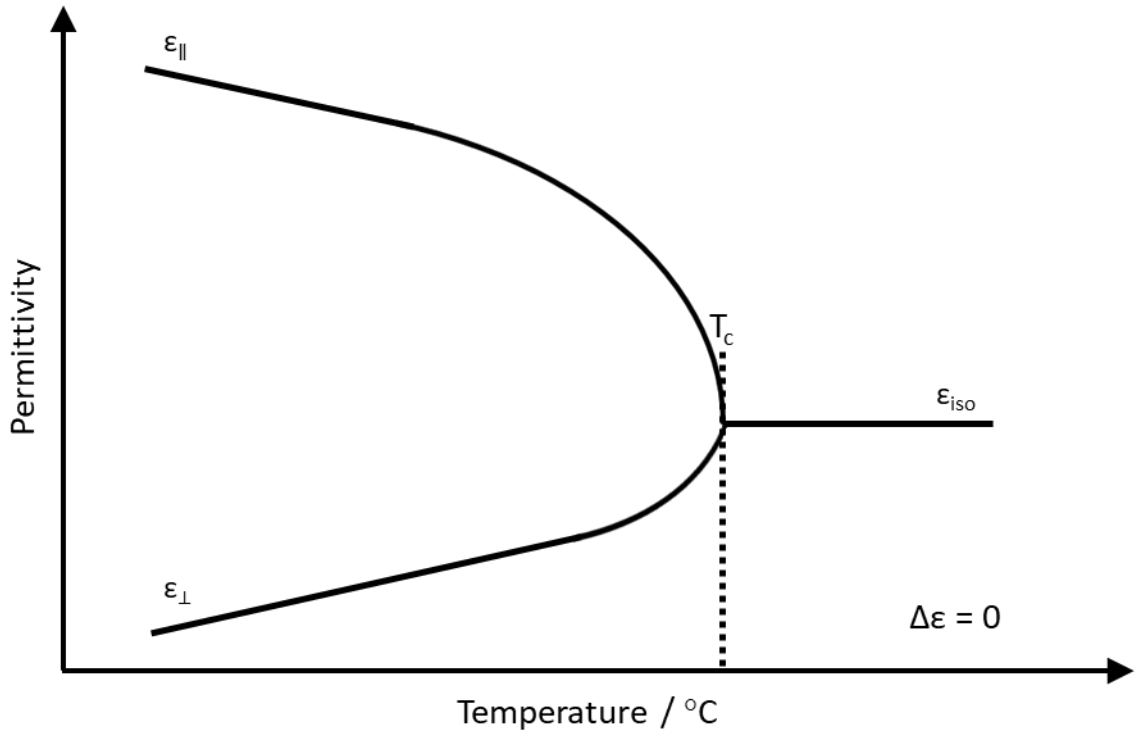

Figure 1.5: Diagram showing the change that occurs in dielectric anisotropy from the transition from the liquid crystal to isotropic liquid phase, T_c.[80]

If the dielectric anisotropy is positive, it is also possible for the liquid crystal director to be reoriented on the application of an electric field placed in a direction differing from the alignment of the director. If the electric field is strong enough, there is a Frederiks transition to align the phase with the electric field, which occurs to minimise the energy of the system. The Frederiks transition is the process by which some liquid crystals can align in the direction of an electric field, which is exploited in the design of liquid crystal devices.[79]

The dielectric properties can be measured by dielectric spectroscopy, which can be used to probe the electronic properties of the material by the application of an alternating current across varying frequencies. Many of these properties are related to the permittivity of the liquid crystal, including the conductivity (σ), impedance (Z, with

Z' and Z'' being the impedance parallel and perpendicular to the director respectively) and capacitance (C). With d being the sample thickness, ω the angular frequency, ε_0 the dielectric permittivity in a vacuum, and A the area of the electrode, σ, C and Z are related to the permittivity through the equations:[81, 82]

$$\sigma = i\omega\varepsilon_0\varepsilon$$

Equation 1.3: Equation defining the components of the conductivity.

$$C = \frac{\varepsilon'\varepsilon_0 A}{d}$$

Equation 1.4: Equation defining the components of capacitance.

a) $$Z = Z' - Z''$$

b) $$Z' = \frac{\varepsilon''}{(\varepsilon'^2 + \varepsilon''^2)\omega C_0}$$

c) $$Z'' = \frac{\varepsilon'}{(\varepsilon'^2 + \varepsilon''^2)\omega C_0}$$

Equation 1.5: Equations defining the components of a) impedance, b) impedance parallel to the director, and c) impedance perpendicular to the director.

The conductivity and permittivity are dependent on the temperature, and also upon the phase of the material, with significant changes in electronic properties occurring upon a phase transition.

1.2.4 Conductive Liquid Crystals

Liquid crystals which can undertake charge carrier transport, either of ions or electrons, are viable candidates as material components within energy storage and generation devices.[67] Liquid crystals with ionic species are suitable for use in many different ion conductive materials, such as in batteries, fuel cells and capacitors. The long alkyl chains of liquid crystal molecules can help to form ion conductive channels by insulating and separating these regions, generally leading to anisotropic conductivity (depending on the phase of the liquid crystal).[83] The greater fluidity of liquid crystals compared to solids makes them suitable for flexible electronics.[84]

Ion transport through liquid crystals is enabled by the integration of ionic or polar groups within the molecular structure of the mesogen.[67] Non-ionic materials with polar groups can be doped with salts to give ionic conductivity, as the doped ions can move through the liquid crystal phase by movement between attractive polar groups.[85] A wide range of different ions have been integrated into liquid crystal molecules, including quaternary ammonium (**59**, Scheme 1.16.a), phosphonium (**60**, Scheme 1.16.b) and guanidinium ions (**61**, Scheme 1.16.c), and aromatic species such as imidazolium (**62**, Scheme 1.16.d) and pyridinium (**63**, Scheme 1.16.e).[60]

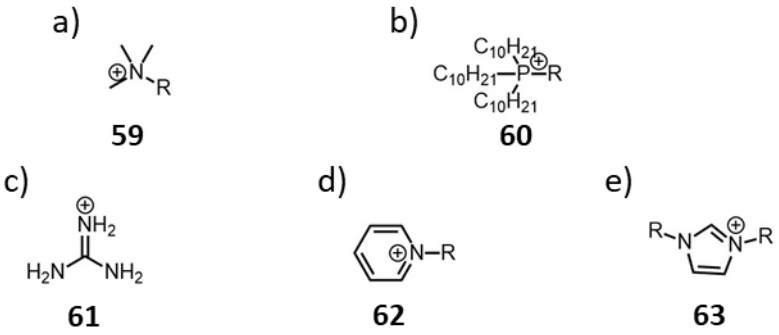

Scheme 1.16: A series of common cations in ionic liquid crystal molecules, showing a) quaternary ammonium, b) quaternary phosphonium, c) guanidinium, d) imidazolium, and e) pyridinium.[60]

The choice of ion and counter ion of an ionic liquid crystal also has a significant impact on the conductivity, with the weaker interactions between the two ions generating higher conductivities, as the counter anion is more able to freely move throughout the bulk phase and so carry charge. Therefore, counter ions with some degree of a delocalised charge give better electronic properties for electrolytes. Liquid crystals that have lower viscosities also show increased ionic conductivities.[83]

The type of liquid crystal phase determines the behaviour of ion transport through the bulk phase. As the insulating regions within the material prevents the ions moving through the whole of the phase, the ion movement is normally restricted to ion channels that are formed between the insulating regions. The anisotropy of the ion movement is dependent on the liquid crystal structure formed. Columnar phases give the formation of 1D-directional ion transport (Figure 1.6.a), with conductivity being restricted to the direction of the alignment of the columns, while smectic phases produce channels that

give 2D-directional ion transport (Figure 1.6.b), with movement of ions restricted between different layers of the phase. It is also possible to create bicontiunous phases which form 3D-directional ion transport, as they produce interconnecting ion channels that enable the ion transport to occur in any direction. Due to the variety of liquid crystal structures that can be created, many different mesogenic phases can be designed for specific properties and applications.[67]

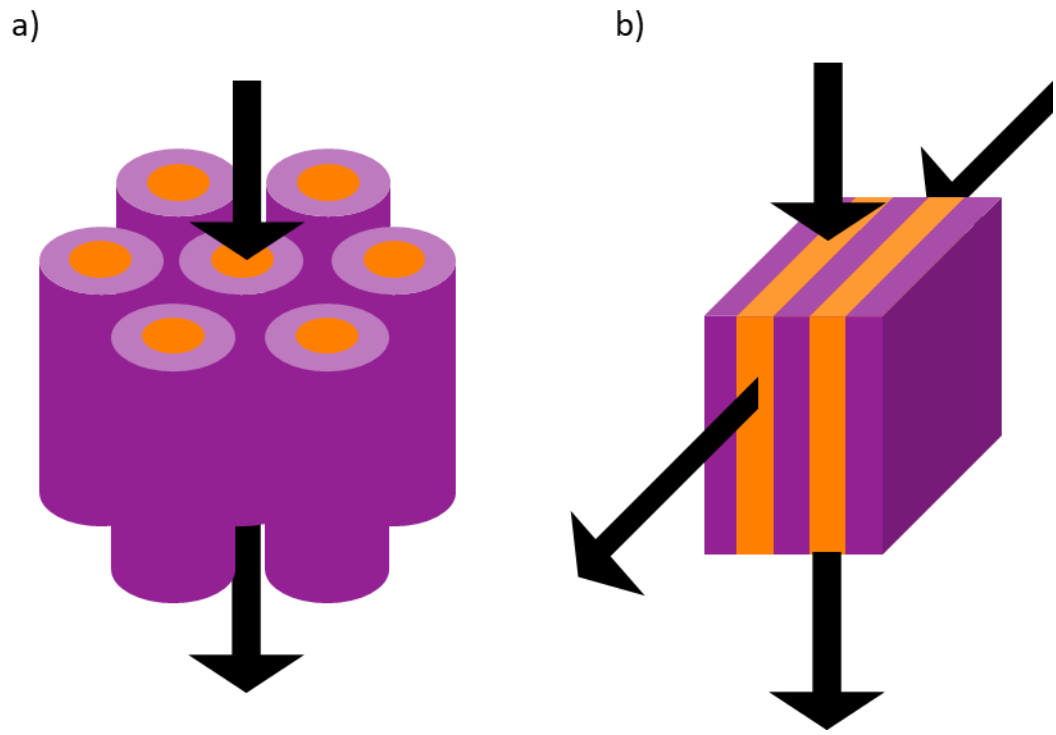

Figure 1.6: Diagram of the control of direction of conductivity within liquid crystal phases, showing a) columnar with 1D conductivity, and b) smectic with 2D conductivity.[86]

Liquid crystals are of interest as electrolytes as part of lithium-ion batteries (Figure 1.7). Lithium-ion batteries are an important technology for energy storage, and are being widely deployed in electric vehicles and renewable power storage.[87] Lithium batteries employ liquid electrolytes due to their high energy densities. However, liquid electrolytes have low ion selectivity and are highly volatile, which leads to significant safety risks from fires and leakage of the electrolyte. The issues with liquid electrolytes increases the difficulty of widespread adoption of these technologies.[85]

Liquid crystals offer an alternative to organic liquid electrolytes. Liquid crystals are non-volatile, reducing the risks of combustion, and are not prone to leakage, but can

still enable a good mobility of ions to ensure ion conductivity. Liquid crystal phases are also fluid enough to display similar ease of processability and interfacial compatibility as liquids.[88] Liquid crystals have therefore been designed as battery electrolytes, with phases used including columnar,[67] smectic[88] or bicontinuous.[86]

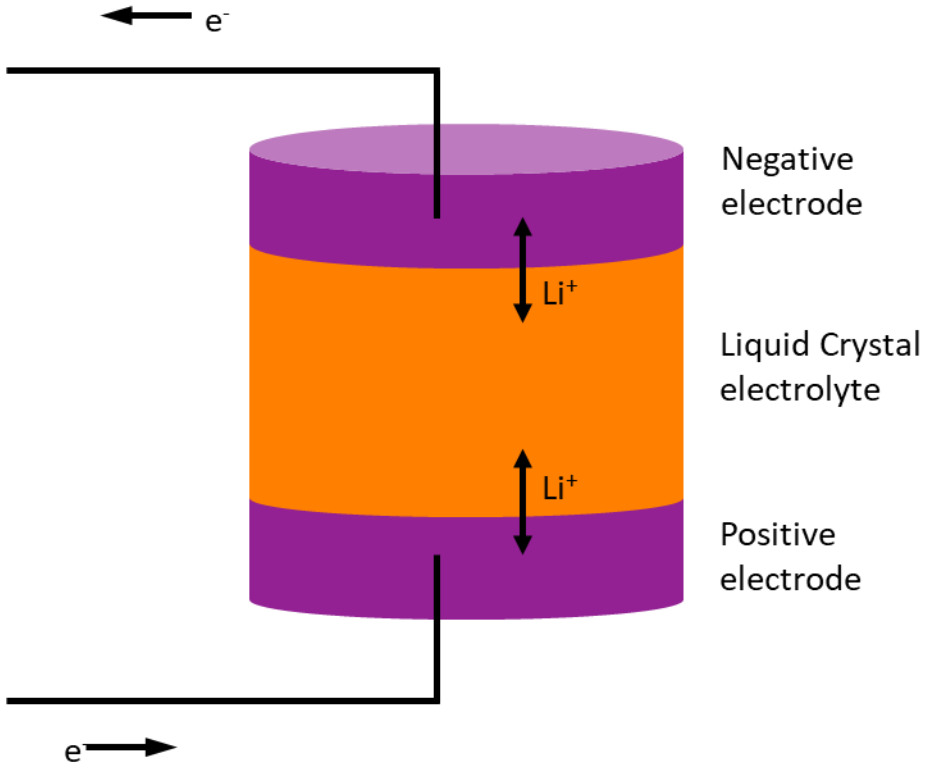

Figure 1.7: Schematic image of a lithium battery with a liquid crystal electrolyte.[88]

An additional issue seen with lithium-ion batteries is dendrite formation. Lithium batteries that make use of lithium metal anodes offer greatly increased theoretical energy densities compared to current lithium batteries.[87] However, inhomogeneous deposition of lithium on the electrodes means that over time batteries can slowly grow dendritic structures of lithium through the electrolyte. The growth of dendrites can eventually result in the battery short-circuiting if the two electrodes connect.[89] Liquid crystal electrolytes with strong anchoring to the substrate and even distribution of Li across the electrode surface are able to suppress the formation of these dendrites, which results in an increased stability and longer lifespan of the lithium batteries.[90, 91]

To be suitable electrolytes in lithium-ion batteries, the liquid crystals chosen require good chemical and mechanical stability, good processability, and good interfacial

connectivity with the electrodes.[83] With a combination of solid and liquid properties, liquid crystal phases are in an ideal position to fulfil these requirements.[92] One of the main challenges is ensuring that the liquid crystals can reach suitable conductivity so they can be used as functional electrolyte materials, as many ionic liquid crystals show low conductivity compared to liquid electrolytes.[83]

Liquid crystal phases require conductivities that are at least 10^{-2}-10^{-3} S cm^{-1} at room temperature to be suitable as electrolytes.[67] The first thermotropic liquid crystal lithium-ion battery electrolyte, developed by Sakuda *et al* in 2015 (Scheme 1.17), showed stable and reversible charge-discharge cycles across a smectic LC doped with $LiN(TFSI)_2$. However, a conductivity of below 10^{-5} S cm^{-1} was seen at room temperature, with the conductivity primarily coming from the doping Li ions and the ability of the liquid crystal phase to support their movement (with similar undoped liquid crystals having conductivities of 10^{-8} S cm^{-1}).[88] Liquid crystal electrolytes have been enhanced since them, having higher conductivities able to reach up to 10^{-3}-10^{-4} S cm^{-1},[93, 94] using molecular modifications such as the addition of ethylene oxide units.[95, 96]

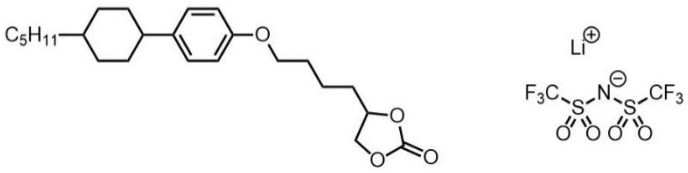

Scheme 1.17: Molecular structure of first thermotropic liquid crystal electrolyte with lithium salt dopant.[88]

Table 1.1: List of the conductivities of liquid crystal electrolytes that have been developed. Numerous series of systems have been developed that reach the region of 10^{-3}-10^{-5} S cm^{-1}.

Publication	**Conductivity at RT/ S cm^{-1}**
Sakuda *et al*[88]	10^{-5}
Onuma *et al*[93]	3×10^{-4}
Dong *et al*[96]	4×10^{-5}
Shimura *et al*[94]	10^{-3}
Kerr *et al*[91]	10^{-4}

The conductivities that have been reached in liquid crystals electrolytes show they hold potential for modification and improvement to enhance their system, but still show charge transport that is unable to reach that that can be achieved with liquid electrolytes. Further work is still needed to allow liquid crystal electrolytes to reach the required conductivity for their utility within lithium ion batteries.

Ensuring a good alignment of the liquid crystal phase can help ensure higher conductivities, as ionic liquid crystals often have poor conductivity when lacking macroscopic alignment over a large area. Ensuring a well aligned system over a large domain can significantly increase the conductivity of the materials, but is also challenging to achieve within devices. The anisotropy can also be increased with longer alkyl chain lengths, which improves the segregation of domains.[83]

To ensure the maintenance of the phase alignment, the mesogen phases often require stabilisation, as the phase alignment can be disrupted by phase transitions from temperature fluctuations. Crystallisation at ambient temperatures can lead to the formation of grain boundary defects, resulting in significant disruption of the macroscopic alignment.[97]

One route for the stabilisation of the liquid crystal phase is *via* polymerising the liquid crystal into polymer films. The polymerisation preserves the structure of the liquid crystal against phase transition, so ensures the alignment of the material remains consistent despite any changes in temperature. Thermal polymerisation is generally avoided as the heat disrupts the aligned structure. Instead photopolymerisation processes are used to ensure that the alignment of the liquid crystal domain is preserved during the formation of the polymer.[83] Forming nanostructured polymers from liquid crystal phases can enhance the conductive properties of polymers compared to the same polymers formed with an amorphous structure, due to ion channels that penetrate through the structure of the phase, which result in higher conductivity polymers.[98]

As the conductivity of columnar materials is primarily restricted to the direction of the columns, and the impact that liquid crystal alignment has upon its conductivity, it is important to be able to both control the direction of the alignment of the columns, and to ensure a uniaxial alignment of the liquid crystal. Columnar materials are aligned on

a substrate in two different ways: either by homeotropic alignment, with the columns coming up from the surface of the substrate (Figure 1.8.a), or by planar alignment, with the columns aligned parallel to the substrate (Figure 1.8.b). Homeotropically aligned phases can be identified by a lack of birefringence when imaging the homeotropically aligned material under a cross-polariser, as the optical axis is aligned with the axis of the columns, meaning there is no rotation of light by the mesogen phase.[63]

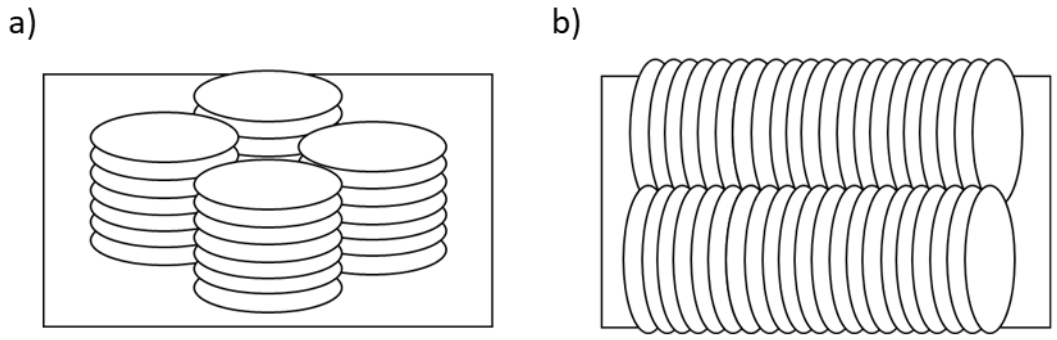

Figure 1.8: Diagrams of the potential alignment of columnar phases on a substrate: showing a) homeotropic alignment, and b) planar alignment.

A variety of different techniques can be used to control the alignment of discotic materials for the creation of a uniform, uniaxial planar alignment, primarily by controlling the application of the liquid crystal to the substrate. These methods include Zone Casting, in which the liquid crystal is applied to a moving substrate through a nozzle while dissolved in solution with a concentration gradient between the nozzle and the substrate (Figure 1.9),[99] and Langmuir-Blodgett Deposition, in which liquid crystal films are grown from solution at the interface between air and the solution, followed by a transfer to a solid substrate by vertical dipping.[100]

Applying a uniform homeotropic alignment of molecules over a large area can be more challenging due to the limited number of techniques available for forming homeotropic structures compared to planar alignments. Homeotropic alignments rarely form spontaneously on a single substrate. Discotic liquid crystals are often able to spontaneously align into homeotropic alignment from the isotropic phase when placed between two solid substrates, independent of the thickness of the film, but will rarely show successful homeotropic alignment when on a single substrate exposed to air.[63]

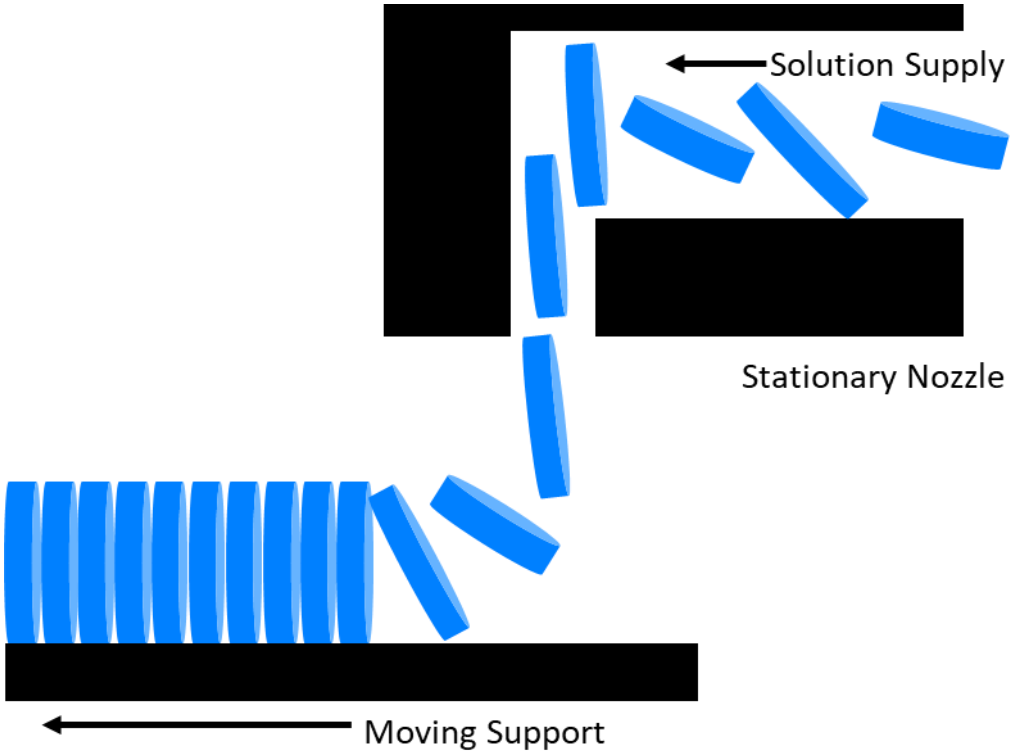

Figure 1.9: Schematic diagram of Zone Casting technique for a homogenous aligned columnar phase.[99]

Unlike with calamitic liquid crystals, the discotic liquid crystals do not normally align with an applied electric field, meaning this cannot be used as a method to control discotic liquid crystal alignment within devices.[101] However, columnar materials that homeotropically align on applying an electric field have been developed. Discotic liquid crystals that can be align by an electric field is achieved by either possessing a hydrogen bonding network that provides a route to respond to an electric field, or with oligothiophene side chains upon the outer chains of the molecule.[102]

Bicontinuous phases, however, do not require alignment in the manner of other liquid crystal phases. Bicontinuous phases can provide 3D-ion transport, due to interconnecting ion channels throughout their phases. The 3D-ion transport means that bicontinuous phases do not produce the domain boundaries that are present within other liquid crystal phases that lower the conductivity when improperly aligned, making them more resistant to temperature fluctuations than other conductivity liquid crystals.[103] Bicontinuous materials that are stable at low temperatures can be used as unaligned liquid crystals in devices, which avoids the need for the challenging alignment of the liquid crystal phase within a device.[83]

Ionic dopants can also be added to mesogen phases to enhance the conductivity, by increasing the bulk phase charge carrier density. Lithium ions, such as $LiNTf_2$ and other lithium salts which have anions that have a delocalised negative charge, can be used to make the liquid crystals suitable materials for lithium-ion batteries. However, the addition of dopants can significantly alter the structure of the liquid crystal phase, including destabilising the liquid crystal phase to instead give an isotropic liquid.[83]

Halide transporting systems can also be designed for different applications other than battery electrolytes. Cationic mesogens with iodide counter anions are of interest for use in dye-sensitised solar cells, which widely use I^-/I^-_3 as a redox couple within the electrolyte. Smectric liquid crystals can concentrate iodide ions between smectic layers, leading to locally high concentrations of iodide ions that favour the exchange reaction between I^- and I^-_3.[104] As with ion batteries, liquid crystals are attractive as transport membranes due to their reduced volatility compared to liquid electrolytes currently in use. Proton conducting liquid crystals are also of interest, for use within fuel cells.[67] Protons can move through proton conducting systems by a hopping mechanism through a hydrogen bonding network created by mixing a lipotropic liquid crystal with water.[105]

It is possible to construct liquid crystal conductive materials such that their ion transport properties can be turned on and off in response to a stimulus. This was achieved by Soberat *et al* by using a liquid crystal which can interchange between two different columnar phases, rectangular columnar and hexagonal columnar, on a change in temperature (with the hexagonal columnar phase being at a higher temperature than the rectangular columnar phase). The rectangular columnar phase has fixed ions so prevents ion movement, while ions can move freely in the hexagonal columnar phase so has a much higher ion conductivity. Therefore, by heating and cooling the liquid crystal phase, the ion conductivity can be increased and decreased.[106]

Liquid crystals have also been developed that undergo conductivity through the transport of electrons. These materials act as organic semiconductors, making them suitable for use in organic field-effect transistors (OFETs),[84] photovoltaic devices,[107] organic light emitting diodes (OLEDs)[108] and electroluminescent devices.[67] Electron transport through liquid crystal phases is facilitated through the overlap of π-conjugated core groups between different mesogen molecules (Figure 1.10).[73]

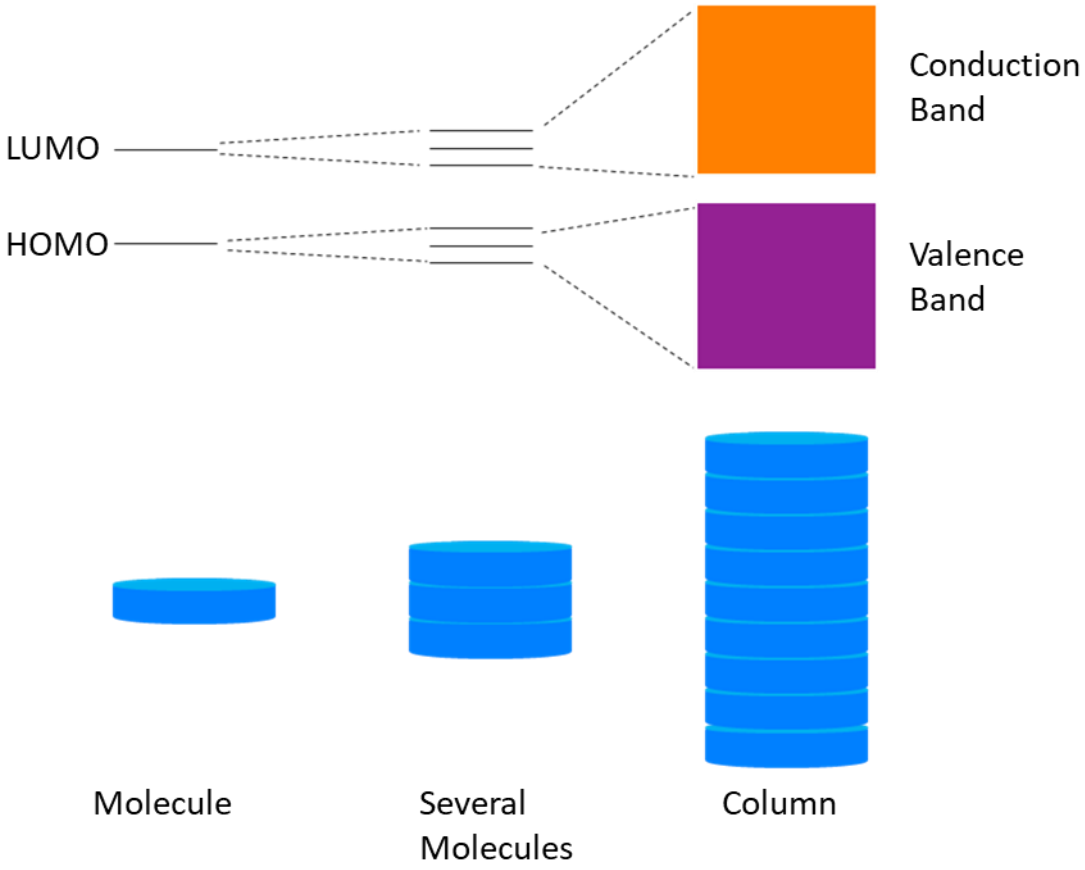

Figure 1.10: Schematic diagram of the change from individual energy levels to broad energy bands as the stacking of molecules of an organic semiconductor in a column increases.[73]

The molecules have a higher degree of mobility than crystalline organic semi-conductors, which reduces the degree of π-orbital overlap that drives the electron movement of these systems compared to crystalline semi-conductors. With good long range orientational order, the orbital overlap between adjacent molecules expands to cover macroscopic distances, giving molecular wires with band-like conduction.[73] The charge transport is described by a hopping mechanism, where a charge carrier transports charge between two neighbouring molecules. The more ordered the system, the better the overlap of π-orbitals, which gives a better charge transfer.[55]

As with ionic conductive materials, the electron transport is highly anisotropic, as it is restricted to the alignment of the π-conjugated groups[67] (typically of a factor of 10^3 in triphenylene liquid crystals).[55] This anisotropy can persist into the crystal phase if the

structures of the liquid crystal phase that allow for charge transfer are preserved, but is lost on heating to the isotropic phase as the orbital overlap is reduced.[55] Cooling rapidly to a glassy solid to prevent crystallisation and domain formation can be used to improve the charge carrying ability by helping to preserve the liquid crystal structure.[73]

Because of their good π-orbital overlap, discotic liquid crystals have been widely studied for use as semiconductors,[63] while calamitic liquid crystals have been studied much less.[109] Calamitic molecules tend to have a poorer overlap of π-orbitals in the liquid crystal phase, so tend to show a lower charge transport.[67] However, smectic liquid crystal phases have been developed with high electron transport capability *via* the formation of 2D channels for π-π stacking and π-CH interactions.[67]

The electron transport is dependent on the molecular structure of the conjugated groups. It can be enhanced by doping with heteroatoms such as nitrogen and sulfur to tune the HOMO and lowest unoccupied molecular orbital (LUMO) to improve electron transport.[67, 110] Other routes to improve the electron transport include expanding the conjugated cores, which leads to higher mobilities. However, doing so can negatively impact the processability by reducing the solubility of the molecules and increasing the melting point of the material.[67] Metal complexes can be integrated into columnar mesogens to increase the electron transport compared to metal free equivalents.[111]

For electron conducting columnar liquid crystals, different applications require different alignments upon a substrate. Homogenous alignments are required for columnar phases used for OFETs, while homeotropic alignments are desired for columnar phases in OLEDs and organic photovoltaic devices.[112]

As with ionic liquid crystals, electron conducting liquid crystals can have their conductivity enhanced by doping the phases with either electron donors or acceptors. These improve the conductivity by enabling charge transfer between electron poor and electron rich species. Doping triphenylene discotic materials with dopants such as trinitrofluorene can enhance the conductivity by a factor of more than 10^7.[113]

1.3 Overview

The aromatic character of certain carbocation ring species grants them much greater stability than other carbocations, making them accessible as potential functional materials. The manipulation of cyclopropenium through amination can form species with unique properties, with high stability, low oxidation potential and weak ion interaction that makes the species of interest for exploitation in functional materials. Cyclopropenium, and their analogue cousin tropylium, have shown themselves capable species for catalysts, reagents and ligands.

Since their discovery, the variety of liquid crystal phases that are known have been greatly expanded, with a great variety of phases having been discovered which are able to form between solids and liquids. As the range of materials has expanded, new applications for these materials have been investigated, with interest moving from displays towards designing liquid crystals as functional materials, particularly as components of electronic devices, taking advantage of fluid materials that show a greater degree of order than liquids. Ionic liquid crystals are being studied in particular as ion conductive materials, which show potential as safer replacements for liquid electrolytes in batteries and other systems. However, to be of use in electronic devices, these materials must overcome the challenges in optimising their properties, including improving the conductivity to useful levels and ensuring that issues with alignment can be dealt with.

As stable ionic species, aromatic cations seem to be suitable species to integrate ionic character into liquid crystals. However, there has been little study of liquid crystals with either cyclopropenium or tropylium species incorporated within, with the first paper demonstrating their synthesis published in 2020, showing the formation of liquid crystals with aminocyclopropenium headgroups.[32] The use of aromatic carbocationic species as part of liquid crystals therefore represents an opportunity to formulate new structures of conductive liquid crystals.

1.4 References

1. A. Balaban, D. Oniciu, A, Katritzky, *Chem. Rev.*, 2004, **104**, 2777.
2. K. Komatsu, T. Kitagawa, *Chem. Rev.*, 2003, **103**, 4, 1371.
3. W. Lin, *J. Chinese Chem. Soc.*, 1955, **2**, 37.
4. K. Potts, J. Baum, *Chem. Rev.*, 1974, **74**, 2, 189.
5. R. Breslow, *J. Am. Chem. Soc.*, 1957, **79**, 19, 5318.
6. R. Breslow, H. Chang, *J. Am. Chem. Soc.*, 1961, **83**, 10, 2367.
7. R. Breslow, J. Groves, *J. Am. Chem. Soc.*, 1970, **92**, 984.
8. R. Kerber, C. Hsu, *J. Am. Chem. Soc.*, 1973, **95**, 10, 3239.
9. R. Breslow, C. Yuan, *J. Am. Chem. Soc.*, 1958, **80**, 22, 5991.
10. J. White, M. Bromley, *Tetrahedron Lett.*, 1993, **34**, 25, 4091.
11. R. West, D. Zecher, W. Goyert, *J. Am. Chem. Soc.*, 1970, **92**, 1, 149.
12. C. Vanos, T. Lambert, *Chem. Sci.*, 2010, **1**, 705.
13. B. Kelly, T. Lambert, *Org. Lett.*, 2011, **13**, 740.
14. B. Kelly, T. Lambert, *J. Am. Chem. Soc.*, 2009, **131**, 13930.
15. H. Yoshida, M. Nakajima, T. Ogata, K. Matsumoto, R. Acheson, J. Wallis, *Bull. Chem. Soc. Jpn.*, 1983, **56**, 10, 3015.
16. S. Yoneda, H. Kojima, *Bull. Chem. Soc. Jpn.*, 1988, **61**, 5, 1793.
17. J. Curnow, D. MacFarlane, K. Walst, *Chem. Commun*., 2011, **47**, 10248.
18. Y. Yan, S. Robinson, T. Vaid, M. Sigman, M. Sanford, *J. Am. Chem. Soc.*, 2021, 143, **33**, 13450.
19. Z. Yoshida, Y. Tawara, *J. Am. Chem. Soc.*, 1971, **93**, 2573.
20. J. Bandar, T. Lambert, *Synthesis*, 2013, **45**, 2485.
21. R. Weiss, K. Schloter, *Tetrahedron Lett.*, 1975, **16**, 40, 3491.
22. M. Taylor, P. Surman, G. Clark, *J. Chem. Soc. Chem. Commun.*, 1994, **21**, 2517.
23. J. Bandar, PhD Thesis, Columbia University, 2014.
24. J. Bandar, A. Tanaset, T. Lambert, *Chemistry*, 2015, **21**, 20, 7365.
25. R. Weiss, M. Hertel, *J. Chem. Soc. Chem. Commun.*, 1980, **5**, 223.
26. O. Curnow, M. Polson, K. Walst, R. Yunis, *RSC Adv.*, 2018, **8**, 28313.
27. R. Weiss, T. Brenner, F. Hampel, A. Wolski, *Angew. Chem. Int. Ed*., 1995, **34**, 4, 439.

28. J. Butchard, O. Curnow, D. Garrett, R. Maclagan, *Angew. Chem. Int. Ed.*, 2006, **45**, 7550.
29. R. Weiss, M. Rechinger, F. Hampel, A. Wolski, *Angew. Chem. Int. Ed.*, 1995, **34**, 4, 441.
30. A. Wallace, C. Jayasinghe, M. Polson, O. Curnow, D. Crittenden, *J. Am. Chem. Soc.*, 2015, **137**, 49, 15528.
31. O. Curnow, M. Holmes, L. Ratten, K. Walst, R. Yunis, *RSC Adv.*, 2012, **29**, 10794.
32. J. Litterscheidt, J. Bandar, M. Ebert, R. Forschner, K. Bader, T. Lambert, W. Frey, A. Bühlmeyer, M. Brändle, F. Schluz, S. Laschat, *Angew. Chem. Int. Ed.*, 2020, **59**, 26, 10557.
33. Y. Jiang, J. Freyer, P. Cotanda, S. Brucks, K. Killops, J. Bandar, C. Torsitano, N. Balsara, T. Lambert, L. Campos, *Nat. Commun.*, 2014, **6**, 5950.
34. N. Steinman, R. Starr, S. Brucks, C. Belay, R. Meir, J. Golenser, L. Campos, A. Domb, *Macromolecules*, 2019, **52**, 9, 3543.
35. H. Huang, T. Lambert, *J. Am. Chem. Soc*., 2021, **143**, 7247.
36. H. Huang, Z. Strater, T. Lambert, *J. Am. Chem. Soc.*, 2020, **142,** 1698.
37. W. Ji, H. Huang, X. Huang, X. Zhang, D. Zheng, T. Ding, J. Chen, T. Lambert, D. Qu, *J. Mater. Chem. A.*, 2020, **8**, 17156.
38. B. Paren, R. Raghunathan, I. Knudson, J. Freyer, L. Campos, K. Winey, *Polym. Chem.*, 2019, **10**, 2832.
39. W. Doering, L. Knox, *J. Am. Chem. Soc*., 1954, **76**, 3203.
40. J. Wagner, D. McDonald, M. Duncan, *J. Phys. Chem. Lett.* 2018, **9**, 16, 4591.
41. M. Tamm, B. Dreβel, R. Fröhlich, *J. Org. Chem.* 2000, **65**, 20, 6795.
42. J. Dauben, A. Gadeckt, K. Harmon, D. Pearson, *J. Am. Chem. Soc.*, 1957, **79**, 4557.
43. D. Geske, *J. Am. Chem. Soc.*, 1959, **81**, 16, 4145.
44. J. Krynitsky, R. Bost, *J. Am. Chem. Soc.*, 1947, **69**, 8, 1918.
45. R. West, K. Kusada, *J. Am. Chem. Soc.*, 1968, **90**, 26, 7354.
46. M. Battiste, *Chemistry and Industry*, 1961, **17**, 550.
47. Y. Lou, Y. He, J. Kendall, D. Lemal, *J. Org. Chem.*, 2003, **68**, 10, 3891.
48. U. Tran, G Oss, D. Pace, J. Ho, T. Nguyen, *Chem. Sci.*, 2018, **9**, 5145.

49. D. Lyons, R. Crocker, T. Nguyen, *Chem. Eur. J.*, 2018, **24**, 10959.
50. D. Andrienko, *J. Mol. Liq.*, 2018, **267**, 520.
51. F. Reinitzer, *Monatsh. Chem.*, 1888, **9**, 421.
52. M. Schadt, *Nature Electronics*, 2018, **1**, 481.
53. H. Kawamoto, *Proceedings of the IEEE*, 2002, **90**, 4, 460.
54. T. Kato, J. Uchida, T. Ichikawa, T. Sakamoto, *Angew. Chem. Int. Ed.*, 2018, **57**, 16, 4355.
55. T. Wöhrle, I. Wurzbach, J. Kirres, A. Kostidou, N. Kapernaum, J. Litterscheidt, J. Haenle, P. Staffeld, A. Baro, F. Giesselmann, S. Laschat, *Chem. Rev.*, 2016, **116**, 3, 1139.
56. T. Niori, T. Sekine, J. Watanabe, T. Furukawa, H. Takezoe, *J. Mater. Chem.*, 1996, **6**, 7, 1231.
57. R. Reddy, C. Tschierske, *J. Mater. Chem.*, 2006, **16**, 907.
58. G. Nealon, R. Greget, C. Dominguez, Z. Nagy, D. Giullon, J. Gallani, B. Donnio, *Beilstein J. Org. Chem.*, 2012, **8**, 349.
59. S. Ghosh, N. Begum, S. Turlapati, S. Roy, A. Das, N. Rao, *Jour. Mater. Chem. C*, 2014, **2**, 425.
60. A. Fernandez, P. Kouwer, *Int. J. Mol. Sci.*, 2016, **17**, 5, 731.
61. S. Chandrasekhar, B. Sadashiva, K. Suresh, *Pramana*, 1977, **9**, 5, 471.
62. B. Kaafarani, *Chem. Mater.*, 2011, **23**, 378.
63. S. Sergeyev, W. Pisula, Y. Geerts, *Chem. Soc. Rev.*, 2007, **36**, 1902.
64. M. Stępień, B. Donnio, J. Sessler, *Chem. Eur. J.*, 2007, **13**, 6853.
65. T. Wöhrle, J. Kirres, M. Kaller, M. Mansueto, S. Tussetschläger, S. Laschat, *J. Org. Chem.*, 2014, **79**, 21, 10143.
66. S. Laschat, A. Baro, N. Steinke, F. Giesselmann, C. Hägele, G. Scalia, R. Judele, E. Kapatsina, S. Sauer, A. Schreivogel, M. Tosoni, *Angew. Chem. Int. Ed.*, 2007, **46**, 4832.
67. T. Kato, M. Yoshio, T. Ichikawa, B. Soberats, H. Ohno, M. Funahashi, *Nat. Rev. Mater.*, 2017, **2**, 17001.
68. H. Kayal, PhD Thesis, University of Windsor, 2012.
69. R. Zniber, R. Achour, M. Cherkaoui, L. Gehringer, D. Guillon, *J. Mater. Chem.*, 2002, **12**, 2208.

70. N. Terasawa, N. Tanigaki, H. Monobe, K, Kiyohara, *J. Fluor. Chem.*, 2006, **127**, 8, 1096.
71. J. Pakash, A. Chandran, A. Biradar, *Rep. Prog. Phys.*, 2017, **80,** 016601.
72. D. Broer, C. Bastiaansen, M. Debije, A. Schenning, *Angew. Chem. Int. Ed.*, 2012, **51**, 7102.
73. J. Lagerwall, G. Scalia, *Curr. Appl. Phys.*, 2012, **12**, 6, 1387.
74. M. Zhou, P. Nemade, X. Lu, X. Zeng, E. Hatakeyama, R. Noble, D. Gin, *J. Am. Chem. Soc.*, 2007, **129**, 9574.
75. M. Sadati, A. Apik, J. Armas-Perez, J. Martinez-Gonzalez, J. Hernandez-Ortiz, N. Abbott, J. de Pablo, *Adv. Funct. Mater.*, 2015, **25**, 6050.
76. A. Ward, *Dielectric Materials for Advanced Applications*, National Research Centre, Cairo, 2016.
77. A. Mohamed, E. Paleologos, in Fundamentals of Geoenviromental Engineering, Butterworth-Heinemann, Oxford, 2018, ch. 16, pp. 581.
78. M. Zakerhamidi, H. Majles Ara, A. Maleki, *Jour. Mol. Liq.*, 2013, **181**, 77.
79. J. Lagerwall, in Fluids, Colloids and Soft Materials: An Introduction to Soft Matter Physics, ed. A. Nieves, A. Puertas, John Wiley & Sons, Hoboken, 2016, ch. 16, 307–340.
80. C. Macros, J. Pena, J. Torres, J. Santos, *Sensors*, 2012, **12**, 3204.
81. A. Barrera, C. Binet, F. Dubois, P. Hébert, P. Supiot, C. Foissac, U. Maschke, *Molecules*, 2021, **26**, 2873.
82. K. Deshmuhk, S. Sankaran, B. Ahamed, K. Sadasivuni, K. Pasha, D. Ponnamma, P. Sreekanth, K. Chidambaram, Dielectric Spectroscopy Kalim Deshmukh, Elsevier, Amsterdam, 2017, ch. 10, pp,. 237.
83. K. Goossens, K. Lava, C. Bielawski, K. Binnemans, *Chem. Rev.*, 2016, **116**, 8, 4643.
84. Y. Funatsu, A. Sonoda, M. Funahashi, *J. Mater. Chem. C*, 2015, **9**, 1982.
85. S. Wang, A. Wang, C. Yang, R. Gao, X. Liu, J. Chen, Z. Wang, Q. Zeng, X. Liu, H. Zhou, L. Zhang, *J. Power Sources*, 2018, **395**, 137.
86. T. Kato, *Angew. Chem. Int. Ed.*, 2010, **49**, 7847.
87. K. Liu, Z. Wang, L. Shi, S. Jungsuttiwong, S. Yuan, *Journal of Energy Chemistry*, 2021, **59**, 320.

88. J. Sakuda, E. Hosono, M. Yoshio, T. Ichikawa, T. Matsumoto, H. Ohno, H. Zhou, T. Kato, *Adv. Funct. Mater.*, 2015, **25**, 1206.
89. D. Cao, X. Sun, Q. Li, A. Natan, P. Xiang, H. Zhu, *Matter*, 2020, **3**, 1, 57.
90. Z. Ahmad, Z. Hong, V. Viswanathan, *PNAS*, 2020, **117**, 43, 26672.
91. D. Gopalakrishnan, S. Alkatie, A. Cannon, S. Rajendran, N. Thangavel, N. Bhagirath, E. Ryan, L. Arava, *Sustainable Energy Fuels*, 2021, **5**, 1488.
92. R. Kerr, S. Miller, R. Shoemaker, B. Elliott, D. Gin, *J. Am. Chem. Soc.,* 2009, **131**, 44, 15972.
93. T. Onuma, E. Hosono, M. Takenouchi, J. Sakuda, S. Kajiyama, M. Yoshio, T. Kato, *ACS Omega,* 2018, **3**, 1, 159.
94. H. Shimura, M. Yoshio, K. Hoshino, T. Mukai, H. Ohno, T. Kato, *Am. Chem. Soc*., 2008, **130**, 5, 1759
95. Z. Liu, B. Dong, M. Misra, Y. Sun, J. Strzalka, S. Patel, F. Escobedo, P. Nealey, C. Ober, *Adv. Funct. Mater*., 2019, **29**, 1805220.
96. B. Dong, Z. Liu, M. Misra, J. Strazalka, J. Niklas, O. Poluektov, F. Escobedo, C. Ober, P. Nealey, S. Patel, *ACS Nano,* 2019, **13**, 7665.
97. B. Mu, J. Chen, K. Chen, C. Zhang, D. Chen, *J. Mater. Chem. C,* 2021, **9**, 8029.
98. S. Cao, M. Yoshio, A. Seki, *Crystals,* 2020, **10**, 4, 276.
99. A. Tracz, J. Jeszka, M. Watson, W. Pisula, K. Mullen, T. Pakula, *J. Am. Chem. Soc*., 2003, **125**, 7, 1682.
100. B. Laursen, K. Norgaard, N. Reitzel, J. Simonsen, C. Nielsen, J. Als-Nielsen, T. Bjornholm, T. Solling, M. Nielsen, O. Bunk, K. Kjaer, N. Tchebotareva, M. Watson, K. Mullen, J. Piris, *Langmuir,* 2004, **20**, 10, 4139.
101. S. Chanrasakhar, in Handbook of Liquid Crystals, John Wiley & Sons, Hoboken, 1998, part 3, ch. 8, pp. 749.
102. N. Hu, R. Shao, Y. Shen, D. Chen, N. Clark, D. Walba, *Adv. Mater.*, 2014, **26**, 13, 2066.
103. T. Ichikawa, M. Yoshio, A. Hamasaki, T. Mukai, H. Ohno, T. Kato, *J. Am. Chem. Soc.,* 2007, 129, **35**, 10662.
104. N. Yamanaka, R. Kawano, W. Kubo, T. Kitamura, Y. Wada, M. Watanabe, S. Yanagida, *Chem. Commun.,* 2005, **6**, 740.

105. S. Ueda, J. Kagimoto, T. Ichikawa, T. Kato, H. Ohno, *Adv. Mater.*, 2011, **23**, 27, 3071.
106. B. Soberats, M. Yoshio, T. Ichikawa, X. Zeng, H. Ohno, G. Ungar, T. Kato, *J. Am. Chem. Soc.*, 2015, **137**, 13212.
107. M. Kumar, S. Kumar, *Polymer*, 2017, **49**, 85.
108. Y. Wang, Y. Liao, C. Cabry, D. Zhou, G. Xie, Z. Qu, D. Bruce, W. Zhu, *J. Mater. Chem. C*, 2017, **5**, 3999.
109. M. Yang, J. Hanna, H. Iino, *J. Mater. Chem. C*, 2019, **7**, 13192.
110. T. Yasuda, T. Shimizu, F. Liu, G. Ungar, T. Kato, *J. Am. Chem. Soc.*, 2011, **133**, 3437.
111. P. Schouten, J. Warman, M. de Haas, M. Fox, H. Pan, *Nature*, 1991, **353**, 736.
112. H. Bisoyi, Q. Li, *Prog. Mater. Sci.*, 2019, **104**, 1.
113. P. Kumar, S. Kumar, V. Lakshminarayanan, *J. Phys. Chem. B*, 2008, **112**, 4865.

CHAPTER 2

CONDUCTIVE CYCLOPROPENIUM LIQUID CRYSTALS

Synopsis

This Chapter discusses the synthesis of novel liquid crystal materials using a molecular design of a triaryl-substituted cyclopropenium, substituted with long alkyloxy chains. The effects of varying alkyl chain lengths and counter anions of these compounds are discussed. The cyclopropenium compounds were studied by measurement of their structural, thermal and electrochemical properties, revealing the presence of two columnar phases depending on the alkyl chain length. The dielectric spectroscopy of the materials shows a trend of increasing conductivity with weaker counter anions and shorter chain lengths, and also reveals that the conductivity is unaffected by the phase or alignment of the compounds for those materials forming hexagonal columnar phases. The columnar phase formed seems to have a significant impact on the ability to retain these properties in the solid phase. The inclusion of lithium salts was shown to not improve the conductivity of the material.

Acknowledgements

The following people are gratefully acknowledged for their contribution to this Chapter: Harry Litt prepared the glass cells, performed much of the dielectric measurements, developed software for the analysis of the data and undertook the DSC measurements. Dr Silvio Poppe undertook the XRD measurements. William D. Carswell undertook the TGA measurements, and Len Lauchan undertook the FTIR measurements. Dr Gang Cheng undertook the XPS measurements, and Dr Paul McGonigal and Dr Michal Kohout undertook the DFT calculations.

2.1 Introduction

Aromatic species are widely used as part of ionic mesogens, particularly pyridinium and imidazolium species.[1-4] Despite cyclopropenium being the simplest possible charged aromatic species,[5] it has not been widely investigated as a functional part of liquid crystal structures (Scheme 2.1.a).[6] Given their planar structure, symmetrical nature and distributed charged aromatic structure,[7] triphenyl-substituted cyclopropeniums show the potential for use as cores for discotic ionic liquid crystals, as they provide an aromatic structure to enable the stacking of molecules into columnar structures when combined with long alkyl chain units.[4] Making use of this molecular design, a new class of ion charge transporting liquid crystals can be envisioned (Scheme 2.1.b).

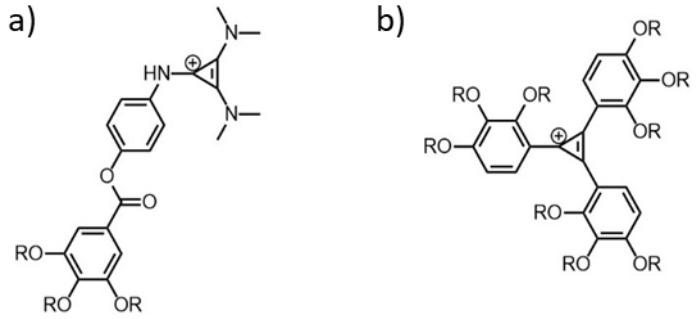

Scheme 2.1 Structure of two liquid crystals, showing a) a previously synthesised cyclopropenium columnar liquid crystal,[7] and b) the cyclopropenium molecules discussed in this Chapter.

This Chapter describes the synthesis of a series of cyclopropenium discotic mesogens, and presents the study of their phase behaviour and electronic properties. The liquid crystal phases are seen only for molecules with long alkyl chains and small halide counter ions. The appearance of two distinct liquid crystal phases was seen with the changes of the length of alkyl chains. Intriguingly, the compounds display a lack of change in their conductivity on phase transition, with the trend of conductivity against temperature being unchanged upon phase transition from liquid-to-liquid crystal or liquid crystal-to-solid. They also show a lack of anisotropy, with no change in conductivity on a change in alignment. The longer chain compounds departed from the series in the solid phase, with neither the conductivity nor the lack of anisotropy persisting on cooling beyond the liquid crystal phase. Lithium salts were added to a cyclopropenium compound to investigate the materials' potential source as an electrolyte for lithium batteries, which showed that the presence of lithium salts interfered with the transport of charge through the medium.

2.2 Results and Discussion

2.2.1 Cyclopropenium Liquid Crystals

Cyclopropenium compounds were synthesised (Scheme 2.2) by substitution with tri-1,2,3(*n*-alkyloxy)benzene molecules, possessing alkyloxy groups of a range of different chain lengths. The tri-1,2,3(*n*-alkyloxy)benzene precursors (**1a-g**) were synthesised by a Williamson ether synthesis with pyrogallol and bromoalkanes, with straight chain or branched bromoalkanes.[8]

The cyclopropenium compounds (**DCn**·X, with n being the number of carbon atoms in the alkyl chain and X being the counter anion) were prepared by a Friedel-Crafts reaction with **1a-g** and tetrachlorocyclopropene acting as an electrophile (**2**).[9] The synthesised cyclopropeniums after the Friedel-Crafts reactions exclusively possessed chloride counter anions. The counter anion of the cyclopropenium was altered by two ion exchange reactions.

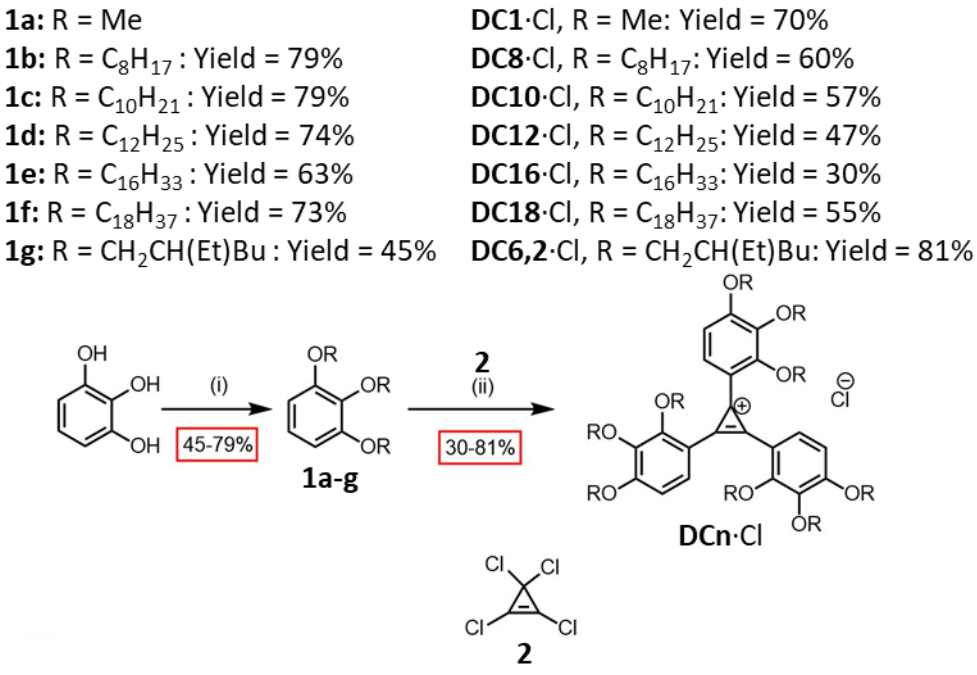

Scheme 2.2: Scheme of the synthesis of substituted cyclopropenium compounds. Reagents and conditions: (i) R-Br, K_2CO_3, KI, 18-crown-6, Me_2CO, reflux, 15 h; (ii) 1). C_3Cl_4, $AlCl_3$, $CHCl_3$, 80 °C, 1 h; 2). $CHCl_3$, 0 °C, 1 h; 3). $CHCl_3$, 50 °C, 16 h.

The ^{1}H NMR spectrum (Figure 2.1) showed that the Friedel-Crafts reaction occurred at the 4-position of the benzene ring selectively, as shown by the two aromatic doublets (in the range of 7.00 – 8.10 ppm, each 3H). The proton signals of the alkyl carbon bonded to the oxygen atoms were significantly more deshielded than the other alkyl protons.

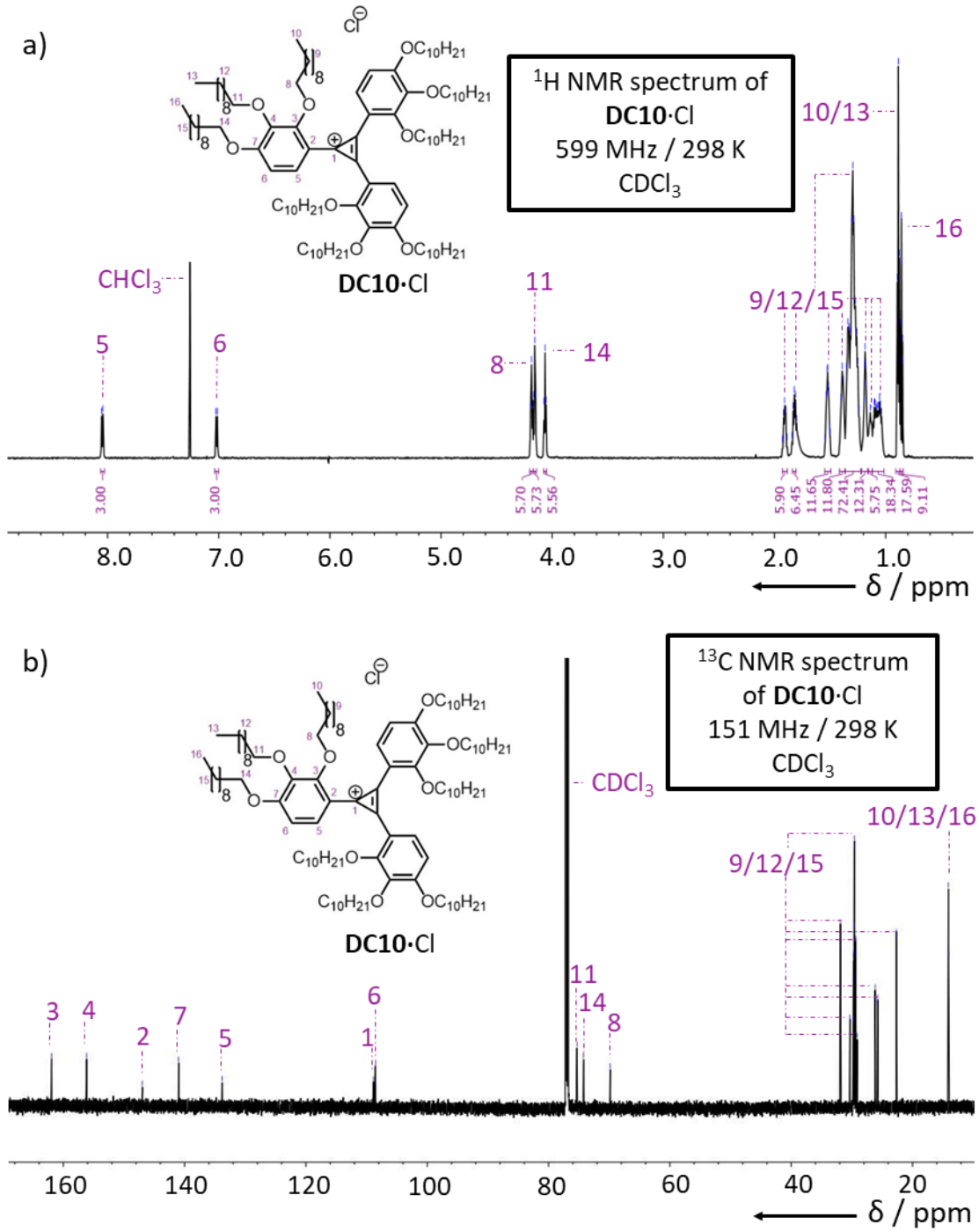

Figure 2.1: NMR spectra of **DC10**·Cl, showing the a) ^{1}H spectrum, and b) ^{13}C spectrum.

The yields seen were around 50-60% for most of the cyclopropenium compounds, with most of the lost yield occurring during the recrystallisation after column chromatography. The impurities being removed seemed to be of a similar solubility as the product, which made the separation with a good yield difficult. Achieving good purity of these compounds was initially challenging due to degradation that could occur under certain conditions during column chromatography or recrystallisation.

Elemental analysis confirmed that no aluminium was present in the isolated compound, with the chloride ion forming as the counter anion. This was confirmed by counter anion exchange, which involved removing the positive charge upon the cyclopropenium by the addition of an alcohol by washing with a basic aqueous solution of sodium acetate, and then removing the alcohol with an acid. On the regeneration of the cyclopropenium with hydrochloric acid, to give a chloride anion, there was no change in properties relative to the starting material. (Scheme 2.3) An alcohol intermediate was identified, rather than a cyclopropene bearing an acetate group, which was confirmed by isolating the intermediate **DC12**·OH.

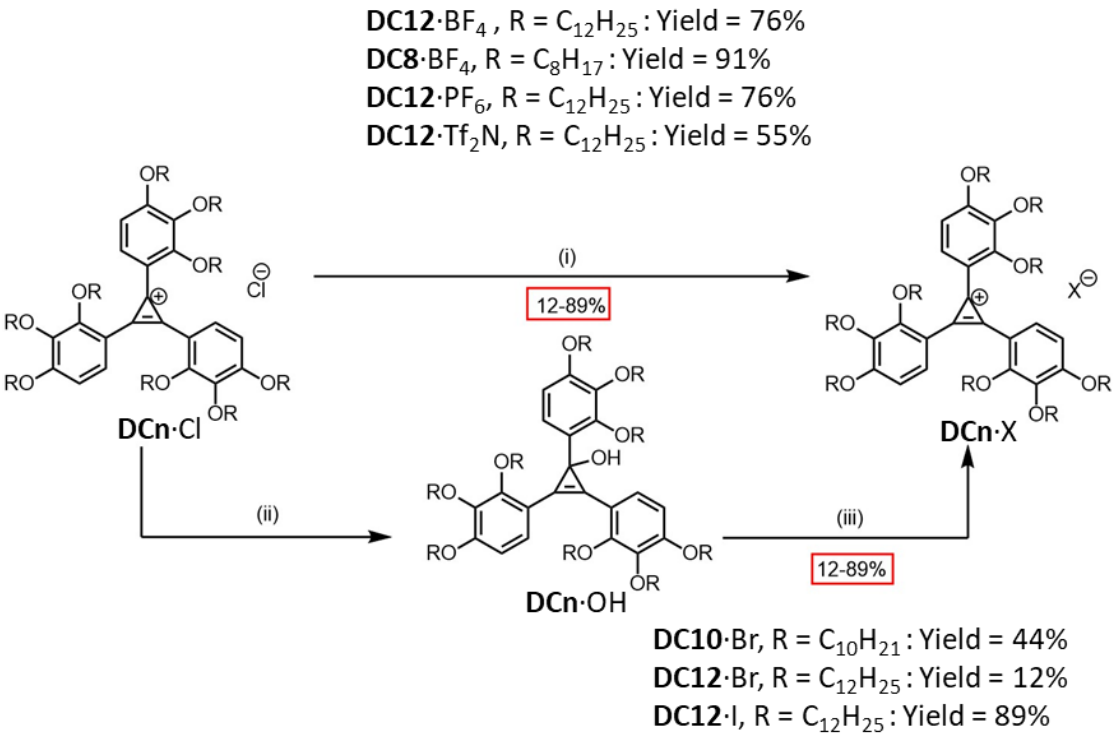

Scheme 2.3: Scheme of the ion exchange of cyclopropenium compounds. Reagents and conditions: (i) AgX, CH_2Cl_2, MeCN, RT, 15 min; (ii) NaOAc, H_2O, CH_2Cl_2, RT; (iii) CH_2Cl_2, HX, H_2O, RT.

The confirmation of the formation of a chloride counter ion by the Friedel-Crafts synthesis of cyclopropenium enabled a second method of counter ion exchange (Scheme 2.3), with silver salts forming a silver chloride precipitate as they exchanged to give the product.

Once fully synthesised, the cyclopropenium compounds were investigated by polarised microscopy (POM) and differential scanning calorimetry (DSC) to study the phase behaviour of the materials, and to determine which of cyclopropenium the materials that showed liquid crystal phases (Table 2.1).

Table 2.1: List of all the prepared cyclopropenium compounds, phase transition temperatures to a liquid crystal (T_K) and isotropic phase (T_I), where appropriate on heating.

Compound	**R Chain**	**Counter Ion X**	**T_K (°C)**	**T_I (°C)**
DC1·Cl	Me	Cl	N/A	103
DC8·Cl	C_8H_{17}	Cl	26	75
DC10·Cl	$C_{10}H_{21}$	Cl	35	56
DC12·Cl	$C_{12}H_{25}$	Cl	46	82
DC16·Cl	$C_{16}H_{33}$	Cl	35	50
DC18·Cl	$C_{18}H_{37}$	Cl	54	62
DC6,2·Cl	$CH_2CH(Et)Bu$	Cl	N/A	N/A
DC10·Br	$C_{10}H_{21}$	Br	36	60
DC12·Br	$C_{12}H_{25}$	Br	43	63
DC12·I	$C_{12}H_{25}$	I	N/A	-7
DC12·BF_4	$C_{12}H_{25}$	BF_4	N/A	37
DC12·PF_6	$C_{12}H_{25}$	PF_6	N/A	-3
DC12·$(Tf)_2N$	$C_{12}H_{25}$	$(Tf)_2N$	N/A	-15
DC8·BF_4	C_8H_{17}	BF_4	N/A	N/A

All cyclopropenium compounds prepared with long straight chain alkyl groups and chloride counter anions showed the appearance of a liquid crystal above RT. The liquid crystal phase formation could be seen by POM, which showed the materials were birefringent in this region (Figure 2.2). Similar textures to those seen in the liquid crystal phases could be seen in the solid phases.

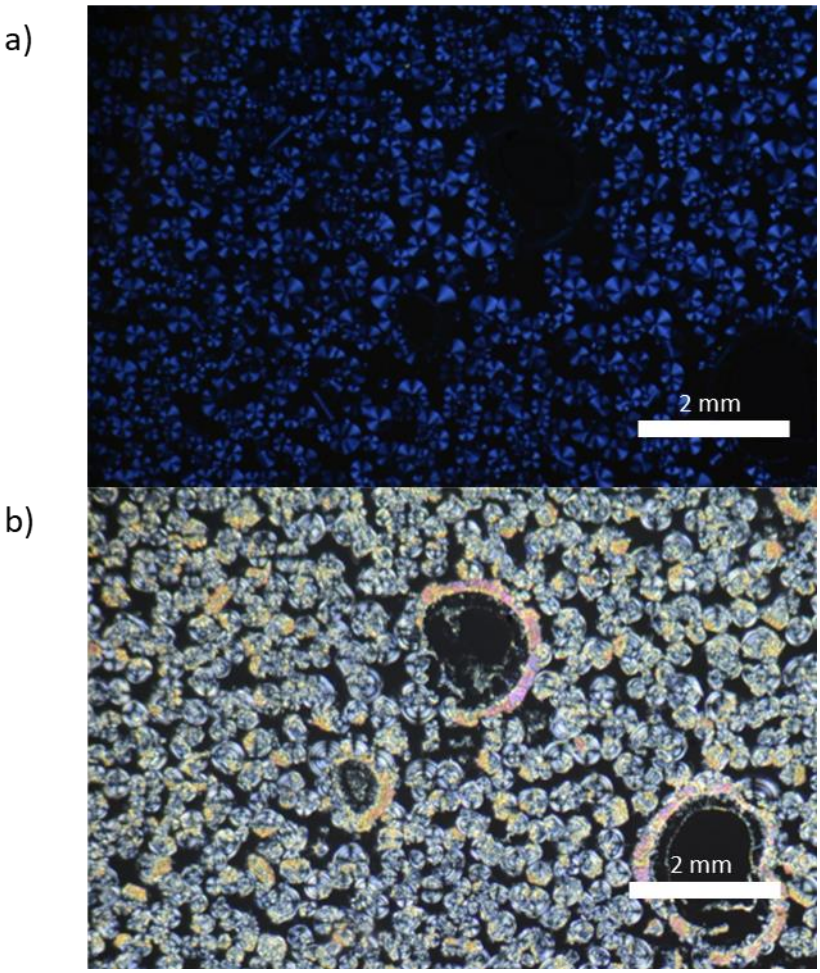

Figure 2.2: POM image of **DC12**·Cl at a) 50 °C, showing the birefringent liquid crystal phase including Maltese cross textures, and b) RT, showing similar textures appearing in the solid phase as those in the liquid crystal phase.

The compound with the shortest alkyl chain R groups, **DC1**·Cl, showed no liquid crystal phase and instead had a high melting point above 100 °C. This is due to **DC1**·Cl lacking long disordered alkyl chains that prevents the molecule from packing too tightly, as a critical chain length must be reached for the formation of a liquid crystal phase.[10]

The cyclopropenium compound with branched ethylheptyl alkyl chains, **DC6,2**·Cl, showed no liquid crystal or solid phase behaviour, and instead maintained a liquid phase over the whole range of investigated temperatures, including down to -30 °C. This can be explained by the branched alkyl chains being sufficiently sterically bulky such that they disrupt the formation of columnar packing. Unlike the other cyclopropeniums, the **DC6,2**·Cl (along with the ether from which it was prepared) has several stereogenic centres on the carbons where the alkyl chains branch. The mixture of different

diastereoisomers formed contribute to the large number of ^{13}C NMR peaks, as well as contributing to the ionic liquid phase persisting at low temperature.

The cyclopropenium compounds with larger counter anions, iodide or multi-atomic ions, also do not show a liquid crystal phase. The larger counter anions appear to disrupt the columnar structure of the liquid crystal, and instead result in a reduced melting point. Most of the compounds with larger counter anions were ionic liquids at RT. As such, liquid crystal phases for these materials are restricted to those with chloride and bromide counter ions.

The compounds with shorter alkyl chains, **DC8**·Cl, **DC10**·Cl, **DC12**·Cl, **DC10**·Br and **DC12**·Br, also showed the appearance of a crystal-crystal transition that could be observed below 0 °C by DSC (Figure 2.3).

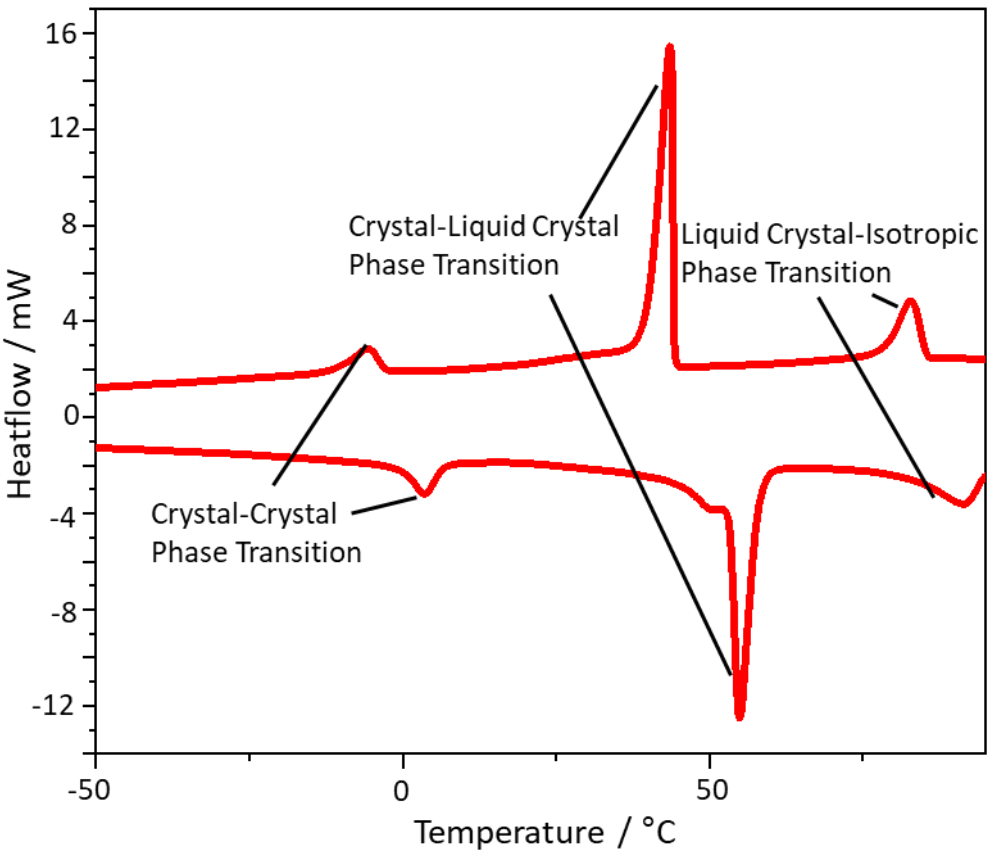

Figure 2.3: The DSC curve of **DC12**·Cl, showing three distinct phase transitions occurring.

Table 2.2: Phase transitions of cyclopropenium liquid crystal compounds identified by DSC: crystal-crystal phase transition (T_C), crystal-liquid crystal phase transition (T_K), and liquid crystal-isotropic phase transition (T_I). The temperatures and transition enthalpies are given for both the first cooling and second heating cycle. Where no phase transition is given, it was not detected for the compound in the temperature range used.

Compound	T_C / °C (ΔH / kJ mol^{-1}) Heating	T_C / °C (ΔH / kJ mol^{-1}) Cooling	T_K / °C (ΔH / kJ mol^{-1}) Heating	T_K / °C (ΔH / kJ mol^{-1}) Cooling	T_I / °C (ΔH / kJ mol^{-1}) Heating	T_I / °C (ΔH / kJ mol^{-1}) Cooling
DC8·Cl	20 (3.6)	14 (3.6)	26 (1.4)	39 (1.7)	75 (11.4)	79 (11.4)
DC10·Cl	-	-	35 (6.5)	40 (6.6)	56 (1.4)	54 (1.5)
DC12·Cl	0 (16.7)	-2 (14.4)	46 (44.6)	44 (51.0)	82 (17.5)	85 (17.2)
DC16·Cl	-	-	35 (140.5)	N/A*	50 (27.3)	36 (N/A*)
DC18·Cl	-45 (9.1)	-62 (7.8)	54 (175.6)	N/A*	62 (2.0)	55 (N/A*)
DC10·Br	6 (2.80)	N/A*	36 (31.2)	40 (31.4)	60 (10.6)	57 (11.6)
DC12·Br	-1 (13.4)	-1 (12.6)	43 (65.6)	46 (67.5)	63 (7.9)	58 (7.9)

*For **DC16**·Cl and **DC18**·Cl, the cooling T_K and T_I phase transitions were mixed so that the beginning of the T_K could not be clearly identified, and neither transition enthalpy could be calculated. For the **DC10**·Br phase transitions, the T_C transition was only seen as a discrete transition on heating, and not on cooling.

The T_K and T_I phase transitions of the larger compounds, **DC16**·Cl and **DC18**·Cl, were seen to merge on cooling, while on heating the liquid crystal phase transitions are still visible as discrete phase transitions (Table 2.2).

The materials were then investigated by thermogravimetric analysis (TGA) to observe their stability with regards to temperature (Figure 2.4).

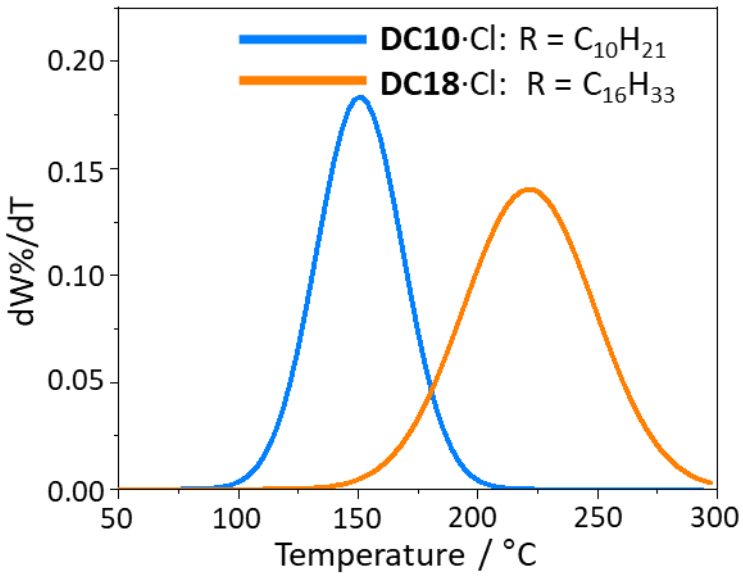

Figure 2.4: DTG curves of **DC10**·Cl and **DC18**·Cl.

The calculated Derivative Thermogravimetry (DTG) spectra shows that the compounds maintain their structure up to 100 °C before beginning to decompose, with the heavier **DC16**·Cl and **DC18**·Cl compounds seeming to be more resilient to degradation than the lighter compounds (**DC8**·Cl, **DC10**·Cl and **DC12**·Cl), with degradation beginning at a higher temperature. While the thermal stability is equivalent to liquid electrolytes,[11] the thermal stability is significantly lower than other ionic liquid crystals[12] or liquid crystal polymers.[13] The lower thermal stability means these cyclopropenium compounds lack one of the advantages over liquid electrolytes possessed by other liquid crystal electrolytes.

2.2.2 Liquid Crystal Phase Behaviour and Electrochemistry

The compounds that showed liquid crystal phases by DSC and POM were investigated by X-ray diffraction (XRD) to identify the mesogen phases that the cyclopropenium materials formed.

XRD analysis of the materials showed the formation of two different columnar phases seen in the liquid crystal materials, depending on the chain lengths (Table 2.3). The short chain compounds (**DC8**·Cl, **DC10**·Cl, **DC10**·Br, **DC12**·Cl and **DC12**·Br) show the appearance of a hexagonal columnar phase. The longer chain compounds **DC16**·Cl and **DC18**·Cl show instead a rectangular columnar phase (Figure 2.5).

Table 2.3: XRD data from the cyclopropenium liquid crystals, showing the detected mesophase and the temperature it was detected at.

Compound	Temperature / °C	Mesophase	Lattice Parameter / Å
DC8·Cl	90*	Col_{hex}	a = 25.7
DC10·Cl	52	Col_{hex}	a = 28.0
DC12·Cl	60	Col_{hex}	a = 30.2
DC16·Cl	50	Col_{rec} – c2mm	a = 66.3 b = 30.9
DC18·Cl	60	Col_{rec} – c2mm	a = 71.9 b = 31.3
DC10·Br	70*	Col_{hex}	a = 28.3
DC12·Br	50	Col_{hex}	a = 54.7

*During the DSC first heating cycle, **DC8**·Cl and **DC10**·Br still show a liquid crystal phase at this temperature, alongside the liquid phase.

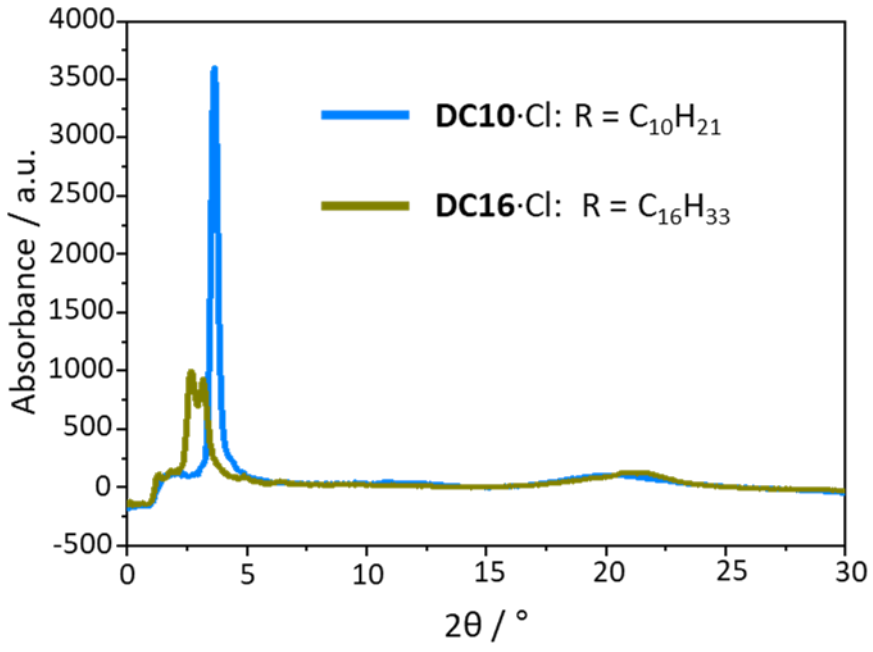

Figure 2.5: WAXD scattering profiles of hexagonal columnar **DC10**·Cl (at 52 °C) and rectangular columnar **DC16**·Cl (at 50 °C) liquid crystal samples.

Using the data from the XRD spectra in the liquid crystal phase, electron density plots of **DC10**·Cl and **DC16**·Cl (Figure 2.6) were calculated and plotted, using a standard method of Fourier reconstruction of the electron density from the XRD spectra by the general formula for 2D periodic systems;

$$\rho = \sum_{hk} \sqrt{I(hk)} \exp\left[2\pi i(hx + ky) + i\varphi(hk)\right]$$

Equation 2.1: Equation defining the general formula for electron density of 2D periodic systems used for a Fourier transform for electron density map.

With ρ being defined as the electron density, *h*, *k*, and *l* being the miller indices, *I* being the corrected intensity and φ being the phase angle of the Fourier transform.[14] These showed the structure of the two different phase symmetries possessed by the molecular structures, giving visualisations of the two liquid crystal phases, with higher density showing the core of the columns, and lower for the more diffuse alkyl regions, and showing a tight packing of the columns in both phases.

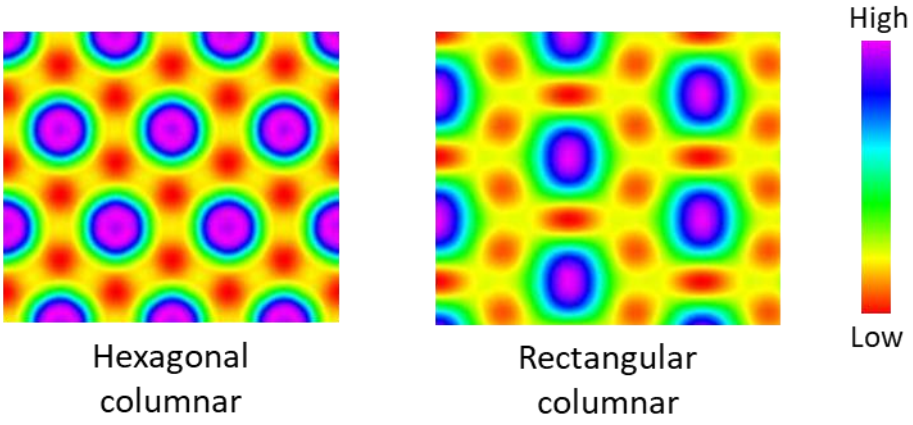

Figure 2.6: Electron density maps of **DC10**·Cl (left) and **DC16**·Cl (right) in their liquid crystal phases, showing the phases as hexagonal columnar and rectangular columnar respectively.

XRD measurements taken at RT identified solid phases in all the compounds measured. For compounds **DC10-12**·Cl and Br, two peaks could be identified for the packing of the alkyl peaks, showing a mixture of both fluid peaks and hexatically packed peaks, showing the solid phase has some degree of fluidity (Figure 2.7).

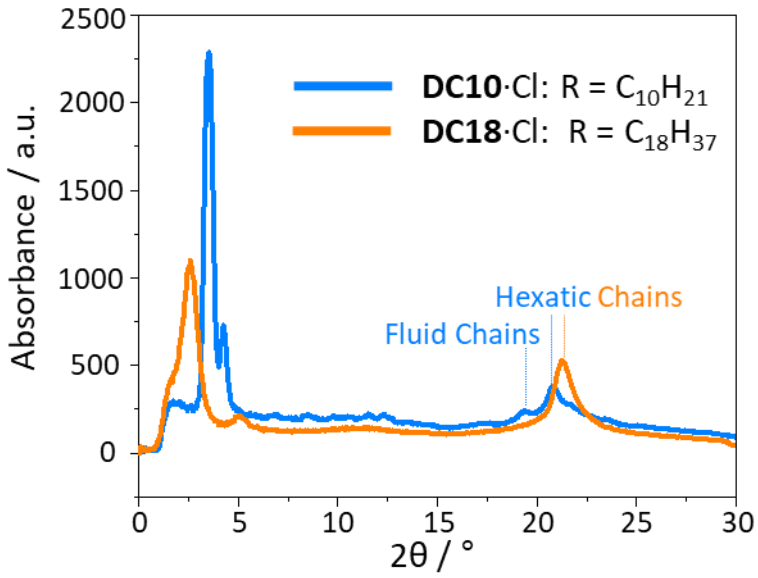

Figure 2.7: XRD spectra at RT of **DC10**·Cl and **DC18**·Cl, showing chain packings in the alkyl region.

The RT XRD of the **DC18**·Cl does not show any fluid alkyl chains, instead having only a single peak for packed alkyl chains that suggest a hexatic packing. The less ordered structure of the hexagonal columnar phase may assist in the fluid chains persisting into the solid phase for the hexagonal columnar materials (with a similar structure to the liquid crystal for both phases) while not persisting for the rectangular columnar materials.[15]

FTIR spectroscopy was also performed to show the difference in the solid state structures between **DC10**·Cl and **DC18**·Cl, with FTIR spectra taken for both compounds at RT (Figure 2.8). The positions of the C-H peaks can show a change in the crystallinity of alkyl chains,[16] with shifts in peak position seen between liquid and crystalline phases to a lower wavenumber for more ordered packing.[17, 18]

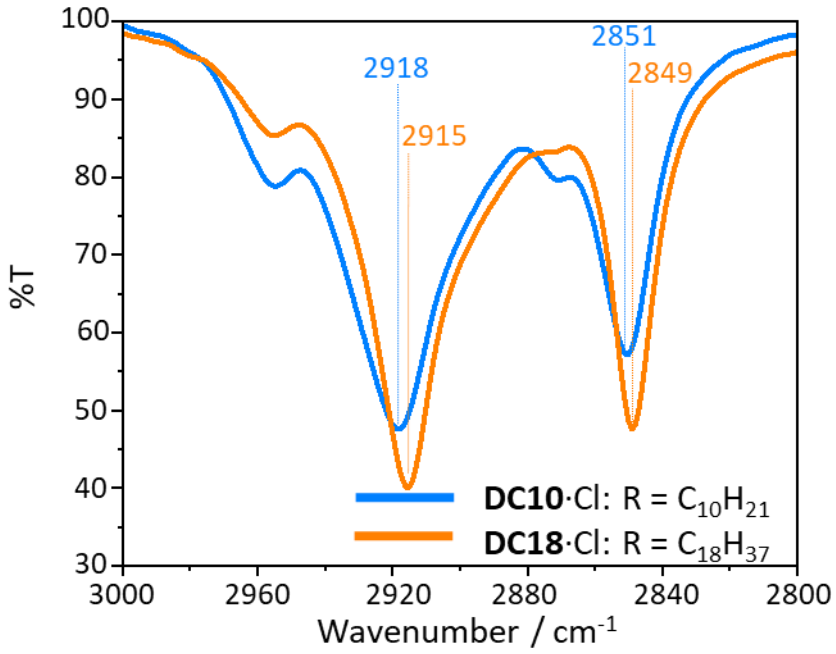

Figure 2.8: FTIR spectrum between 3000 and 2800 cm^{-1} of **DC10**·Cl and **DC18**·Cl at RT.

The peak of the asymmetric CH_2 mode of **DC18**·Cl showed a peak at a lower wavenumber (with a difference of about 3 cm^{-1}) compared to the **DC10**·Cl peak. A similar difference was seen in the symmetric CH_2 stretch, with a lower **DC18**·Cl peak (by about 2 cm^{-1}) compared to **DC10**·Cl (Table 2.4). The trend of lower wavenumber C-H peaks for the **DC18**·Cl in the FTIR spectra shows that the alkyl chains are packed with greater crystallinity in the solid phase compared to the hexagonal columnar **DC10**·Cl.

Table 2.4: Table of the difference in the CH_2 FTIR peaks between **DC10**·Cl and **DC18**·Cl.

Compound	**CH_2 Asymmetric Stretch Peak / cm^{-1}**	**CH_2 Symmetric Stretch Peak / cm^{-1}**
DC10·Cl	2918	2851
DC18·Cl	2915	2849

Density functional theory (DFT) calculations were performed for the **DCn** cations. The flat **DC12** cation was shown with a width of 42.5 Å. However, the semi-empirical optimisation showed a width of 39.7 Å, from the non-flat arrangement of the alkyl peaks (Figure 2.9). The aromatic cyclopropenium and phenyl substituents core remained flat for the semi-empirical optimisation. The diameter of the molecules was larger than the distance between cores seen in XRD, suggesting a highly dense packing in the hexagonal columnar phase.[19]

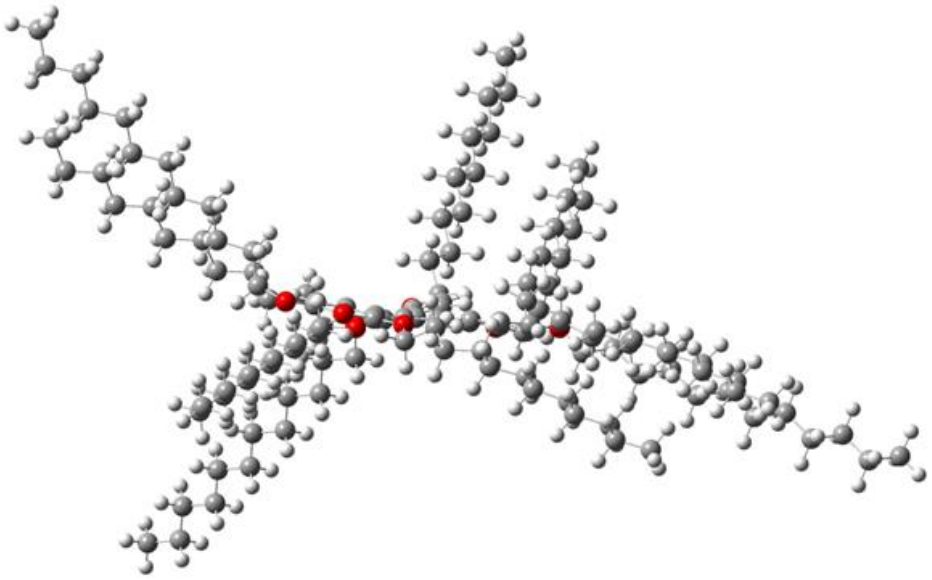

Figure 2.9: A semi-empirical optimised structure of the **DC12** cyclopropenium cation.

Electrostatic potential (ESP) maps were calculated for the **DC1** and **DC8** cations, alongside **DC2** and **DC4** cyclopropenium cations (which were not synthesised), as well as several other alkyl-substituted cations. The ESP maps (Figure 2.10) shows that the charge is highly delocalised across the cation, with the positive charge being distributed into the alkyl chain region rather than being restricted to the aromatic centre. The charges that were calculated for the central positions of the **DC** cations are much lower than those calculated in ESP maps for other alkyl substituted cations, pyridinium and imidazolium, both of which showed a much greater concentration of the positive charge on the central cation.

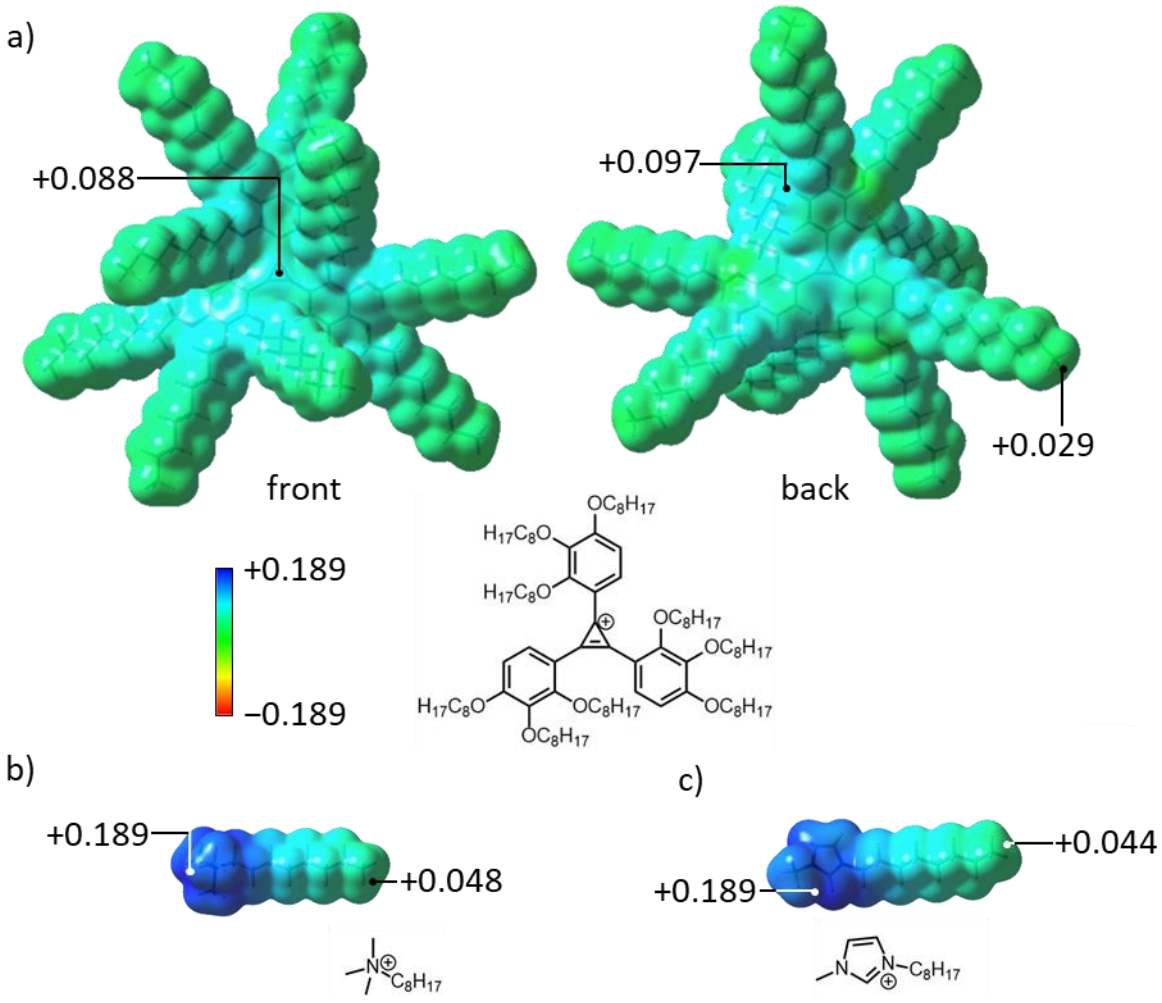

Figure 2.10: ESP maps of a) the front and back of the **DC8** cation, b) trimethyloctylammonium, and c) methyloctylimidazolium, showing the diffuse charge across the different cations.

The calculated potential at the centre of the cation showed little difference between the four cations studied (**DC1**, **DC2**, **DC4**, **DC8**). ESP maps of the larger cations show that the alkyl regions all had a positive electrostatic potential, though with higher charges closer to aromatic region (Figure 2.11). This suggests that the alkyl regions would be able to form interactions with the counter anions of the cyclopropenium molecules, rather than just the central aromatic regions.

X-ray Photoelectron Spectroscopy (XPS) measurements were performed to investigate the environments of the elements within the compounds at RT in the solid phase, particularly of the counter anions. The XPS **DC10**·Cl spectra show a single oxygen peak with a single oxygen environment. The XPS showed two distinct carbon peaks, which were assigned by comparison to Lomon *et al.* The sp^3 and sp^2 carbon environment peaks

merged together into a single large peak. The signals for carbon in an environment bonded to oxygen can still be identified as a separate peak at a higher binding energy.[20] The merger of the sp^3 and sp^2 peaks supports the ESP maps showing the high degree of delocalisation of charge out onto the alkyl chains and electron donation into the molecular centre by the lack of separation between the binding energies of the two environments.

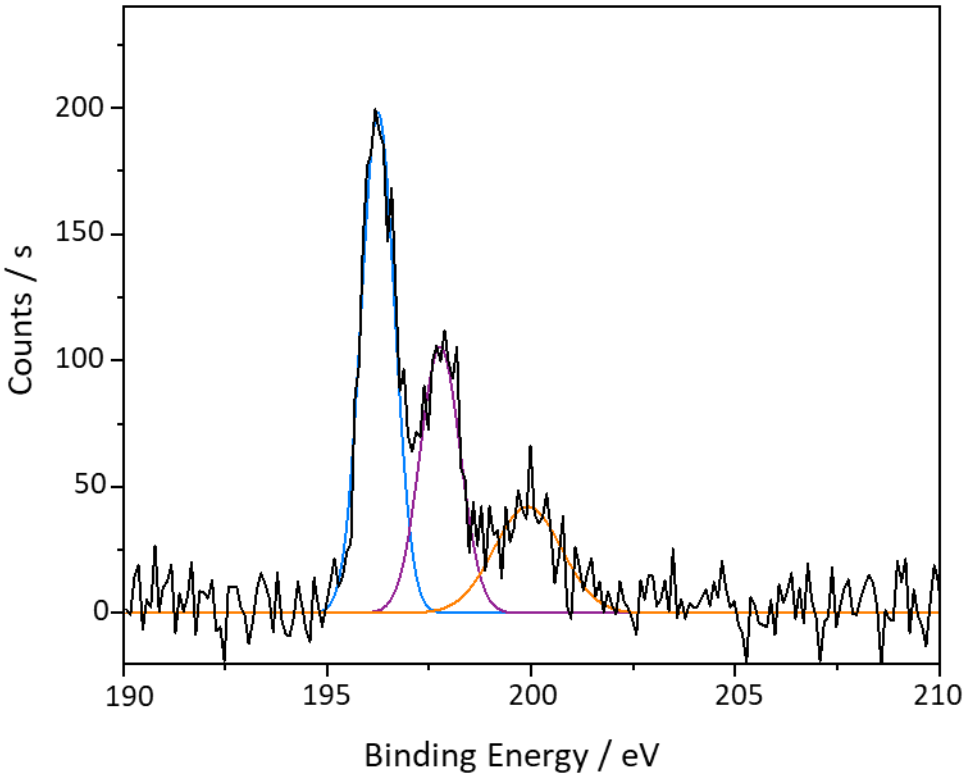

Figure 2.11: XPS spectra of chlorine 2p of **DC10**·Cl, showing three distinct environments with peak-fitting traces overlaid.

DC10·Cl has three distinct chloride peaks from the XPS, at binding energies of 196 eV, 198 eV and 200 eV. By comparison with similar ionic charged species, such as guanidinium chloride ionic liquids studied by Santos *et al*, the peaks at 196 eV and 198 eV correspond to free chloride ions within the solid cyclopropenium to $2p_{3/2}$ for the 196 eV peak and to $2p_{1/2}$ for the 198 eV (Figure 2.11), showing the presence of peak splitting in the free chloride ions.[21]

The smallest chloride peak at 200 eV shows the formation of a covalent interaction, rather than being an ionic species, as seen by Jian *et al*. The covalent environment may be from chlorine directly bonded to the cyclopropenium centre of the molecule.[22] The three chloride peaks had relative intensities of a 5:3:2 ratio, with the majority of the chloride

ions being in the environment of the two peaks corresponding to free chloride ions not bound to the cation. The conductivity is likely expected to arise from the free chloride ions, as they will have the highest mobility.

Cyclic voltammetry (CV) data of the cyclopropenium compounds shows an irreversible reduction that occurred between -1.1 and -1.3 V (Figure 2.12). The irreversible reduction shows that the cyclopropenium compounds do not have the electrochemical stability possessed by aminocyclopropenium species, lacking their reversible reduction or oxidation.[23]

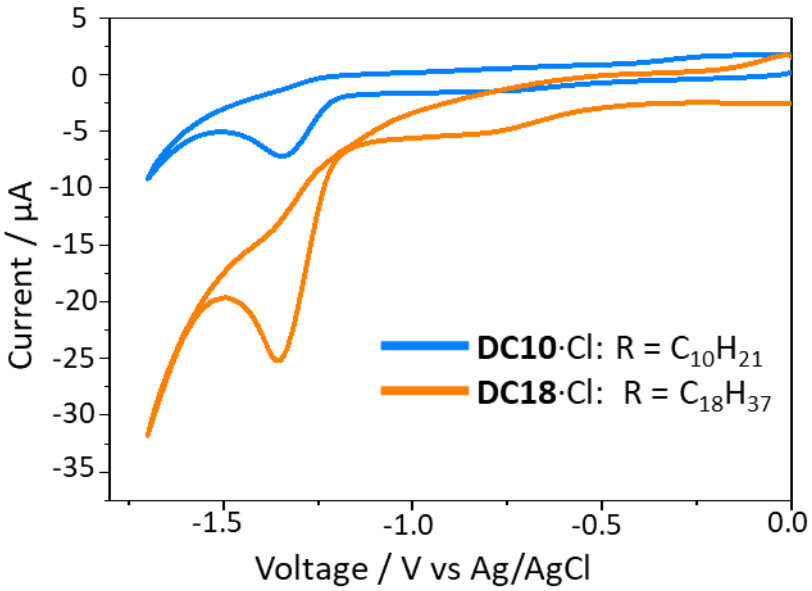

Figure 2.12: Cyclic voltammograms of **DC10**·Cl and **DC18**·Cl.

UV-vis spectroscopy was also performed for each of the liquid crystal cyclopropenium compounds (alongside non-mesogenic **DC1**·Cl), with each compound showing an onset of absorption occuring between 393 and 398 nm (Figure 2.13). The cyclopropenium compounds all showed little variation in either absorption onset or reduction potential with changes in the chain length or counter anion, as the cationic active region remained unchanged.

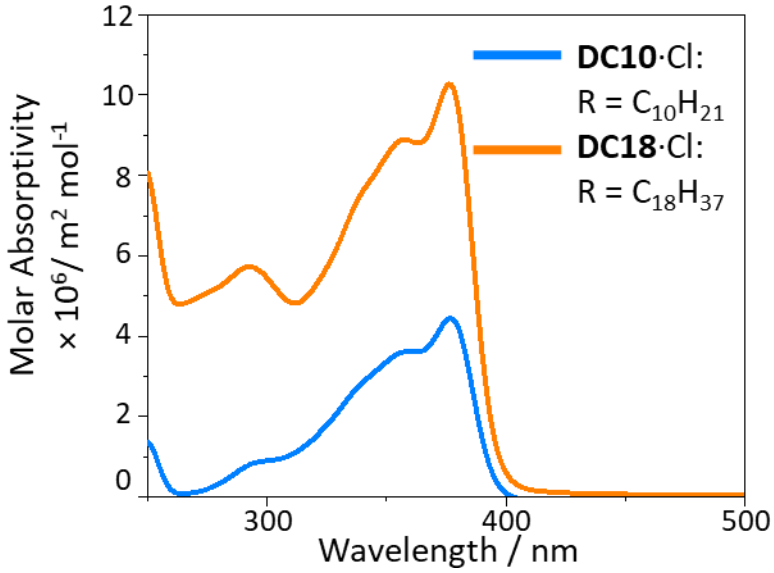

Figure 2.13: UV-vis spectra of **DC10**·Cl and **DC18**·Cl.

Using the UV-vis and CV measurements, the LUMO and LUMO-HOMO gap were calculated for each compound separately, along with an estimation of the HOMO energy (Table 2.5), using the methods documented by Leonat *et al.*[24]

Table 2.5 Reduction onset and onset of absorption for each cyclopropenium compounds **DC1-18**·Cl and **DC10-12**·Br derived from CV, and the estimated values LUMO and HOMO of the compound from this.

Compound	E_{red}^{onset} / V vs Ag/AgCl	E_{LUMO} / eV vs Ferrocene	λ_{onset} / nm	E_{gap} / eV	E_{HOMO} / eV
DC1·Cl	-1.16	-2.73	393	3.16	-5.89
DC8·Cl	-1.21	-2.68	396	3.14	-5.82
DC10·Cl	-1.20	-2.69	395	3.14	-5.83
DC12·Cl	-1.27	-2.62	398	3.12	-5.74
DC16·Cl	-1.28	-2.61	397	3.13	-5.74
DC18·Cl	-1.22	-2.67	396	3.14	-5.81
DC10·Br	-1.24	-2.65	393	3.16	-5.81
DC12·Br	-1.22	-2.67	398	3.12	-5.79

The energies of the LUMO and HOMO estimated by UV-vis and CV remained consistent for all materials, due to their identical electrochemically active region. No significant difference occurred on changing the counter ion to a bromide ion, due to electrochemical activity being concentrated on the cyclopropenium. The range of the HOMO and LUMO gap is commonly used to assign the stability range of electrolytes, which in turn determines the electrodes that can be used. Though the cyclopropenium mesogens have lower reductive potentials than liquid electrolytes (around 1.3 V for organic electrolytes),

allowing for lower reduction potentials to be accessed, the irreversible reduction of the cyclopropeniums means they have lower stabilities than other electrolytes, showing they are limited as electrolytes due to lacking long-term stability.[25, 26]

2.2.3 Dielectric Measurements

Dielectric measurements were performed on the mesogenic materials (as well as ionic liquid **DC6,2**·Cl) to study their conductive properties, comparing the impacts of the different phases on their electronic properties. The compounds were heated to the isotropic phase and added to pre-assembled indium tin oxide (ITO) coated glass cells by the mechanism of capillary action, using a series of guard ring cells (Figure 2.14).

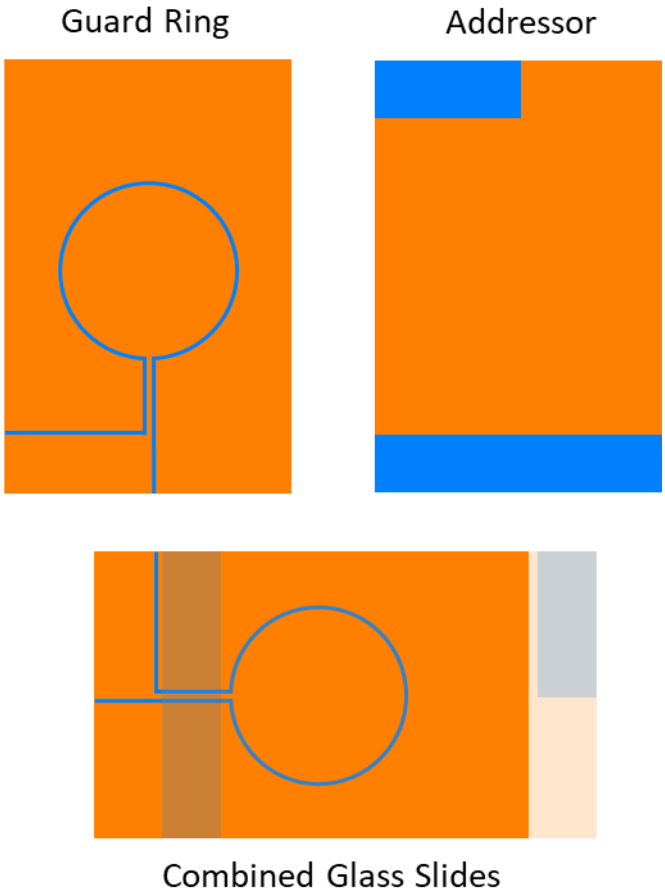

Figure 2.14: Schematic of the ITO pattern used for guard ring LC cells. The left-hand side shows the guard ring substrate and the right-hand side shows the addressor substrate. The bottom image shows the combined slides, with the two sides not fully overlapping with sections of each side exposed to allow for connections to a circuit to be applied. The orange regions represent areas coated in ITO, while blue is free from ITO.

The cyclopropenium compounds self-assembled in the guard ring cells into a homeotropic alignment, confirmed by the lack of birefringence in the POM images at the

liquid crystal phase of guard ring cells (Figure 2.15). This is in contrast to images of the materials taken outside of confined glass cells where birefringence textures were readily seen.[27] The homeotropic alignment was maintained during the dielectric measurements.

Figure 2.15: Image of **DC10**·Br taken under polarised microscope under dielectric measurement. No birefringence of the material can be seen while measurements were taken.

Dielectric measurements of the compounds were performed over a range of frequency and temperatures, cooling from the isotropic phase and measuring across the frequency range at each temperature for each compound. The materials showed a fall in real and imaginary permittivity with increased frequency, the real permittivity reaching a plateau at higher frequencies (Figure 2.16).

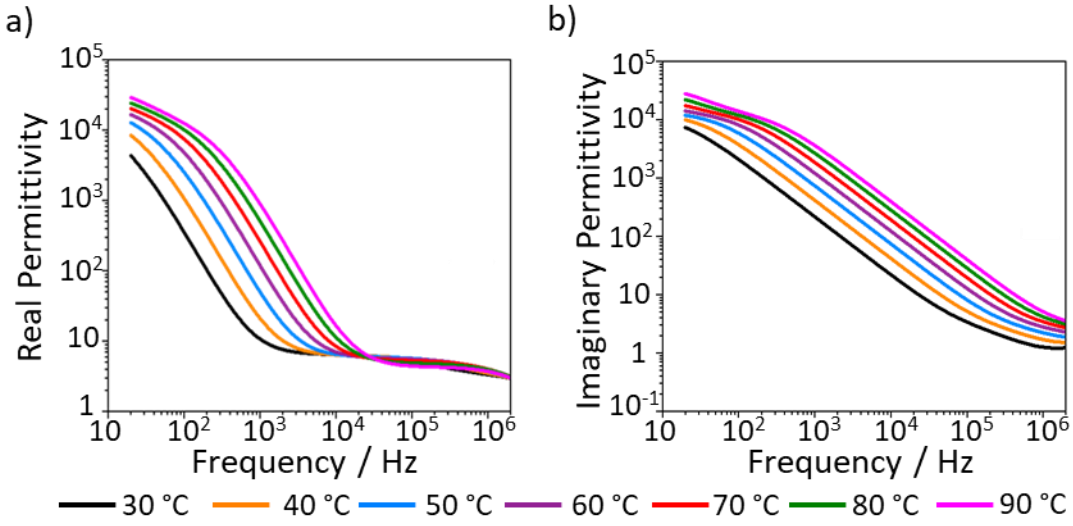

Figure 2.16: Graphs of a) real permittivity and b) imaginary permittivity against frequency for **DC10**·Cl over a range of temperatures.

The conductance also varied with a change in frequency, with the conductance rising to a plateau region of steady conductance. This plateau region, where conductivity is independent of the frequency, corresponds to the dc conductivity.[28] As the frequency increases further, dipole reorientation mechanisms of charge transfer become available as well as the movement of ionic species, and so the conductance begins to rise again with frequency.[29]

Taking the conductivity from between the plateau region (between 10^3 and 10^4 Hz) of the conductance curves, by calculating conductivity from the conductance and the surface area and thickness of the guard ring cells, the trend of conductivity against temperature for each cyclopropenium mesogen (and ionic liquid **DC6,2·**Cl) could be observed (Figure 2.17).

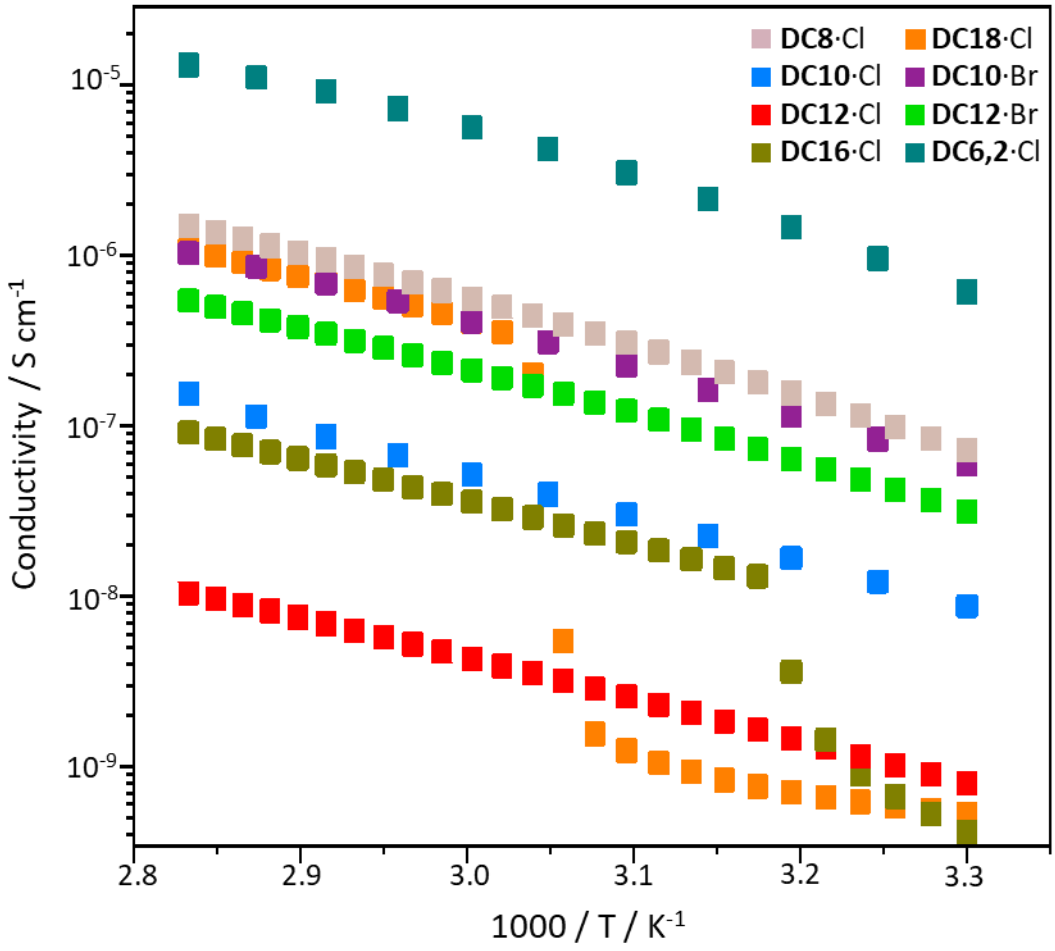

Figure 2.17: A graph of conductivity against temperature for cyclopropenium materials in guard ring cells at 10^3 Hz.

For all the hexagonal columnar materials (**DC8**·Cl, **DC10**·Cl, **DC12**·Cl, **DC10**·Br and **DC12**·Br), the trends of conductivity against temperature are unchanged over the whole temperature range – there is continuous variation with temperature over the liquid, liquid crystal and solid phases. **DC12**·Cl was measured down to -10 ºC, and the same conductivity trend that was observed for the 80-30 ºC region was seen to persist into the negative degree temperatures (Figure 2.37, Appendix 2.6.3). The ionic conductivity persists across the two phase transitions of each compound. The free chloride ions that are identified by XPS in **DC10**·Cl at RT show that ions should be able to move freely in the solid phase, supporting the conductivity being preserved at low temperatures.

For the rectangular columnar cyclopropenium compounds **DC16**·Cl and **DC18**·Cl, upon undergoing the transition from liquid through liquid crystal and then to the solid phase, the conductivity falls off dramatically. Note that the phase transitions are shifted by a few degrees relative to those observed by DSC, which can be ascribed to the changes to the phase transition from being constrained in the glass cell as well as the slower cooling rate.

The effect on conductivity matches the effects observed for the real and imaginary permittivity on changing temperature. For the hexagonal columnar compounds, the permittivity of the curves undergoes a small change with temperature and are not affected by the phase transition of the cyclopropenium compounds. **DC16**·Cl and **DC18**·Cl instead undergo a fall in permittivity with these phase transitions (Figure 2.18).

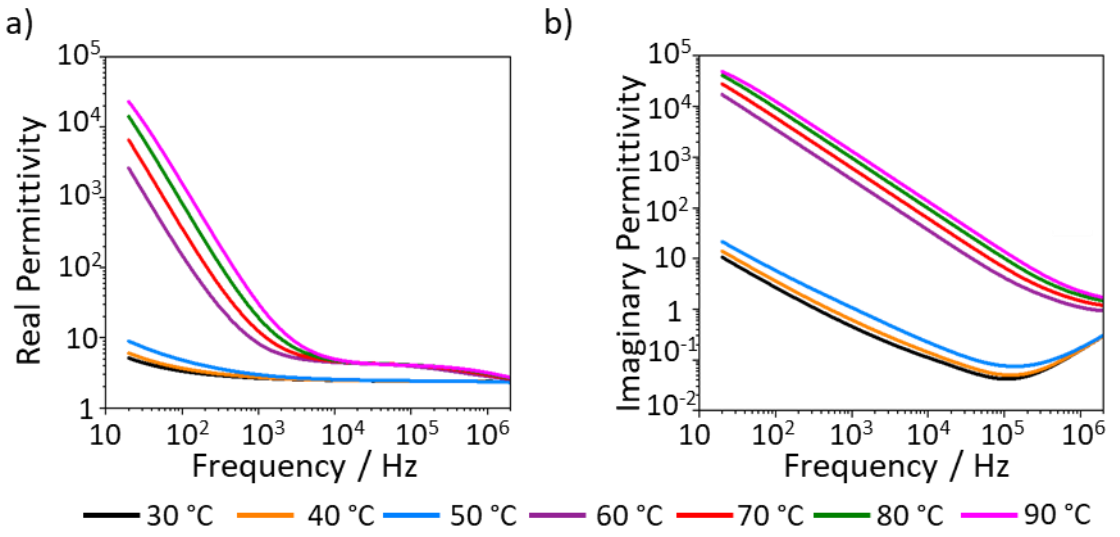

Figure 2.18: Graphs of a) real permittivity and b) imaginary permittivity against frequency for **DC18**·Cl over a range of temperatures, showing a drop in permittivity on a phase transition.

The consistent conductivity through all three phases of the hexagonal materials can be rationalised due to the chloride ions being able to move freely through the alkyl chain regions in the solid phase. The diffuse charge seen by ESP maps shows that the counter anion would be able to interact with the alkyl chains, particularly close to the central aromatic region, and so implies that counter anion movement through these regions is important for their conductivity.

The difference between the hexagonal and rectangular columnar compounds might be explained by the different alkyl chain behaviour in the solid phase. RT measurement of the XRD of the **DC10** and **DC12** show a degree of alkyl chain fluidity in the solid phase, while XRD measurement of the **DC18**·Cl shows no fluidity. Therefore, the greater alkyl chain fluidity in the smaller compounds would allow for ion transport though the alkyl chain region to continue effectively in the solid phase, by the movement of free counter ions identified by XPS in **DC10**·Cl. Meanwhile the loss of conductivity in the larger compounds at low temperature can be explained by the reduced alkyl chain fluidity in the solid phase, meaning the fall in conductivity on cooling for **DC16**·Cl and **DC18**·Cl may be attributed to a transition to the solid phase. The columnar structure and fluidity granted by the mesogen phase are seen as necessary for the conductivity in the solid phase.

All compounds showed Arrhenius behaviour[30] in the liquid phase, with the exception of the **DC6,2**·Cl, and the hexagonal columnar materials showed Arrhenius behaviour continuing throughout the whole temperature range. This meant that the activation enthalpy of the charge transfer could be calculated in each case (Table 2.6).

Table 2.6: The conductivity at 30 °C and activation enthalpy of charge transfer calculated for each compound from the dielectric spectroscopy.

Compound	**Conductivity at 30 °C / S cm^{-1}**	**Regions Of Arrhenius Behaviour**	**E_a/ eV**
DC8·Cl	7.18×10^{-8}	Full Temperature Range	0.54
DC10·Cl	8.76×10^{-9}	Full Temperature Range	0.52
DC12·Cl	7.95×10^{-10}	Full Temperature Range	0.49
DC16·Cl	4.16×10^{-10}	≥ 42 °C	0.48
DC18·Cl	5.25×10^{-10}	≥ 58 °C	0.46
DC10·Br	6.01×10^{-8}	Full Temperature Range	0.54
DC12·Br	3.15×10^{-8}	Full Temperature Range	0.51
DC6,2·Cl	6.11×10^{-7}	N/A	N/A

For the hexagonal columnar materials, the conductivity decreased with a decrease in the alkyl chain length (Table 2.6), with the highest conductivity being for **DC8**·Cl and the lowest being held by **DC12**·Cl. This is rationalised by the materials possessing a higher density of charged species as the proportion of the compound made up of the alkyl chains decreases. However, this trend is not seen to continue with rectangular columnar **DC16**·Cl and **DC18**·Cl.

Both the **DC10** and **DC12** cyclopropeniums show an increase in conductivity with bromide ions. This can be explained by the fact that the bromide is a more weakly coordinating counter anion than the chloride, and thus would be less tightly bound to the cyclopropenium and so more able to undergo charge transport.

The ionic liquid **DC6,2**·Cl, which had only a liquid phase over the measured temperature range, showed a higher conductivity than all of the liquid crystal materials, even where all materials were in the liquid phase. This might be attributed to the shorter radii of the branched cation (compared to **DC8**·Cl, which has the same molecular weight as the **DC6,2**·Cl), giving a greater density of chloride in the material.

The liquid crystals developed show an extremely wide range of conductivity compared to similar systems, with the properties of the liquid crystal phase persisting into the solid phase that make them of potential as conductive materials able to operate at much lower temperatures than other conductive mesogens, while still having their ready processibility by being stable on heating and cooling to and from the isotropic phase. However, the conductivity of the liquid crystals is low, with the highest 30 ºC conductivity limited to below 10^{-7} S cm^{-1}, equivalent to previously developed carbonate derived liquid crystals. This is significantly lower than the required 10^{-2}-10^{-3} S cm^{-1} for viable electrolytes. It is also lower than conductivity achieved for other conductive liquid crystals, such as the first developed ionic liquid crystal electrolyte by Sakuda eta al, as well further improved mesogen electrolyte systems that have come since with polyether groups within alkyl chains, which have reached 10^{-3}-10^{-4} S cm^{-1}.[31, 32, 33, 34] Improving the conductivity of the cyclopropenium compounds is important to match other mesogens that have been developed for electrolytes.

2.2.4 Anisotropy Measurements

The mesogen anisotropy was tested by dielectric spectroscopy using glass cells in which the ITO electrodes were placed perpendicular to the alignment of the columns. These in-plane cells were prepared with a specific design to ensure a flow of current that was perpendicular to the alignment of the homeotropic columnar structures (Figure 2.19).

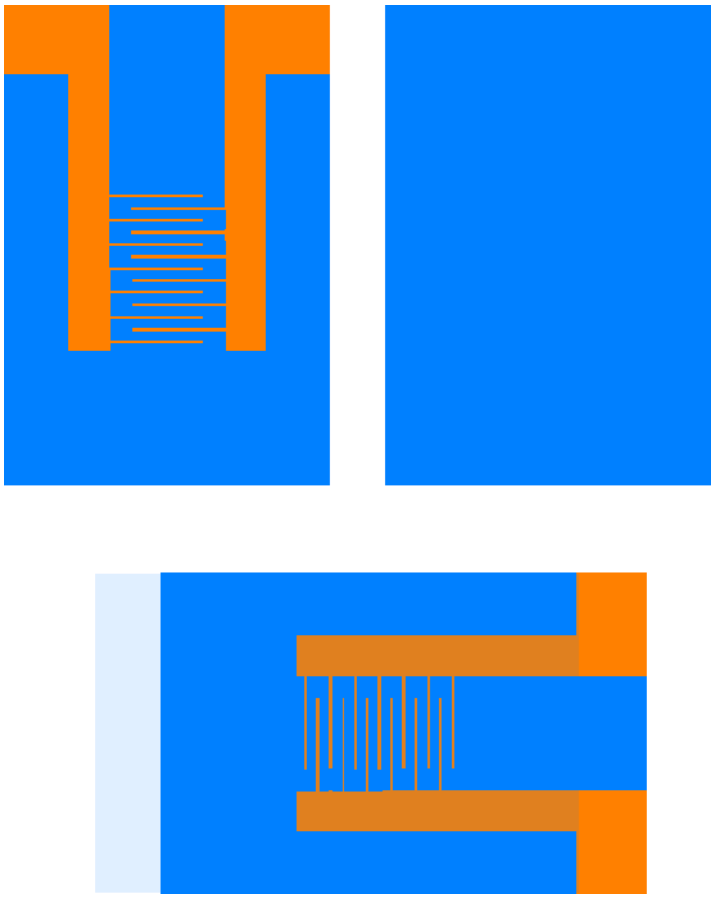

Figure 2.19: Schematic of the ITO pattern used for the in-plane electrode LC cells. The separate slides are shown in left and right, and the bottom image shows the combined glass slides, with areas on each side exposed. The orange regions represents the areas coated in ITO, and the blue regions those free from ITO.

The homeotropic alignment was confirmed by POM images of materials in the in-plane cells showing no birefringence. **DC10**·Cl and **DC18**·Cl were measured to observe the conductive anisotropy of the two columnar phases (Figure 2.20). Conductivity could not be calculated directly from the dielectric spectroscopy, due to no defined contact surface area or cell gap distance. Instead, it was assumed that the conductivities in the isotropic phase would be identical to the measurements of the guard ring cells, to find a conversion factor to calculate the conductivity for the other phases.

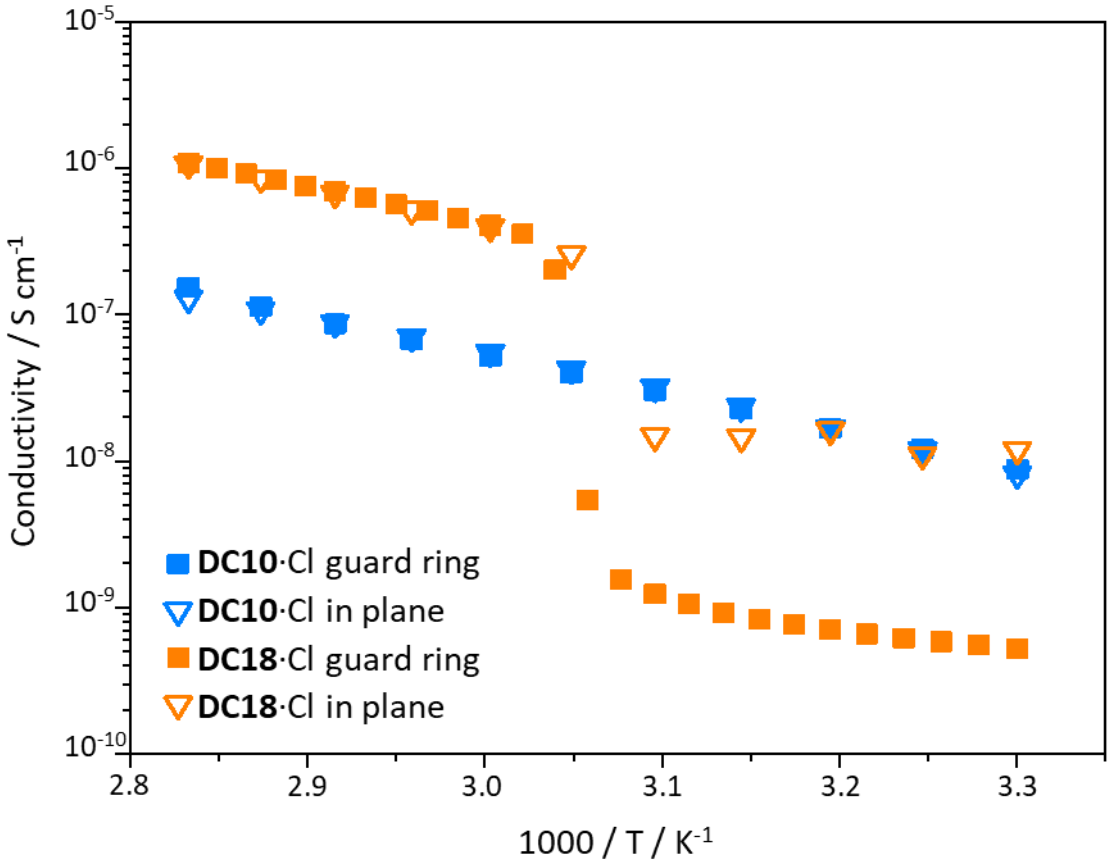

Figure 2.20: The comparisons of the guard ring and in plane estimated conductivities.

For the hexagonal columnar **DC10**·Cl, no anisotropy was observed in any phases. For the rectangular columnar **DC18**·Cl, anisotropy appeared as it transitioned from the liquid phase to liquid crystal and then to the solid phase, with the conductivity perpendicular to the plane of the column alignment being higher than the conductivity parallel to the plane. The lack of anisotropy supports the indication that the counter ions conduct by movement through the alkyl regions, as previously suggested by the differences in the XRD of the solid phase between the larger and smaller compounds. Anisotropic behaviour would be expected if the ion transport were constrained by the columns (Figure 2.21), so the isotropic conductivity implies the alkyl chain fluidity allows for the ion conductivity, giving liquid-like conductivity in the mesogen and solid phases which explains both the lack of change of conductivity on phase transition and the isotropic conductivity. For **DC18**·Cl, anisotropy emerges at lower temperatures favouring ion transport in directions perpendicular to the alignment of the columns, which might be explained by the formation of ion channels perpendicular to the previous homeotropic column alignment, as the more ordered chains may mean it is easier for ions to move between columns than along them.

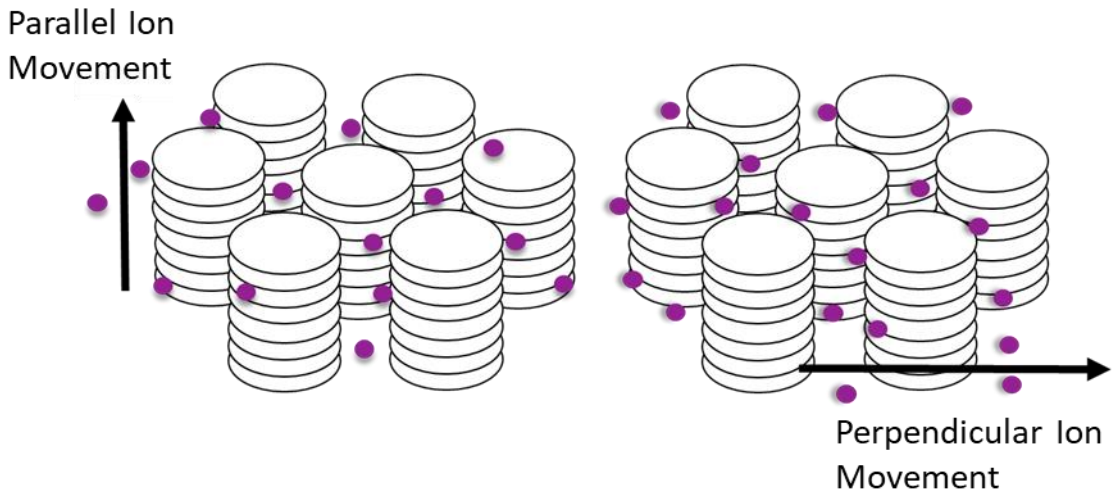

Figure 2.21: A representation of the movement of ions independent of the alignment of the columns.

2.2.5 Lithium Doped Materials

One approach to try to increase the conductivity of the cyclopropenium compounds was to dope them with salts, as an attempt to increase the charge carrier density, and in turn show their potential as materials for electrolytes in lithium batteries. **DC10**·Br was doped with lithium salt LiBr at 10 mol% loading. LiBr was chosen to match **DC10**·Br's counter ion. The **DC10**·Br doped with LiBr was studied by DSC, which showed no significant change in the phase behaviour (Figure 2.22).

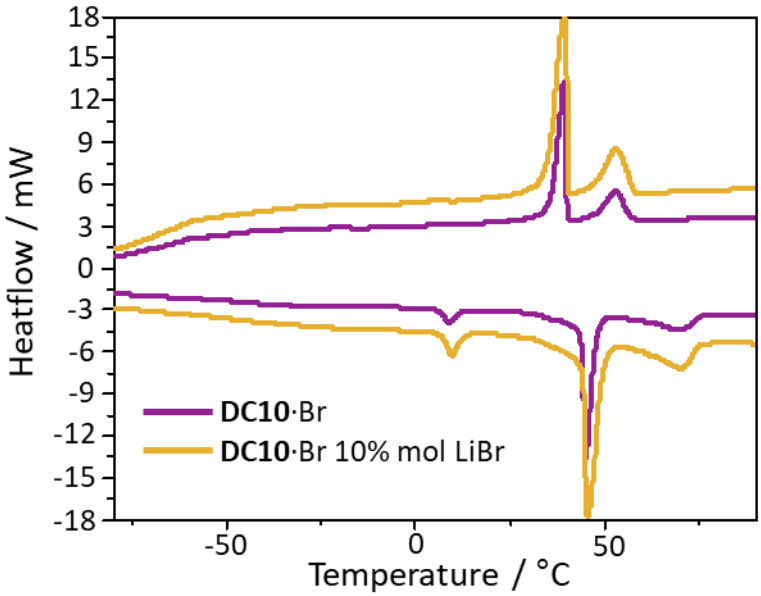

Figure 2.22: The DSC of **DC10**·Br of the undoped and doped with 10% mol LiBr materials.

The dielectric studies of the doped sample, compared to the undoped sample, showed a reduction in the conductivity on the addition of the LiBr (Figure 2.23).

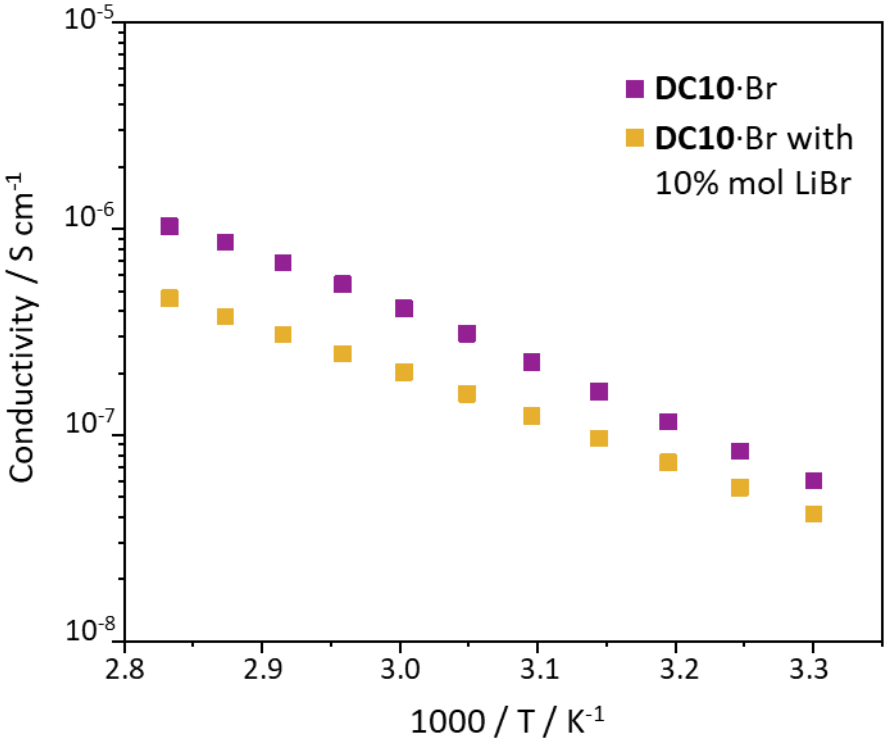

Figure 2.23: The conductivity against temperature of two **DC10**·Br samples, of the undoped and doped with 10% mol LiBr materials.

The addition of the LiBr both showed a reduced conductivity. The reduction in conductivity from adding additional ion carriers can be explained by an instability of the LiBr mixture with the cyclopropenium. When measuring with glass cells that possessed thin cell gaps, the undoped samples were seen to consistently short while the LiBr doped samples showed no shorting. This may arise from the additional ions assembling as layers of ions at the electrodes, acting as an insulating protective layer which prevents this shorting. Given the disruption in the flow of ions from the addition of the lithium salts, it seems that LiBr doping is not effective as a means of improving the conductivity of these compounds. This can be compared to other liquid crystal electrolytes, which show significant conductivity by the doping of liquid crystal phases with lithium ions.[31] The materials developed here require improvement to be able to form a stable phase with lithium ions, so they might be used as electrolytes, and to enable them to have their conductivity bolstered by dopants as can be done for other liquid crystal electrolytes, which is currently not possible for these materials.

2.3 Conclusions

In summary, a new structure for ionic discotic liquid crystals based on symmetrical cyclopropenium cores was developed. The cyclopropenium liquid crystals were studied using a range of different analytical techniques, confirming the presence of columnar liquid crystalline structures and with properties heavily dependent on the length of alkyl chain side groups, showing hexagonal and rectangular columnar phases. The dielectric spectroscopy of these materials was investigated, which demonstrated that the conductivity was independent of the phase for the hexagonal columnar materials. The conductivity was maintained across three phases of matter due to the freedom of movement through the alkyl regions which retain fluidity into the solid phase due to the structure given by the liquid crystal phases, and the halide ions being unconstrained by the cationic sites due to the highly-diffuse nature of charge within the triaryl cyclopropenium centres. Perpendicular studies showed that it was also independent of the phase alignment. The lack of anisotropy is unusual for columnar materials, and makes these compounds of interest for use in devices where the strict alignment of liquid crystals is very difficult. While the materials are currently limited by their low room temperature conductivity compared to similar ionic liquid crystal materials, their unique ion movement retention across phase transitions shows their potential in which they might be developed as a new series of functional conductive mesogenic materials.

2.4 Future Work

Future work should continue to evaluate the effectiveness of the cyclopropenium compounds as functional materials in batteries, by beginning with their effectiveness and stability as electrolytes by linear sweep voltammetry. Further work should continue with investigations of methods to optimise their properties, in particular looking at ways to increase their conductivity in order to take advantage of their lack of limitation by phase behaviour. Methods may include looking at the use of salts that may integrate better with the cyclopropenium compounds, such as smaller lithium chloride. Another potential route to enhance the materials is to alter the alkyl chains to enable improved mixing of lithium salts in the cyclopropenium mesogens phase, such as the inclusion of glycol ethers[35] in the alkyl region, as has been performed for other similar liquid crystal electrolytes,[36] to help improve their ability to transport charge through the material.

2.5 Experimental Methods

2.5.1 Specific Experimental Methods

Instrumentation and Analytical Techniques: TGA (Thermogravimetric Analysis) was performed using a PerkinElmer Pyris 1 TGA. DSC (Differential Scanning Calorimetry) was performed using a PerkinElmer DSC 8500. Microscope images were recorded with an Olympus CX50 microscope at ×10 magnification using a Linkam LTS420 heating mantle to heat the sample while being imaged. An X Series 2 ICP-MS was used for trace aluminium and trace silver detection. Dielectric measurements were performed using an Agilent E4980A dielectric bridge, with measurements taken at intervals of 2 °C or 5 °C while cooling with a 5 min stabilisation time at each discrete temperature. SAXD (Small-Angle X-ray Diffraction) and WAXD (Wide-Angle X-ray Diffraction) measurements were taken using a Siemens Kristalloflex 760H with a Vantec 500 detector from Bruker. FTIR measurements were taken with a PerkinElmer Frontier FTIR spectrometer equipped with a Specac Quest ATR accessory with extended range diamond puck. XPS measurements were performed with a Thermo Scientific K-Alpha X-Ray Photoelectron Spectrometer System. An X Series 2 ICP-MS was used for trace aluminium and trace silver detection. Fourier transform infrared (FTIR) spectroscopy measurements were taken with a PerkinElmer Frontier FTIR spectrometer equipped with a Specac Quest ATR accessory with extended range diamond puck.

2.5.2 Synthetic Procedures

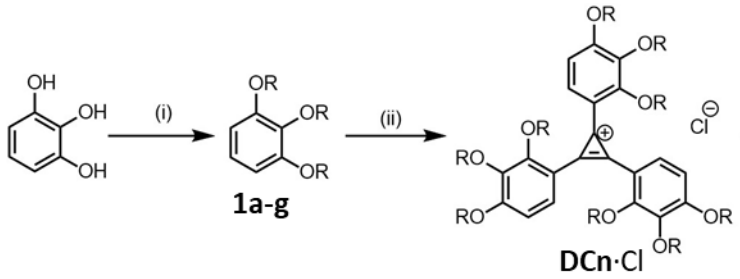

Scheme 2.4: Synthetic route used to prepare the cyclopropenium salts. R is an alkyl group in each case. Reagents and conditions: (i) R-Br, K_2CO_3, KI, 18-crown-6, Me_2CO, reflux, 15 h, 26–79%; (ii) 1). C_3Cl_4, $AlCl_3$, $CHCl_3$, 80 °C, 1 h; 2). $CHCl_3$, 0 °C, 1 h; 3). $CHCl_3$, 50 °C, 16 h, 30–81%.

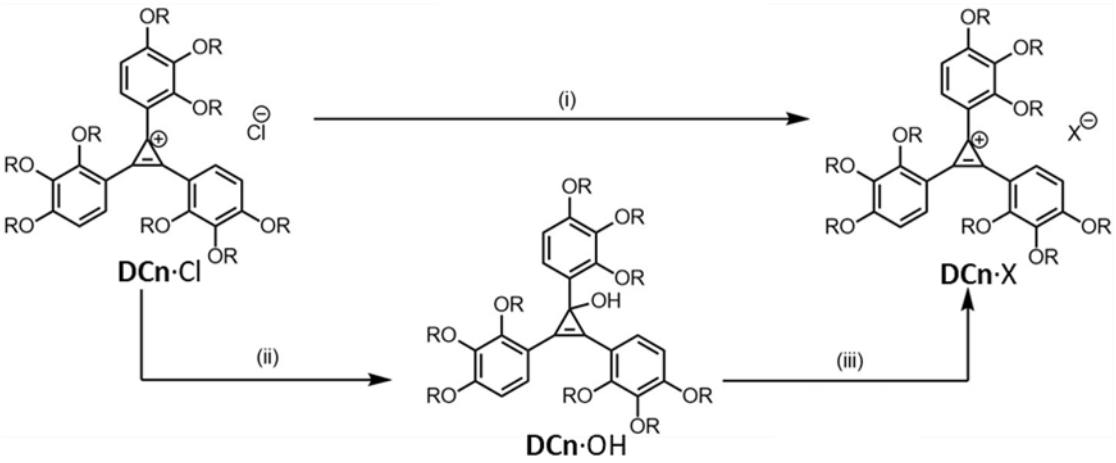

Scheme 2.5: Synthetic route used to undergo ion exchange of the cyclopropenium salts. R is an alkyl group in each case. Reagents and conditions: (i) **DCn**·Cl, AgX, CH_2Cl_2, MeCN, RT, 15 min, 55-91%; (ii) **DCn**·Cl, NaOAc, H_2O, CH_2Cl_2, RT; (iii) CH_2Cl_2, HX, H_2O, RT, 12-85% over two steps.

*Synthesis of 1,2,3-Tri(alkyloxy)benzene (**1**)*

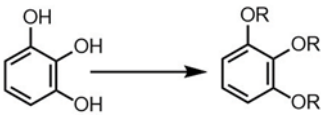

General procedure: Pyrogallol (20.0 mmol, 1 equiv.), K_2CO_3 (202 mmol, 10 equiv.), KI (6.06 mmol, 0.3 equiv.) and 18-crown-6 (0.8 mmol, 0.04 equiv.) were added into a 500 ml round bottom flask and dissolved in $(CH_3)_2CO$ (160 mL). The reaction mixture was stirred for 5 min, followed by the addition of the desired bromoalkane (90.0 mmol, 4.5 equiv.) and the reaction mixture was refluxed for 16 h. The mixture was then either allowed to cool to RT, or hexanes was added (100 mL), before filtering under vacuum to remove solids. The solvent was then removed under reduced pressure to yield a crude solid. The crude solid was dissolved in hexanes (50 mL) and washed with a saturated aqueous solution of NH_4Cl (30 mL), before being dried over $MgSO_4$, filtered, and evaporated to dryness. The crude product was then purified by either column chromatography (Teledyne Isco Combiflash Rf+ system, 40 g SiO_2, hexanes/EtOAc gradient elution [1:0 to 0:1]) or triturated with hot Me_2CO (3 × 50 mL), filtered and the combined organic phases concentrated under reduced pressure to yield the pure desired product.

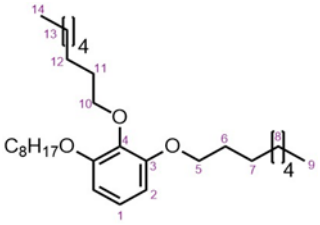

1,2,3-Tri(*n*-octyloxy)benzene (1b). The product was obtained from pyrogallol (2.40 g, 20.0 mmol) and 1-bromooctane (15.5 mL, 90.0 mmol) after filtering in acetone and purification by column chromatography as an orange liquid (6.55 g, 15.9 mmol, 79% yield). **^{1}H NMR** (600 MHz, $CDCl_3$) δ 6.90 (t, J = 8.3 Hz, 1H, H_1), 6.54 (d, J = 8.3 Hz, 2H, H_2), 3.99 – 3.94 (m, 6H, H_5/H_{10}), 1.83– 1.78 (m, 4H, H_6), 1.77 – 1.73 (m, 2H, H_{11}) 1.51 – 1.44 (m, 6H, H_7/H_{12}), 1.37 – 1.26 (m, 24H, H_8/H_{13}), 0.89 (t, J = 6.8 Hz, 9H, H_9/H_{14}). **^{13}C NMR** (151 MHz, $CDCl_3$) δ 153.5 (C_3), 138.6 (C_4), 123.2 (C_1), 107.0 (C_2), 73.5 (C_{10}), 69.3 (C_5), 32.1 (alkyl-C), 32.0 (alkyl-C), 30.5 (C_{11}), 29.7 (alkyl-C), 29.6 (alkyl-C), 29.5 (alkyl-C), 29.4 (alkyl-C), 26.3 (alkyl-C), 26.3 (alkyl-C), 22.8 (alkyl-C), 22.8 (alkyl-C), 14.2 (C_{14}), 14.2 (C_9). **HRMS-ASAP** *m/z* = 462.4076 $[M]^+$, calculated for $C_{30}H_{54}O_3$ = 462.4073.

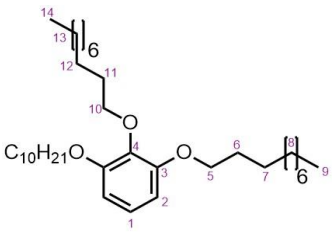

1,2,3-Tri(*n*-decyloxy)benzene (1c). The product was obtained from pyrogallol (2.40 g, 20.0 mmol) and 1-bromodecane (18.7 mL, 90.0 mmol) after filtering in acetone and purification by column chromatography as an off-white solid (8.51 g, 15.9 mmol, 79% yield). **M.P.** 18 – 19 °C. **^{1}H NMR** (600 MHz, $CDCl_3$) δ 6.90 (t, J = 8.3 Hz, 1H, H_1), 6.55 (d, J = 8.3 Hz, 2H, H_2), 4.00 – 3.95 (m, 6H, H_5/H_{10}), 1.84- 1.79 (m, 4H, H_6), 1.79 - 1.74 (m, 2H, H_{11}), 1.52 – 1.45 (m, 6H, H_7/H_{12}), 1.37 – 1.24 (m, 36H, H_8/H_{13}), 0.90 (t, J = 6.9 Hz, 9H, H_9/H_{14}).**^{13}C NMR** (151 MHz, $CDCl_3$) δ 153.6 (C_3), 138.6 (C_4), 123.2 (C_1), 106.9 (C_2), 73.5 (C_{10}), 69.2 (C_5), 32.1 (alkyl-C), 32.1 (alkyl-C), 30.5 (C_{11}), 29.9 (alkyl-C), 29.8 (alkyl-C), 29.8 (alkyl-C), 29.8 (alkyl-C), 29.7 (alkyl-C), 29.6 (alkyl-C), 29.6 (alkyl-C), 29.6 (alkyl-C), 29.5 (alkyl-C), 26.3 (alkyl C), 26.3 (C_7/C_{12}), 22.8 (alkyl-C), 22.8 (alkyl-C), 14.2 (C_9/C_{14}). **HRMS-ASAP** *m/z* = 546.4995 $[M]^+$, calculated for $C_{36}H_{66}O_3$ = 546.5012.

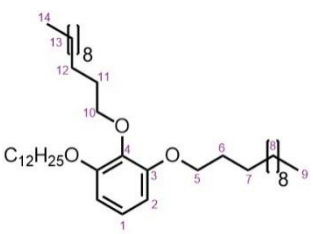

1,2,3-Tri(*n*-dodecyloxy)benzene (1d). The product was obtained from pyrogallol (2.40 g, 20.0 mmol) and 1-bromododecane (22.0 mL, 90.0 mmol) after filtering in acetone and hexanes and purification by trituration as an off-white solid (8.89 g, 14.1 mmol, 74% yield). **M.P.** 38 – 39 °C. **^{1}H NMR** (600 MHz, $CDCl_3$) δ 6.90 (t, J = 8.3 Hz, 1H, H_1), 6.54 (d, J = 8.3

Hz, 2H, H_2), 3.98 – 3.93 (m, 6H, H_5/H_{10}), 1.82 – 1.77 (m, 4H, H_6), 1.76 - 1.72 (m, 2H, H_{11}), 1.50 – 1.43 (m, 6H, H_7/H_{12}), 1.35 – 1.24 (m, 48H, H_8/H_{13}), 0.88 (t, *J* = 6.9 Hz, 9H, H_9/H_{14}). **^{13}C NMR** (151 MHz, $CDCl_3$) δ 153.6 (C_3), 138.6 (C_4), 123.2 (C_1), 107.0 (C_2), 73.5 (C_{10}), 69.2 (C_5), 32.1 (alkyl-C), 32.1 (alkyl-C), 30.5 (C_{11}), 29.9 (alkyl-C), 29.9 (alkyl-C), 29.8 (alkyl-C), 29.8 (alkyl-C), 29.8 (alkyl-C), 29.8 (alkyl-C), 29.6 (alkyl-C), 29.6 (Alkyl-C), 29.5 (alkyl-C), 29.5 (alkyl-C), 26.3 (alkyl-C), 26.2 (alkyl-C), 22.8 (alkyl-C), 14.3 (C_9/C_{14}). **HRMS-ASAP** *m/z* = 630.5962 $[M]^+$, calculated for $C_{42}H_{78}O_3$ = 630.5951.

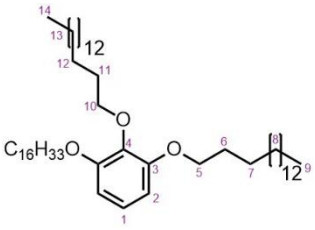

1,2,3-Tri(*n*-hexadecyloxy)benzene (1e). The product was obtained from pyrogallol (2.40 g, 20.0 mmol), and 1-bromohexadecane (27 mL, 90.0 mmol) after filtering in acetone and hexanes and purification by trituration as an off-white solid (10.69 g, 11.9 mmol, 63% yield). **M.P.** 55 – 57 °C. **^{1}H NMR** (600 MHz, $CDCl_3$) δ 6.90 (t, *J* = 8.3 Hz, 1H, H_1), 6.54 (d, *J* = 8.3 Hz, 2H, H_2), 3.98 – 3.93 (m, 6H, H_5/H_{10}), 1.82 – 1.76 (m, 4H, H_6), 1.76 – 1.71 (m, 2H, H_{11}), 1.51 – 1.41 (m, 6H, H_7/H_{12}), 1.37 – 1.21 (m, 72H, H_8/H_{13}), 0.88 (t, *J* = 6.9 Hz, 9H, H_9/H_{14}). **^{13}C NMR** (151 MHz, $CDCl_3$) δ 153.6 (C_3), 138.6 (C_4), 123.2 (C_1), 107.0 (C_2), 73.5 (C_{10}), 69.2 (C_5), 32.1 (alkyl-C), 30.5 (C_{11}), 29.9 (alkyl-C), 29.9 (alkyl-C), 29.8 (alkyl-C), 29.8 (alkyl-C), 29.6 (alkyl-C), 29.6 (alkyl-C), 29.5 (alkyl-C), 26.3 (alkyl-C), 26.3 (alkyl-C), 22.8 (alkyl-C), 14.3 (C_9/C_{14}). **HRMS-ASAP** *m/z* = 798.7825 $[M]^+$, calculated for $C_{30}H_{54}O_3$ = 798.7829.

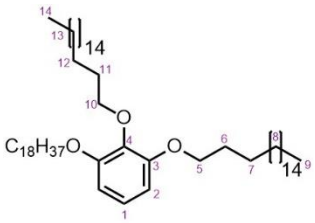

1,2,3-Tri(*n*-octadecyloxy)benzene (1f). The product was obtained from pyrogallol (1.09 g, 8.64 mmol), and 1-bromooctodecane (15.1 mL, 44.4 mmol) after filtering in acetone and hexanes and purification by trituration as an off-white solid (5.58 g, 6.32 mmol, 73% yield). **M.P.**: 55 – 57 °C. **^{1}H NMR** (600 MHz, $CDCl_3$) δ 6.90 (t, *J* = 8.3 Hz, 1H, H_1), 6.54 (d, *J* = 8.3 Hz, 2H, H_2), 3.98 – 3.92 (m, 6H, H_5/H_{10}), 1.82 – 1.76 (m, 4H, H_6), 1.76 – 1.71 (m, 2H, H_{11}), 1.50 – 1.43 (m, 6H, H_7/H_{12}), 1.37 – 1.32 (m, 6H, H_8/H_{13}), 1.31 – 1.22 (m, 78H, H_8/H_{13}), 0.88 (t, *J* = 6.9 Hz, 9H, H_9/H_{14}). **^{13}C NMR** (151 MHz, $CDCl_3$) δ 153.6 (C_3), 138.6 (C_4), 123.2 (C_1), 107.0 (C_2), 73.5 (C_{10}), 69.3 (C_5), 32.1 (alkyl-C), 30.5 (C_{11}), 29.9 (alkyl-C), 29.9 (alkyl-C), 29.9 (alkyl-C), 29.9 (alkyl-C), 29.8 (alkyl-C), 29.8 (alkyl-C),

29.8 (alkyl-C), 29.8 (alkyl-C), 29.6 (alkyl-C), 29.6 (alkyl-C), 29.5 (alkyl-C), 26.3 (alkyl-C), 26.3 (alkyl-C), 22.9 (alkyl-C), 14.3 (C_9/C_{14}). **HRMS-ASAP** *m/z* = 882.8763 $[M]^+$, calculated for $C_{60}H_{114}O_3$ = 882.8768.

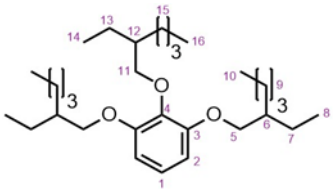

1,2,3-Tri(2-ethylhexyloxy)benzene (1g). The product was obtained from pyrogallol (2.40 g, 20.0 mmol), and 1-bromo-2-ethylhexane (16 mL, 90.0 mmol) after filtering in acetone and purification by column chromatography as a colourless liquid (4.18 g, 9.03 mmol, 45% yield). **^{1}H NMR** (599 MHz, $CDCl_3$) δ 6.90 (t, *J* = 8.3 Hz, 1H, H_1), 6.54 (d, *J* = 8.3 Hz, 2H, H_2), 3.91 – 3.75 (m, 6H, H_5/H_{11}), 1.76 – 1.72 (m, 2H, H_6), 1,72 – 1.68 (m, 1H, H_{12}), 1.64 – 1.58 (m, 1H, alkyl-H), 1.57 – 1.51 (m, 2H, alkyl-H), 1.49 – 1.42 (m, 4H, alkyl-H), 1.42 – 1.37 (m, 3H, alkyl-H), 1.34 – 1.28 (m, 12H, alkyl-H), 0.95 – 0.86 (m, 18H, H_8/H_{10}/H_{14}/H_{16}). ^{13}C NMR (151 MHz, $CDCl_3$) δ 153.7 (C_3), 137.8 (C_4), 123.0 (C_1), 106.1 (C_2), 75.9 (C_{11}), 71.1 (C_5), 41.0 (C_7/C_9/C_{11}/C_{13}), 40.6 (C_6), 39.6 (C_6), 39.1 (C_{12}), 33.7 (alkyl-C), 31.9 (alkyl-C), 31.6 (alkyl-C), 30.5 (alkyl-C), 29.3 (alkyl-C), 29.1 (alkyl-C), 28.8 (alkyl-C), 27.0 (alkyl-C), 25.2 (alkyl-C), 23.8 (alkyl-C), 23.7 (alkyl-C), 23.2 (alkyl-C), 23.1 (alkyl-C), 22.8 (alkyl-C), 22.8 (alkyl-C), 14.1 (methyl-C), 14.1 (methyl-C), 14.0 (methyl-C), 11.2 (methyl-C), 11.1 (methyl-C), 10.8 (methyl-C). **HRMS–ASAP** *m/z* = 463.4045 $[M+H]^+$, calculated for $C_{30}H_{55}O_3$ = 463.4107.

*Synthesis of tris(n-1,2,3 tri(Alkyloxy)phenyl)cyclopropenium chloride (**DCn**·Cl).*

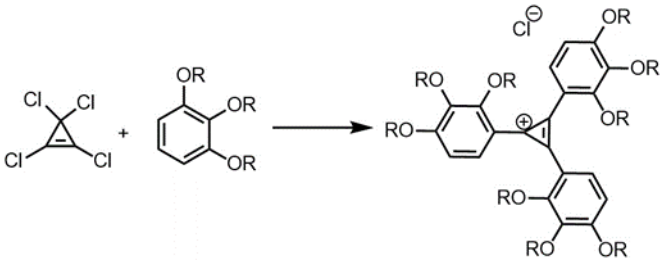

General procedure: 2 (0.82 mmol, 1.1 equiv.) and $AlCl_3$ (0.75 mmol, 1 equiv.) were added to an oven dried microwave vial under an N_2 atmosphere in $CHCl_3$ (0.1 mL or 0.5 mL) sonicated for 5 min before being heated to 80 °C for 1 h. The mixture was then cooled to 0 °C and 1,2,3-trialkyloxybenzene (1.5 mmol, 2 equiv.) dissolved in $CHCl_3$ (1.5 mL or 17 mL) was added to the vial and left to stir for 60 min. The mixture was then heated to 50 °C and 1,2,3-trialkyloxybenzene (1.5 mmol, 2 equiv.) in $CHCl_3$ (1.5 mL or

5 mL) was added and the mixture left to stir overnight at 50 °C. Where necessary, the crude mixture was dissolved in hexanes (25 mL) and filtered, before removing the solvent under reduced pressure. The mixture was then purified by column chromatography (Teledyne Isco Combiflash Rf+ system, 12 g SiO_2, CH_2Cl_2/MeOH gradient elution [1:0 to 17:3]) and the solvent removed under reduced pressure. Where necessary, the product was further purified by either recrystallisation or trituration with MeCN (5 mL) depending on the solubility.

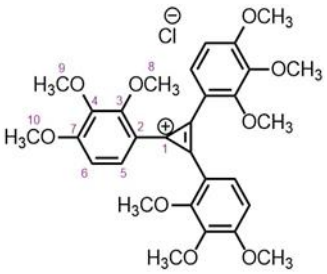

Tris(1,2,3-trimethoxyphenyl)cyclopropenium Chloride (DC1·Cl). The product was obtained from **2** (73 mg, 0.41 mmol) and **1a** (total 0.50 g, 0.75 mmol) in $CHCl_3$ (added in quantities of 0.1 mL, 1.5 mL, 1.5 mL) after column chromatography and trituration as a colourless solid (0.30 g, 0.52 mmol, 70% yield). **M.P.** 100 - 103 °C. **^{1}H NMR** (599 MHz, $CDCl_3$) δ 8.11 (d, *J* = 7.9 Hz, 3H, H_5), 7.09 (d, *J* = 7.9 Hz, 3H, H_6), 4.09 (s, 9H, H_8), 4.06 (s, 9H, H_9), 3.96 (s, 9H, H_{10}). **^{13}C NMR** (151 MHz, $CDCl_3$) δ 162.4 (C_3), 156.4 (C_4), 146.7 (C_2), 141.3 (C_7), 133.7 (C_5), 108.5 (C_6), 108.1 (C_1), 62.4 (C_9), 61.7 (C_{10}), 57.2 (C_8). **HRMS–ASAP** *m/z* = 537.2104 $[M\text{-}Cl]^+$, calculated for $C_{30}H_{33}O_9$ = 537.2119.

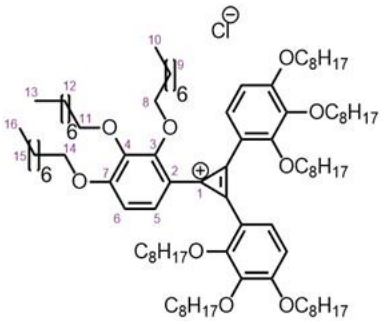

Tris(1,2,3-tri(*n*-octyloxy)phenyl)cyclopropenium Chloride (DC8·Cl). The product was obtained from **2** (0.10 g, 0.56 mmol) and **1b** (1.00 g, 2.16 mmol) in $CHCl_3$ (added in quantities of 0.1\mL, 1.5 mL, 1.5 mL) after column chromatography and recrystallisation as a yellow solid (0.48 g, 0.34 mmol, 60% yield). **M.P.** 74 - 76 °C. **^{1}H NMR** (700 MHz, $CDCl_3$) δ 8.05 (d, *J* = 8.8 Hz, 3H, H_5), 7.02 (d, *J* = 8.8 Hz, 3H, H_6), 4.18 (t, *J* = 6.5 Hz, 6H, H_8), 4.13 (t, *J* = 6.7 Hz, 6H, H_{11}), 4.07 (t, *J* = 6.5 Hz, 6H, H_{14}), 1.93 – 1.89 (m, 6H, alkyl-H), 1.84 – 1.81 (m, 6H, alkyl-H), 1.55 – 1.51 (m, 12H, alkyl-H), 1.41 – 1.37 (m, 12H, alkyl-H), 1.36 - 1.33 (m, 18H, alkyl-H), 1.32 - 1.29 (m, 24H, alkyl-H), 1.22 – 1.18 (m, 6H, alkyl-H), 1.15 – 1.08 (m, 18H, alkyl-H), 1.07 – 1.03 (m, 6H, alkyl-H), 0.91 – 0.89 (m, 18H, H_{10}/H_{13}), 0.83 (t, *J* = 7.2 Hz, 9H, H_{16}). **^{13}C NMR** (151 MHz, $CDCl_3$) δ 162.1 (C_3), 156.3 (C_4), 147.1 (C_2), 141.2 (C_7), 134.0 (C_5), 109.0 (C_1), 108.7 (C_6), 75.4 (C_{11}), 74.4 (C_{14}), 69.9 (C_8), 32.1 (alkyl-C), 32.0 (alkyl-C), 31.9 (alkyl-C), 30.5 (alkyl-C), 29.9 (alkyl-C), 29.7 (alkyl-C), 29.5 (alkyl-C), 29.5 (alkyl-C), 29.5

(alkyl-C), 29.4 (alkyl-C), 29.3 (alkyl-C), 29.3 (alkyl-C), 26.3 (alkyl-C), 26.2 (alkyl-C), 25.9 (alkyl-C), 22.9 (alkyl-C), 22.8 (alkyl-C), 22.7 (alkyl-C), 14.3 (methyl-C), 14.2 (methyl-C), 14.2 (methyl-C). **MS-MALDI** (DTCB matrix with CH_2Cl_2) *m/z* = 1420.0 $[M\text{-}Cl]^+$, calculated for $C_{93}H_{159}O_9$ = 1420.2.

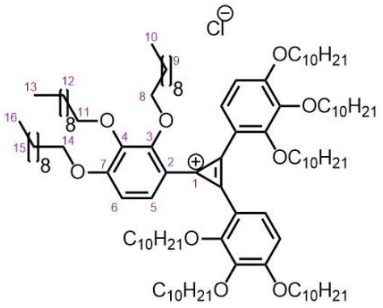

Tris(1,2,3-tri(*n*-decyloxy)phenyl)cyclopropenium Chloride (DC10·Cl). The product was obtained from **2** (0.14 g, 0.82 mmol) and **1c** (1.77 g, 3.24 mmol) in $CHCl_3$ (added in quantities of 0.1 mL, 1.5 mL, 1.5 mL) after column chromatography and recrystallisation as a yellow solid (0.79 g, 0.47 mmol, 57% yield). **M.P.** 54 - 58 °C. **^{1}H NMR** (599 MHz, $CDCl_3$) δ 8.05 (d, *J* = 7.9 Hz, 3H, H_5), 7.02 (d, *J* = 7.9 Hz, 3H, H_6), 4.19 (t, *J* = 6.5 Hz, 6H, H_8), 4.16 (t, *J* = 6.5 Hz, 6H, H_{11}), 4.06 (t, *J* = 6.5 Hz, 6H, H_{14}), 1.93 – 1.89 (m, 6H, alkyl-H), 1.83 – 1.80 (m, 6H, alkyl-H), 1.55 – 1.49 (m, 12H, alkyl-H), 1.41 – 1.37 (m, 12H, alkyl-H), 1.36 – 1.32 (m, 18H, alkyl-H), 1.31 – 1.25 (m, 48H, alkyl-H), 1.20 – 1.16 (m, 12H, alkyl-H), 1.15 – 1.12 (m, 6H, alkyl-H), 1.11 – 1.02 (m, 18H, alkyl-H), 0.89 (t, *J* = 6.6 Hz, 18H, H_{10}/H_{13}), 0.86 (t, 6.6 Hz, 9H, H_{16}). **^{13}C NMR** (176 MHz, $CDCl_3$) δ 162.1 (C_3), 156.3 (C_4), 147.1 (C_2), 141.1 (C_7), 134.0 (C_5), 109.1 (C_1), 108.7 (C_6), 75.5 (C_{11}), 74.4 (C_{14}), 70.0 (C_8), 32.1 (alkyl-C), 32.1 (alkyl-C), 32.1 (alkyl-C), 30.5 (alkyl-C), 29.9 (alkyl-C), 29.9 (alkyl-C), 29.9 (alkyl-C), 29.8 (alkyl-C), 29.8 (alkyl-C), 29.7 (alkyl-C), 29.6 (alkyl-C), 29.6 (alkyl-C), 29.5 (alkyl-C), 29.5 (alkyl-C), 29.5 (alkyl-C), 29.3 (alkyl-C), 26.3 (alkyl-C), 26.2 (alkyl-C), 25.9 (alkyl-C), 22.9 (alkyl-C), 22.9 (alkyl-C), 22.9 (alkyl-C), 14.3 (methyl-C), 14.3 (methyl-C). **MS-MALDI** (DTCB matrix with CH_2Cl_2) *m/z* = 1637.2 $[M\text{-}Cl]^+$, calculated for $C_{111}H_{195}O_9$ = 1637.5.

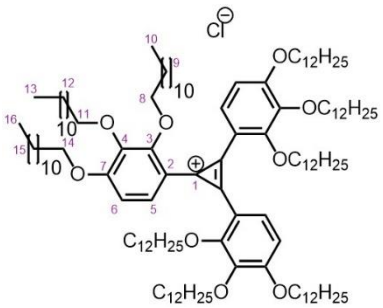

Tris(1,2,3-tri(*n*-dodecyloxy)phenyl)cyclopropenium Chloride (DC12·Cl). The product was obtained from **2** (0.14 g, 0.82 mmol) and **1d** (total 1.80 g, 3.00 mmol) in $CHCl_3$ (added in quantities of 0.1 mL, 1.5 mL, 1.5 mL) after column chromatography and recrystallisation as a pale yellow solid (0.51 g, 0.35 mmol, 47% yield). **M.P.** 83 - 86 °C. **^{1}H NMR** (599 MHz, $CDCl_3$) δ 8.05 (d, *J* = 8.8 Hz, 3H, H_5), 7.01 (d, *J* = 8.9 Hz, 3H, H_6), 4.18 (t, *J* = 7.6 Hz, 6H, H_8), 4.16 (t, *J* = 7.6 Hz, 6H, H_{11}), 4.06 (t, *J* = 7.6 Hz, 6H, H_{14}), 1.94 – 1.87 (m, 6H, alkyl-H), 1.85 – 1.79 (m, 6H, alkyl-H), 1.55 – 1.49 (m,

12H, alkyl-H), 1.41 – 1.36 (m, 12H, alkyl-H), 1.36 – 1.31 (m, 18H, alkyl-H), 1.31 – 1.24 (m, 78H, alkyl-H), 1.23 – 1.21 (m, 12H, alkyl-H), 1.21 – 1.12 (m, 18H, alkyl-H), 1.12 – 1.02 (m, 18H, alkyl-H), 0.88 – 0.85 (m, 27H, $H_{10}/H_{13}/H_{16}$). **^{13}C NMR** (151 MHz, $CDCl_3$) δ 162.1 (C_3), 156.3 (C_4), 147.1 (C_2), 141.1 (C_7), 134.0 (C_5), 109.0 (C_6), 108.7 (C_1), 75.5 (C_{11}), 74.4 (C_8), 70.0 (C_{14}), 32.1 (alkyl-C), 32.1 (alkyl-C), 30.5 (alkyl-C), 29.9 (alkyl-C), 29.9 (alkyl-C), 29.9 (alkyl-C), 29.8 (alkyl-C), 29.8 (alkyl-C), 29.8 (alkyl-C), 29.8 (alkyl-C), 29.8 (alkyl-C), 29.6 (alkyl-C), 29.5 (alkyl-C), 29.5 (alkyl-C), 29.5 (alkyl-C), 29.3 (alkyl-C), 26.3 (alkyl-C), 26.2 (alkyl-C), 25.9 (alkyl-C), 22.8 (alkyl-C), 22.8 (alkyl-C), 22.8 (alkyl-C), 14.2 (methyl-C), 14.2 (methyl-C). **MS-MALDI** (DTCB matrix with CH_2Cl_2) *m/z* = 1925.6 $[M\text{-}Cl]^+$, calculated for $C_{129}H_{232}O_9$ = 1925.8.

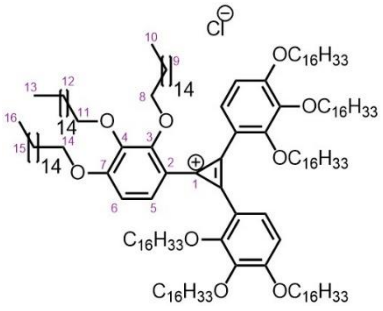

Tris(1,2,3-tri(*n*-hexadecyloxy)phenyl)cyclopropenium Chloride (DC16·Cl). The product was obtained from **2** (74 mg, 0.41 mmol) and **1e** (total 1.20 g, 1.50 mmol) in $CHCl_3$ (added in quantities of 0.5 mL, 17 mL, 5 mL) after column chromatography and recrystallisation as a yellow solid (0.28 g, 0.11 mmol, 30% yield). **M.P.** 50 – 52 °C. **^{1}H NMR** (599 MHz, $CDCl_3$) δ 8.05 (d, *J* = 5.0 Hz, 3H, H_5), 7.02 (d, *J* = 5.0 Hz, 3H, H_6), 4.19 (t, *J* = 6.1 Hz, 6H, H_8), 4.16 (t, *J* = 6.1 Hz, 6H, H_{11}), 4.06 (t, *J* = 6.1 Hz, 6H, H_{14}), 1.93 – 1.89 (m, 6H, alkyl-H), 1.84 – 1.80 (m, 6H, alkyl-H), 1.55 – 1.49 (m, 12H, alkyl-H), 1.42 – 1.36 (m, 12H, alkyl-H), 1.35 – 1.32 (m, 12H, alkyl-H), 1.31 – 1.21 (m, 162H, $H_9/H_{12}/H_{15}$), 1.20 – 1.11 (m, 18H, alkyl-H), 1.11 – 1.02 (m, 18H, alkyl-H), 0.88 (t, *J* = 8.0 Hz, 27H, $H_{10}/H_{13}/H_{16}$). **^{13}C NMR** (151 MHz, $CDCl_3$) δ 162.1 (C_3), 156.3 (C_4), 147.1 (C_2), 141.1 (C_7), 134.1 (C_5), 109.1 (C_1), 108.7 (C_6), 75.5 (C_{11}), 74.4 (C_{14}), 70.0 (C_8), 32.1 (alkyl-C), 30.5 (alkyl-C), 30.0 (alkyl-C), 30.0 (alkyl-C), 29.9 (alkyl-C), 29.9 (alkyl-C), 29.9 (alkyl-C), 29.9 (alkyl-C), 29.9 (alkyl-C), 29.9 (alkyl-C), 29.8 (alkyl-C), 29.8 (alkyl-C), 29.8 (alkyl-C), 29.8 (alkyl-C), 29.6 (alkyl-C), 29.6 (alkyl-C), 29.6 (alkyl-C), 29.5 (alkyl-C), 29.5 (alkyl-C), 29.3 (alkyl-C), 26.4 (alkyl-C), 26.3 (alkyl-C), 26.0 (alkyl-C), 22.9 (alkyl-C), 14.3 (methyl-C). **MS-MALDI** (DTCB matrix with CH_2Cl_2) *m/z* = 2430.1 $[M\text{-}Cl+H]^+$, calculated for $C_{165}H_{304}O_9$ = 2430.3.

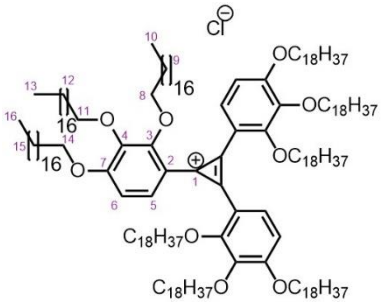

Tris(1,2,3-tri(*n*-octadecyloxy)phenyl)cyclopropenium Chloride (DC18·Cl). The product was obtained from **2** (73 mg, 0.41 mmol) and **1f** (total 1.32 g, 1.50 mmol) in $CHCl_3$ (added in quantities of 0.5 mL, 17 mL, 5 mL) after column chromatography and recrystallisation as a white solid (0.55 g, 0.21 mmol, 55% yield). **M.P.** 61 - 63 °C. **^{1}H NMR** (599 MHz, $CDCl_3$) δ 8.05 (d, *J* = 7.9 Hz, 3H, H_5), 7.02 (d, *J* = 7.9 Hz, 3H, H_6), 4.21 – 4.13 (m, 12H, H_8/H_{11}), 4.06 (t, *J* = 6.5 Hz, 6H, H_{14}), 1.94 – 1.88 (m, 6H, alkyl-H), 1.83 – 1.80 (m, 6H, alkyl-H), 1.55 – 1.49 (m, 12H, alkyl-H), 1.42 – 1.35 (m, 18H, alkyl-H), 1.29 – 1.23 (m, 222H, alkyl-H), 1.17 – 1.13 (m, 12H, alkyl-H), 1.08 – 1.03 (m, 12H, alkyl-H), 0.88 (t, *J* = 6.6 Hz, 27H, H_{10}/H_{13}/H_{16}). **^{13}C NMR** (151 MHz, $CDCl_3$) δ 161.1 (C_3), 156.3 (C_4), 147.1 (C_2), 141.1 (C_7), 134.1 (C_5), 109.1 (C_6), 108.7 (C_1), 75.5 (C_{11}), 74.5 (C_{14}), 70.1 (C_8), 32.1 (alkyl-C), 30.5 (alkyl-C), 30.0 (alkyl-C), 30.0 (alkyl-C), 29.9 (alkyl-C), 29.9 (alkyl-C), 29.9 (alkyl-C), 29.9 (alkyl-C), 29.9 (alkyl-C), 29.9 (alkyl-C), 29.8 (alkyl-C), 29.8 (alkyl-C), 29.8 (alkyl-C), 29.8 (alkyl-C), 29.8 (alkyl-C), 29.6 (alkyl-C), 29.6 (alkyl-C), 29.5 (alkyl-C), 29.5 (alkyl-C), 29.5 (alkyl-C), 29.3 (alkyl-C), 26.4 (alkyl-C), 26.3 (alkyl-C), 26.0 (alkyl-C), 22.8 (alkyl-C), 14.3 (methyl-C). **MS-MALDI** (DTCB matrix with CH_2Cl_2) *m/z* = 2684.4 $[M\text{-}Cl+H]^+$, calculated for $C_{183}H_{340}O_9$ = 2684.6.

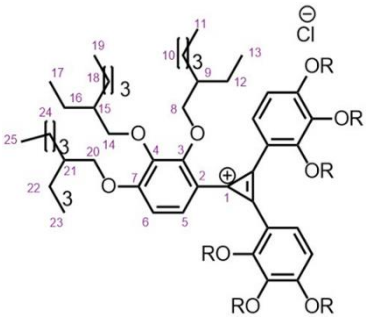

Tris(1,2,3-tri(2-ethylhexyloxy)phenyl)cyclopropenium Chloride (DC6,2·Cl). The product was obtained from **2** (0.15 g, 0.82 mmol) and **1g** (total 1.42 g, 3.07 mmol) in $CHCl_3$ (added in quantities of 0.1 mL, 1.5 mL, 1.5 mL) after column chromatography as a brown liquid (0.88 g, 0.605 mmol, 81% yield). **^{1}H NMR** (600 MHz, $CDCl_3$) δ 7.99 – 7.92 (m, 3H, H_3), 7.00 – 6.94 (m, 3H, H_4), 4.15 – 4.10 (m, 3H, H_8 or H_{14}), 4.10 – 4.03 (m, 6H, H_8 or H_{14}), 4.03 -3.99 (m, 3H, H_8 or H_{14}), 3.95 (d, *J* = 6.0 Hz, 6H, H_{20}), 1.87 – 1.82 (m, 3H, alkyl-H), 1.82 – 1.77 (m, 3H, alkyl-H), 1.63 – 1.56 (m, 6H, alkyl-H), 1.56 – 1.45 (m, 15H, alkyl-H), 1.44 – 1.41 (m, 3H, alkyl-H), 1.40 – 1.31 (m, 27H, alkyl-H), 1.20 – 1.15 (m, 3H, alkyl-H), 1.14 – 1.03 (m, 18H, alkyl-H), 1.04 – 1.00 (m, 3H, alkyl-H), 1.00 – 0.94 (m, 18H, methyl-H), 0.94 – 0.88 (m, 18H, methyl-H), 0.79 (t, *J* = 7.2 Hz, 9H, methyl-H), 0.59 (t, *J* = 7.3 Hz, 9H, methyl-H). **^{13}C NMR** (151 MHz, $CDCl_3$) δ 162.4 (aromatic-C), 156.7 (aromatic-C), 147.0 (aromatic-C), 141.4 (C_7), 134.0

(C_5), 108.9 (C_6), 108.4 (aromatic-C), 78.9 (alkyloxy-C), 77.6 (C_{20}), 72.4 (alkyloxy-C), 40.7 (alkyl-C), 40.0 (alkyl-C), 39.5 (alkyl-C), 30.6 (alkyl-C), 30.5 (alkyl-C), 29.9 (alkyl-C), 29.4 (alkyl-C), 29.2 (alkyl-C), 29.0 (alkyl-C), 23.8 (alkyl-C), 23.7 (alkyl-C), 23.7 (alkyl-C), 23.3 (alkyl-C), 23.2 (alkyl-C), 23.1 (alkyl-C), 14.3 (methyl-C), 14.2 (methyl-C), 14.2 (methyl-C), 11.3 (methyl-C), 11.3 (methyl-C), 11.2 (methyl-C), 10.8 (methyl-C). **MS–ASAP** *m/z* = 1422.2 $[M+H-Cl]^+$, calculated for $C_{93}H_{160}O_9$ = 1421.2.

*Counter Ion Exchange of Cyclopropenium via Alcohol Intermediate (**DCn**·X)*

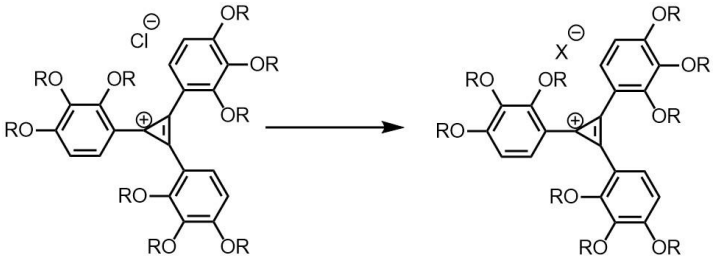

General procedure: Tris(1,2,3-tri(*n*-alkyloxy)phenyl)cyclopropenium chloride (0.11 mmol, 1 equiv) was dissolved in CH_2Cl_2 (50 mL), and the solution was washed with NaOAc solution (50 mL, 0.37 M) three times. The solution was then washed with aqueous hydrohalogenic acid (15 mL, 1 M) and filtered. The solvent was removed under reduced pressure, and the product was then either isolated or recrystallised in MeCN (15 mL) before further drying to isolate the product.

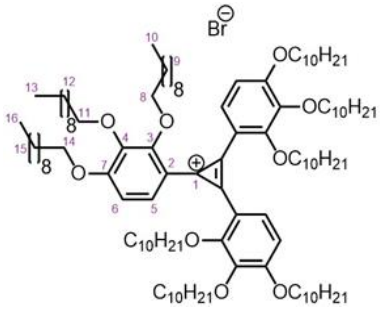

Tris(1,2,3-tri(*n*-decyloxy)phenyl)cyclopropenium Bromide (DC10·Br). The product was obtained from **DC10**·Cl (0.78 g, 0.46 mmol) and hydrobromic acid (15 mL, 1 M) after recrystallisation as a yellow solid (0.46 g, 0.27 mmol, 44% yield). **M.P.** 58 - 60 °C. **^{1}H NMR** (600 MHz, $CDCl_3$) δ 8.05 (d, *J* = 8.9 Hz, 3H, H_6), 7.02 (d, *J* = 8.9 Hz, 3H, H_5), 4.18 (t, *J* = 6.5 Hz, 6H, H_8), 4.15 (t, *J* = 6.7 Hz, H_{11}), 4.06 (t, *J* = 6.5 Hz, 6H, H_{14}), 1.93 - 1.87 (m, 6H, alkyl-H), 1.84 – 1.79 (m, 6H, alkyl-H), 1.55 – 1.48 (m, 12H, alkyl-H), 1.41 – 1.36 (m, 12H, alkyl-H), 1.34 – 1.23 (m, 72H, alkyl-H), 1.20 – 1.15 (m, 12H, alkyl-H), 1.15 – 1.01 (m, 24H, alkyl-H), 0.88 (t, *J* = 7.1 Hz, 18H, H_{10}/H_{13}), 0.85 (t, *J* = 7.2 Hz, 9H, H_{16}). **^{13}C NMR** (151 MHz, $CDCl_3$) δ 162.1 (C_3), 156.3 (C_4), 147.1 (C_2), 141.1 (C_7), 134.0 (C_5), 109.1 (C_6), 108.7 (C_1), 75.5 (C_{11}), 74.5 (C_{14}), 70.0 (C_8), 32.1 (alkyl-C), 32.0 (alkyl-C), 32.0 (alkyl-C), 30.5 (alkyl-C), 30.0 (alkyl-C),

29.9 (alkyl-C), 29.9 (alkyl-C), 29.8 (alkyl-C), 29.7 (alkyl-C), 29.7 (alkyl-C), 29.5 (alkyl-C), 29.5 (alkyl-C), 29.5 (alkyl-C), 29.5 (alkyl-C), 29.5 (alkyl-C), 29.2 (alkyl-C), 26.3 (alkyl-C), 26.2 (alkyl-C), 25.9 (alkyl-C), 22.8 (alkyl-C), 22.8 (alkyl-C), 22.8 (alkyl-C), 14.2 (methyl-C), 14.2 (methyl-C). **MS-MALDI** (DTCB matrix with CH_2Cl_2) *m/z* = 1637.1 $[M\text{-}Cl]^+$, calculated for $C_{111}H_{195}O_9$ = 1637.5.

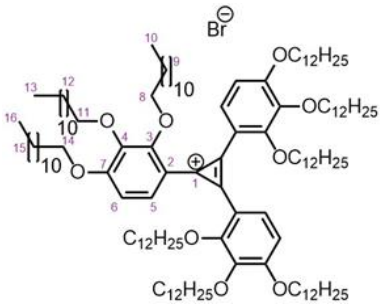

Tris(1,2,3-tri(*n*-dodecyloxy)phenyl)cyclopropenium Bromide (DC12·Br). The product was obtained from **DC12**·Cl (0.41 g, 0.20 mmol) and aqueous hydrobromic (15 mL, 1 M) after recrystallisation as a yellow solid (50 mg, 0.025 mmol, 12% yield). **M.P.** 63 - 65 °C. **^{1}H NMR** (600 MHz, $CDCl_3$) δ 8.07 (d, *J* = 8.9 Hz, 3H, H_6), 7.04 (d, *J* = 8.9 Hz, 3H, H_5), 4.19 (t, *J* = 6.5 Hz, 6H, H_8), 4.16 (t, *J* = 6.7 Hz, H_{11}), 4.07 (t, *J* = 6.5 Hz, 6H, H_{14}), 1.94 - 1.87 (m, 6H, alkyl-H), 1.85 – 1.79 (m, 6H, alkyl-H), 1.55 – 1.48 (m, 12H, alkyl-H), 1.42 – 1.36 (m, 12H, alkyl-H), 1.36 – 1.32 (m, 18H, alkyl-H), 1.32 – 1.24 (m, 78H, alkyl-H), 1.24 – 1.21 (m, 12H, alkyl-H), 1.21 – 1.00 (m, 24H, alkyl-H), 0.90 – 0.85 (m, H_{10}/H_{13}/H_{16}). **^{13}C NMR** (151 MHz, $CDCl_3$) δ 162.1 (C_3), 156.3 (C_4), 147.3 (C_2), 141.1 (C_7), 134.3 (C_5), 109.2 (C_6), 108.8 (C_1), 75.5 (C_{11}), 74.5 (C_{14}), 70.1 (C_8), 32.1 (alkyl-C), 32.1 (alkyl-C), 30.5 (alkyl-C), 30.0 (alkyl-C), 29.9 (alkyl-C), 29.9 (alkyl-C), 29.9 (alkyl-C), 29.9 (alkyl-C), 29.8 (alkyl-C), 29.8 (alkyl-C), 29.8 (alkyl-C), 29.8 (alkyl-C), 29.6 (alkyl-C), 29.6 (alkyl-C), 29.6 (alkyl-C), 29.5 (alkyl-C), 29.5 (alkyl-C), 29.3 (alkyl-C), 26.4 (alkyl-C), 26.3 (alkyl-C), 26.0 (alkyl-C), 22.8 (alkyl-C), 14.3 (methyl-C), 14.2 (methyl-C). **MS-MALDI** (DTCB matrix with CH_2Cl_2) *m/z* = 1925.5 $[M\text{-}Br+H]^+$, calculated for $C_{129}H_{232}O_9$ = 1925.8.

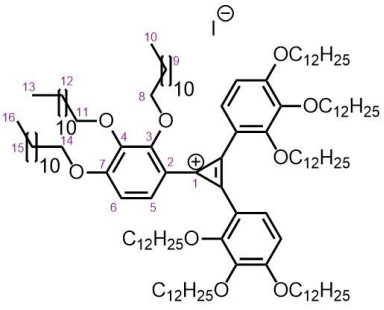

Tris(1,2,3-tri(*n*-dodecyloxy)phenyl)cyclopropenium Iodide (DC12·I). The product was obtained from **DC12**·Cl (0.23 g, 0.11 mmol) and hydroiodic acid (15 mL, 1 M) as a brown liquid (200 mg, 0.098 mmol, 89% yield). **M.P.** -7 °C. **^{1}H NMR** (599 MHz, $CDCl_3$) δ 8.10 (d, *J* = 7.9 Hz, 3H, H_5), 7.01 (d, *J* = 7.9 Hz, 3H, H_6), 4.22 – 4.15 (m, 12H, H_8), 4.11 (t, *J* = 6.5 Hz, 6H, H_{14}), 1.94 - 1.88 (m, 6H, alkyl-H), 1.86 – 1.81 (m, 6H, alkyl-H), 1.55 – 1.51 (m, 12H, alkyl-H), 1.42 – 1.38 (m, 12H, alkyl-H), 1.37 – 1.32 (m, 18H, alkyl-H), 1.32 – 1.24 (m, 78H, v), 1.24 – 1.21 (m, 12H alkyl-H),

1.21 – 1.02 (m, 36H, alkyl-H), 0.91 – 0.85 (m, 27H, $H_{10}/H_{13}/H_{16}$). **^{13}C NMR** (151 MHz, $CDCl_3$) δ 161.9 (C_3), 156.4 (C_4), 147.3 (C_2), 141.1 (C_7), 134.6 (C_5), 109.0 (C_6), 108.9 (C_1), 75.5 (C_{11}), 74.6 (C_{14}), 70.0 (C_8), 32.1 (alkyl-C), 32.1 (alkyl-C), 30.6 (alkyl-C), 30.0 (alkyl-C), 30.0 (alkyl-C), 29.9 (alkyl-C), 29.9 (alkyl-C), 29.9 (alkyl-C), 29.8 (alkyl-C), 29.8 (alkyl-C), 29.8 (alkyl-C), 29.8 (alkyl-C), 29.6 (alkyl-C), 29.6 (alkyl-C), 29.6 (alkyl-C), 29.5 (alkyl-C), 29.5 (alkyl-C), 29.3 (alkyl-C), 26.4 (alkyl-C), 26.3 (alkyl-C), 26.0 (alkyl-C), 22.9 (alkyl-C), 14.3 (methyl-C), 14.3 (methyl-C). **MS-MALDI** (DTCB matrix with CH_2Cl_2) *m/z* = 1925.5 $[M\text{-}I+H]^+$, calculated for $C_{129}H_{232}O_9$ = 1925.8.

*Counter Ion Exchange of Cyclopropenium with Silver Salts (**DCn**·X)*

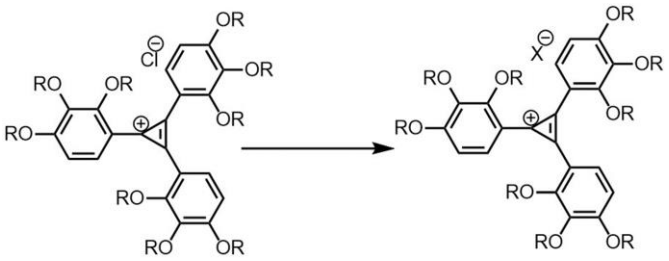

General procedure: Tris(1,2,3-tri(*n*-alkyloxy)phenyl)cyclopropenium chloride (0.150 mmol, 1 equiv.) was dissolved in a CH_2Cl_2 (30 mL) and MeCN (10 mL) solvent mixture with AgX (0.150 mmol, 1 equiv.), and the solution was left to stir for 15 min at RT. The precipitate was removed from the solution by filtration. The solvent was then removed under reduced pressure to isolate the product.

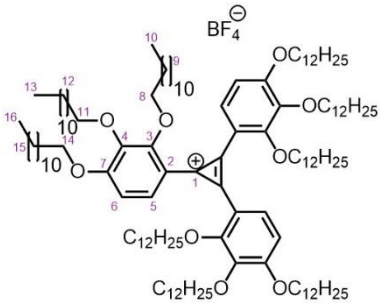

Tris(1,2,3-tri(*n*-dodecyloxy)phenyl)cyclopropenium Tetrafluoroborate (DC12·BF_4). The product was obtained from **DC12**·Cl (0.30 g, 0.15 mmol) and $AgBF_4$ (29 mg, 0.15 mmol) as a yellow solid (0.23 g, 0.11 mmol, 76% yield). **M.P.** 37 °C. **^{1}H NMR** (599 MHz, $CDCl_3$) δ 8.01 (d, *J* = 7.9 Hz, 3H, H_5), 7.00 (d, *J* = 7.9 Hz, 3H, H_6), 4.20 – 4.13 (m, 12H, H_8/H_{11}), 4.06 (t, *J* = 6.5 Hz, 6H, H_{14}), 1.93 – 1.88 (m, 6H, alkyl-H), 1.84 – 1.80 (m, 6H, alkyl-H), 1.55 – 1.49 (m, 12H, alkyl-H), 1.42 – 1.36 (m, 12H, alkyl-H), 1.35 – 1.31 (m, 18H, alkyl-H), 1.31 – 1.25 (m, 78H, alkyl-H), 1.23 – 1.21 (m, 12H, alkyl-H), 1.20 – 1.03 (m, 36H, alkyl-H), 0.89 – 0.86 (m, 27H, $H_{10}/H_{13}/H_{16}$). **^{13}C NMR** (151 MHz, $CDCl_3$) δ 162.1 (C_3), 156.3 (C_4), 147.1 (C_2), 141.1 (C_7), 133.9 (C_5), 109.0 (C_1), 108.7 (C_6), 75.5 (C_{11}), 74.4 (C_{14}), 69.9 (C_8), 32.1 (alkyl-C), 32.1 (alkyl-C), 30.5

(alkyl-C), 29.9 (alkyl-C), 29.9 (alkyl-C), 29.9 (alkyl-C), 29.9 (alkyl-C), 29.8 (alkyl-C), 29.8 (alkyl-C), 29.8 (alkyl-C), 29.8 (alkyl-C), 29.8 (alkyl-C), 29.6 (alkyl-C), 29.6 (alkyl-C), 29.5 (alkyl-C), 29.5 (alkyl-C), 29.3 (alkyl-C), 26.3 (alkyl-C), 26.3 (alkyl-C), 25.9 (alkyl-C), 22.9 (alkyl-C), 22.9 (alkyl-C), 22.8 (alkyl-C), 14.3 (methyl-C), 14.2 (methyl-C). **MS-MALDI** (DTCB matrix with CH_2Cl_2) *m/z* = 1925.5 $[M\text{-}BF_4+H]^+$, calculated for $C_{129}H_{232}O_9$ = 1925.8.

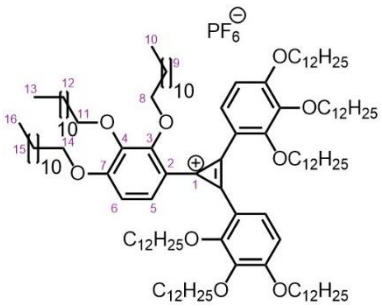

Tris(1,2,3-tri(*n*-dodecyloxy)phenyl)cyclopropenium Hexafluorophosphate (DC12·PF_6). The product was obtained from **DC12**·Cl (245 mg, 0.125 mmol) and $AgPF_6$ (33 mg, 0.13 mmol) as an orange liquid (0.24 g, 0.11 mmol, 91% yield). **^{1}H NMR** (600 MHz, $CDCl_3$) δ 8.03 (d, *J* = 7.9 Hz, 3H, H_5), 7.02 (d, *J* = 7.9 Hz, 3H, H_6), 4.18 (t, *J* = 6.6 Hz, 6H, H_{14}), 4.15 (t, *J* = 6.7 Hz, 6H, H_{14}), 4.06 (t, *J* = 6.5 Hz, 6H, H_{14}), 1.94 – 1.87 (m, 6H, alkyl-H), 1.85 – 1.79 (m, 6H, alkyl-H), 1.56 – 1.49 (m, 12H, alkyl-H), 1.42 – 1.36 (m, 12H, alkyl-H), 1.36 – 1.32 (m, 18H, alkyl-H), 1.31 – 1.24 (m, 72H, alkyl-H), 1.24 – 1.21 (m, 12H, alkyl-H), 1.21 – 1.12 (m, 18H, alkyl-H), 1.11 – 1.01 (m, 36H, alkyl-H), 0.91 – 0.84 (m, 27H, $H_{10}/H_{13}/H_{16}$). **^{13}C NMR** (151 MHz, $CDCl_3$) δ 162.1 (C_3), 156.3 (C_4), 147.3 (C_2), 141.1 (C_7), 134.0 (C_5), 109.0 (C_1), 108.8 (C_6), 75.4 (C_{11}), 74.4 (C_{14}), 69.9 (C_8), 32.1 (alkyl-C), 32.1 (alkyl-C), 30.5 (alkyl-C), 29.9 (alkyl-C), 29.9 (alkyl-C), 29.9 (alkyl-C), 29.9 (alkyl-C), 29.9 (alkyl-C), 29.8 (alkyl-C), 29.8 (alkyl-C), 29.8 (alkyl-C), 29.8 (alkyl-C), 29.8 (alkyl-C), 29.6 (alkyl-C), 29.5 (alkyl-C), 29.5 (alkyl-C), 29.5 (alkyl-C), 29.3 (alkyl-C), 26.3 (alkyl-C), 26.3 (alkyl-C), 25.9 (alkyl-C), 22.9 (alkyl-C), 22.8 (alkyl-C), 22.8 (alkyl-C), 14.3 (methyl-C), 14.2 (methyl-C). **MS-MALDI** (DTCB matrix with CH_2Cl_2) *m/z* = 1925.5 $[M\text{-}PF_6+H]^+$, calculated for $C_{129}H_{232}O_9$ = 1925.8.

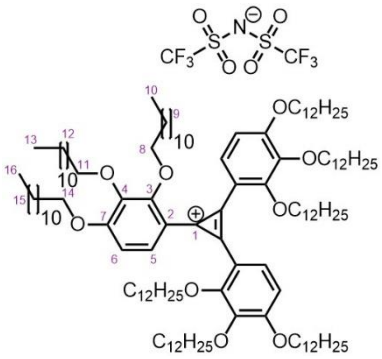

Tris(1,2,3-tri(n-dodecyloxy)phenyl)cyclopropenium Bis(trifluoromethane)sulfonimide (DC12·$(Tf_2)N$). The product was obtained from **DC12**·Cl (0.30 g, 0.15 mmol) and $Ag(Tf)_2N$ (29 mg, 0.15 mmol) as a yellow liquid (0.23 g, 0.11 mmol, 76% yield). **^{1}H NMR** (600 MHz, $CDCl_3$) δ 7.99 (d, *J* = 7.9 Hz, 3H, H_5), 6.98 (d, *J* = 7.9 Hz, 3H, H_6), 4.18 – 4.14 (m, 12H, H_8/H_{11}), 4.06 (t, *J* = 6.5 Hz,

6H, H_{14}), 1.93 – 1.88 (m, 6H, alkyl-H), 1.84 – 1.79 (m, 6H, alkyl-H), 1.55 – 1.50 (m, 12H, alkyl-H), 1.41 – 1.37 (m, 12H, alkyl-H), 1.36 – 1.32 (m, 18H, alkyl-H), 1.31 – 1.25 (m, 78H, alkyl-H), 1.23 – 1.21 (m, 12H, alkyl-H), 1.20 – 1.12 (m, 36H, alkyl-H), 1.11 – 1.01 (m, 36H, alkyl-H), 0.89 – 0.86 (t, *J* = 6.6 Hz, 27H, $H_{10}/H_{13}/H_{16}$). **^{13}C NMR** (151 MHz, $CDCl_3$) δ 162.1 (C_3), 156.3 (C_4), 147.2 (C_2), 141.1 (C_7), 133.9 (C_5), 108.9 (C_6), 108.7 (C_1), 75.5 (C_{11}), 74.4 (C_{14}), 69.9 (C_8), 32.1 (alkyl-C), 32.1 (alkyl-C), 30.5 (alkyl-C), 29.9 (alkyl-C), 29.9 (alkyl-C), 29.9 (alkyl-C), 29.9 (alkyl-C), 29.8 (alkyl-C), 29.8 (alkyl-C), 29.8 (alkyl-C), 29.8 (alkyl-C), 29.8 (alkyl-C), 29.6 (alkyl-C), 29.6 alkyl-C), 29.5 (alkyl-C), 29.5 (alkyl-C), 29.3 (alkyl-C), 26.3 (alkyl-C), 26.2 (alkyl-C), 25.9 (alkyl-C), 22.9 (alkyl-C), 22.8 (alkyl-C), 22.8 (alkyl-C), 14.3 (methyl-C), 14.2 (methyl-C). **MS-MALDI** (DTCB matrix with CH_2Cl_2) *m/z* = 1925.5 $[M\text{-}(Tf)_2N+H]^+$, calculated for $C_{129}H_{232}O_9$ = 1925.8.

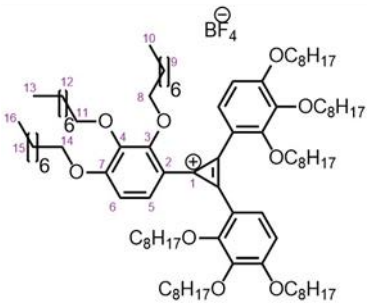

Tris(1,2,3-tri(n-octyloxy)phenyl)cyclopropenium Tetrafluoroborate (DC8·BF_4). The product was obtained from **DC8**·Cl (33 mg, 0.02 mmol) and $AgBF_4$ (25 mg, 0.13 mmol) as a brown liquid (20 mg, 0.01 mmol, 55% yield). **^{1}H NMR** (700 MHz, $CDCl_3$) δ 8.02 (d, *J* = 8.8 Hz, 3H, H_5), 7.02 (d, *J* = 8.8 Hz, 3H, H_6), 4.18 (t, *J* = 6.5 Hz, 6H, H_{12}), 4.16 (t, *J* = 6.7 Hz, 6H, H_8), 4.06 (t, *J* = 6.5 Hz, 6H, H_{16}), 1.93 – 1.88 (m, 6H, alkyl-H), 1.84 – 1.80 (m, 6H, alkyl-H), 1.56 – 1.49 (m, 12H, alkyl-H), 1.41 – 1.36 (m, 12H, alkyl-H), 1.35 – 1.28 (m, 42H, alkyl-H), 1.22 – 1.18 (m, 6H, alkyl-H), 1.16 – 1.07 (m, 18H, alkyl-H), 1.06 – 1.01 (m, 6H, alkyl-H), 0.90 (t, *J* = 7.3 Hz, 18H, H_{10}/H_{13}), 0.83 (t, *J* = 7.3 Hz, 9H, H_{16}). **^{13}C NMR** (151 MHz, $CDCl_3$) δ 162.1 (C_3), 156.3 (C_4), 147.3 (C_2), 141.1 (C_7), 133.9 (C_5), 109.0 (C_6), 108.7 (C_1), 75.4 (C_{11}), 74.4 (C_{14}), 69.9 (C_8), 32.0 (alkyl-C), 31.9 (alkyl-C), 31.9 (alkyl-C), 30.5 (alkyl-C), 29.9 (alkyl-C), 29.7 (alkyl-C), 29.5 (alkyl-C), 29.5 (alkyl-C), 29.5 (alkyl-C), 29.4 (alkyl-C), 29.3 (alkyl-C), 29.3 (alkyl-C), 26.3 (alkyl-C), 26.2 (alkyl-C), 25.9 (alkyl-C), 22.8 (alkyl-C), 22.8 (alkyl-C), 22.7 (alkyl-C), 14.2 (methyl-C), 14.2 (methyl-C), 14.2 (methyl-C). **MS-MALDI** (DTCB matrix with CH_2Cl_2) *m/z* = 1420.8 $[M\text{-}BF_4]^+$, calculated for $C_{93}H_{159}O_9$ = 1421.2.

2.6 Appendix of Supplementary Data and Discussion

2.6.1 Differential Scanning Calorimetry

DSC was performed on each compound over three heating cooling cycles, from 100 °C to -90 °C, at a heating rate of 10 °C min^{-1}.

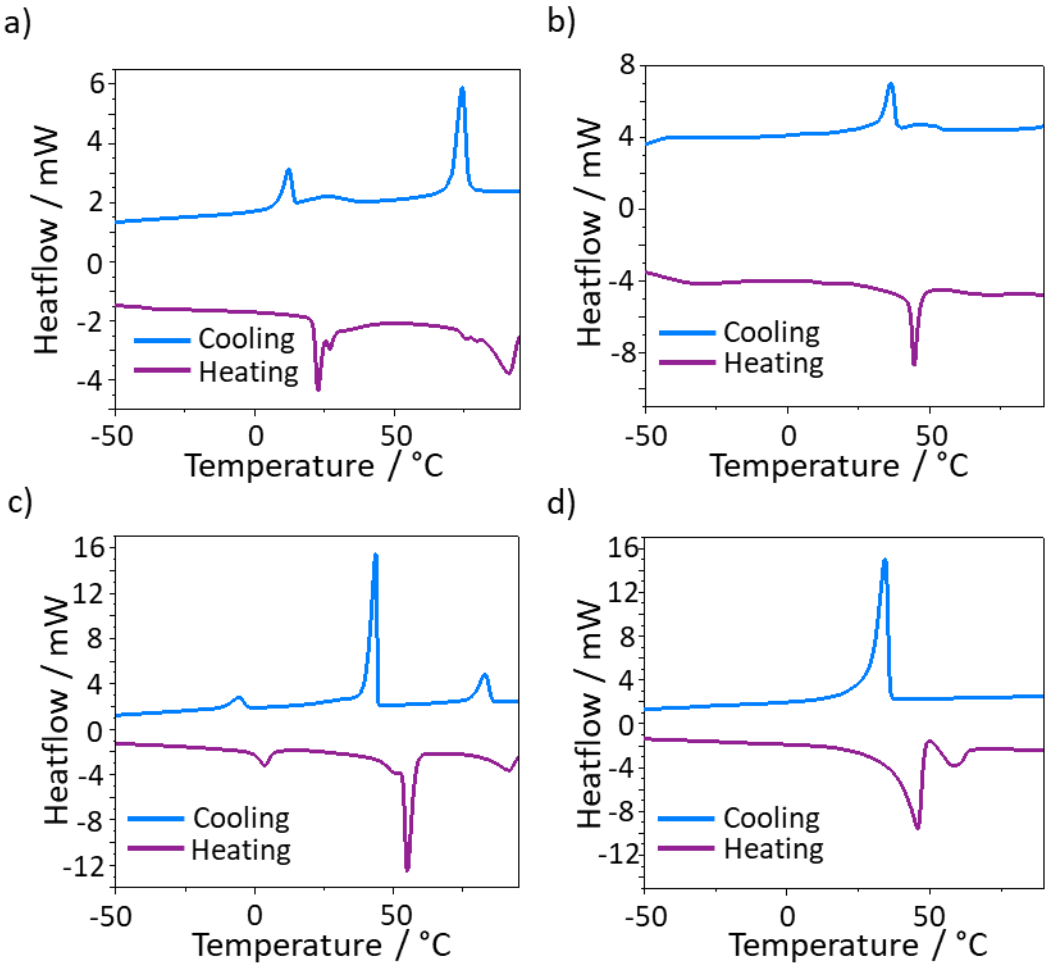

Figure 2.24: DSC of a) **DC8**·Cl, b) **DC10**·Cl, c) **DC12**·Cl, and d) **DC16**·Cl.

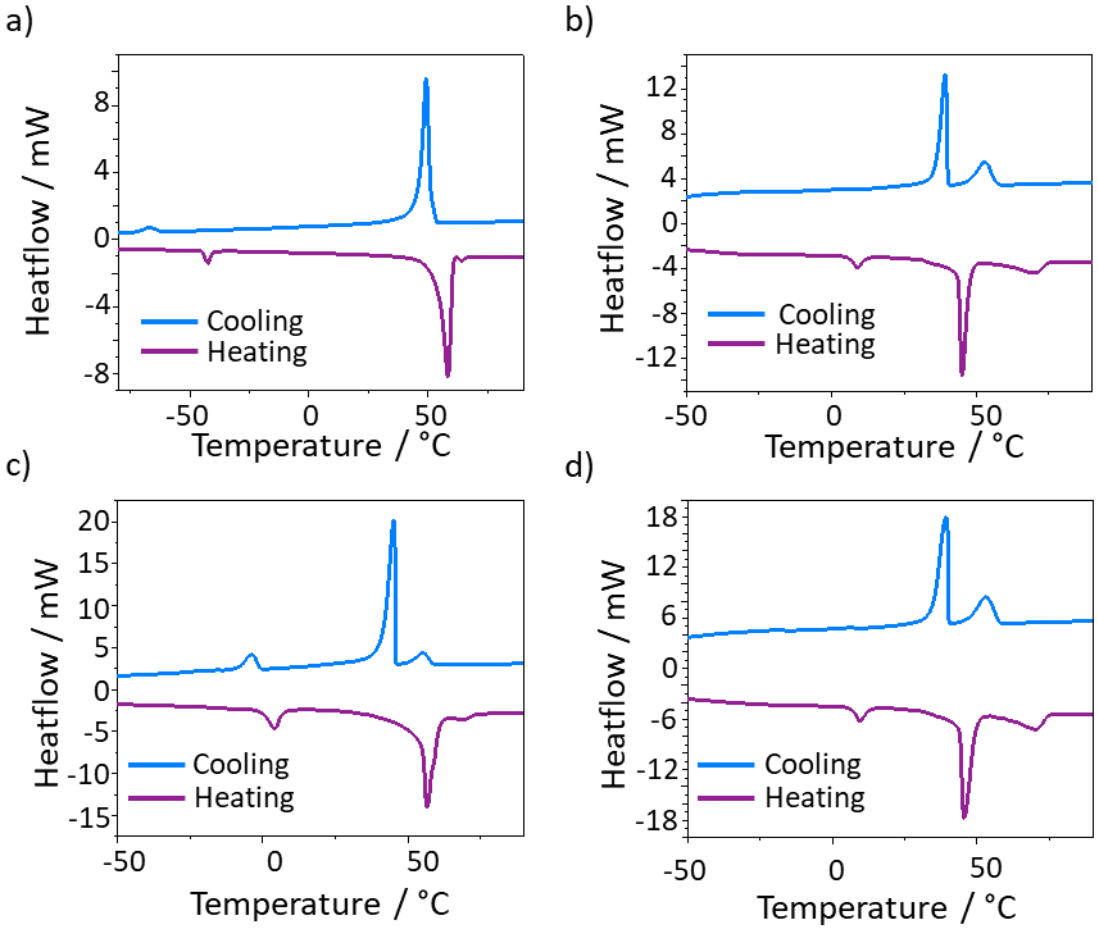

Figure 2.25: DSC of a) **DC18**·Cl, b) **DC10**·Br, c) **DC12**·Br, and d) **DC10**·Br with 10% LiBr.

2.6.2 Thermogravimetric Analysis

TGA was performed on each compound heating to 300 °C at a rate of 10 °C / min.

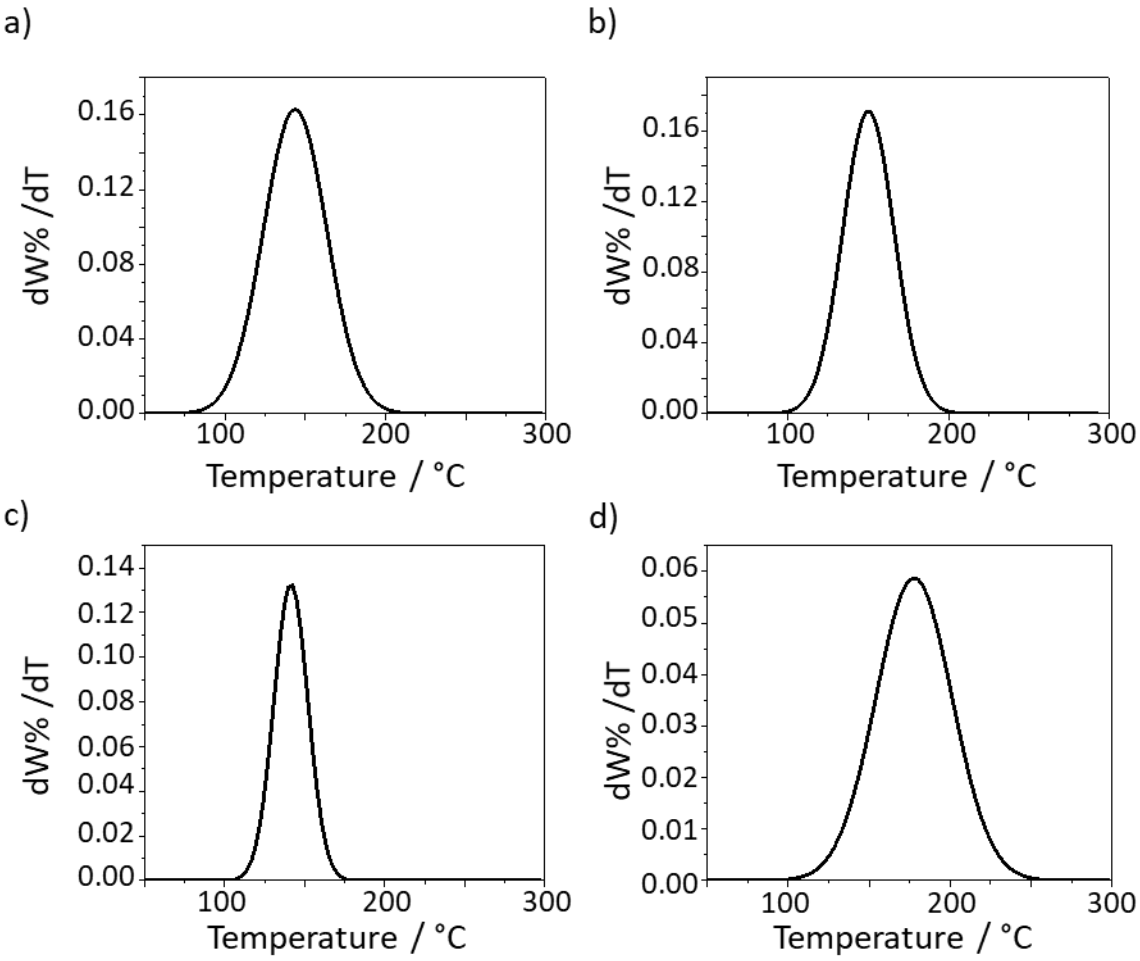

Figure 2.26: DTG curves of a) **DC8**·Cl, b) **DC10**·Cl, c) **DC12**·Cl, and d) **DC16**·Cl.

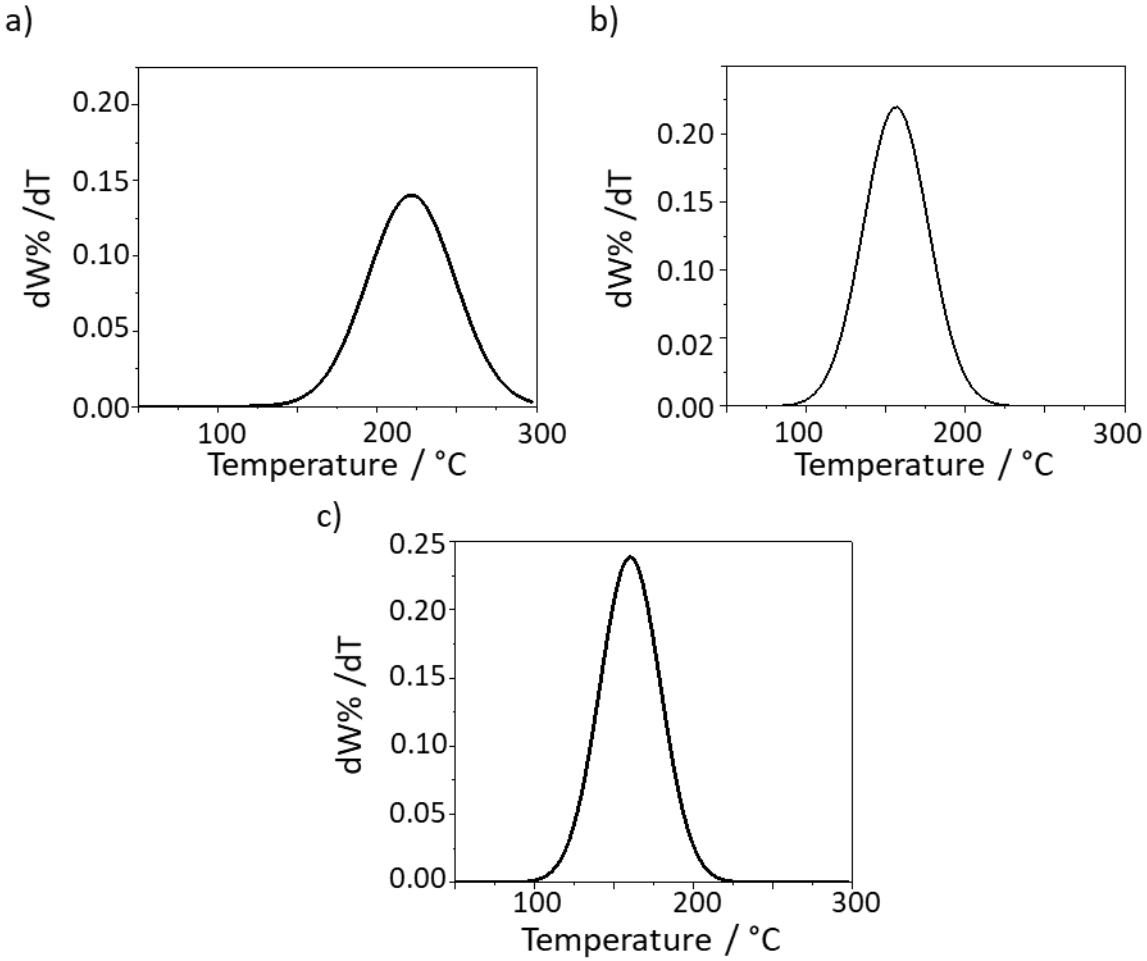

Figure 2.27: DTG curves of a) **DC18**·Cl, b) **DC10**·Br, and c) **DC12**·Br.

2.6.3 Dielectric Measurements

The guard ring cells used for the dielectric measurements were fabricated from patterned ITO coated glass, using a guarded electrode design lacking alignment layers. A photolithography process was used to produce the ITO pattern on the glass substrates. A uniform cell gap was created using a bulk cell construction process, giving comparable cell gaps between cells. Two patterned ITO plates were sandwiched together, one of which consisted of a 3x4 array of the guard ring substrate design with spacer beads evenly deposited onto its surface, the other with a 3x4 array of the addressor substrate design with a thermal glue pattern deposited on the surface. The assembled plates were vacuum sealed, pressed and baked to cure the glue, producing a 3x4 array of cells. The cells were then separated by scribing the glass plates on both sides to leave access to all the electrodes (Figure 2.14).

The individual cell gaps were measured using UV-vis reflectance spectroscopy on the empty cells by taking the average of five measurements from the centre and a measurement from each corner of the cells. Wires were soldered to the exposed ITO of the cell to connect the three electrodes to the dielectric bridge. Empty cell dielectric measurements were taken at a range of voltages, frequencies and temperatures to ensure the cells were appropriate for use and to determine the empty cell capacitance. This was then used to calculate the permittivity of the cyclopropenium compounds using the ratio of the filled to empty cell capacitance.

The cells were filled with the cyclopropenium compounds in the isotropic phase (~100°C) through capillary action. Dielectric measurements were taken using an Agilent E4980A dielectric bridge on cooling from the isotropic phase at a rate of 1 °C min^{-1} whilst being studied through POM with a Leica microscope to determine the alignment when cooled into the LC phase. The temperature was stabilised for 1 min before taking each dielectric measurement at frequencies in the range of 20 Hz – 2 MHz for each temperature with an applied voltage of 1 V_{rms}. The temperature was maintained using a Linkam hot stage temperature controller.

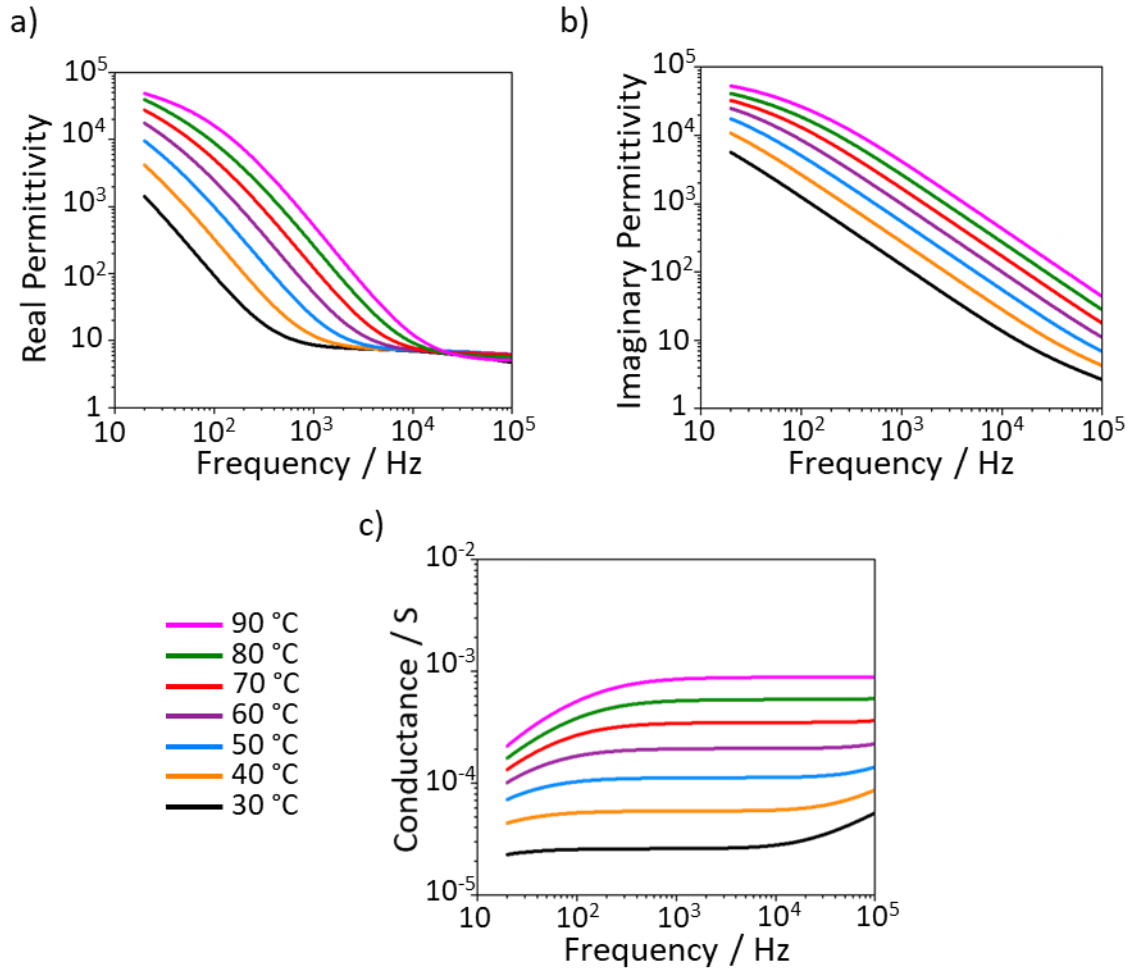

Figure 2.28: Dielectric measurements of **DC8**·Cl, showing a) real permittivity, b) imaginary permittivity, and c) conductance against frequency.

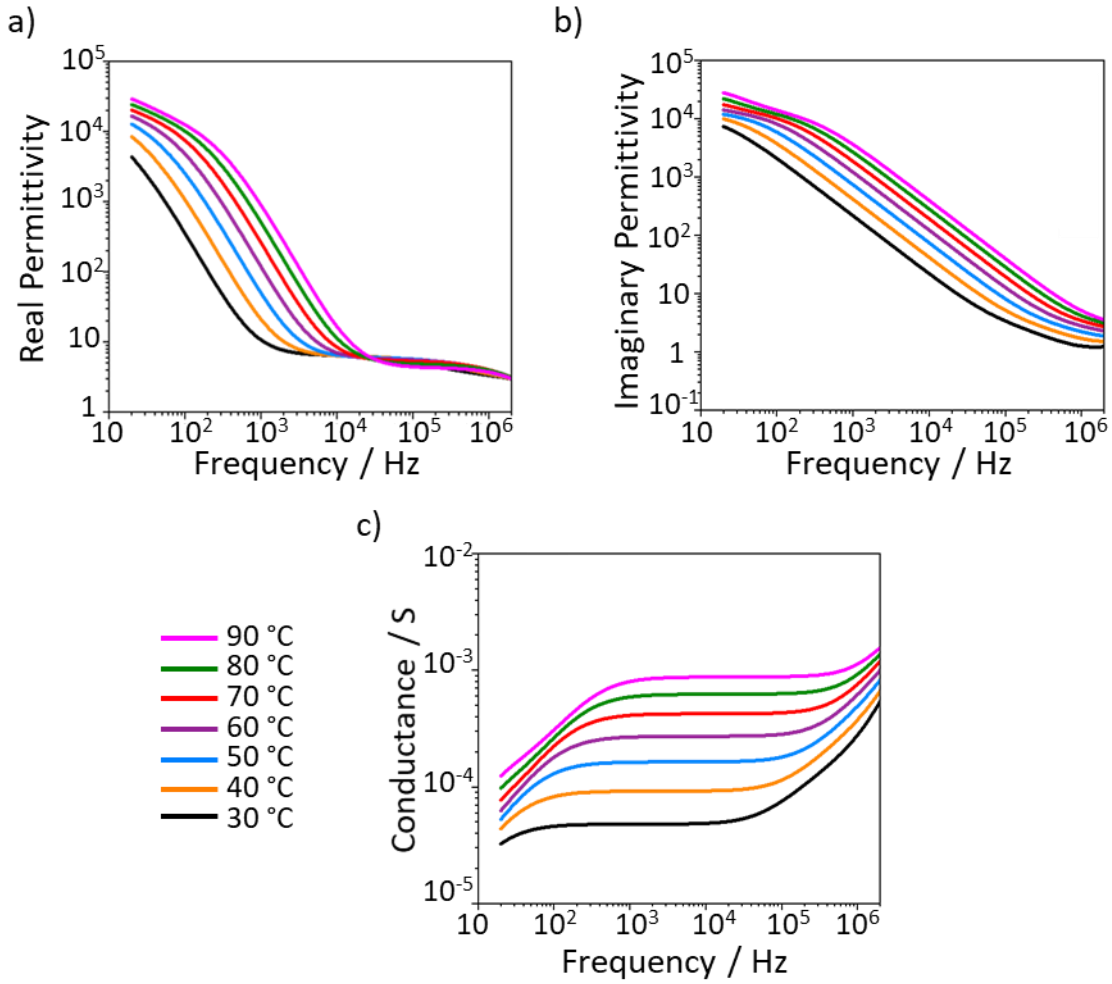

Figure 2.29: Dielectric measurements of **DC10**·Cl, showing a) real permittivity, b) imaginary permittivity, and c) conductance against frequency.

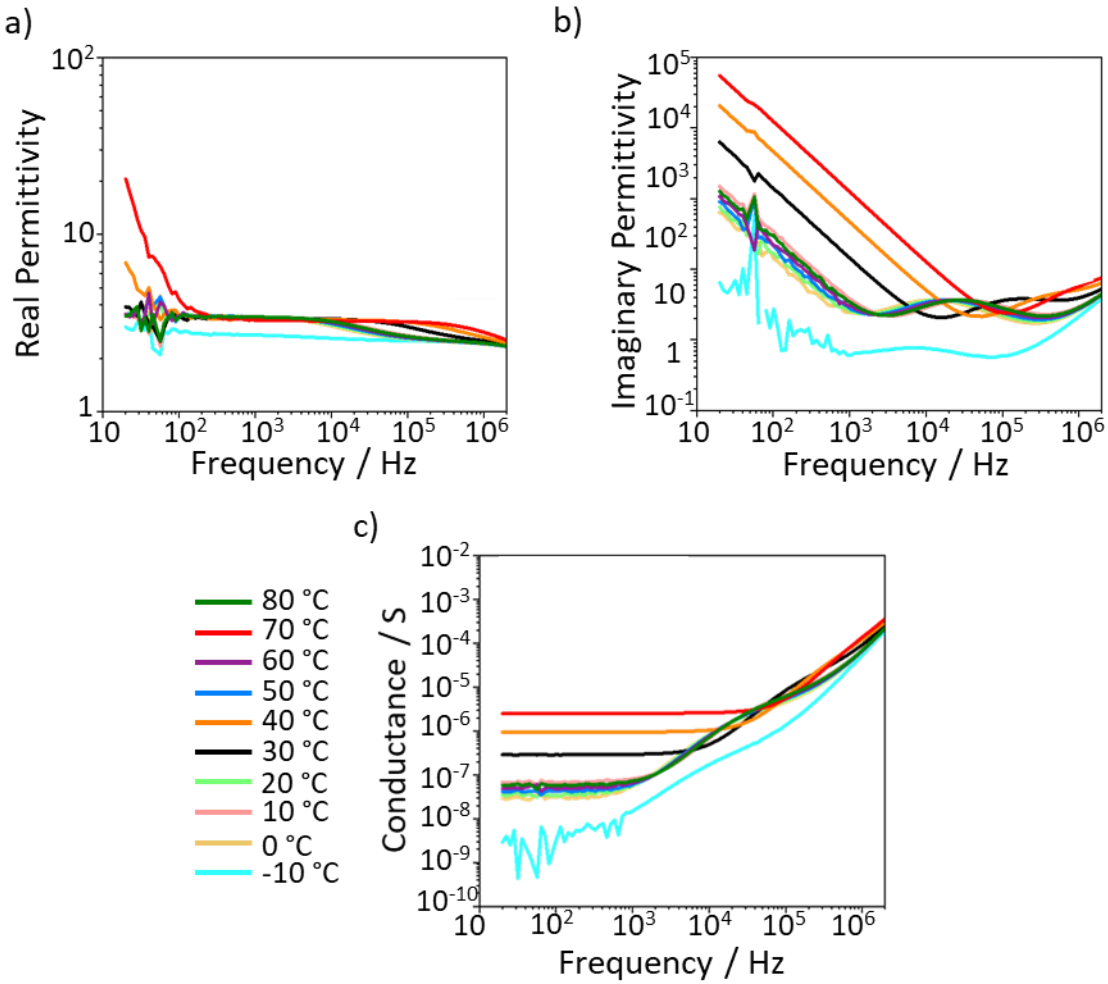

Figure 2.30: Dielectric measurements of **DC12**·Cl, showing a) real permittivity, b) imaginary permittivity, and c) conductance against frequency.

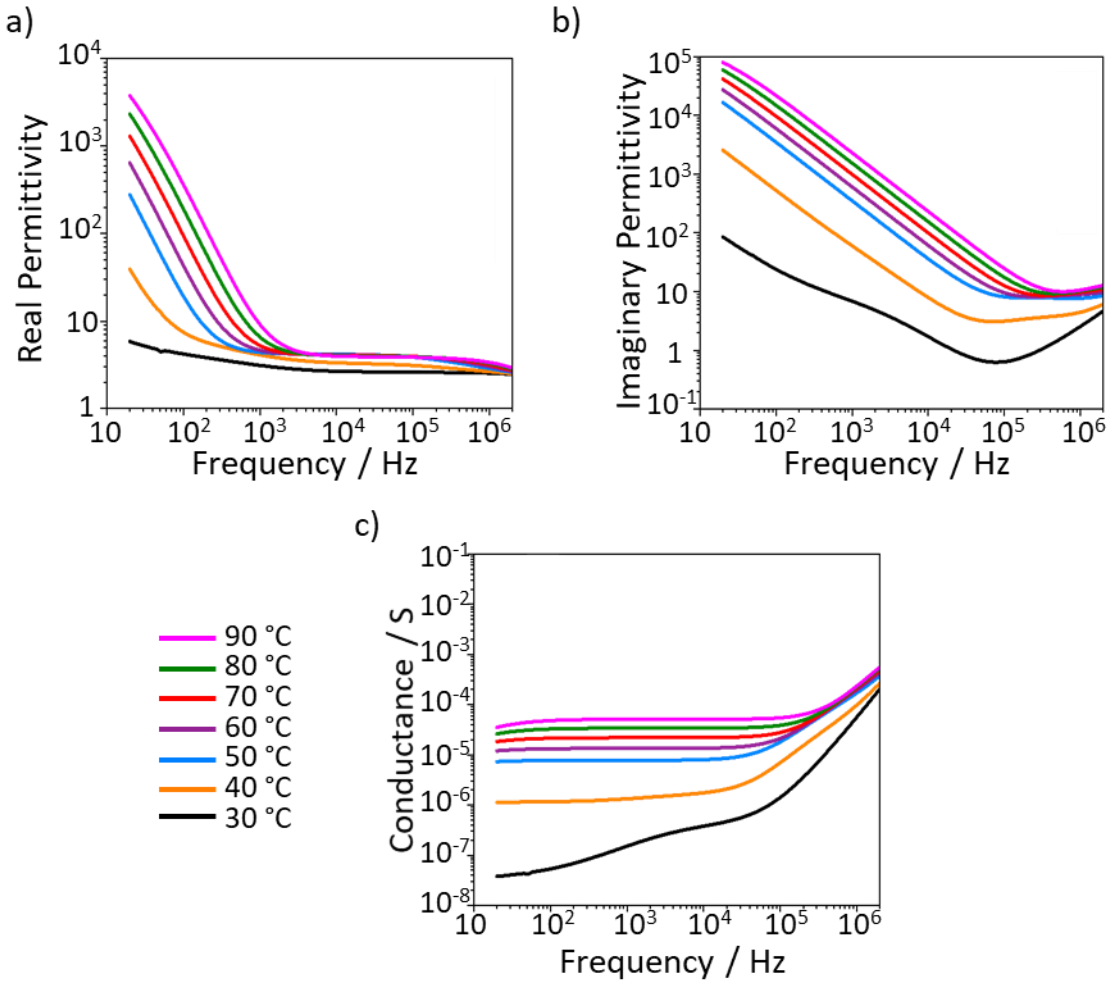

Figure 2.31: Dielectric measurements of **DC16**·Cl, showing a) real permittivity, b) imaginary permittivity, and c) conductance against frequency.

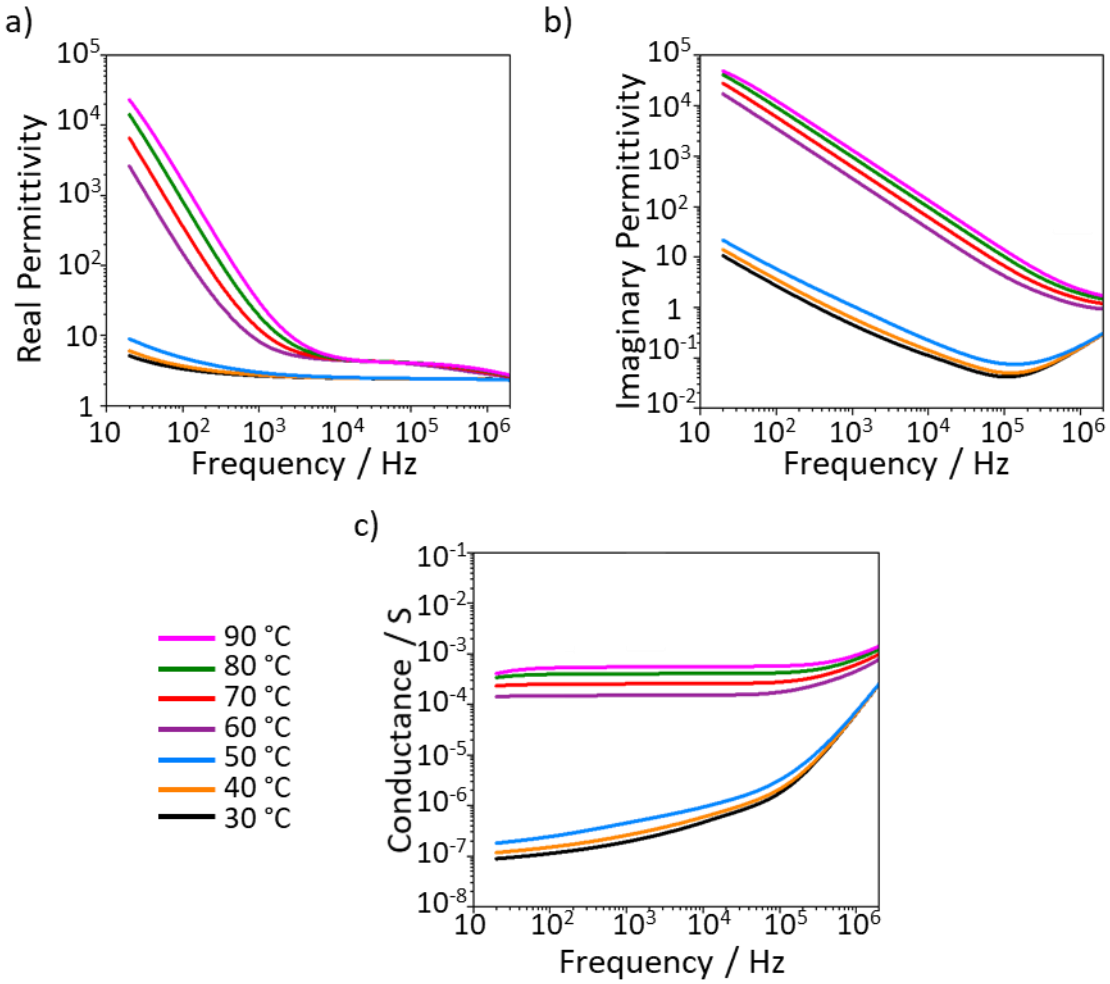

Figure 2.32: Dielectric measurements of **DC18**·Cl, showing a) real permittivity, b) imaginary permittivity, and c) conductance against frequency.

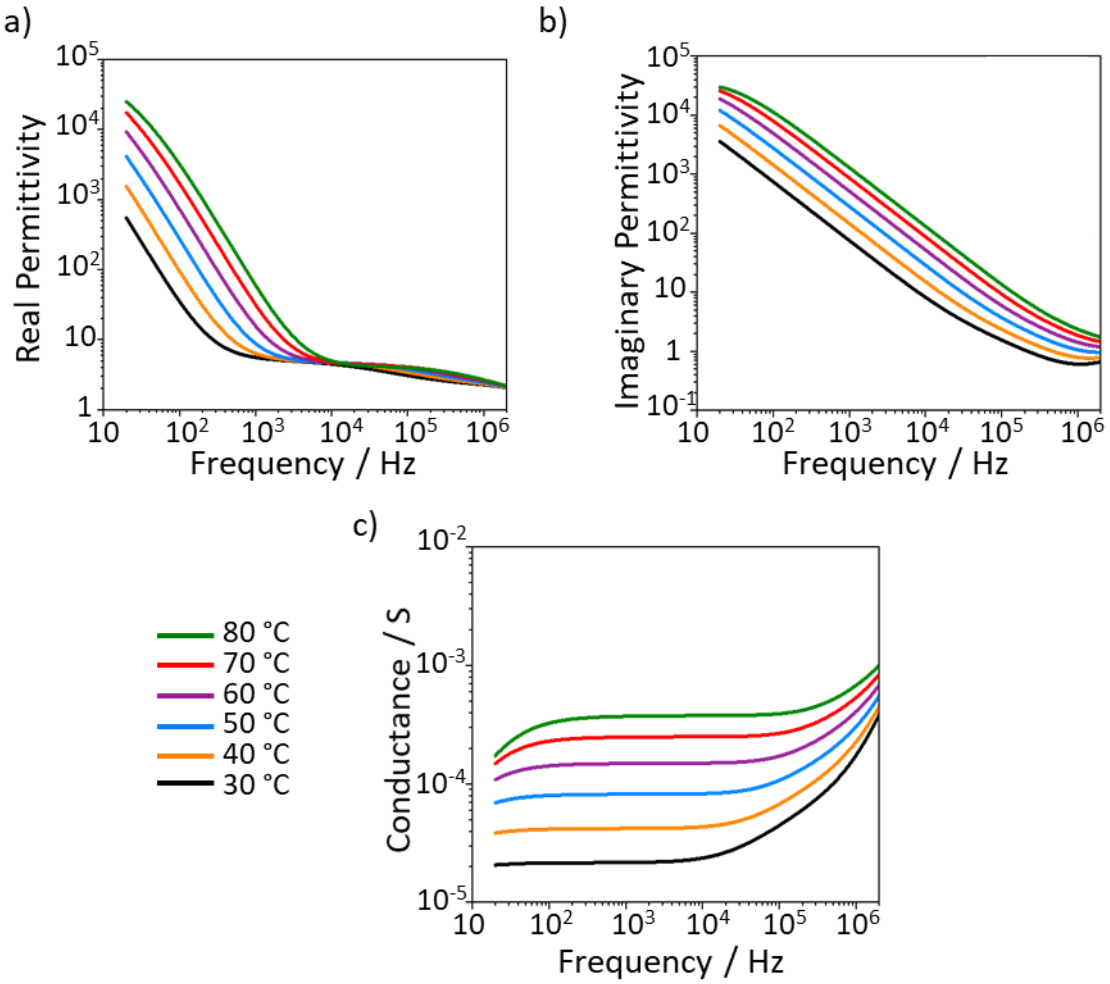

Figure 2.33: Dielectric measurements of **DC10**·Br, showing a) real permittivity, b) imaginary permittivity, and c) conductance against frequency.

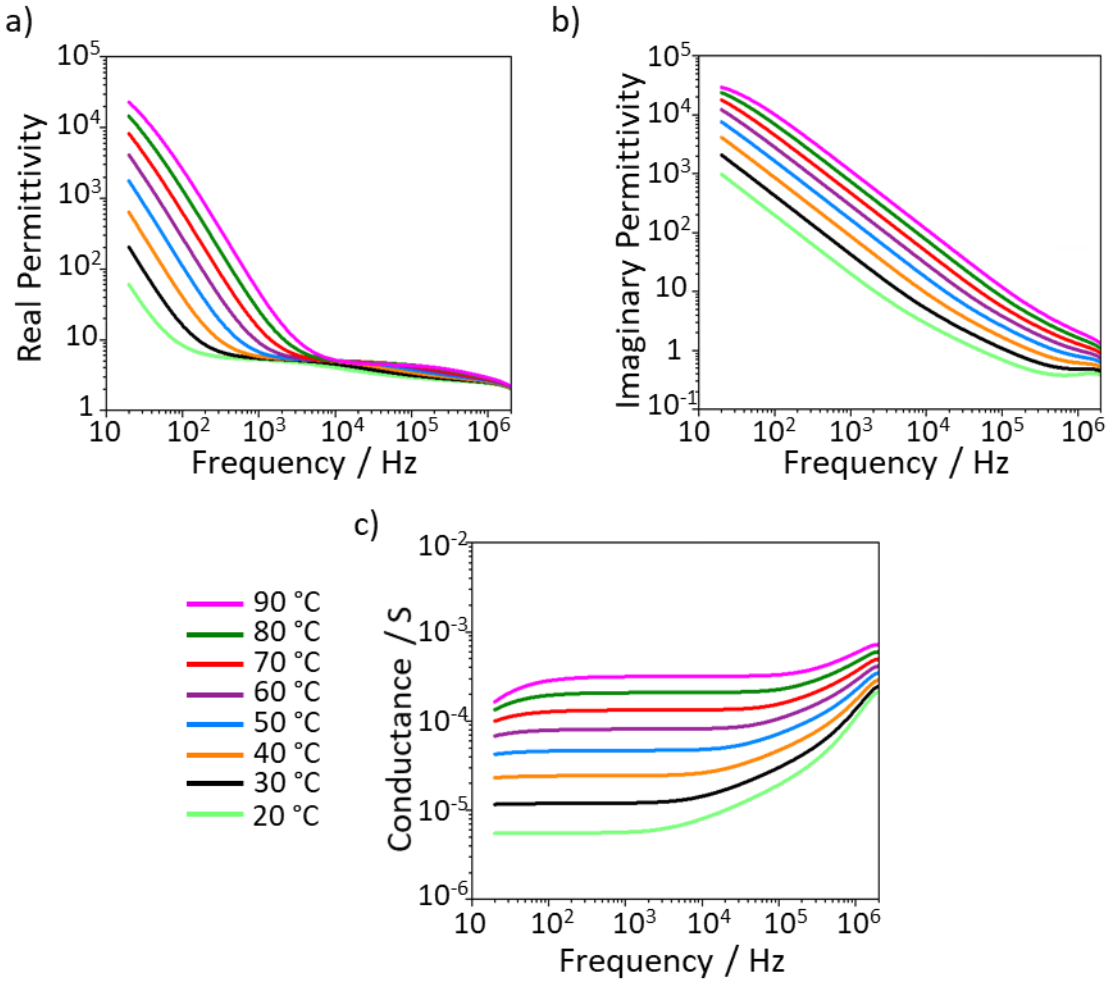

Figure 2.34: Dielectric measurements of **DC12**·Br, showing a) real permittivity, b) imaginary permittivity, and c) conductance against frequency.

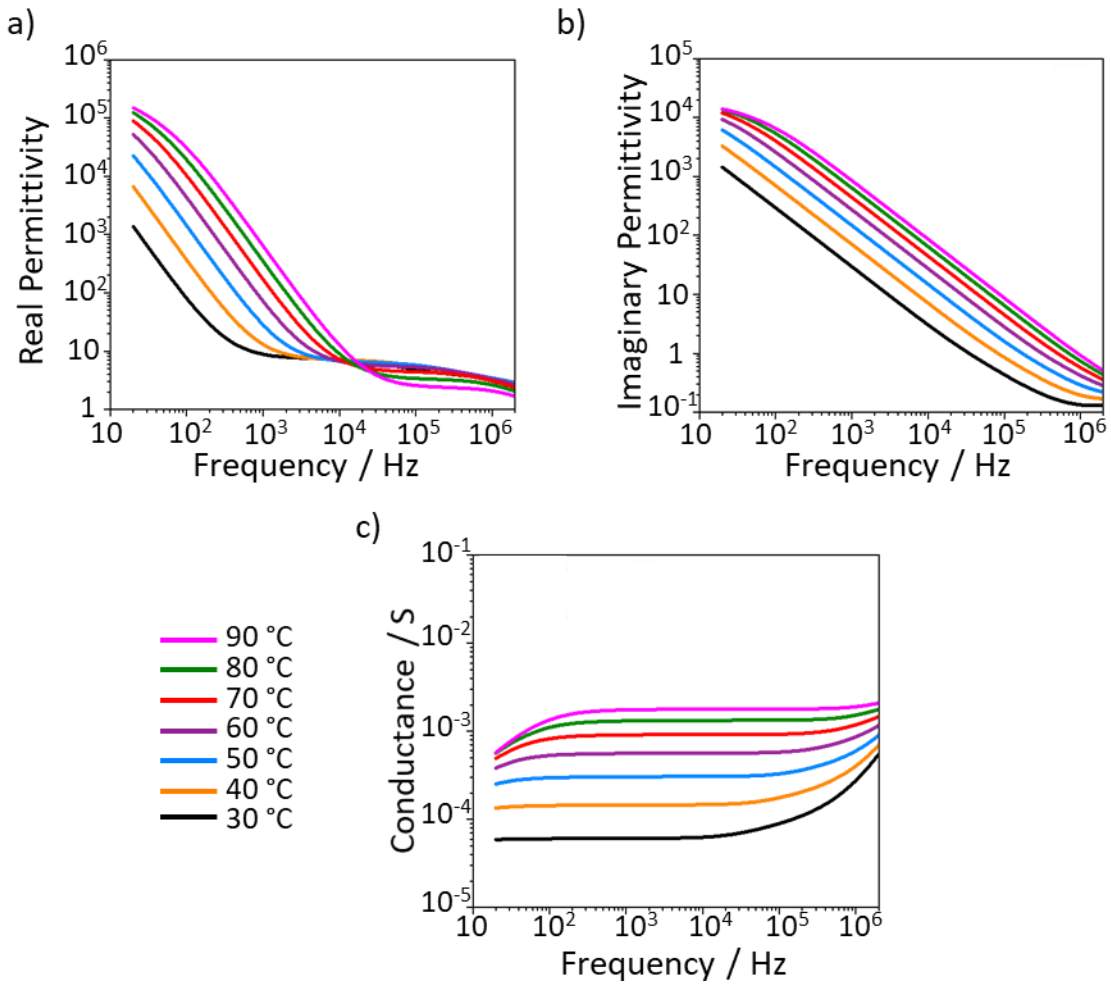

Figure 2.35: Dielectric measurements of **DC6,2**·Cl, showing a) real permittivity, b) imaginary permittivity, and c) conductance against frequency.

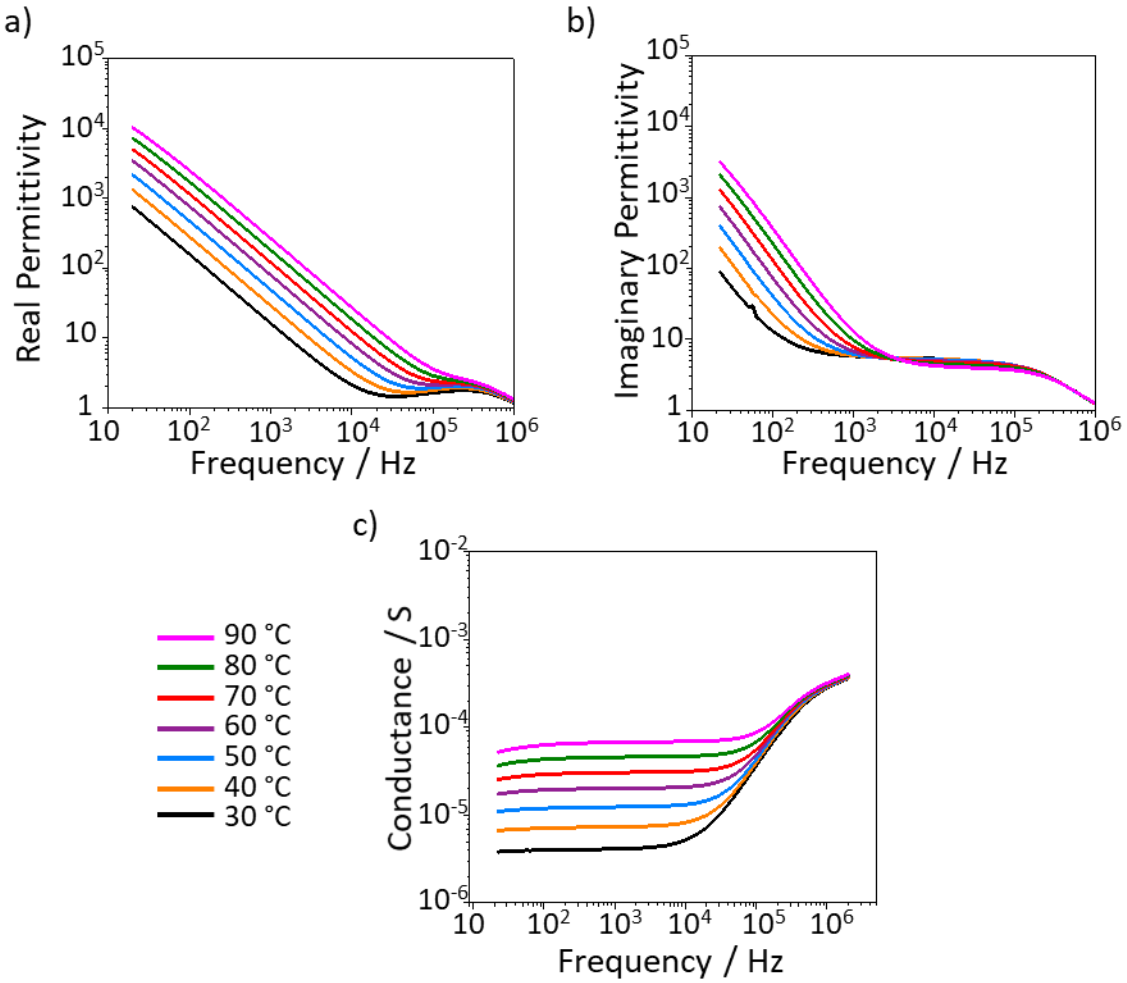

Figure 2.36: Dielectric measurements of **DC10**·Br doped with 10% LiBr, showing a) real permittivity, b) imaginary permittivity, and c) conductance against frequency.

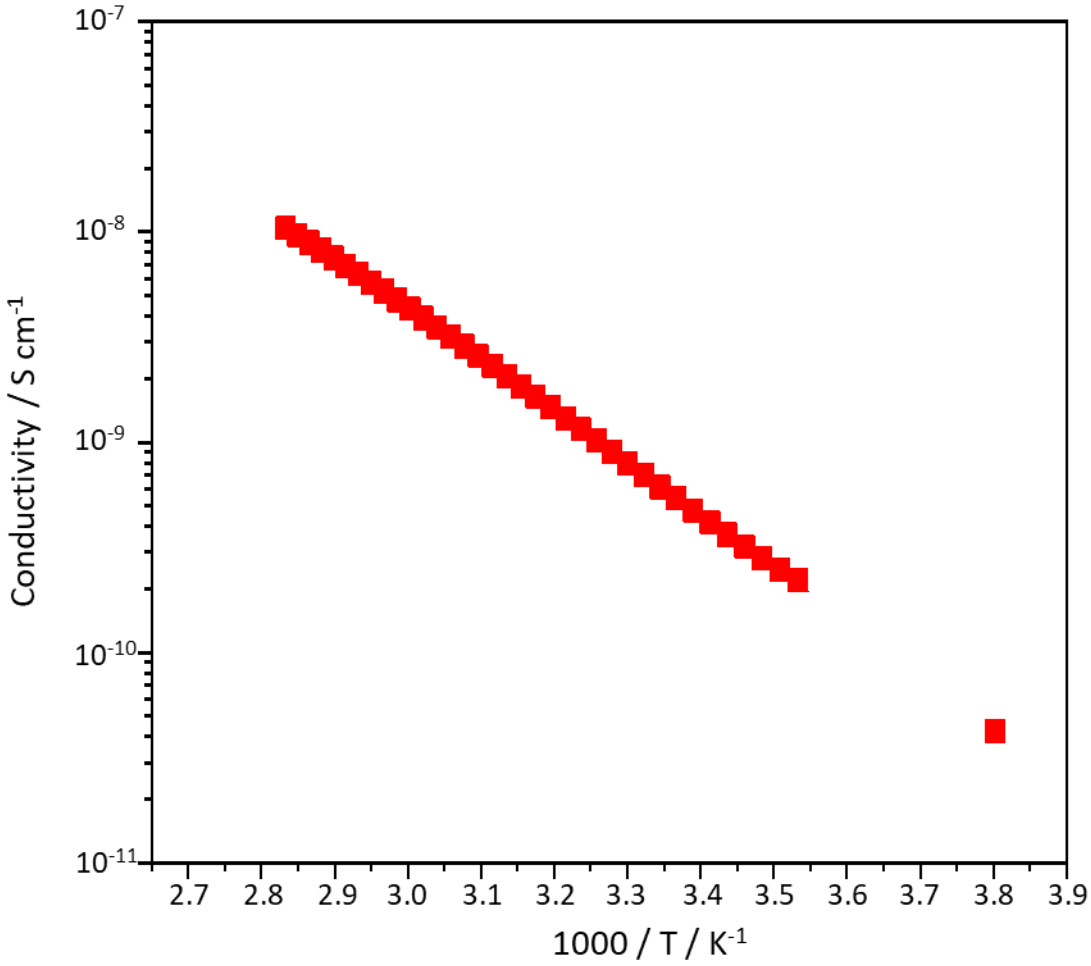

Figure 2.37: Full range of conductivity against temperature measurements for **DC12**·Cl.

2.6.4 Cyclic Voltammetry

CV was performed using an EmStat3 potentiostat in 1 mM solutions of CH_2Cl_2 with 0.1 M of NBu_4PF_6 electrolyte, at a scan rate of 0.1 V s^{-1}. A glassy carbon working electrode, a platinum counter electrode and a AgCl/Ag reference electrode were used.

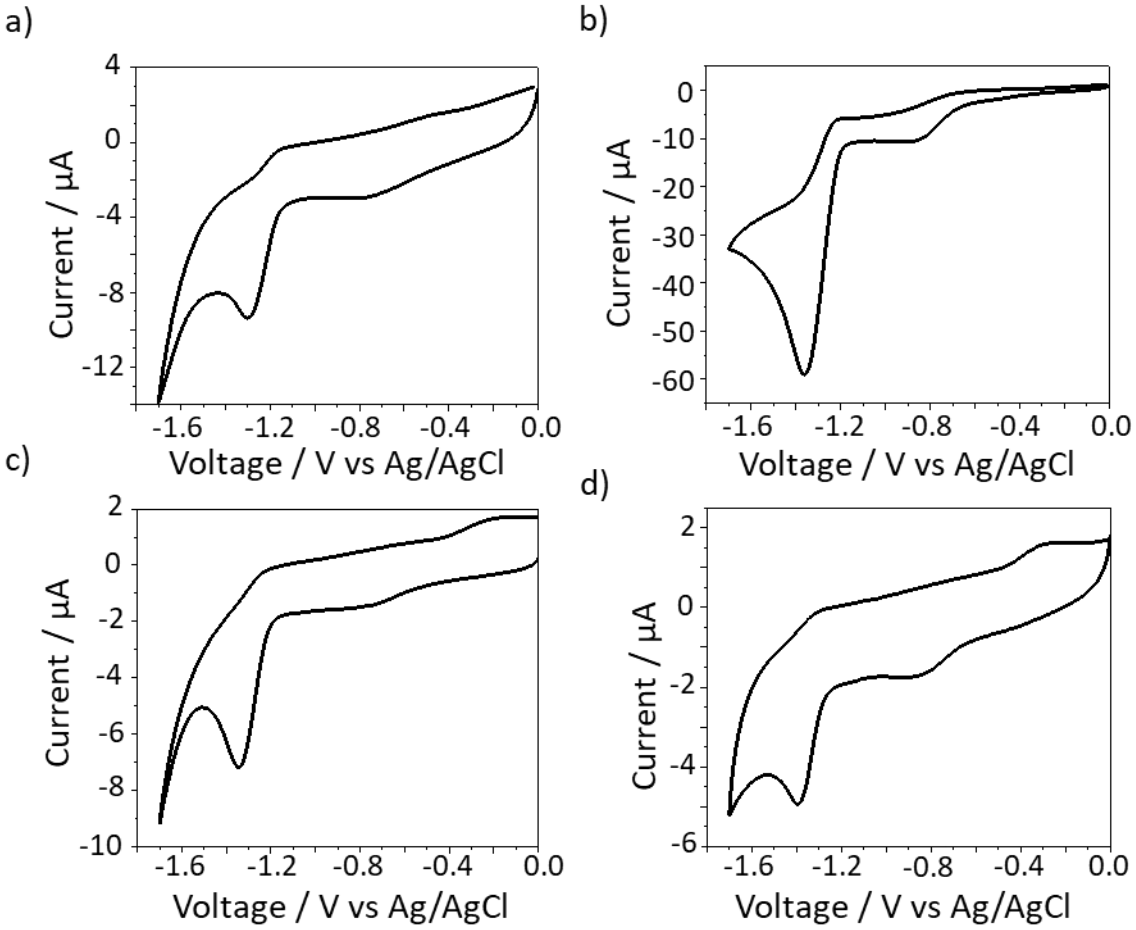

Figure 2.38: Cyclic voltammograms of cyclopropenium compounds at 1 mM concentration in CH_2Cl_2 with NBu_4PF_4 electrolyte at 0.1 M concentration, showing a) **DC1**·Cl, b) **DC8**·Cl, c) **DC10**·Cl and d) **DC12**·Cl.

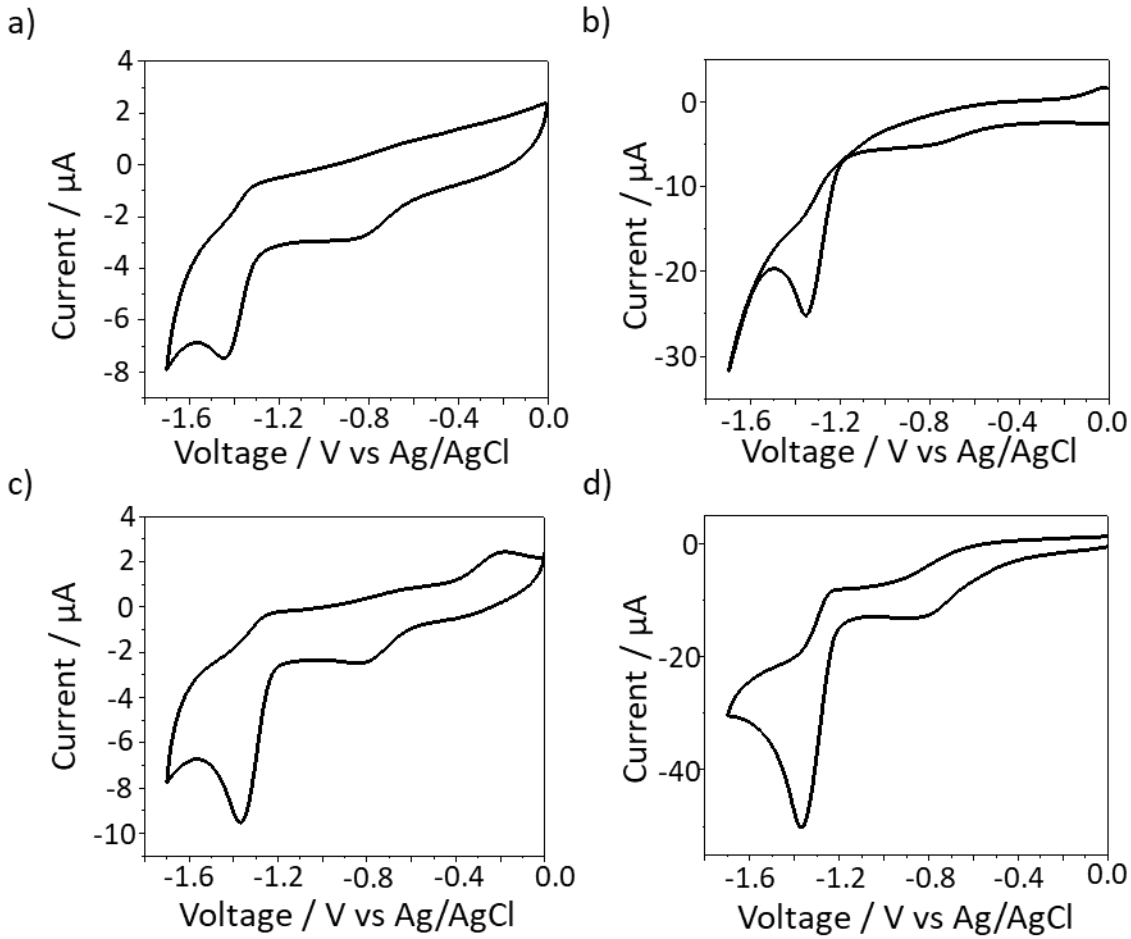

Figure 2.39: Cyclic voltammograms of cyclopropenium compounds at 1 mM concentration in CH_2Cl_2 with NBu_4PF_4 electrolyte at 0.1 M concentration, showing a) **DC16**·Cl, b) **DC18**·Cl, c) **DC10**·Br and d) **DC12**·Br.

2.6.5 UV-vis Spectroscopy

UV-vis spectroscopy was performed on each compound in the range of 200-800 nm wavelengths through a 10 mm path length cuvette, in a $CHCl_3$ solution at 0.001-0.01 mM concentration.

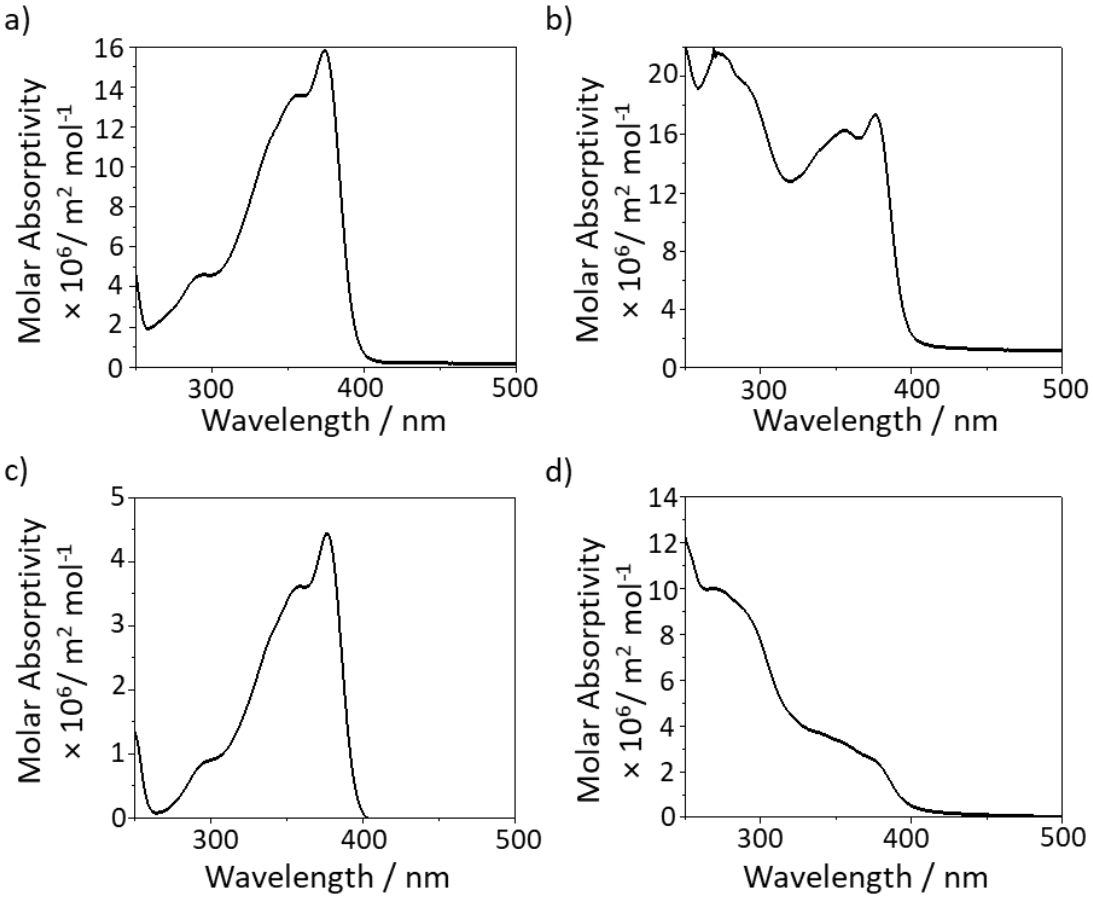

Figure 2.40: UV-vis spectra of cyclopropenium compounds in $CHCl_3$, showing a) **DC1**·Cl at 0.002 mM concentration, b) **DC8**·Cl at 0.002 mM concentration, c) **DC10**·Cl at 0.01 mM concentration and d) **DC12**·Cl at 0.01 mM concentration.

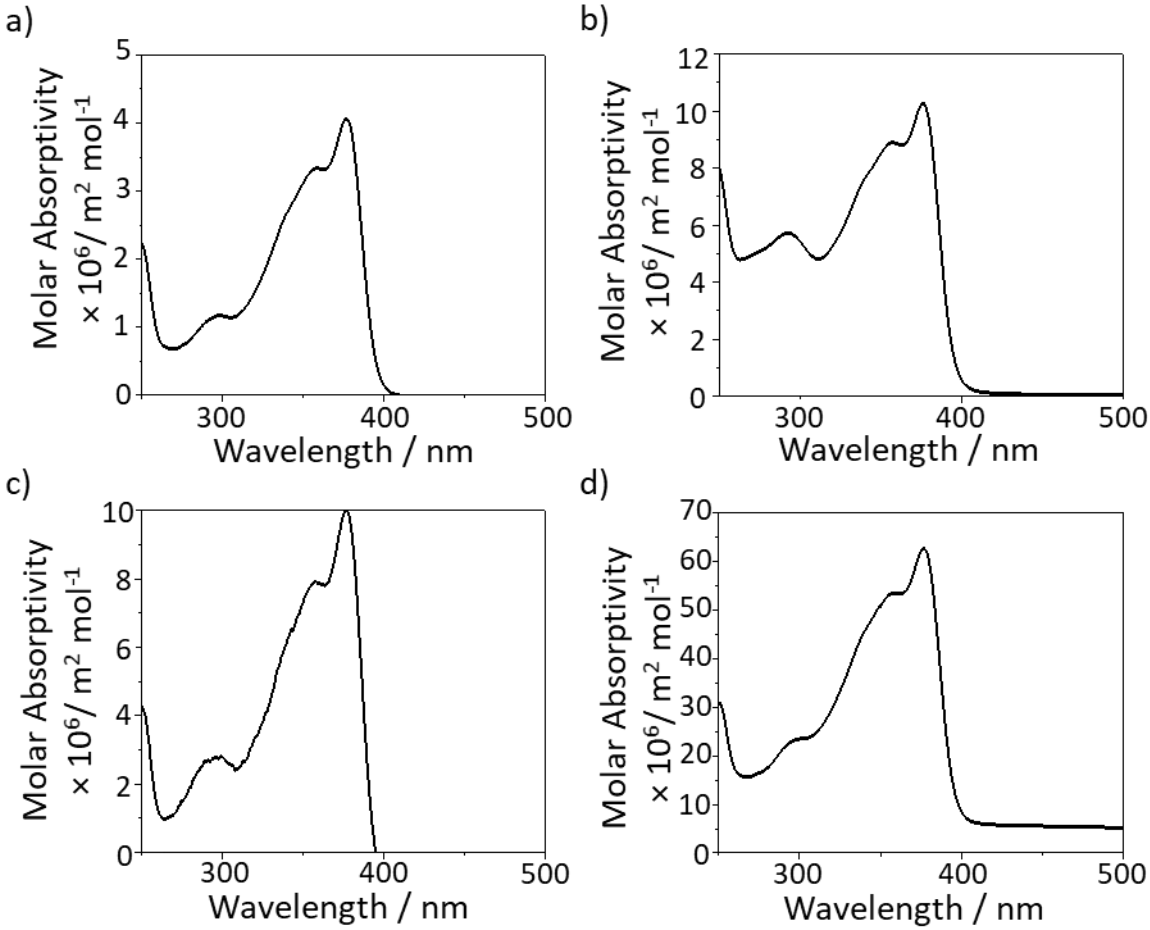

Figure 2.41: UV-vis spectra of cyclopropenium compounds in $CHCl_3$, showing a) **DC16**·Cl at 0.01 mM concentration, b) **DC18**·Cl at 0.01 mM concentration, c) **DC10**·Br at 0.01 mM concentration and d) **DC12**·Br at 0.001 mM concentration.

2.6.6 X-Ray Diffraction Spectroscopy

The XRD measurements were performed with samples on glass slides by heating from RT. The detector to sample distances were 26.90 cm for SAXD experiments (measuring time: 30 min) and 9.00 cm for WAXD experiments (measuring time: 15 min).

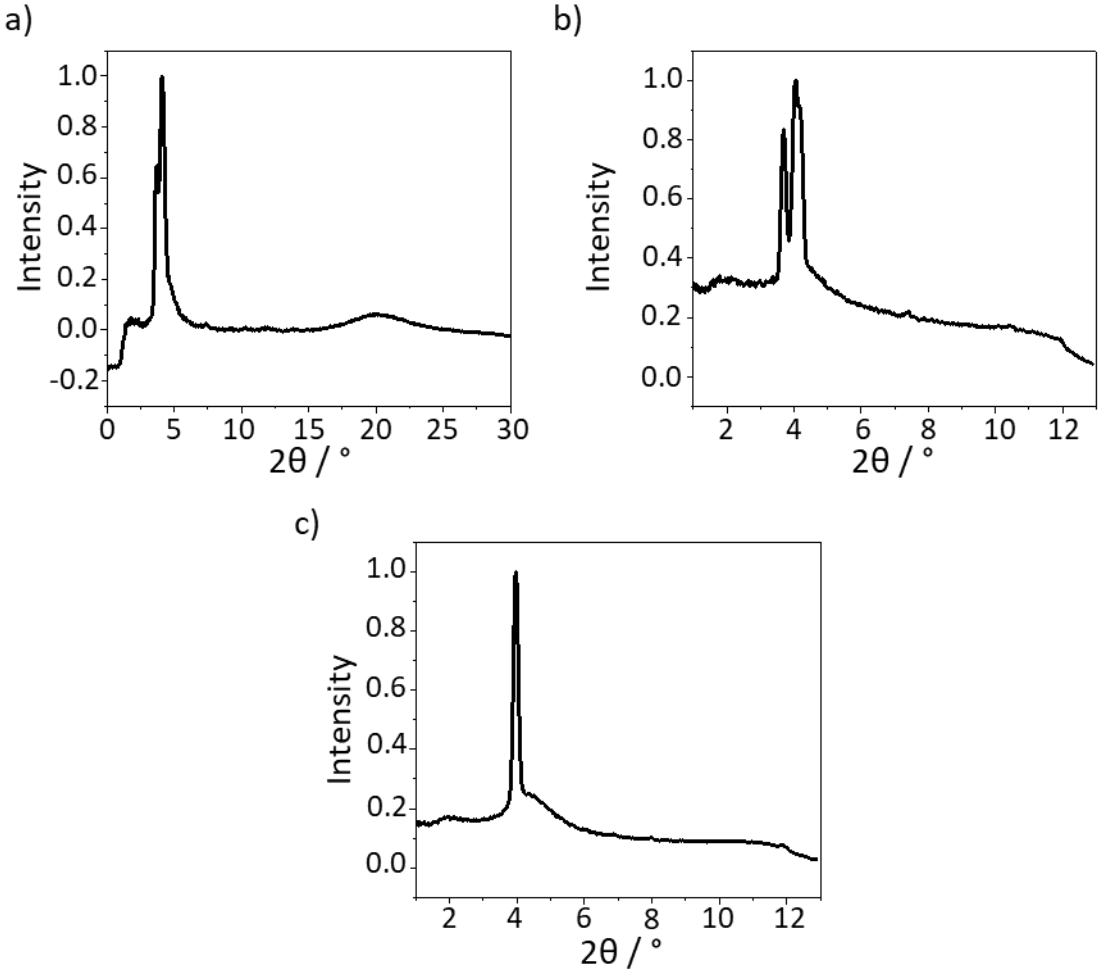

Figure 2.42: XRD spectra of **DC8**·Cl, showing a) WAXD spectrum at 70 °C, b) SAXD spectrum at 70 °C, and c) SAXD spectrum at 90 °C.

Table 2.7: Data from the XRD patterns of **DC8**·Cl at 70 ºC.

2 θ	**θ**	***d*-value / nm**
3.689	1.845	2.395
4.034	2.017	2.190
4.206	2.103	2.101
7.334	3.667	1.205
10.031	5.015	0.882
10.995	5.497	0.805
20.203	10.101	0.440

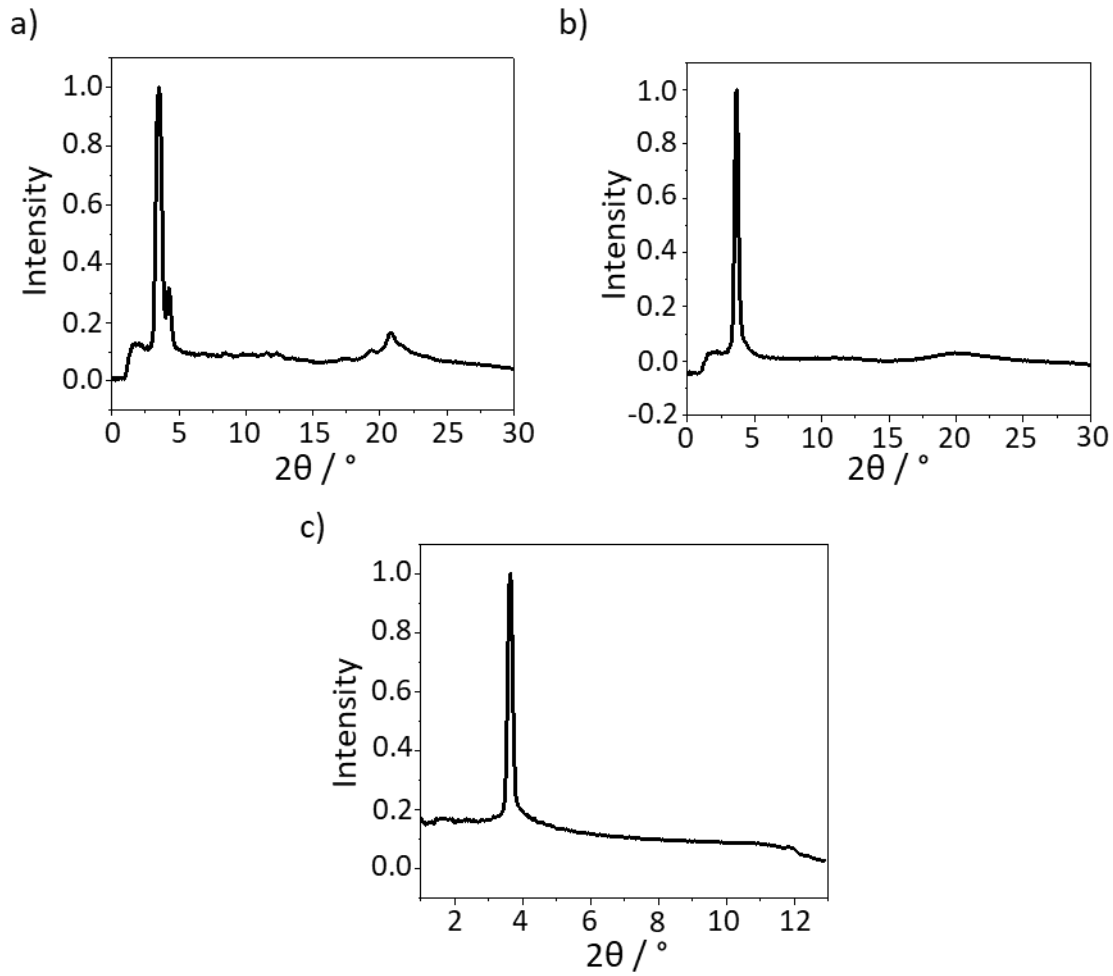

Figure 2.43: XRD spectra of **DC10**·Cl, showing a) WAXD spectrum at RT, b) WAXD spectrum at 52 °C, and c) SAXD spectrum at 52 °C.

Table 2.8: Data from the peaks of the XRD patterns of **DC10**·Cl at RT.

2 θ	**θ**	***d*-value / nm**
3.505	1.753	2.521
4.238	2.119	2.085
6.817	3.409	1.297
8.490	4.245	1.042
10.481	5.240	0.844
11.533	5.766	0.767
12.302	6.151	0.719
19.473	9.737	0.456
20.843	10.422	0.426
21.540	10.770	0.413
23.327	11.664	0.381

Table 2.9: Data from the peaks of the XRD patterns of **DC10**·Cl at 52 ºC.

2 θ	**θ**	***d*-value / nm**
3.640	1.820	2.427
9.581	4.790	0.923
10.884	5.442	0.813
20.295	10.147	0.438

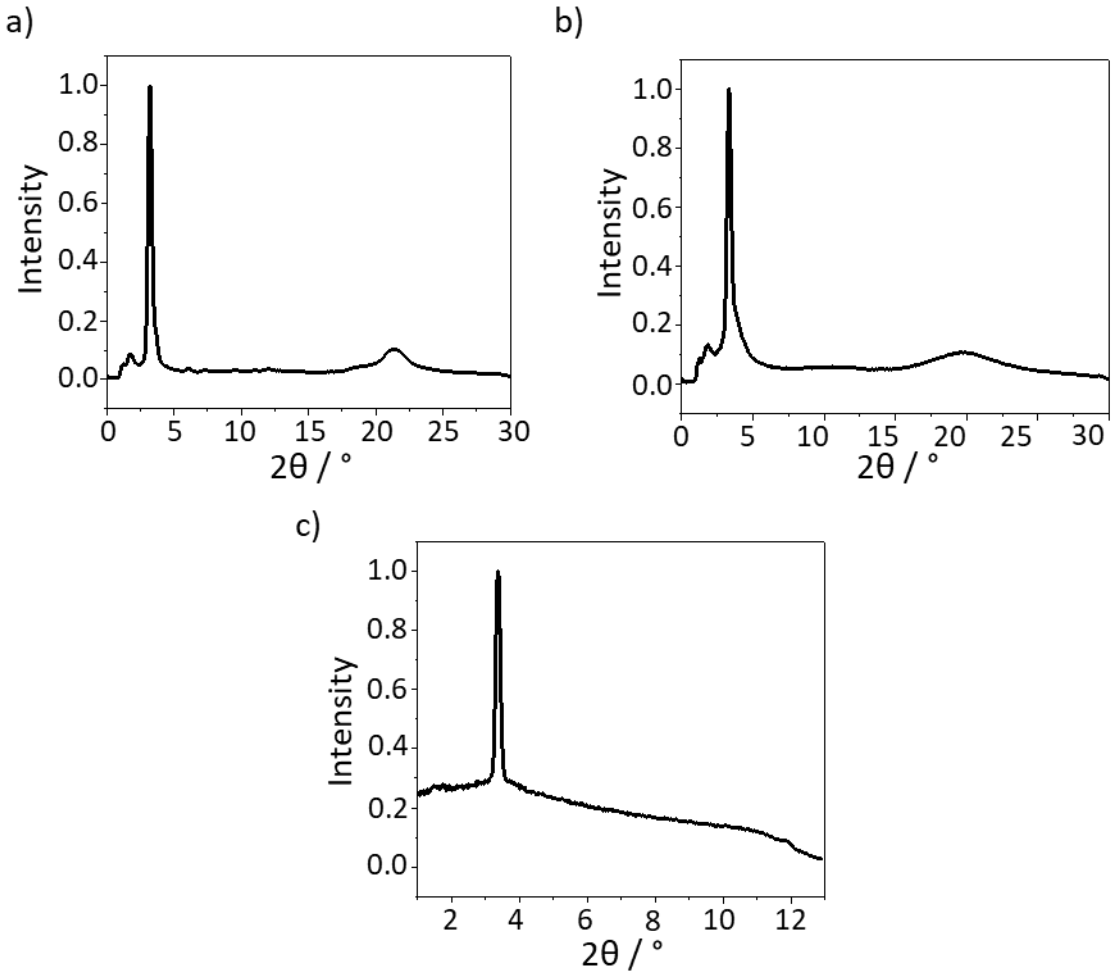

Figure 2.44 XRD spectra of **DC12**·Cl, showing a) WAXD spectrum at RT, b) WAXD spectrum at 60 °C, and c) SAXD spectrum at 60 °C.

Table 2.10: Data from the XRD patterns of **DC12**·Cl at RT.

2 θ	**θ**	***d*-value / nm**
3.223	1.612	2.741
3.622	1.811	2.439
6.053	3.026	1.460
7.300	3.650	1.211
8.102	4.051	1.091
9.522	4.761	0.929
11.017	5.509	0.803
12.020	6.010	0.736
18.767	9.384	0.473
21.383	10.692	0.416

Table 2.11: Data from the XRD patterns of **DC12**·Cl at 60 ºC.

2 θ	**θ**	***d*-value / nm**
3.375	1.687	2.618
5.835	2.918	1.515
8.899	4.450	0.994
20.008	10.004	0.444

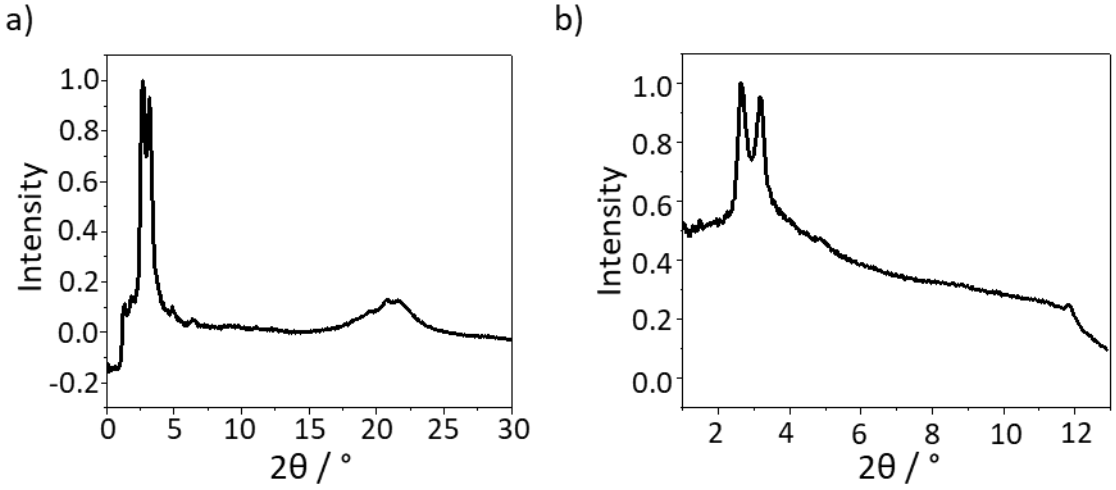

Figure 2.45: XRD spectra of **DC16**·Cl, showing a) WAXD spectrum at 50 °C, b) SAXD spectrum at 50 °C.

Table 2.12: Data from the XRD patterns of **DC16**·Cl at 50 ºC.

2 θ	**θ**	***d*-value / nm**
2.664	1.332	3.317
3.156	1.578	2.799
4.874	2.437	1.813
6.387	3.194	1.384
19.576	9.788	0.453
20.864	10.432	0.426
21.577	10.789	0.412

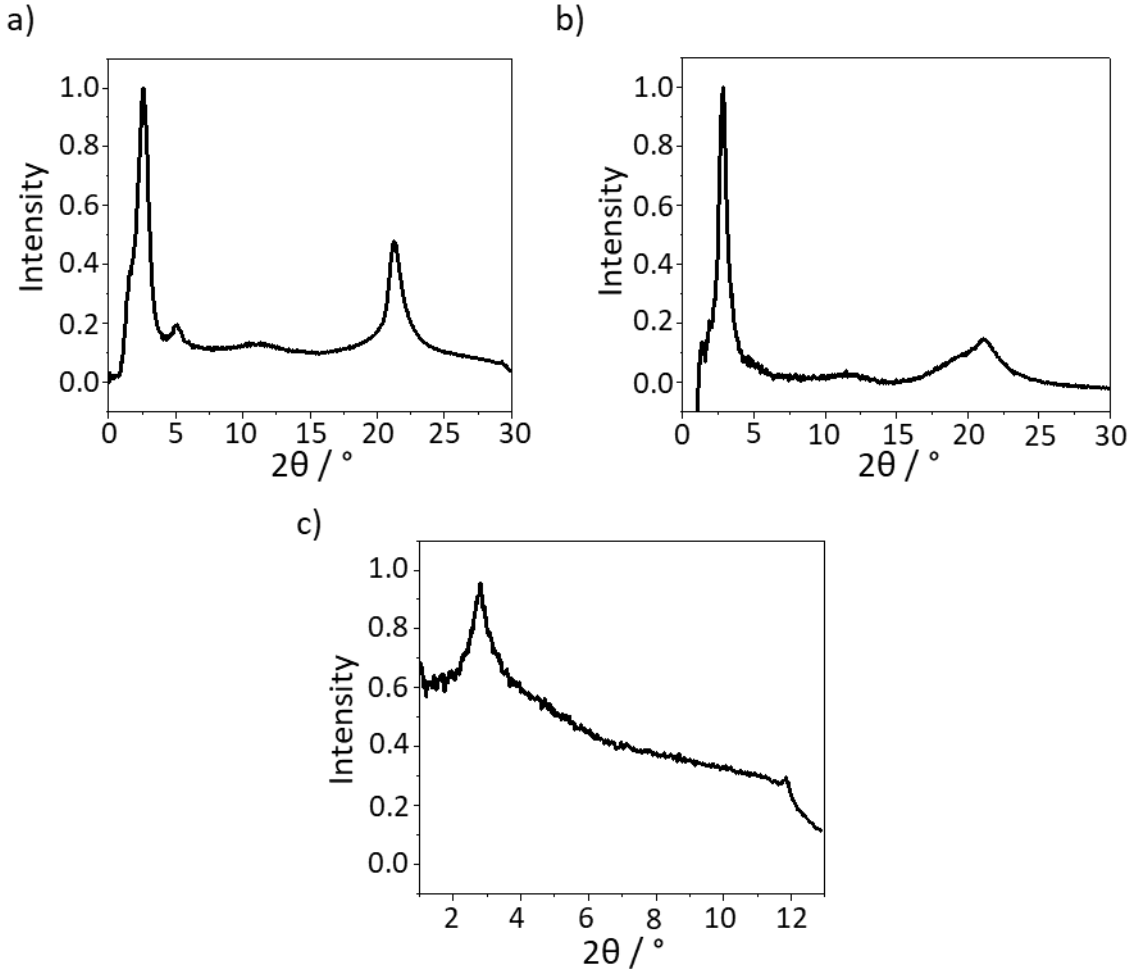

Figure 2.46: XRD spectra of **DC18**·Cl, showing a) WAXD spectrum at RT, b) WAXD spectrum at 60 °C, and c) SAXD spectrum at 60 °C.

Table 2.13: Data from the XRD patterns of **DC18**·Cl at RT.

2 θ	**θ**	***d*-value / nm**
2.556	1.278	3.457
5.043	2.521	1.752
21.324	10.662	0.417

Table 2.14: Data from the XRD patterns of **DC18**·Cl at 60 ºC.

2 θ	**θ**	***d*-value / nm**
2.789	1.394	3.168
18.984	9.492	0.467
21.210	10.605	0.419

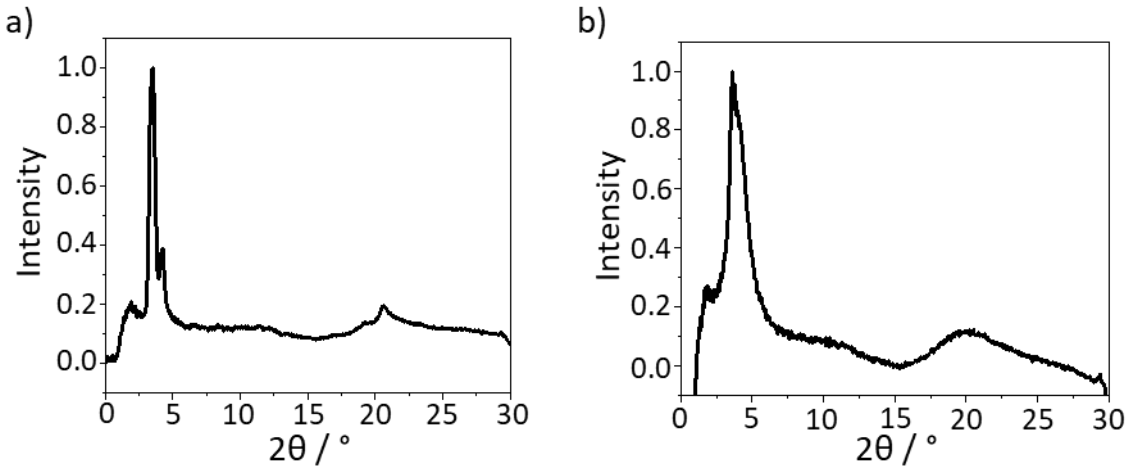

Figure 2.47: XRD spectra of **DC10**·Br, showing WAXD spectra at a) RT, and b) 70 °C.

Table 2.15: Data from the XRD patterns of **DC10**·Br at 70 ºC.

2 θ	**θ**	***d*-value / nm**
3.607	1.804	2.449
4.022	2.011	2.197
20.187	10.094	0.440

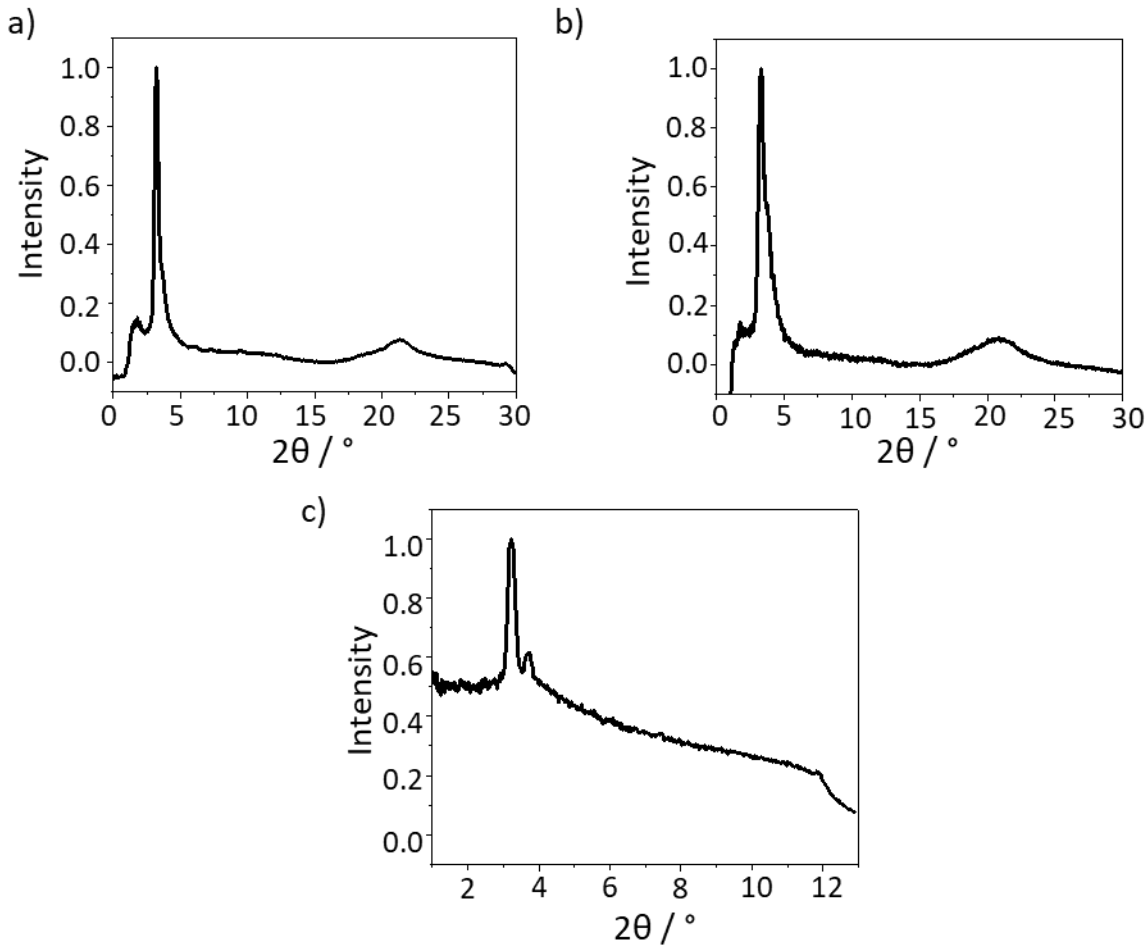

Figure 2.48: XRD spectra of **DC12**·Br, showing a) WAXD spectrum at RT, a) WAXD spectrum at 50 °C, and c) SAXD spectrum at 50 °C.

Table 2.16: Data from the XRD patterns of **DC12**·Br at RT.

2 θ	**θ**	***d*-value / nm**
18.752	9.376	0.473
21.304	10.652	0.417

Table 2.17: Data from the XRD patterns of **DC12**·Br at 50 ºC.

2 θ	**θ**	***d*-value / nm**
3.231	1.615	2.735
3.695	1.847	2.391
18.476	9.238	0.480
20.867	10.433	0.426

2.6.7 Density Functional Theory Calculations

The cyclopropenium cation structure was drawn and results visualised using Gaussview. The DFT calculations were performed in two sets, both using Gaussian 16[19]. For both sets, the geometry of the triphenylcyclopropenium cation core was optimised using a B3LYP[37] functional with 6-31G(d.p) basis set.[38, 39, 40] For the first set of calculations, the terminal alkyl chains were then added to the core, and the structure optimisation was performed using a multilayer approach keeping the basis set constant for the central core and using a reduced 3-21g basis set for the surrounding alkyl chains. This was carried out to give a planar structure of the most extended conformer. For the second set of calculations, frequency calculations were performed to confirm the lack of any negative vibrational frequencies. Electrostatic potential maps are plotted at an electron density isovalue of 0.001.

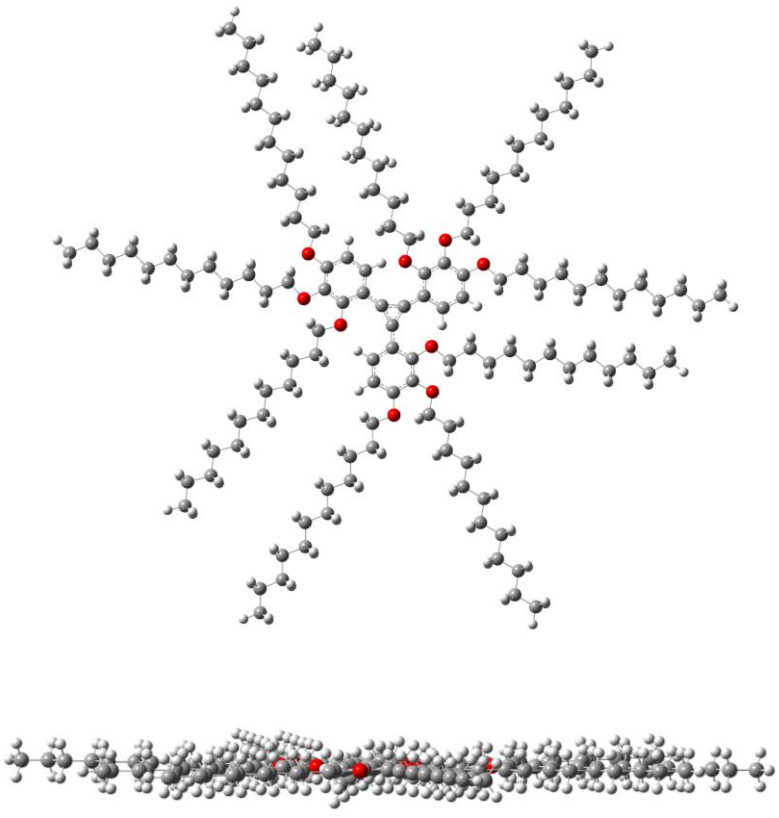

Figure 2.49: The Guassian optimised structure of the DC12 cation, showing a width of 42.5 Å, and a significantly lower height (~3 Å).

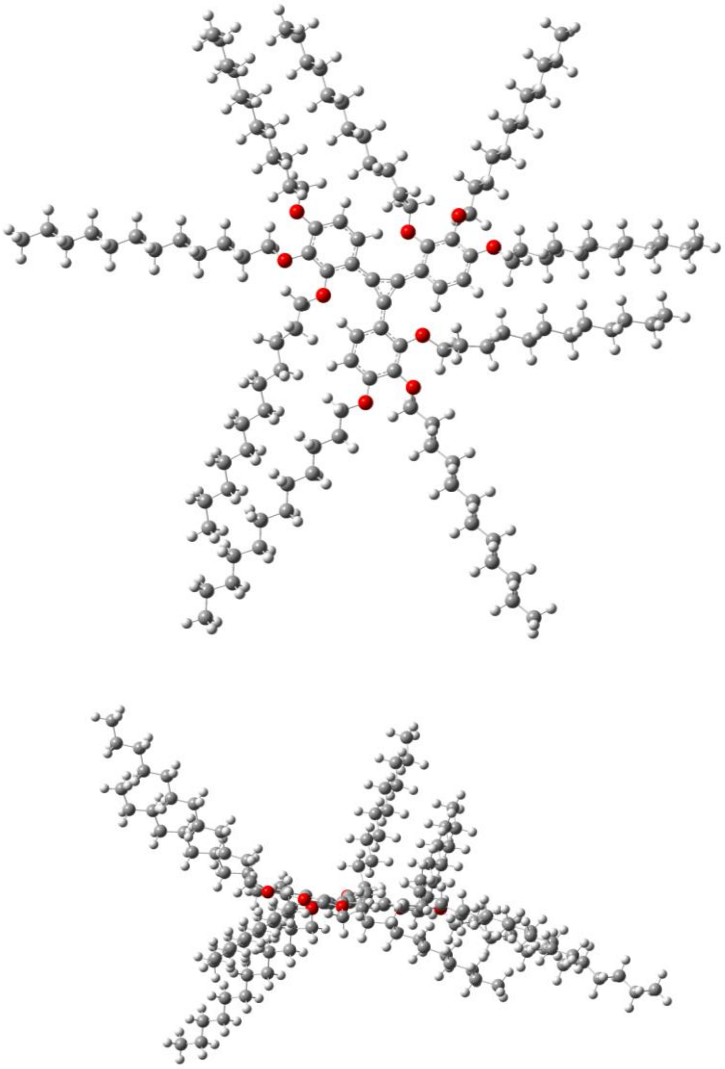

Figure 2.50: Semi-empirical optimisation with AM1 base set (Gaussian) structure of the **DC12** cation, showing a width of 39.7 Å and a mean height of 24.5 Å.

Table 2.18: Width of the **DCn** cations with the arrangement as shown in Figure 2.49.

Cation	Mean width / Å
DC8	30.9
DC10	35.9
DC12	42.3
DC14	45.8
DC16	50.7
DC18	55.7

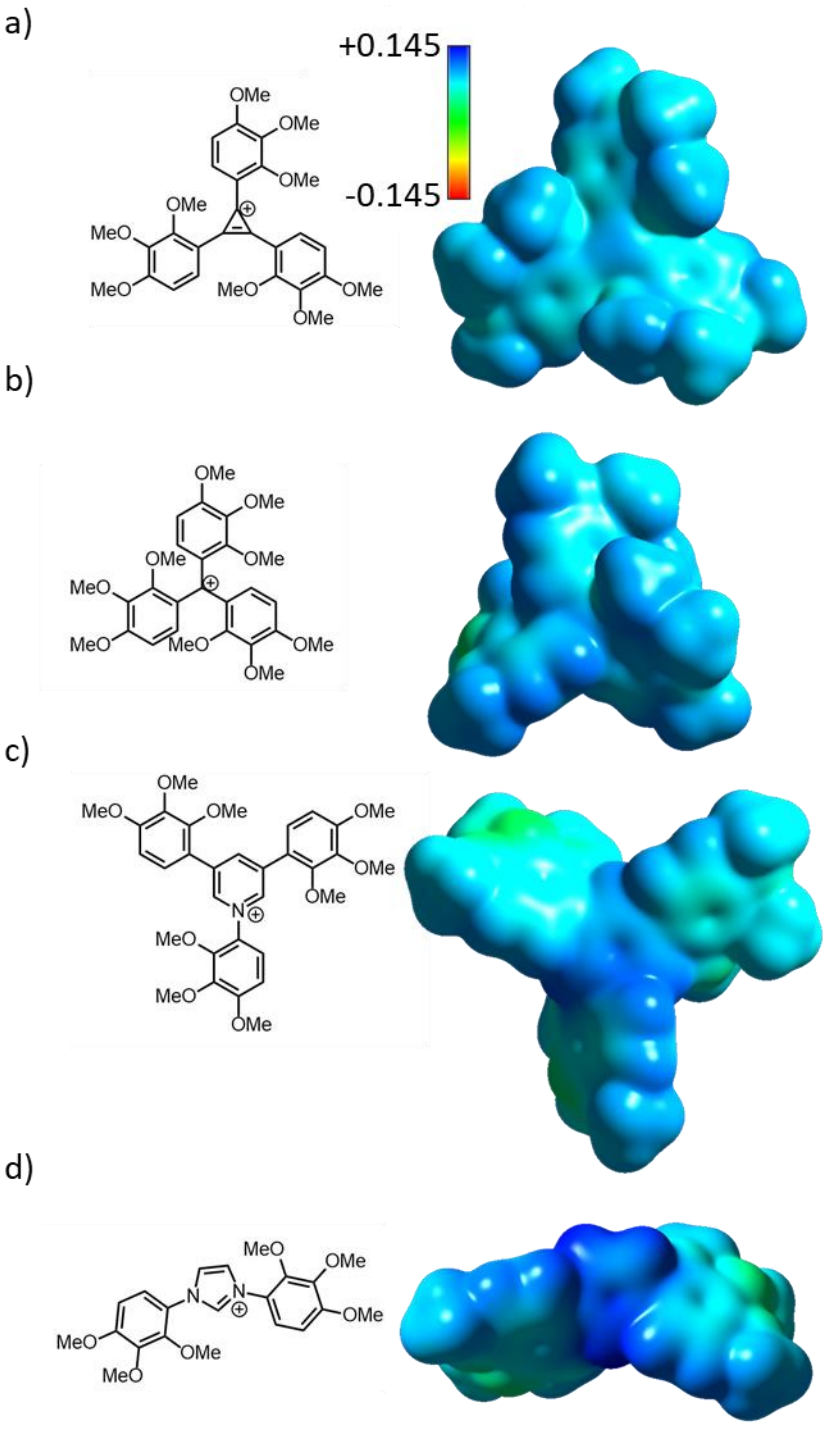

Figure 2.51: ESP maps of a) **DC1** cation, b) tris(1,2,3-trimethoxy)phenylmethyl cation, c) tris(1,2,3-trimethoxy)phenylpyridinium cation, and d) di(1,2,3-trimethoxy)imidazolium cation.

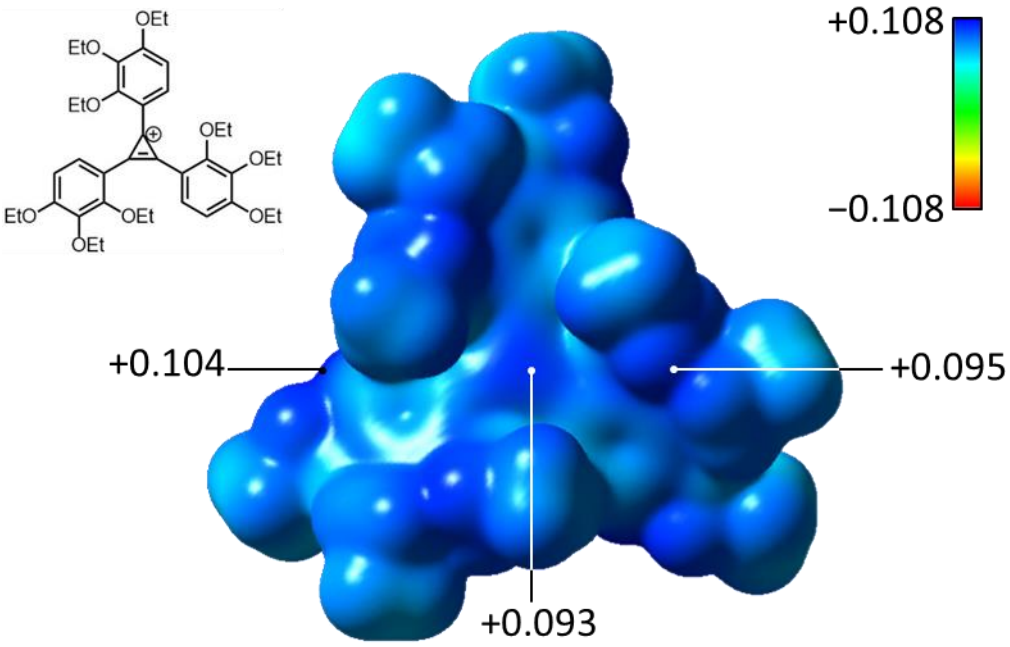

Figure 2.52: ESP map of **DC2** cation.

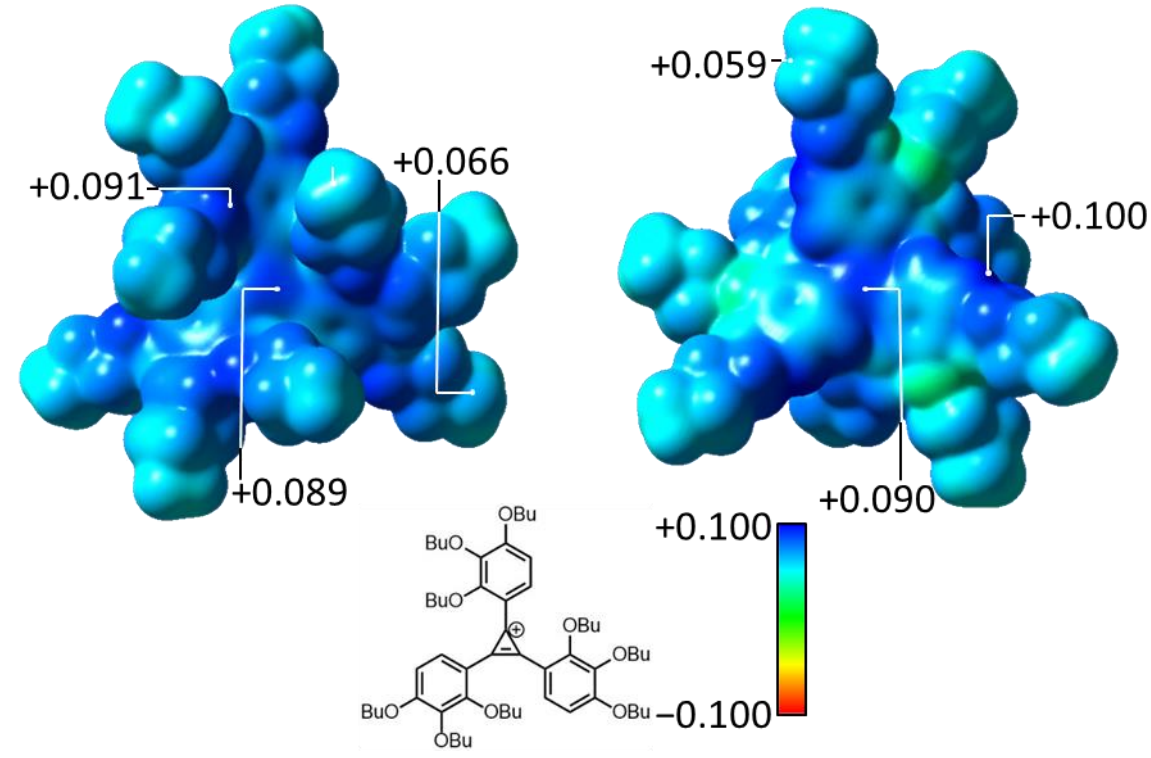

Figure 2.53: ESP map of **DC4** cation.

2.6.8 Fourier Transformed Infrared Spectroscopy

FTIR measurements were performed for both compounds at RT.

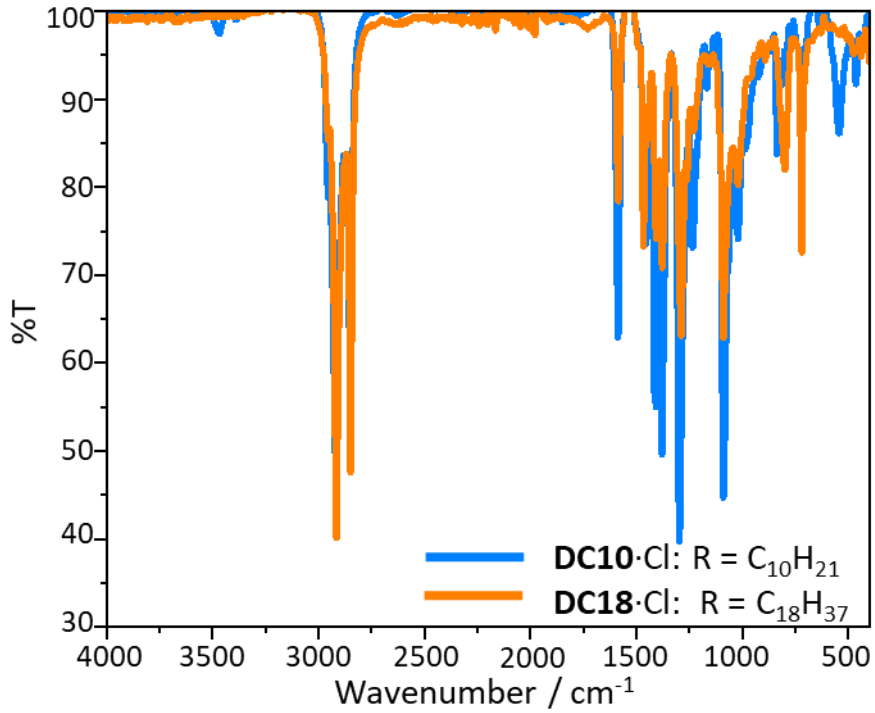

Figure 2.54: FTIR spectra of **DC10**·Cl and **DC18**·Cl.

2.6.9 X-Ray Photoelectron Spectroscopy

XPS experiments were each performed at RT from 0 to 1350 eV, with a spot size of 200 µm and 0.5 eV energy step.

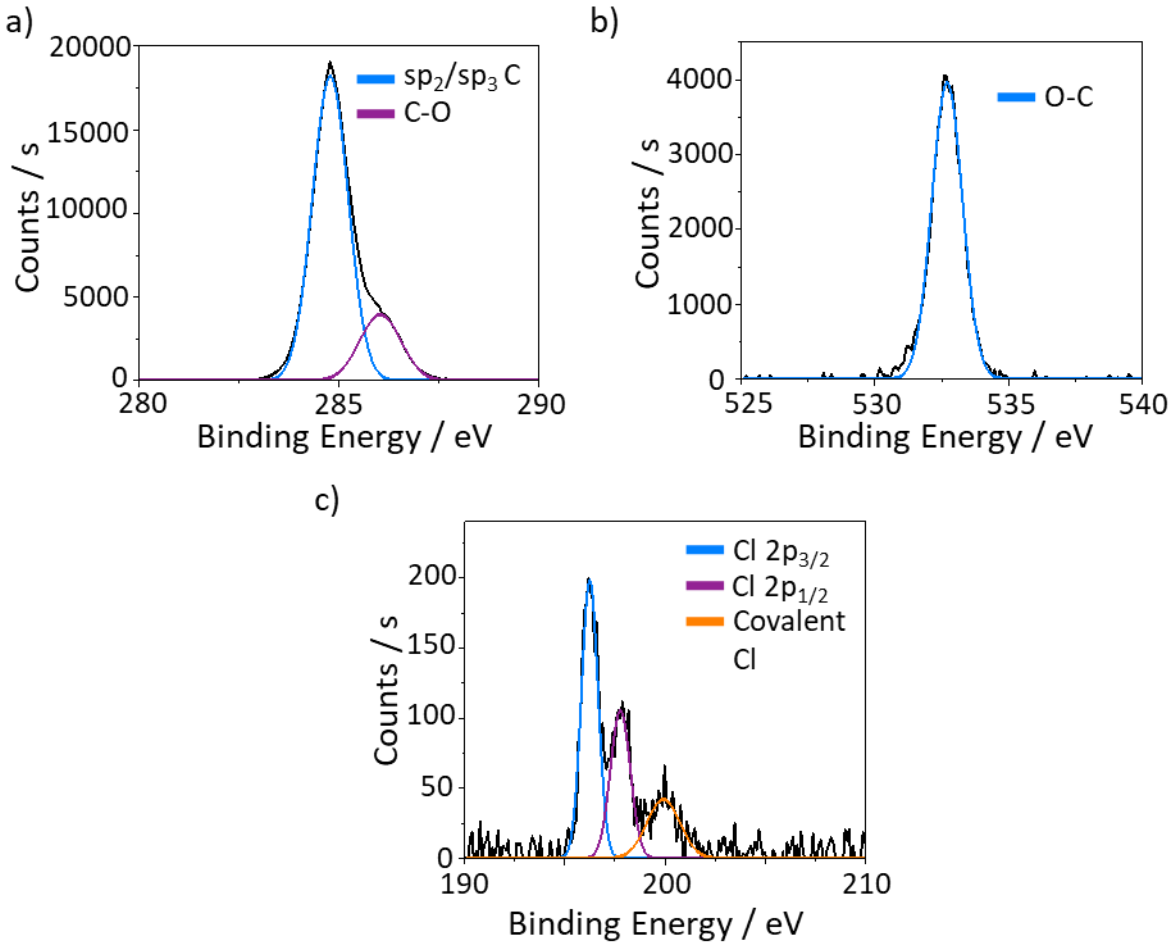

Figure 2.55: XPS spectra of **DC10**·Cl for a) C1s, b) O1s and c) Cl2p.

2.7 References

1. A. Fernandez, P. Kouwer, *Int. J. Mol. Sci.*, 2016, **17**, 731.
2. K. Axenov, S. Laschat, *Materials*, 2011, **4**, 206.
3. S. Kumar, S. Pal, *Tetrahedron Lett.*, 2005, **46**, 15, 2607.
4. K. Goossens, K. Lava, C. Bielawski, K. Binnemans, *Chem. Rev.* 2016, **116**, 8, 4643.
5. R. Breslow, *J. Am. Chem. Soc.*, 1957, **79**, 19, 5318.
6. J. Litterscheidt, J. Bandar, M. Ebert, R. Forschner, K. Bader, T. Lambert, W. Frey, A. Bühlmeyer, M. Brändle, F. Schluz, S. Laschat, *Angwe. Chem. Int. Ed.*, 2020, **59**, 26, 10557.
7. R. Breslow, H. Chang, *J. Am. Chem. Soc.*, 1961, **83**, 10, 2367.
8. P. Imin, M. Imit, A. Adronov, *Macromolecules*, 2011, **44**, 23, 9138.
9. R. West, D. Zecher, W. Goyert, *J. Am. Chem. Soc.*, 1970, **92**, 1, 149.
10. M. Avilés, C. Sánchez, R. Pamies, J. Sanes, M. Bermúdez, *Lubricants*, 2019, **7**, 9, 72.
11. Q. Zhang, S. Liu, Z. Lin, K. Wang, M. Chen, K. Xu, W. Li, *Nano Energy*, 2020, **74**, 104860.
12. J. Yao, Y. You, H. Liu, L. Dong, C. Xiong, *Jour. Mater. Sci.*, 2011, **46**, 3343.
13. X. Cao, J. Cheng, X. Zhang, D. Zhou, Y. Tong, *Int. J. Electrochem. Sci.*, 2020, **15**, 677.
14. S. Poppe, A. Lehmann, A. Scholte, M. Prehm, X. Zeng, G. Ungar, C. Tschierske, *Nat. Commun.*, 2015, **6**, 8637.
15. R. Termine, A. Golemme, *Int. J. Mol. Sci*, 2021, ***22***, 2, 877.
16. H. Li, S. Santhosh Babu, S. Turner, D. Neher, M. Hollamby, T. Seki, S. Yagai, Y. Deguchi, H. Möhwald, T. Nakanishi, *J. Mater. Chem. C*, 2013, **1**, 1943.
17. R. Snyder, H. Strauss, *J. Phys. Chem.*, 1982, **86**, 5145.
18. M. Porter, T. Bright, D. Allara, C. Chidsey, *J. Am. Chem. Soc.*, 1987, **109**, 3559.
19. Gaussian 16, Revision C.01, M. Frisch, G. Trucks, H. Schlegel, G. Scuseria, M. Robb, J. Cheeseman, G. Scalmani, V. Barone, G. Petersson, H. Nakatsuji, X. Li, M. Caricato, A. Marenich, J. Bloino, B. Janesko, R. Gomperts, B. Mennucci, H. Hratchian, J. Ortiz, A. Izmaylov, J. Sonnenberg, D. Williams-Young, F. Ding, F. Lipparini, F. Egidi, J. Goings, B. Peng, A. Petrone, T. Henderson, D. Ranasinghe, V. Zakrzewski, J. Gao, N. Rega,

G. Zheng, W. Liang, M. Hada, M. Ehara, K. Toyota, R. Fukuda, J. Hasegawa, M. Ishida, T. Nakajima, Y. Honda, O. Kitao, H. Nakai, T. Vreven, K. Throssell, J. Montgomery, J. Peralta, F. Ogliaro, M. Bearpark, J. Heyd, E. Brothers, K. Kudin, V. Staroverov, T. Keith, R. Kobayashi, J. Normand, K. Raghavachari, A. Rendell, J. Burant, S. Iyengar, J. Tomasi, M. Cossi, J. Millam, M. Klene, C. Adamo, R. Cammi, J. Ochterski, R. Martin, K. Morokuma, O. Farkas, J. Foresman, D. Fox, Gaussian, Inc., Wallingford CT, 2016.

20. J. Lomon, P. Chaiyabin, T. Saisopa, K. Seawsakul, N. Saowiang, K. Promsakha, P. Poolcharuansin, N. Pasaja, A. Chingsungneon, R. Supruangnet, N. Chanlek, H. Nakajima, P. Songsiriritthigul, *J. Phys.: Conf. Ser.*, 2018, **1144**, 012048.
21. A. Santos, R. Blundell, P. License, *Phys. Chem. Chem. Phys.*, 2015,**17**, 11839.
22. D. Jian, K. Mumtani, V. Gustin, S. Gunduz, G. Celik, I. Waluyo, A. Hunt, A. Co, U. Ozkan, *ChemElectroChem*. 2018, **5**, 14, 1966.
23. J. Bandar, T. Lambert, *Synthesis*, 2013, **45**, 2485.
24. L. Leonat, G. Sbârcea, I. Brânzoi, *U. P. B. Sci. Bull. Series B*, 2013, **75**, 3, 111.
25. M. Gauthier, T. Carney, A. Grimaud, L. Giordano, N. Pour, H. Chang, D. Fenning, S. Lux, O. Paschos, C. Bauer, F. Maglia, S. Lupart, P. Lamp, Y. Shao-Horn, *J. Phys. Chem. Lett.*, 2015, **6**, 4653.
26. J. Goodenough, K. Park, *J. Am. Chem. Soc.*, 2013, **135**, 1167.
27. S. Sergeyev, W. Pisula, Y. Geerts, *Chem. Soc. Rev.*, 2007, **36**, 1902.
28. S. Halder, A. Dey, S. Sil, P. Ray, *J. Mater. Sci. Mater. Electron*, 2021, **32**, 168.
29. A. Ward, *Dielectric Materials for Advanced Applications*, National Research Centre, Cairo, 2016.
30. M. Sienkowska, H. Monobe, P. Kaszynski, Y. Shimizu, *J. Mater. Chem.*, 2007, **17**, 1392.
31. J. Sakuda, E. Hosono, M. Yoshio, T. Ichikawa, T. Matsumoto, H. Ohno, H. Zhou, T. Kato, *Adv. Funct. Mater.*, 2015, **25**, 1206.
32. J. Uchida, B. Soberats, M. Gupta, T. Kato, *Adv. Mater.*, 2022, **34**, 2109063.
33. Z. Liu, B. Dong, M. Misra, Y. Sun, J. Strzalka, S. Patel, F. Escobedo, P. Nealey, C. Ober, *Adv. Funct. Mater.*, 2019, **29**, 1805220.
34. B. Dong, Z. Liu, M. Misra, J. Strazalka, J. Niklas, O. Poluektov, F. Escobedo, C. Ober, P. Nealey, S. Patel, *ACS Nano*, 2019, **13**, 7665.
35. M. Strauss, I. Hwang, A. Evans, A. Natraj, X. Anguilar-Enriquez, I. Castano, E. Roesner, J. Choi, W. Dichtel, *J. Am. Chem. Soc*., 2021, **143**, 17655.

36. B. Dong, Dong, Z. Liu, M. Misra, J. Strazalka, J. Niklas, O. Poluektov, F. Escobedo, C. Ober, P. Nealey, S. Patel, *ACS Nano*, 2019, **13**, 7665.
37. P. Stephens, F. Devlin, C. Chabalowski, M. Frisch, *J. Phys. Chem.*, 1994, **98**, 45, 11623.
38. R. Ditchfield, W. Hehre, J. Pople, *Jour. Chem. Phys.*, 1971, **54**, 2, 724.
39. P. Hariharan, J. Pople, *Theor. Chim. Acta*, 1973, **28**, 213.
40. W. Hehre, R. Ditchfield, J. Pople, *Jour. Chem. Phys.*, 1972, **56**, 5, 2257.

CHAPTER 3

AMINOCYCLOPROPENIUM LIQUID CRYSTALS

Synopsis

This Chapter discusses the synthesis of aminocyclopropenium-centred liquid crystals, based on the cyclopropenium liquid crystals discussed in Chapter 2. A set of aminocyclopropenium compounds was synthesised and initial characterisation undertaken. The liquid crystal character of two compounds was observed at room temperature, with liquid crystals phases forming for a compound possessing a larger counter anion. A greater stability of the aminocyclopropenium compared with the cyclopropenium species was observed from thermal analysis.

Acknowledgements

The following people are gratefully acknowledged for their contribution to this Chapter: Grant Brown undertook the DSC measurements, and William D. Carswell undertook the TGA measurements.

3.1 Introduction

The cyclopropenium mesogens discussed in Chapter 2 demonstrate a number of useful properties, with conductivity being independent of their phase or alignment. However, their potential is limited by low stability and conductivity. Both of these issues might be solved by the introduction of an aminocyclopropenium core, while still using the same pyrogallol-ether groups around the edge (Scheme 3.1). Aminocyclopropenium compounds are more stable than aryl-substituted cyclopropenium compounds,[1] and the weak interaction of counter anions with the electron rich cations should increase the conductivity.[2] Furthermore, the nitrogen atoms would increase the space between the cyclopropenium and the aryl group, allowing larger, weaker counter anions to fit within and still maintain a liquid crystal phase. The aminocyclopropenium has a 4-substitution position on the aryl groups rather than a 5-substitution. The design used emulates the triskelion shape of cyclopropenium compounds discussed in Chapter 2, due to the tertiary amine possessing a 120 ° bond angle. While no longer a fixed planar centre, the phenyl groups would still be able to align planar to the cyclopropenium, and might be expected to maximise the interactions with phenyl groups on neighbouring aminocyclopropeniums, favouring the formation of a liquid crystal.

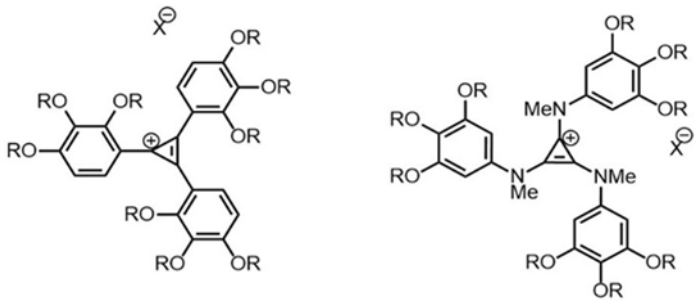

Scheme 3.1: Cyclopropeniums discussed in Chapter 2 and aminocyclopropeniums developed in this Chapter.

This Chapter describes the synthesis and initial characterisation of novel aminocyclopropenium compounds, adapting a number of published synthetic methods to the pyrgallol ethers to make new aminocyclopropenium materials. Initial study of the phase behaviour and thermal stability was undertaken.

3.2 Results and Discussion

3.2.1 Methylated Amine Precursor

The method of synthesis of aminocyclopropenium compounds was through the reaction of pentachlorocyclopropane with a secondary amine.[3, 4] A tris(alkyloxy)methylaniline compound was chosen as the starting material for the aminocyclopropenium. A route to form this was attempted by the bromination of a trialkyloxybenzene (**1a-b**) to make bromo-trialkyloxybenzene (**2a-b**),[5] followed by amination of the bromine group with methylamine.[6] The synthesis was attempted to form the methylated amine product directly, using a copper iodide and hydroxyproline catalysed reaction with **2a-b** and methylamine (Scheme 3.2), without requiring a methylation to be performed. However, this route proved unsuccessful, as the reaction mostly only returning **2a-b**. It is possible that the poor solubility of **2a-b** in highly polar conditions hindered the reaction from proceeding. It is possible that the reaction was performed at too high temperatures for the methyl amine (at reflux), and that lower temperatures may have prevented evaporation of the methylamine allowing the reaction to proceed. However, a full study of the amination of **2a-c** was not performed.

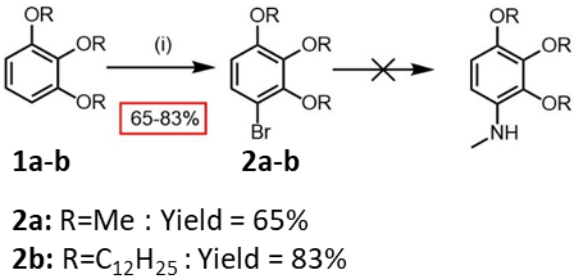

Scheme 3.2: Proposed unsuccessful synthesis of tris(alkyloxy)methylaniline compounds. (i) DBDMH, THF, 0 °C, RT.

Instead a longer route was used, by the nitration of trialkyloxybenzene (**1b-c**) to form trialkyloxynitrobenzene (**3b-c**),[7] followed by a reduction to the trialkyloxyaniline (**4b-c**).[8] Note that **4a** was commercially available so was not required to be synthesised in the previous steps. The methyl group was added by the reaction with NaOMe and paraformaldehyde, followed by $NaBH_4$ to form the tris(alkyloxy)methylaniline (**5a-c**) (Scheme 3.3).[9] The reaction to form **3b-c** occurred exclusively at the 5-position.

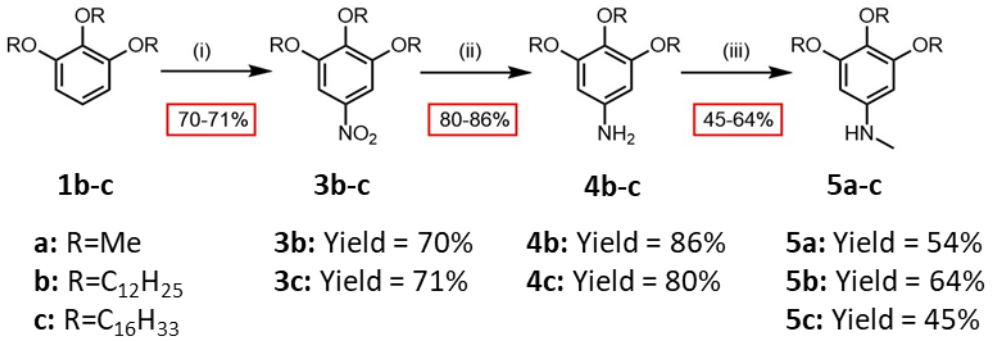

Scheme 3.3: Synthesis of tris(alkyloxy)methylaniline. Reagents and conditions: (i) $NaNO_2$, HNO_3, H_2O, CH_2Cl_2, RT, 4 h; (ii) NH_2NH_2, Pd/C, EtOH, 80 °C, 16 h; (iii) 1). NaOMe, $H(CH_2O)_nOH$, ^iPrOH, 60 °C, 16 h; 2). $NaBH_4$, ^iPrOH, 80 °C, 24 h.

3.2.2 Aminocyclopropenium Synthesis

Aminocyclopropeniums were synthesised from **5a-c** by reaction with pentachlorocyclopropane, in the presence of excess base,[1] to produce the chloride counter anion product (Scheme 3.4).

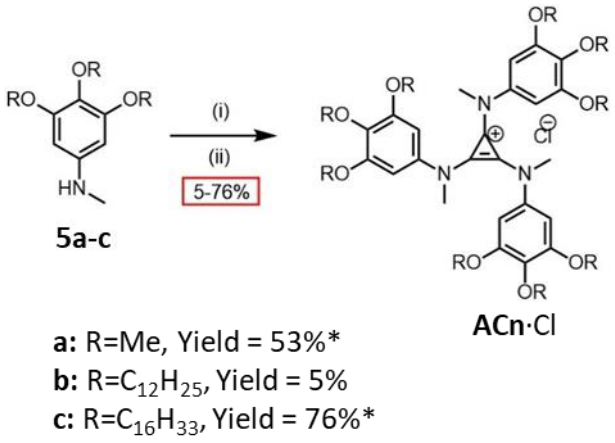

Scheme 3.4: Synthesis of aminocyclopropenium compounds. Reagents and conditions: (i) 1). C_3Cl_5H, NEt_3, CH_2Cl_2, 0 °C, 1 h; 2). RT, 24 h. (*Yields measured without full purification)

Using this method, three aminocyclopropenium compounds with chloride counter anions (**AC1**·Cl, **AC12**·Cl and **AC16**·Cl) were synthesised (Scheme 3.5). From the aminocyclopropenium chlorides two different procedures were used to undertake ion exchange: a reaction with $AgBF_4$ producing a AgCl precipitate (forming **AC12**·BF_4

and **AC16**·BF_4), or by washing with NaI solution to exchange the chloride for an iodide (forming **AC12**·I).

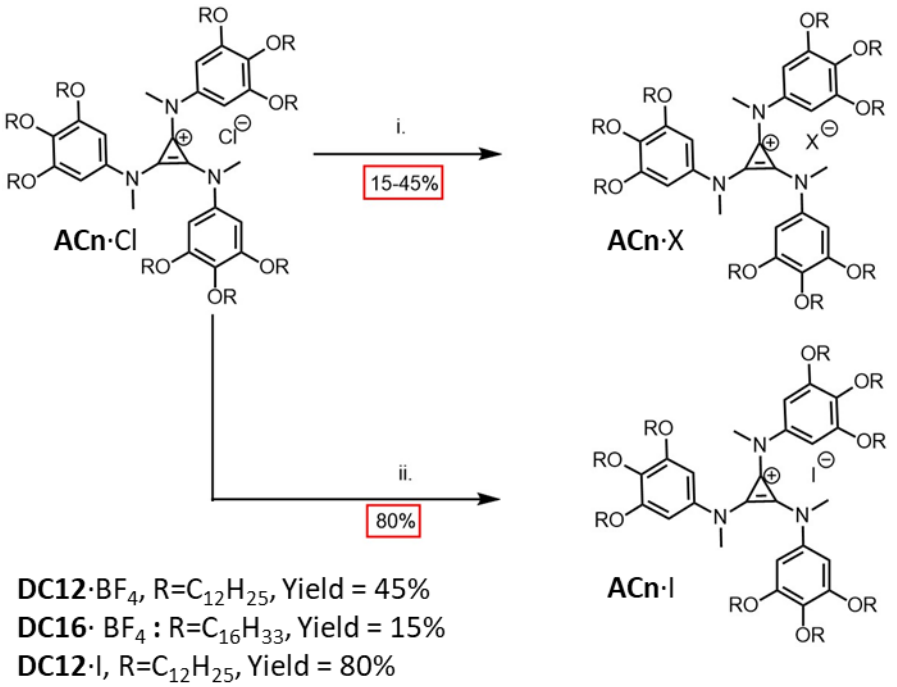

Scheme 3.5: Ion exchange of **ACn**·Cl. Reagents and conditions: (i) AgBF, CH_2Cl_2, CH_3CN, RT, 15 min; (ii) NaI, CH_2Cl_2, H_2O, RT.

Table 3.1: List of all the prepared aminocyclopropenium compounds. Only **AC12**·Cl was obtained with good purity.

Compound	R Chain	Counter Ion X	Yield
AC1·Cl	CH_3	Cl	53%
AC12·Cl	$C_{12}H_{25}$	Cl	5%
AC16·Cl	$C_{16}H_{33}$	Cl	76%
AC12·I	$C_{12}H_{25}$	I	15%
AC12·BF_4	$C_{12}H_{25}$	BF_4	45%
AC16·BF_4	$C_{16}H_{33}$	BF_4	80%

It was found to be difficult to obtain fully clean samples of the aminocyclopropenium materials. While a clean sample could be obtained for **AC12**·Cl, it was isolated with only a 5% yield. A route to obtain the aminocyclopropenium in good yields could not be found. Recrystallisation with acetonitrile and acetone was attempted but was found to be insufficient to fully purify the materials. Only recrystallisation with acetone

followed by precipitation from dichloromethane by acetonitrile was able to isolate clean **AC12**·Cl in low yields.

In addition, the **AC16** compounds were not fully characterised, as there was insufficient material to make sufficiently concentrated solutions to obtain ^{13}C NMR spectra that could show the whole set of carbon peaks (due to losses of material during attempted recrystallisations after the initial recrystallisation to obtain clean samples). However, initial study of the **AC1** and **AC12** aminocyclopropenium materials was undertaken, as part of an effort to direct future research by establishing the compounds that might be suitable as useful materials.

3.2.3 Material Analysis

The phase behaviour of the materials was studied. Each compound was investigated by POM, DSC and TGA. **AC12**·Cl and **AC12**·BF_4 both show birefringence at RT under POM (Figure 3.1).

Figure 3.1: **AC12**·BF_4 under POM cooling to a birefringent liquid crystal phase from the non-birefringent isotropic phase.

The DSC data shows that both **AC12**·Cl and **AC12**·BF_4 have multiple phase transitions that can be attributed to the presence of a liquid crystal phase (Figure 3.2).

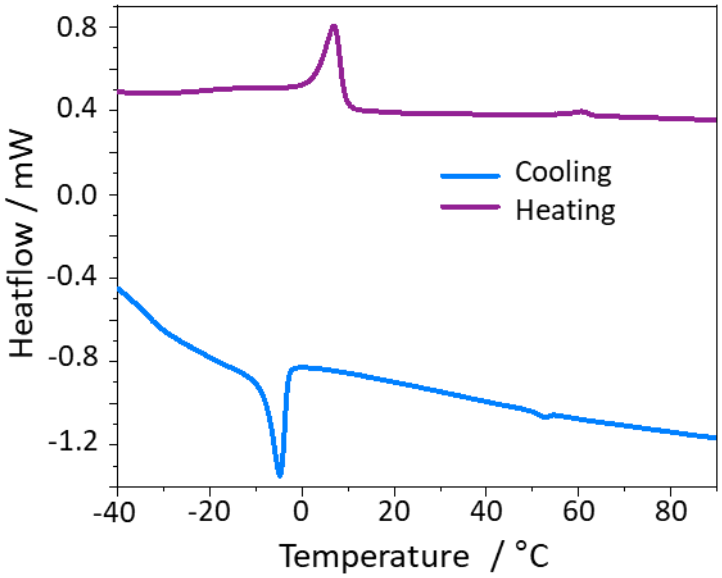

Figure 3.2: DSC of **AC12**·Cl.

AC1·Cl has a solid phase at RT, rather than a liquid crystal phase. The **AC1**·Cl DSC showed peaks of irreversible phase transitions in the first heating cycle, with no phase transitions seen in later cycles (Figure 3.3).

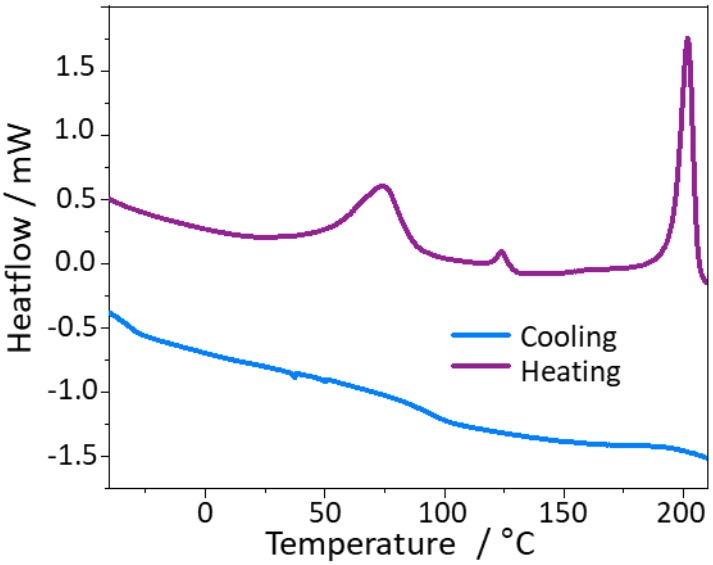

Figure 3.3: DSC of **AC1**·Cl, with irreversible phase transitions and decomposition on the first heating.

AC1·Cl also showed a peak at higher temperatures corresponding to decomposition of the sample. Later DSC runs of **AC1**·Cl that stayed below the decomposition temperature also showed initial phase transitions that were irreversible.

AC12·I instead has a liquid phase at RT, with a phase transition to the solid phase occurring below RT. The results seen for the DSC of the aminocyclopropenium compounds matches the results seen with the cyclopropenium compounds, the major difference being the compound with BF_4 can form a liquid crystal phase, indicating that the more flexible core of the aminocyclopropenium does allow for the integration of larger counter anions.

Table 3.2: Phase transitions of aminocyclopropenium compounds with liquid crystal phases studied by DSC: crystal-liquid crystal phase transition (T_K), and liquid crystal-isotropic or solid-liquid phase transition (T_I).

Compound	T_K (°C) Heating	T_K (°C) Cooling	T_I (°C) Heating	T_I (°C) Cooling
AC12·Cl	3	-3	57	54
AC12·BF_6	0	3	79	71

TGA was performed on all materials, with the aminocyclopropenium compounds all having higher decomposition temperatures than the equivalent cyclopropenium compounds (Figure 3.4), with decomposition beginning at 200-300 °C for the aminocyclopropenium compounds.

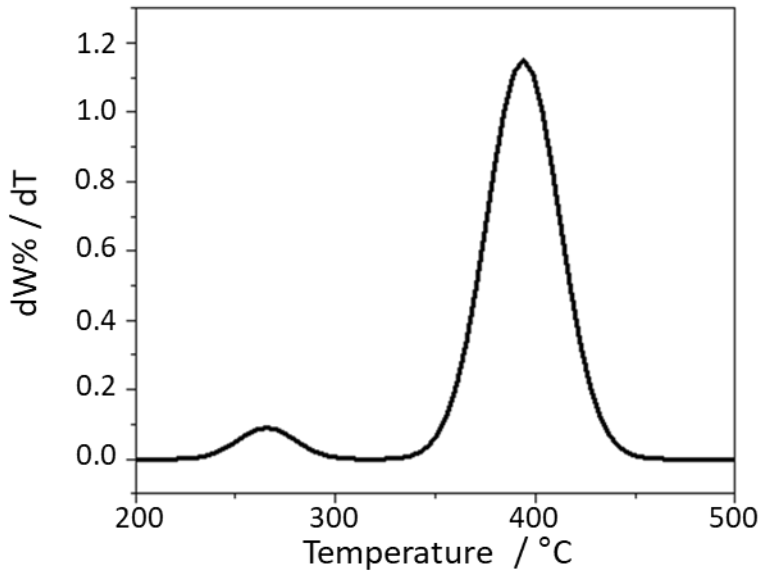

Figure 3.4: DTG of the differential of weight percentage over time against temperature of **AC12**·Cl.

The thermal analysis of the **AC** compounds shows that the phase transitions occur at lower temperatures, with a liquid crystal phase seen at RT, compared to the **DC** compounds. The aminocyclopropenium compounds are also able to form liquid crystal phases with the larger multi-atomic BF_4 anion, while the cyclopropenium compounds could only form a liquid crystal with small halide counter anions.

UV-vis spectra were taken for the liquid crystal compounds **AC12**·Cl and **AC12**·BF_4, as well as non-mesogen **AC1**·Cl (Figure 3.5). Compared to the cyclopropenium equivalents, the UV-vis spectra of the aminocyclopropeniums have a much lower initial wavelength absorbance peak (Table 3.3).

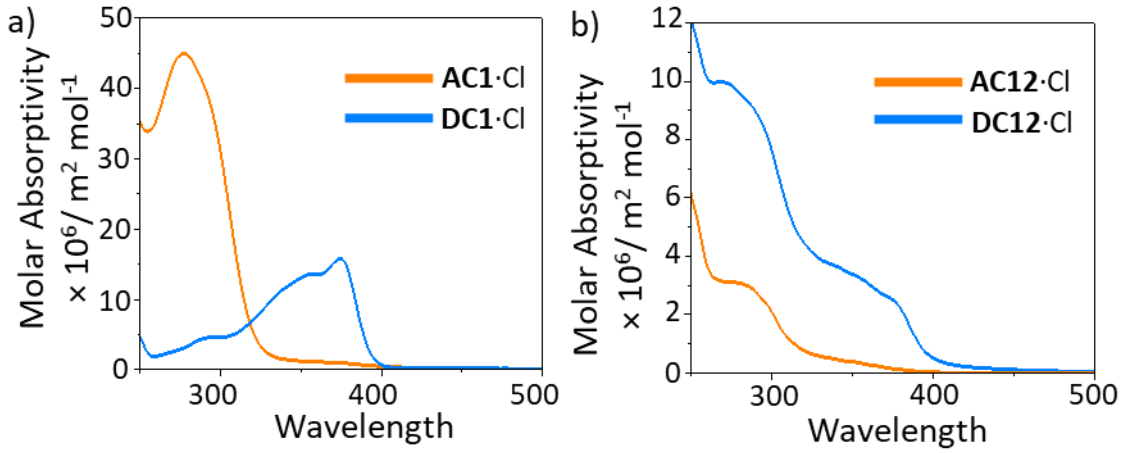

Figure 3.5: UV-vis spectra of a) **AC1**·Cl and **DC1**·Cl, and b) **AC12**·Cl and **DC12**·Cl.

Table 3.3: UV-vis onset wavelength of the absorption of **AC12**·Cl and **AC1**·Cl, and the equivalent DC compounds.

Compound	**λ_{onset} / nm**
AC12·Cl	312
DC12·Cl	398
AC1·Cl	320
DC1·Cl	393

The blue-shift in the UV-vis spectra from the cyclopropenium to the aminocyclopropenium in absorbance at a lower wavelength can be explained by the disruption of conjugation between the cyclopropenium and phenyl groups by the addition of the nitrogen groups, resulting in the higher energy absorption for the aminocyclopropenium.

3.3 Conclusions

In summary, a range of aminocyclopropenium centred compounds designed to form discotic liquid crystals were prepared, and initial analysis was performed upon them. Liquid crystal phases were seen for a dodecyl-functionalised aminocyclopropenium possessing either a Cl or BF_4 counter ion. The aminocyclopropeniums had a higher stability than the cyclopropeniums, and were able to form liquid crystal phases at lower temperatures and with a larger counter anion. The initial investigation of these compounds shows their potential as a development on the earlier cyclopropenium liquid crystals. However, further work is needed to continue the development of the isolation and full characterisation of these compounds.

3.4 Future Work

To enable full characterisation of the compounds, investigations of methods for the purification of the aminocyclopropenium compounds needs to be continued, as only the **AC12**·Cl could be isolated fully pure and only in poor yields. Once a method for isolating these compounds effectively can be developed, full characterisation of the compounds must be completed. XRD should be performed to determine which liquid crystal phases are formed by the aminocyclopropenium compounds. Dielectric spectroscopy should be used to confirm if the aminocyclopropenium has enhanced conductivity compared to cyclopropenium compounds, and if they have the same properties of maintaining their conductivity with phase change and alignment, as well as the impacts of different ions.

Beyond this, future work might investigate the effectiveness of doping, whether the aminocyclopropenium compounds are more amenable to having their phase doped with ionic species compared to the cyclopropenium, with the lone pairs on the amines and larger cavities about the centre should assist the integration of lithium salts. Investigation of the aminocyclopropenium species should be performed to see their effectiveness in battery devices, as well as to the changes to the molecular structure, such as further alterations in the alkyl chain length and counter ions, that may enhance the material properties of these compounds.

3.5 Experimental Methods

3.4.1 Specific Experimental Methods

Instrumentation and Analytical Techniques: TGA (Thermogravimetric Analysis) was performed using a PerkinElmer TGA 8000 or PL Thermal Sciences STA 625. DSC (Differential Scanning Calorimetry) was performed using a PerkinElmer DSC 8000 and Mettler Toledo DSC822. Microscope images were recorded with an Olympus CX50 microscope at ×10 magnification using a Linkam LTS420 heating mantle to heat the sample while being imaged.

3.4.2 Synthetic Procedures

Scheme 3.6: First part of the synthetic route used to prepare the triaminocyclopropenium salts. R is an alkyl group in each case. Reagents and conditions: (i) $NaNO_2$, HNO_3, H_2O, CH_2Cl_2, RT, 4 h, 70-78%; (ii) NH_2NH_2, Pd/C, EtOH, 80 °C, 16 h, 49-86%; (iii) 1). NaOMe, $H(CH_2O)_nOH$, ^iPrOH, 60 °C, 16 h; 2). $NaBH_4$, ^iPrOH, 80 °C, 24 h, 32-64%.

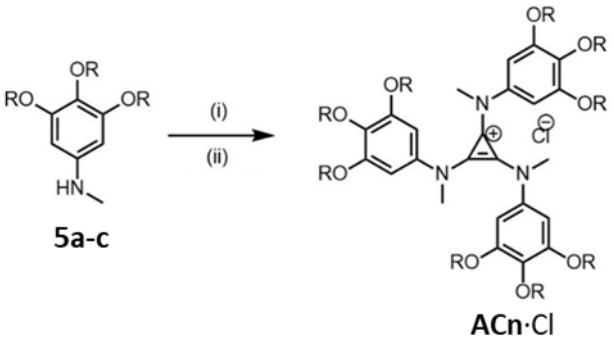

Scheme 3.7: Second part of the synthetic route used to prepare the triaminocyclopropenium salts. R is an alkyl group in each case. Reagents and conditions (i) C_3Cl_5H, NEt_3, CH_2Cl_2, 0 °C, 1 h; (ii) CH_2Cl_2, RT, 24 h, 5-76%;

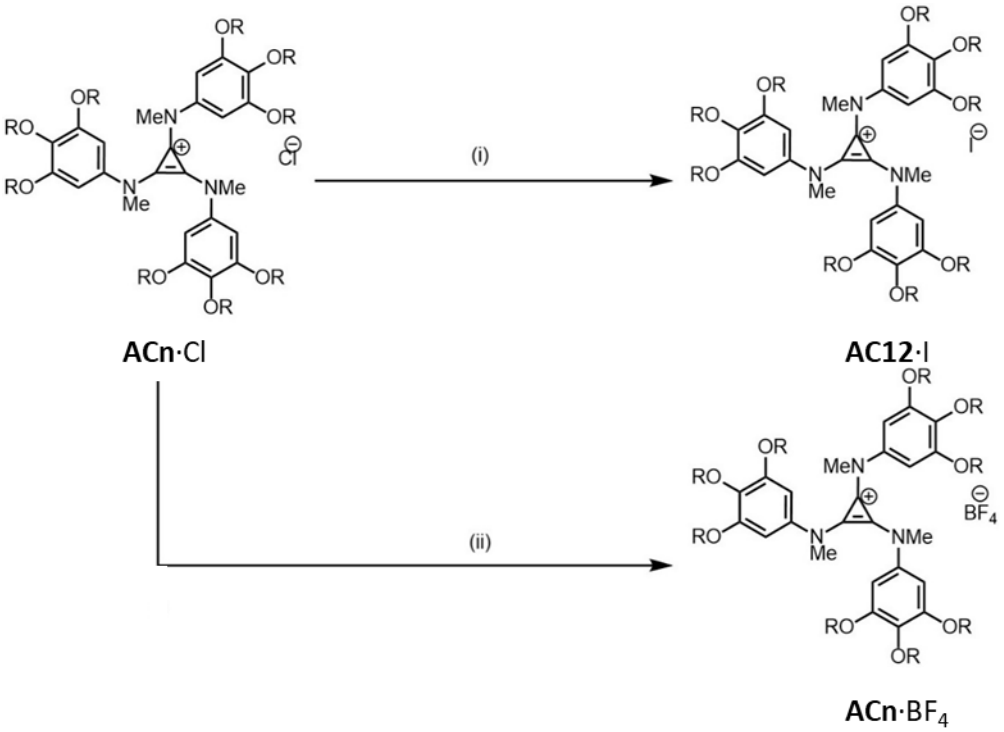

Scheme 3.8: Ion exchange the synthetic route used to prepare the triaminocyclopropenium salts. R is an alkyl group in each case. Reagents and conditions: (i) NaI, CH_2Cl_2, H_2O, RT, 80% (ii) $AgBF_4$, CH_2Cl_2, CH_3CN, RT, 15 min, 15-45%.

*Synthesis of 1-bromo-2,3,4-trialkyloxybenzene (**2**)*

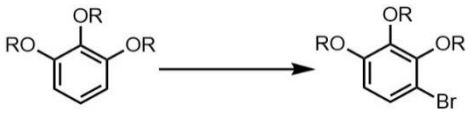

General procedure: 1,2,3-Tris(*n*-alkyl-1-oxy)benzene **(1a/b)** (60.0 mmol, 2.0 equiv.) was added to a round bottom flask, dissolved in THF (100 mL) and cooled to 0 °C. 1,3-Dibromo-5,5-dimethylhydantoin (DBDMH) (30.0 mmol, 1.0 equiv.) in THF (35 mL) was added to the solution, which was left to stir for 14 h. Water (100 mL) was added, and THF removed under reduced pressure. The product was extracted with CH_2Cl_2 (50 mL), and the organic layer dried over $MgSO_4$ and filtered. The solvent was removed under reduced pressure, and the product isolated by column chromatography (Teledyne Isco Combiflash Rf+ system, 80 g SiO_2, Hexanes/EtOAc gradient elution [1:0 to 0:1]) to give the pure product.

1-Bromo-2,3,4-trimethoxybenzene (2a). The product was obtained from **1a** (10.1 g, 60.2 mmol) and DBDMH (8.6 g, 30.0 mmol) as a pale yellow liquid (9.6 g, 38.8 mmol, 65% yield). **^{1}H NMR** (600 MHz, $CDCl_3$) δ 7.20 (d, *J* = 9.0 Hz, 1H, H_2), 6.58 (d, *J* = 9.0 Hz, 1H, H_3), 3.90 (s, 3H, H_9), 3.88 (s, 3H, H_8), 3.84 (s, 3H, H_7). **^{13}C NMR (151 MHz, $CDCl_3$)** 153.5 (C_4), 151.1 (C_5), 143.7 (C_6), 126.9 (C_2), 108.8 (C_3), 108.5 (C_1), 61.2 (C_8), 61.2 (C_9), 56.3 (C_7). **HRMS-ASAP** *m/z* = 246.9968 $[M+H]^+$, calculated for $C_9H_{12}O_3Br$ = 246.9970.

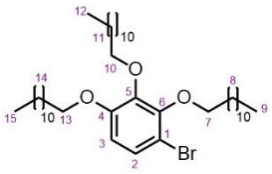

1-Bromo-2,3,4-tri-*n*-dodecyloxybenzene (2b). The product was obtained from **1b** (9.9 g, 14.0 mmol) and DBDMH (2.3 g, 8.1 mmol) as a yellow liquid (8.3 g, 11.6 mmol, 83% yield). **^{1}H NMR** (600 MHz, $CDCl_3$) δ 7.13 (d, *J* = 9.0 Hz, 1H, H_3), 6.52 (d, *J* = 9.0 Hz, 1H, H_2), 4.01 (t, *J* = 6.7 Hz, 2H, H_{10}), 3.96 (t, *J* = 6.6 Hz, 2H, H_7), 3.91 (t, *J* = 6.7 Hz, 2H, H_{13}), 1.81 – 1.76 (m, 4H, H_8/H_{11}), 1.75 – 1.70 (m, 2H, H_{14}), 1.50 – 1.43 (m, 6H, $H_8/H_{11}/H_{14}$), 1.35 – 1.32 (m, 6H, $H_8/H_{11}/H_{14}$), 1.30 – 1.24 (m, 42H, $H_8/H_{11}/H_{14}$), 0.87 (t, *J* = 7.1 Hz, 9H, $H_9/H_{12}/H_{15}$). **^{13}C NMR (151 MHz, $CDCl_3$)** 153.2 (C_4), 150.8 (C_5), 143.3 (C_6), 126.6 (C_3), 109.5 (C_2), 108.7 (C_1), 74.1 (C_{10}), 74.0 (C_7), 69.0 (C_{13}), 32.1 (alkyl-C), 31.7 (alkyl-C), 30.4 (alkyl-C), 30.4 (alkyl-C), 29.9 (alkyl-C), 29.9 (alkyl-C), 29.8 (alkyl-C), 29.8 (alkyl-C), 29.8 (alkyl-C), 29.8 (alkyl-C), 29.7 (alkyl-C), 29.6 (alkyl-C), 29.5 (alkyl-C), 29.5 (alkyl-C), 29.5 (alkyl-C), 29.4 (alkyl-C), 26.2 (alkyl-C), 26.2 (alkyl-C), 26.2 (alkyl-C), 22.8 (alkyl-C), 22.8 (alkyl-C), 22.6 (alkyl-C), 14.3 ($C_8/C_{11}/C_{14}$). **HRMS-ASAP** *m/z* = 709.5133 $[M+H]^+$, calculated for $C_{42}H_{78}O_3Br$ = 709.5134.

*Synthesis of 3,4,5-alkyloxy-1-nitrobenzene (**3**)*

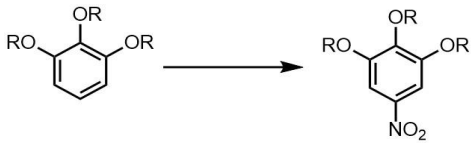

General procedure: 1,2,3-Tris(*n*-alkyl-1-oxy)benzene (7.0 mmol, 4.7 equiv.) and $NaNO_2$ (1.5 mmol, 1.0 equiv.) were added to CH_2Cl_2 (50 mL) and H_2O (2.5 mL). Concentrated nitric acid (5 mL) was then added dropwise. The mixture was left to stir for 4 h. H_2O (20 mL) was added and the product extracted with CH_2Cl_2 (20 mL). The

organic layer was dried with $MgSO_4$, filtered and the solvent removed under reduced pressure. The product was isolated by recrystallisation in MeOH (20 mL).

3,4,5-Tri-*n*-dodecyloxy-1-nitrobenzene (3b). The product was obtained from **1b** (4.1 g, 6.6 mmol), $NaNO_2$ (67 mg, 1.4 mmol) and nitric acid (2.3 mL) as a pale yellow solid (3.0 g, 4.6 mmol, 70% yield). **M.P.** 51 – 52 °C. **^{1}H NMR (600 MHz, $CDCl_3$)** δ 7.47 (s, 2H, H_2), 4.06 (t, *J* = 6.5 Hz, 2H, H_8), 4.03 (t, *J* = 6.5 Hz, 4H, H_5), 1.87 – 1.80 (m, 4H, H_6), 1.77 – 1.71 (m, 2H, H_9), 1.51 - 1.44 (m, 6H, H_6/H_9), 1.39 - 1.32 (m, 6H, H_6/H_9), 1.31 - 1.24 (m, 42H, H_6/H_9), 0.88 (t, *J* = 6.5 Hz, 9H, H_7/H_{10}). **^{13}C NMR (151 MHz, $CDCl_3$)** δ 152.9 (C_3), 144.0 (C_4), 143.3 (C_1), 102.3 (C_2), 74.0 (C_8), 69.6 (C_5), 32.1 (alkyl-C), 32.1 (alkyl-C), 30.5 (alkyl-C), 29.9 (alkyl-C), 29.9 alkyl-C), 29.8 (alkyl-C), 29.8 (alkyl-C), 29.8 (alkyl-C), 29.7 (alkyl-C), 29.5 (alkyl-C), 29.5 (alkyl-C), 29.5 (alkyl-C), 29.3 (alkyl-C), 26.2 (alkyl-C), 26.1 (alkyl-C), 22.9 (alkyl-C), 14.3 (C_7/C_{10}). **HRMS-ASAP** *m/z* = 675.5798 [M^+], calculated for $C_{42}H_{77}NO_5$ = 675.5802.

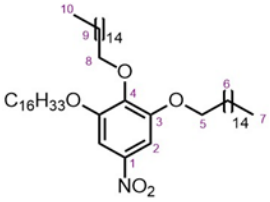

3,4,5-Tri-*n*-hexadecyloxy-1-nitrobenzene (3c). The product was obtained from **1c** (5.6 g, 7.0 mmol), $NaNO_2$ (72 mg, 1.5 mmol) and nitric acid (2.5 mL) as a pale yellow solid (4.2 g, 5.0 mmol, 71% yield). **M.P.** 72 °C. **^{1}H NMR (600 MHz, $CDCl_3$)** δ 7.46 (s, 2H, H_2), 4.05 (t, *J* = 6.5 Hz, 2H, H_8), 4.02 (t, *J* = 6.5 Hz, 4H, H_5), 1.86 – 1.80 (m, 4H, H_6), 1.76 – 1.70 (m, 2H, H_9), 1.50 - 1.43 (m, 6H, H_6/H_9), 1.38 - 1.32 (m, 6H, H_6/H_9), 1.32 - 1.20 (m, 66H, H_6/H_9), 0.87 (t, *J* = 67.0 Hz, 9H, H_7/H_{10}). **^{13}C NMR (151 MHz, $CDCl_3$)** δ 152.8 (C_3), 144.0 (C_4), 143.3 (C_1), 102.3 (C_2), 74.0 (C_8), 69.6 (C_5), 32.1 (alkyl-C), 30.4 (alkyl-C), 29.9 (alkyl-C), 29.9 (alkyl-C), 29.9 (alkyl-C), 29.8 (alkyl-C), 29.8 (alkyl-C), 29.8 (alkyl-C), 29.8 (alkyl-C), 29.7 (alkyl-C), 29.7 (alkyl-C), 29.5 (alkyl-C), 29.5 (alkyl-C), 29.5 (alkyl-C), 29.2 (alkyl-C), 26.2 (alkyl-C), 26.1 (alkyl-C), 22.8 (alkyl-C), 14.3 (C_7/C_{10}). **HRMS-ASAP** *m/z* = 844.7754 [M+H]$^+$, calculated for $C_{54}H_{102}NO_5$ = 844.7758.

*Synthesis of 3,4,5-alkyloxy-1-aniline (**4**)*

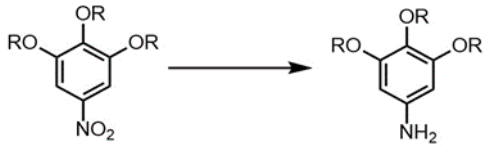

General procedure: 2,4,5-Tris(*n*-alkyloxy)-1-nitrobenzene (4.6 mmol. 1.0 equiv.), Pd/C (5% Pd, 300 mg) and hydrazine monohydrate (30 mmol, 6.5 equiv.) were added to EtOH (50 mL) and heated to 80 °C for 16 h. The mixture was cooled to RT, filtered, and dissolved in CH_2Cl_2 (50 mL). The solution was washed with H_2O (2 × 100 mL), dried with $MgSO_4$, filtered and the solvent removed under reduced pressure. The product was isolated by column chromatography (Manual silica column, eluent Hexanes:EtOAc/9:1).

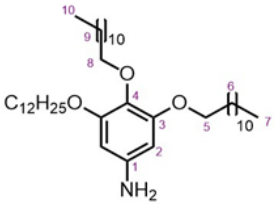

3,4,5-Tri-*n*-dodecyloxy-1-aniline (4b). The product was obtained from **3b** (10.7 g, 15.8 mmol) and hydrazine monohydrate (4.5 mL, 90.0 mmol) as a pale red solid (8.9 g, 13.7 mmol, 86% yield). **M.P.** 71 – 72 °C. **^{1}H NMR (600 MHz, $CDCl_3$)** δ 5.91 (s, 2H, H_2), 3.90 (t, *J* = 6.5 Hz, 4H, H_5), 3.84 (t, *J* = 6.5 Hz, 2H, H_8), 1.80 – 1.74 (m, 4H, H_6), 1.73 – 1.68 (m, 2H, H_9), 1.48 – 1.41 (m, 6H, H_6/H_9), 1.36 – 1.31 (m, 6H, H_6/H_9), 1.31 – 1.22 (m, 48H, H_6/H_9), 0.88 (t, *J* = 6.9 Hz, 9H, H_7/H_{10}). **^{13}C NMR (151 MHz, $CDCl_3$)** δ 153.9 (C_3), 142.4 (C_1), 131.3 (C_4), 94.7 (C_2), 73.7 (C_8), 69.1 (C_5), 32.1 (alkyl-C), 32.1 (alkyl-C), 30.5 (alkyl-C), 29.9 (alkyl-C), 29.9 (alkyl-C), 29.9 (alkyl-C), 29.8 (alkyl-C), 29.8 (alkyl-C), 29.6 (alkyl-C), 29.5 (alkyl-C), 29.5 (alkyl-C), 29.5 (alkyl-C), 26.3 (alkyl-C), 26.3 (alkyl-C), 22.8 (alkyl-C), 14.3 (C_7/C_{10}). **HRMS-ASAP** *m/z* = 645.6090 [M^+], calculated for $C_{42}H_{79}NO_3$ = 645.6060.

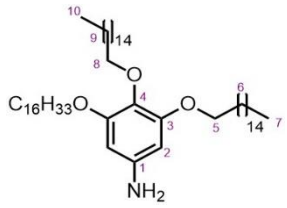

3,4,5-Tri-*n*-hexadecyloxy-1-aniline (4c). The product was obtained from **3c** (6.5 g, 7.7 mmol) and hydrazine monohydrate (1.1 mL, 20.1 mmol) as a pale red solid (5.0 g, 6.1 mmol, 80% yield). **M.P.** 71 – 72 °C. **^{1}H NMR (600 MHz, $CDCl_3$)** δ 5.91 (s, 2H, H_2), 3.90 (t, *J* = 6.5 Hz, 4H, H_5), 3.84 (t, *J* = 6.5 Hz, 2H, H_8), 1.80 – 1.74 (m, 4H, H_6), 1.71 – 1.68 (m, 2H, H_9), 1.48 – 1.42 (m, 6H, H_6/H_9), 1.36 – 1.31(m, 6H, H_6/H_9), 1.31 – 1.22 (m, 66H, H_6/H_9), 0.88 (t, *J* = 6.8 Hz, 9H, H_7/H_{10}). **^{13}C NMR (151 MHz, $CDCl_3$)** δ 153.9 (C_3), 142.4 (C_4), 131.3 (C_1), 94.7 (C_2),

73.7 (C_8), 69.2 (C_5), 32.1 (alkyl-C), 30.5 (alkyl-C), 29.9 (alkyl-C), 29.9 (alkyl-C), 29.9 (alkyl-C), 29.9 (alkyl-C), 29.8 (alkyl-C), 29.8 (alkyl-C), 29.6 (alkyl-C), 29.5 (alkyl-C), 29.5 (alkyl-C), 26.4 (alkyl-C), 26.3 (alkyl-C), 22.8 (alkyl-C), 14.3 (C_7/C_{10}). **HRMS – ASAP** *m/z* = 814.7990 $[M+H]^+$, calculated for $C_{54}H_{104}NO_3$ = 814.8016.

*Synthesis of 3,4,5-alkyloxy-1-methylaniline (**5**)*

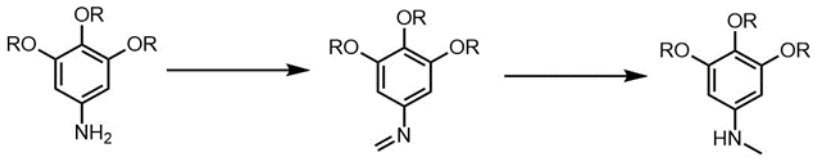

General procedure: 3,4,5-Tris(*n*-alkyloxy)-1-aniline (7.4 mmol, 1.0 equiv.), MeONa (38 mmol, 5.0 equiv), and paraformaldehyde (15 mmol, 2.0 equiv.) were added to ^{i}PrOH (100 mL) and heated to 60 °C for 16 h. The mixture was then cooled to RT and $NaBH_4$ (9.9 mmol. 1.3 equiv.) was added, and the mixture was heated to reflux for 24 h. The mixture was then cooled to RT, and quenched with sat. $NaHCO_3$ solution (50 mL). The product was extracted with EtOAc (3 × 50 mL). The organic fractions were combined and washed with brine (50 mL), dried with $MgSO_4$, filtered and the solvent removed under reduced pressure. The product was isolated by column chromatography (Teledyne Isco Combiflash Rf+ system, 24 g SiO_2, Hexanes/EtOAc gradient elution).

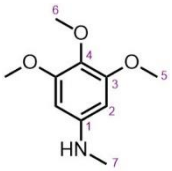

3,4,5-Trimethoxy-*n*-methylaniline (5a). The product was obtained from **4a** (2.9 g, 15.6 mmol), MeONa (4.6 g, 82.2 mmol), paraformaldehyde (1.0 g, 33.3 mmol) and $NaBH_4$ (0.8 g, 21.6 mmol) as a brown oil (1.7 g, 8.4 mmol, 54% yield). **^{1}H NMR (600 MHz, $CDCl_3$)** δ 5.85 (s, 2H, H_2), 3.83 (s, 6H, H_5), 3.76 (s, 3H, H_6), 2.82 (s, 3H, H_7). **^{13}C NMR (151 MHz, $CDCl_3$)** δ 154.1 (C_3), 146.3 (C_1), 130.2 (C_4), 90.1 (C_2), 61.2 (C_6), 56.1 (C_5), 31.3 (C_7). **HRMS – ASAP** *m/z* = 198.1115 $[M+H]^+$, calculated for $C_{10}H_{16}NO_3$ = 198.1130.

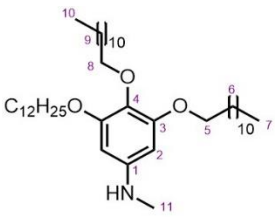

3,4,5-Tri-*n*-dodecyloxy-*n*-methylaniline (5b). The product was obtained from **4b** (4.9 g, 7.4 mmol), MeONa (2.1 g, 37.5 mmol), paraformaldehyde (0.5 g, 15.3 mmol) and $NaBH_4$ (0.4 g, 9.9 mmol) as a brown solid (3.9 g, 17.1 mmol,

64% yield). **M.P.** 42 °C. **^{1}H NMR (600 MHz, $CDCl_3$)** δ 5.86 (s, 2H, H_1), 3.94 (t, *J* = 6.6 Hz, 4H, H_5), 3.84 (t, *J* = 6.6 Hz, 2H, H_8), 2.80 (s, 3H, H_{12}), 1.81 – 1.74 (m, 4H, H_6), 1.74 - 1.68 (m, 2H, H_9), 1.48 - 1.42 (m, 6H, H_6/H_9), 1.35 - 1.31 (m, 6H, H_6/H_9), 1.30 - 1.23 (m, 42H, H_6/H_9), 0.88 (t, *J* = 6.6 Hz, 9H, H_7/H_{10}). **^{13}C NMR (151 MHz, $CDCl_3$)** δ 154.0 (C_3), 145.6 (C_1), 130.8 (C_4), 92.3 (C_2), 73.8 (C_8), 69.3 (C_5), 32.1 (alkyl-C), 32.1 (alkyl-C), 31.5 (C_{11}), 30.5 (alkyl-C), 29.9 (alkyl-C), 29.9 (alkyl-C), 29.9 (alkyl-C), 29.8 (alkyl-C), 29.8 (alkyl-C), 29.6 (alkyl-C), 29.6 (alkyl-C), 29.5 (alkyl-C), 29.5 (alkyl-C), 26.4 (alkyl-C), 26.3 (alkyl-C), 22.7 (alkyl-C), 14.3 (C_7/C_{10}). **HRMS - ASAP** *m/z* = 660.6303 [M+H$^+$], calculated for $C_{43}H_{82}NO_3$ = 660.6289.

3,4,5-Tri-*n*-hexadecyloxy-*n*-methylaniline (5c). The product was obtained from **4c** (4.9 g, 6.0 mmol), MeONa (1.7 g, 30.0 mmol), paraformaldehyde (0.5 g, 13.0 mmol) and $NaBH_4$ (0.3 g, 8.1 mmol) as a brown solid (2.3 g, 2.7 mmol, 45% yield). **M.P.** 52 – 53 °C. **^{1}H NMR (400 MHz, $CDCl_3$)** δ 5.83 (s, 2H, H_2), 3.94 (t, *J* = 6.7 Hz, 6H, H_5), 3.84 (t, *J* = 6.7 Hz, 3H, H_6), 2.79 (s, 3H, H_8), 1.80 - 1.75 (m, 4H, H_6), 1.73 - 1.68 (m, 2H, H_9), 1.48 - 1.42 (m, 6H, H_6/H_9), 1.35 - 1.31 (m, 6H, H_6/H_9), 1.30 - 1.23 (m, 6H, H_6/H_9), 0.87 (t, *J* = 7.0 Hz, 9H, H_7/H_{10}). **^{13}C NMR (151 MHz, $CDCl_3$)** δ 153.8 (C_3), 145.9 (C_4), 130.4 (C_1), 91.9 (C_2), 73.6 (C_8), 69.1 (C_5), 31.9 (C_{12}), 31.2 (alkyl-C), 30.9 (alkyl-C), 30.3 (alkyl-C), 29.8 (alkyl-C), 29.7 (alkyl-C), 29.7 (alkyl-C), 29.6 (alkyl-C), 29.5 (alkyl-C), 29.4 (alkyl-C), 29.3 (alkyl-C), 26.2 (alkyl-C), 26.1 (alkyl-C), 22.7 (alkyl-C), 14.1 (C_7/C_{10}). **HRMS – ASAP** 828.8186 [M+H]$^+$, calculated for $C_{55}H_{106}NO_3$ = 828.8173.

*Synthesis of tris((trialkylphenyl)methyl)aminocyclopropenium chloride (**ACn**·Cl)*

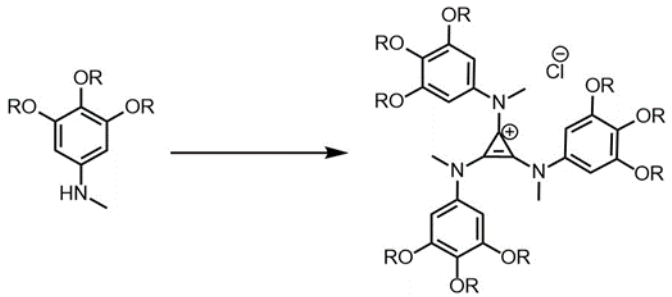

General procedure: Pentachlorocyclopropane (0.62 mmol, 1 equiv.) was added to CH_2Cl_2 (25 mL), cooled to 0 ℃ and 3,4,5-tris(*n*-alkyloxy)-1-methylaniline (2.42 mmol, 4 equiv.) and Et_3N (3.35 mmol, 5.4 equiv.) were added in succession. The reaction was stirred for 1 h at 0 ℃ and then for 24 h at RT. The solvent was removed under reduced pressure and the crude mixture was purified by column chromatography (Teledyne Isco Combiflash Rf+ system, 12 g SiO_2, CH_2Cl_2/MeOH gradient elution [1:0 to 17:3]), and either left without further purification, recrystallised in acetone (20 mL) or dissolved in CH_2Cl_2 (5 mL) and precipitated out with CH_3CN (50 mL) and then filtered to isolate the product.

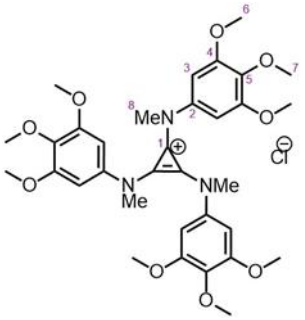

Tris((3,4,5-trimethoxy)-*n*-methyl)aminocyclopropenium chloride – AC1·Cl. The product was obtained from pentachlorocyclopropane (0.3 g, 1.6 mmol), **5a** (1.0 g, 5.2 mmol), and Et_3N (0.9 g, 8.4 mmol) as a brown solid (0.5 g, 0.8 mmol, 53% yield). **M.P.** 119 - 120 °C. **^{1}H NMR (400 MHz, $CDCl_3$)** δ 6.87 (s, 6H, H_3), 3.85 (s, 18H, H_6), 3.76 (s, 9H, H_7), 3.32 (s, 9H, H_8). **^{13}C NMR (151 MHz, $CDCl_3$)** δ 153.8 (C_4), 140.0 (C_1 or C_2), 137.0 (C_5), 118.5 (C_1 or C_2), 101.5 (C_3), 61.0 (C_7), 56.9 (C_6), 42.9 (C_8). **HRMS – ASAP** 624.2950 $[M\text{-}Cl]^+$, calculated for $C_{33}H_{42}N3O_9$ = 624.2921.

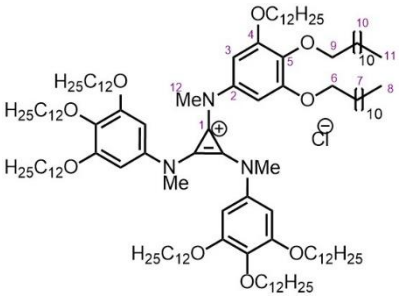

Tris((3,4,5-tri-*n*-dodecyloxy)-*n*-methyl)aminocyclopropenium chloride – AC12·Cl. The product was obtained from pentachlorocyclopropane (22 mg, 0.10 mmol), **5b** (0.35 g, 0.53 mmol), and Et_3N (0.14 g, 0.72 mmol) after precipitation from CH_3CN and CH_2Cl_2 as a brown liquid crystal (10 mg, 0.005 mmol, 5% yield). **M.P.** 57 - 59 °C. **^{1}H NMR (600 MHz, $CDCl_3$)** δ 6.63 (s, 6H, H_3), 3.98 – 3.85 (m, 12H, H_6), 3.84 (t, J = 6.4 Hz, 6H, H_9), 3.30 (s, 9H, H_{12}), 1.77 – 1.72 (m, 12H, H_7), 1.72 – 1.66 (m, 6H, H_{10}), 1.49 – 1.40 (m, 18H, H_7/H_{10}), 1.32 – 1.23 (m, 144H, H_7/H_{10}), 0.88 (t, J = 7.0 Hz, 27H, H_8/H_{11}). **^{13}C NMR (151 MHz, $CDCl_3$)** δ 153.7 (aromatic-C), 139.5 (aromatic-C), 137.2 (C_5), 117.9 (aromatic-C), 102.5 (C_3), 73.6 (C_6), 69.6 (C_9), 43.1 (C_{12}), 32.1 (alkyl-C), 32.1 (alkyl-C), 30.6 (alkyl-C), 30.0 (alkyl-C), 30.0 (alkyl-C), 30.0 (alkyl-C), 29.9 (alkyl-C), 29.9

(alkyl-C), 29.9 (alkyl-C), 29.7 (alkyl-C), 29.6 (alkyl-C), 29.6 (alkyl-C), 29.5 (alkyl-C), 26.3 (alkyl-C), 26.3 (alkyl-C), 22.8 (alkyl-C), 14.3 (methyl-C). **MS-MALDI** (DTCB matrix with CH_2Cl_2) *m/z* = 2012.7 $[M\text{-}Cl+H]^+$, calculated for $C_{132}H_{241}N_3O_9$ = 2012.8.

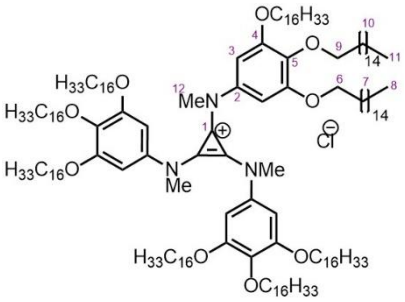

Tris((3,4,5-tri-*n*-hexadecyloxy)-*n*-methyl)aminocyclopropenium chloride – AC16·Cl. The product was obtained from pentachlorocyclopropane (92 mg, 0.55 mmol), **5c** (1.85 g, 2.22 mmol), and Et_3N (0.29 g, 2.86 mmol) after recrystallisation from acetone as an orange solid (1.05 g, 0.42 mmol, 76% yield). **^{1}H NMR (400 MHz, $CDCl_3$)** 6.63 (s, 6H, H_3), 3.88 (t, *J* = 6.4 Hz, 12H, H_6), 3.83 (t, *J* = 6.4 Hz, 6H, H_9), 3.28 (s, 9H, H_{12}), 1.77 – 1.71 (m, 12H, H_7), 1.70 – 1.65 (m, 6H, H_{10}), 1.48 – 1.41 (m, 18H, H_7/H_{10}), 1.30 – 1.23 (m, 216H, H_7/H_{10}), 0.88 (t, *J* = 7.0 Hz, 27H, H_8/H_{11}). **^{13}C NMR (151 MHz, $CDCl_3$).** δ 153.7 (aromatic-C), 139.4 (aromatic-C), 137.2 (aromatic-C), 102.6 (aromatic-C), 73.6 (C_{12}), 69.6 (C_9), 32.0 (alkyl-C), 30.6 (alkyl-C), 30.0 (alkyl-C), 30.0 (alkyl-C), 30.0 (alkyl-C), 29.9 (alkyl-C), 29.9 (alkyl-C), 29.9 (alkyl-C), 29.9 (alkyl-C), 29.8 (alkyl-C), 29.8 (alkyl-C), 29.8 (alkyl-C), 29.6 (alkyl-C), 29.6 (alkyl-C), 29.5 (alkyl-C), 29.4 (alkyl-C), 26.4 (alkyl-C), 26.3 (alkyl-C), 22.8 (alkyl-C), 14.3 (methyl-C). **MS-ESI** *m/z* = 2517.0 $[M+H\text{-}Cl]^+$, calculated for $C_{168}H_{313}N_3O_9$ = 2517.4.

Tris((trialkylphenyl)methyl)aminocyclopropenium ion exchange via sodium iodide

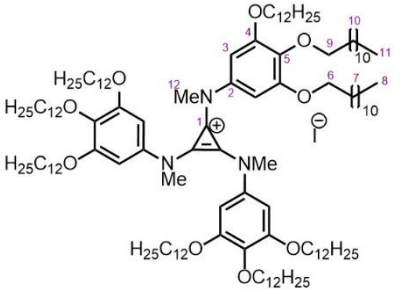

Tris((3,4,5-tri-*n*-dodecyloxy)-*n*-methyl)aminocyclopropenium iodide – AC12·I. **AC12**·Cl (100 mg, 0.05 mmol) was dissolved in CH_2Cl_2 (10 mL). The solution was washed with NaI solution (10 ml, 2.5 mM solution in H_2O) three times. The solution was dried with $MgSO_4$, filtered and the solvent was then removed under reduced pressure to give the product as a yellow liquid (83 mg, 0.04 mmol, 80% yield). **^{1}H NMR (600 MHz, $CDCl_3$)** δ 6.76 (s, 6H, H_3), 3.97 – 3.89 (m, 12H, H_6), 3.84 (t, *J* = 6.4 Hz, 6H, H_9), 3.19 (s, 9H, H_{12}), 1.79 – 1.72 (m, 12H, H_7), 1.71 – 1.65 (m, 6H, H_{10}), 1.48 – 1.41 (m, 18H, H_7/H_{10}), 1.30 – 1.24 (m, 144H, H_7/H_{10}), 0.88 (t, *J* = 7.0 Hz, 27H, H_8/H_{11}). **^{13}C NMR (151 MHz, $CDCl_3$)** δ 153.8

(aromatic-C), 139.5 (aromatic-C), 137.3 (C_5), 118.1 (aromatic-C), 103.3 (C_3), 73.6 (C_6), 70.0 (C_9), 43.2 (C_{12}), 32.1 (alkyl-C), 30.5 (alkyl-C), 29.9 (alkyl-C), 29.9 (alkyl-C), 29.9 (alkyl-C), 29.8 (alkyl-C), 29.7 (alkyl-C), 29.6 (alkyl-C), 29.6 (alkyl-C), 29.5 (alkyl-C), 26.4 (alkyl-C), 26.3 (alkyl-C), 22.8 (alkyl-C), 14.3 (methyl-C), 14.3 (methyl-C). **MS-ESI** *m/z* = 2012.7 $[M\text{-}I+H]^+$, calculated for $C_{132}H_{241}N_3O_9$ = 2012.8.

Tris((trialkylphenyl)methyl)aminocyclopropenium ion exchange via silver salt

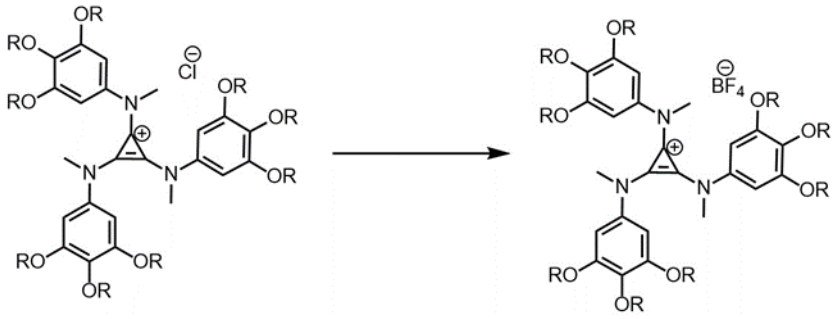

General procedure: Tris((3,4,5-tri-*n*-alkyloxy)-*n*-methyl)aminocyclopropenium chloride (0.05 mmol, 1 equiv.) was dissolved in CH_2Cl_2 (7.5 mL) and CH_3CN (2.5 mL). $AgBF_4$ (0.05 mmol, 1 equiv.) was added, and the mixture stirred for 15 min. The precipitate was removed from the solution by filtration. The solvent was removed under reduced pressure, and the sample was recrystallised in acetone (10 mL), cooled to -8 °C to precipitate out the product, which was isolated by filtration.

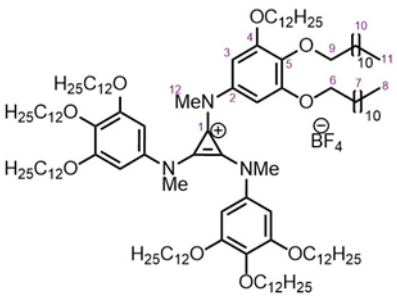

Tris((3,4,5-tri-*n*-dodecyloxy)-*n*-methyl)aminocyclopropenium tetrafluoroborate – AC12·BF_4. The product was obtained from **AC12**·Cl (334 mg, 0.16 mmol) and $AgBF_4$ (33 mg, 0.17 mmol) to give the product as a brown liquid crystal (53 mg, 0.03 mmol, 15% yield). **M.P.** 75 – 79 °C. **^{1}H NMR (600 MHz, $CDCl_3$)** δ 6.56 (s, 6H, H_3), 3.92 – 3.86 (m, 12H, H_6), 3.84 (t, *J* = 6.3 Hz, 6H, H_9), 3.14 (m, 9H, H_{12}), 1.77 – 1.72 (m, 12H, H_7), 1.70 – 1.67 (m, 6H, H_{10}), 1.47 – 1.42 (m, 18H, H_7/H_{10}), 1.31 – 1.23 (m, 144H, H_7/H_{10}), 0.87 (t, *J* = 6.9 Hz, 27H, H_8/H_{11}). **^{13}C NMR (151 MHz, $CDCl_3$)** δ 153.8 (aromatic-C), 139.5 (aromatic-C), 137.3 (C_5), 117.5 (aromatic-C), 102.7 (C_3), 73.6 (C_6), 69.5 (C_9), 42.9 (C_{12}), 32.1 (alkyl-C), 32.1 (alkyl-C), 30.1 (alkyl-C), 30.5 (alkyl-C), 30.0 (alkyl-C), 29.9 (alkyl-C), 29.9 (alkyl-C),

29.9 (alkyl-C), 29.8 (alkyl-C), 29.7 (alkyl-C), 29.6 (alkyl-C), 29.6 (alkyl-C), 29.5 (alkyl-C), 26.3 (alkyl-C), 26.3 (alkyl-C), 22.8 (alkyl-C), 14.2 (methyl-C). **MS-ESI** *m/z* = 2012.9 $[M\text{-}Cl+H]^+$, calculated for $C_{132}H_{241}N_3O_9$ = 2012.8.

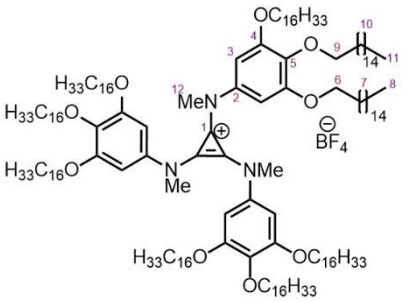

Tris((3,4,5-tri-*n*-hexadecyloxy)-*n*-methyl)aminocyclopropenium tetrafluoroborate - AC16·BF$_4$. The product was obtained from **AC12**·Cl (128 mg, 0.05 mmol) and $AgBF_4$ (16 mg, 0.08 mmol) to give the product as a grey solid (60 mg, 0.02 mmol, 45% yield). **^{1}H NMR (600 MHz, CDCl$_3$)** 6.57 (s, 6H, H_3), 3.92 – 3.87 (m, 12H, H_9), 3.85 (t, *J* = 6.4 Hz, 12H, H_6), 3.12 (s, 9H, H_{12}), 1.78 – 1.73 (m, 12H, H_7), 1.71 – 1.67 (m, 6H, H_{10}), 1.47 – 1.42 (m, 18H, H_7/H_{10}), 1.29 – 1.24 (m, 216H, H_7/H_{10}), 0.88 (t, *J* = 7.0 Hz, 27H, H_8/H_{11}). **^{13}C NMR (151 MHz, CDCl$_3$).** δ 153.8 (aromatic-C), 139.6 (aromatic-C), 137.4 (aromatic-C), 102.8 (aromatic-C), 73.6 (C_{12}), 69.5 (C_9), 42.9 (C_{12}), 32.1 (alkyl-C), 30.6 (alkyl-C), 30.0 (alkyl-C), 30.0 (alkyl-C), 29.9 (alkyl-C), 29.9 (alkyl-C), 29.9 (alkyl-C), 29.9 (alkyl-C), 29.9 (alkyl-C), 29.8 (alkyl-C), 29.8 (alkyl-C), 29.7 (alkyl-C), 29.6 (alkyl-C), 29.5 (alkyl-C), 26.3 (alkyl-C), 26.3 (alkyl-C), 22.9 (alkyl-C), 14.3 (methyl-C). **MS-ESI** *m/z* = 2517.0 $[M+H\text{-}BF_4]^+$, calculated for $C_{168}H_{313}N_3O_9$ = 2517.4.

3.6 Appendix of Supplementary Data and Discussion

3.6.1 – Differential Scanning Calorimetry

DSC was performed on each compound over three heating cooling cycles, from 220 °C to -50 °C, at a heating rate of 10.0 °C min^{-1}.

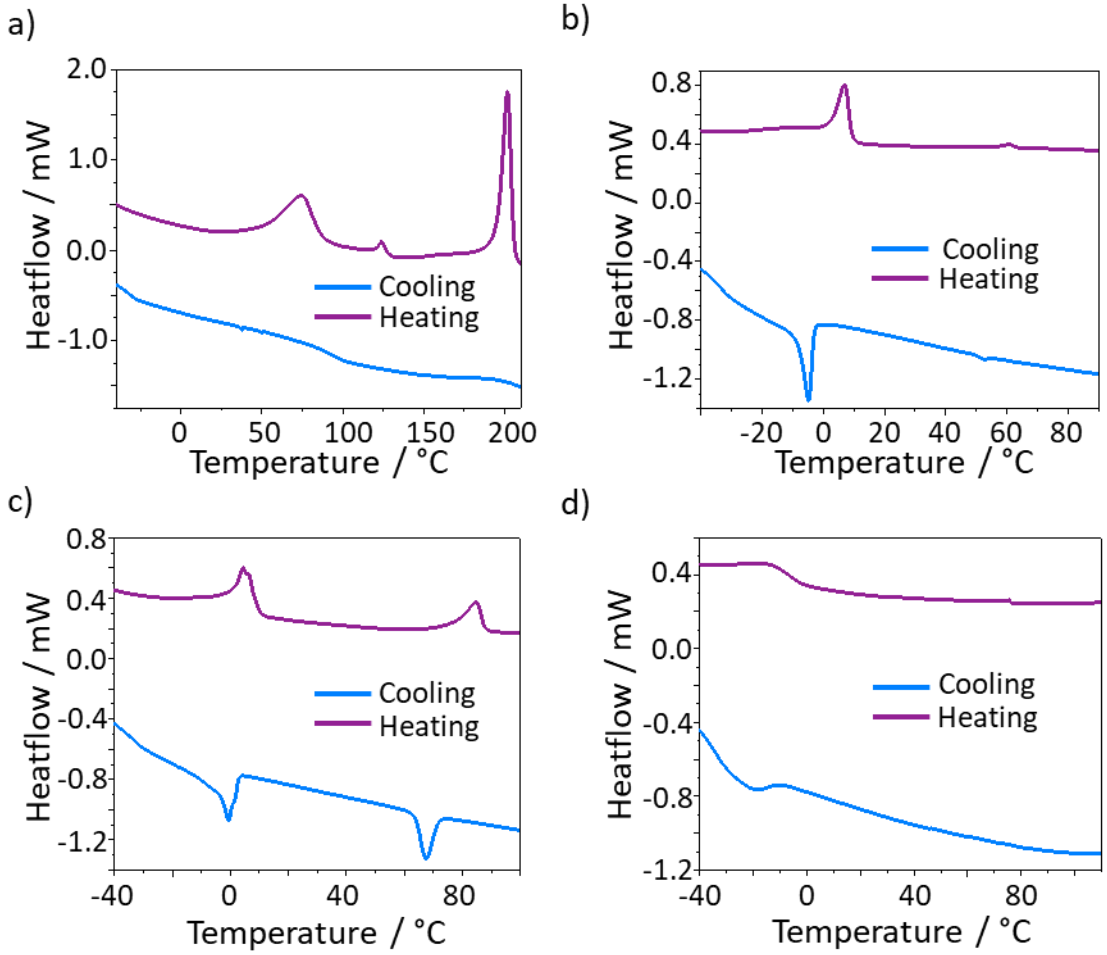

Figure 3.6: DSC of a) **AC1**·Cl, b) **AC12**·Cl, c) **AC12**·BF_4, and d) **AC1**·I.

3.6.2 – Thermogravimetric Analysis

TGA was performed on each compound heating to 500 °C at a rate of 10 °C / min.

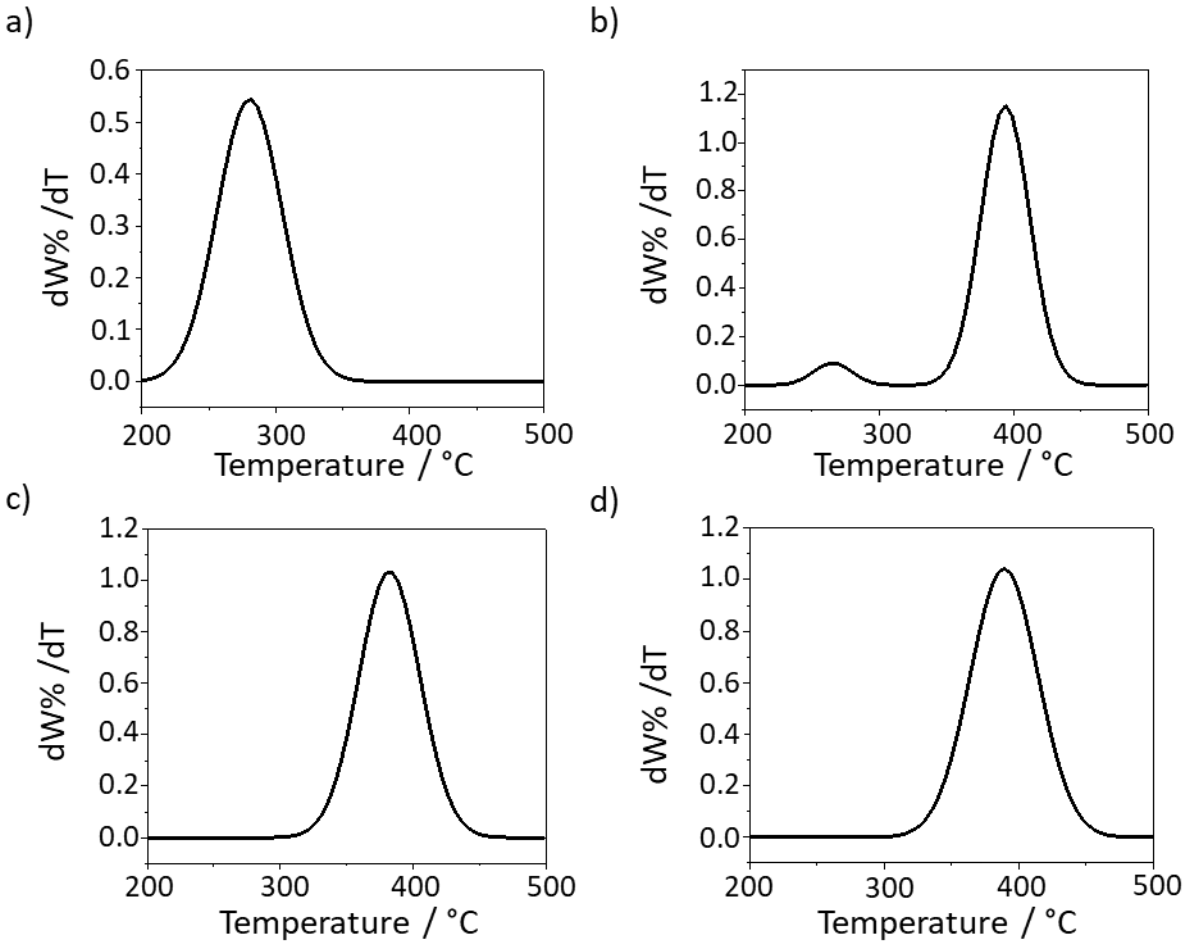

Figure 3.7: DTG curves of a) **AC1**·Cl, b) **AC12**·Cl, c) **AC12**·BF_4, and d) **AC12**·I.

3.6.3 – UV-vis Spectroscopy

UV-vis spectroscopy was performed on each compound in the range of 200-800 nm wavelengths through a 10 mm path length cuvette, in a $CHCl_3$ solution at 0.002-0.01 mM concentration.

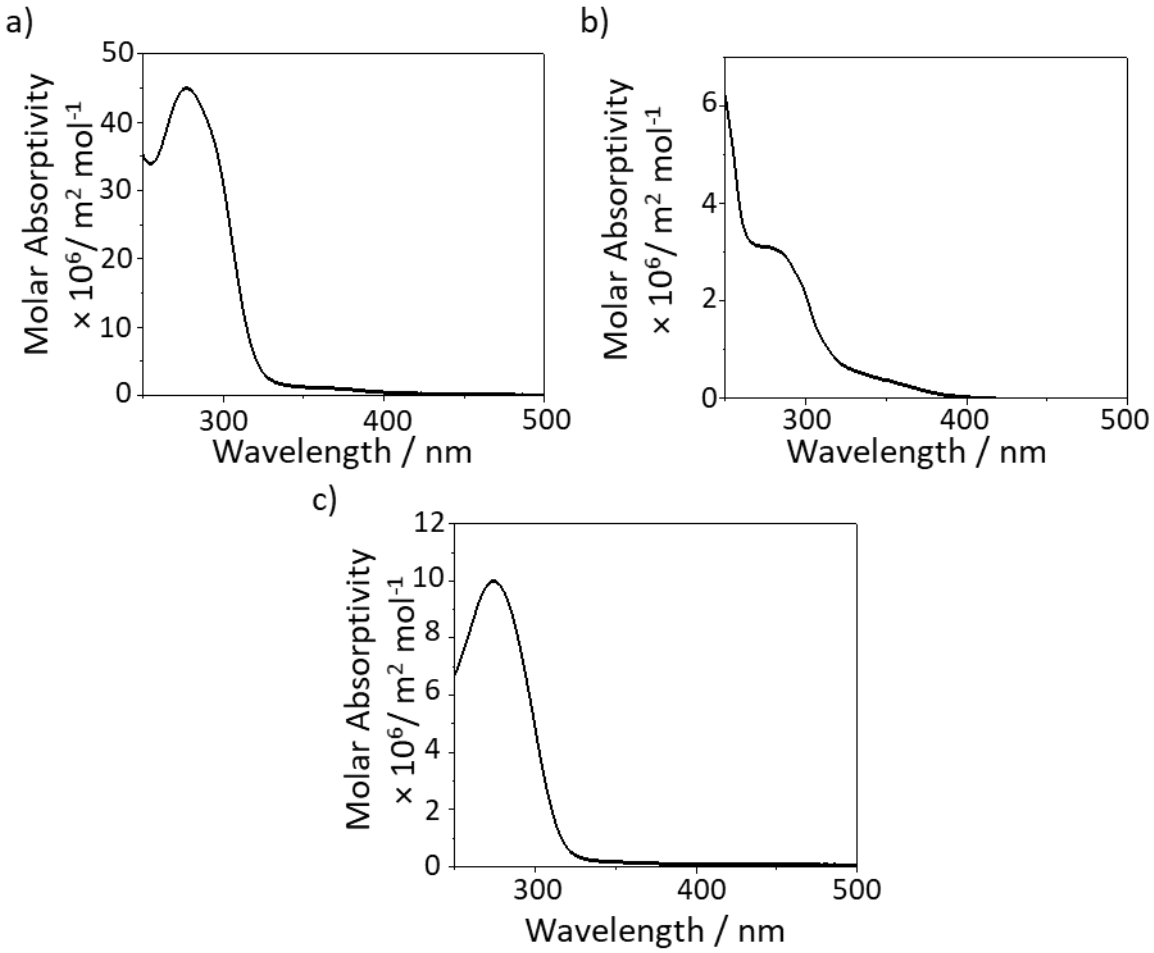

Figure 3.8: UV-vis spectroscopy of cyclopropenium compounds in CH_3Cl, showing a) 0.002 mM of **AC1**·Cl, b) 0.01 mM of **AC12**·Cl, and c) 0.01 mM of **AC12**·BF_4.

3.7 References

1. J. Bandar, T. Lambert, *Synthesis*, 2013, **45**, 2485.
2. K. Komatsu, T. Kitagawa, *Chem. Rev.,* 2003, **103**, 4, 1371.
3. M. Taylor, P. Surman, G. Clark, *J. Chem. Soc. Chem. Commun*., 1994, **21**, 2517.
4. Z. Strater, M. Rauch, S. Jockusch, T. Lambert, *Angew. Chem. Int. Ed*., 2019, **58**, 24, 8049.
5. T. Tsutsui, S. Kusaba, M. Yamashina, M. Akita, M. Yoshizawa, *Chem. Eur. J.*, 2019, **25**, 4320.
6. L. Jiang, X. Lu, H. Zhang, Y. Jiang, D. Ma, *J. Org. Chem.* 2009, **74**, 12, 4542.
7. F. Lincker, P. Bourgun, P. Masson, P. Didier, L. Guidoni, J. Bigot, J. Nicoud, B. Donnio, D. Guillon, *Org. Lett.* 2005, **7**, 8, 1505.
8. Y. Rajan, M. Shellaiah, C. Huang, H. Lin, H. Lin, *Tetrahedron*, 2012, **68**, 38, 7926.
9. A. Gangjee, O. Namjoshi, S. Raghavan, S. Queener, R. Kisliuk, V. Cody, *J. Med. Chem.,* 2013, **56**, 11, 4422.

CHAPTER 4

TROPYLIUM ANALOGUES OF CYCLOPROPENIUM CHEMISTRY

Synopsis

This Chapter discusses the attempted use of octachlorocycloheptatriene to synthesise tropylium analogues of cyclopropenium compounds. Octachlorocycloheptatriene was synthesised *via* the formation of a bicyclic precursor. A Friedel-Crafts reaction was attempted using anisole and trialkyloxybenzene, which progressed slowly and did not lead to an isolatable product. An amination reaction for the formation of an aminotropylium was attempted, which either did not react or showed the degradation of the starting material, along with a side reaction. This shows that tropylium analogues of cyclopropenium cannot be accessed by the same synthetic routes.

Acknowledgement

The following person is gratefully acknowledged for their contribution to this Chapter: Dr Dimitry S. Yufit solved the X-ray structure shown.

4.1 Introduction

Tropylium is the next cation in the sequence of aromatic hydrocarbon cations after cyclopropenium. Both are planar structures (although tropylium can form a boat structure depending on its substituents)[1] and have enhanced stability from their aromatic nature.[2] Therefore, it is plausible that the synthesis of compounds used in cyclopropenium chemistry might be applicable to tropylium chemistry. The investigation of tropylium compounds that are analogues to cyclopropenium compounds could demonstrate the differences arising from the size and symmetry of the central cation.

This Chapter describes the investigation of the synthesis of tropylium compounds comparable to previously synthesised cyclopropenium compounds – first, a tropylium equivalent to the trialkyloxyphenyl-substituted cyclopropeniums shown in Chapter 2, and second, a tropylium equivalent to tris(diethyl)aminocyclopropenium by two different methods that have been reported for aminocyclopropenium.[3, 4] The tropylium compounds began with a chlorinated reagent, using it as an equivalent for the tetrachlorocyclopropene that is used as a reagent for both cyclopropeniums that the tropyliums are analogues of.[5, 6] The starting materials were synthesised by previously performed procedures.[7, 8] The study of both reactions showed the limitations of attempting to adapt these methods to tropyliums, with the Friedel-Crafts reactions exhibiting a much slower and incomplete reaction than with cyclopropenium synthesis, and the amination not giving the formation of any desired product.

4.2 Results and Discussion

4.2.1 Precursor Synthesis

For the synthesis of tropylium cations, the precursor octachlorocycloheptatriene (**1**) was chosen, to be used as a reagent upon which further substitution could be performed. The precursor **1** can be readily induced to form a heptachlorotropylium cation by treatment with $AlCl_3$.

To obtain **1** for later synthesis, a three step synthesis was adapted from a procedure used by Roedig *et al.*[7] Hexachlorocyclopentadiene (**2**) underwent a ring forming reaction with trichloroethene in the presence of $AlCl_3$, giving a bicyclic compound nonochlorobicyclo[3,2,0]hepta-2-ene (**3**). This was then followed by an elimination reaction to form octochlorobicyclo[3,2,0]hepta-2,6-diene (**4**), removing HCl from **3**. On treatment of **4** with $AlCl_3$ while heating to high temperatures, the bicyclic species underwent a ring opening reaction *via* a tropylium species as an intermediate, and giving **1** as the product (Scheme 4.1).[8]

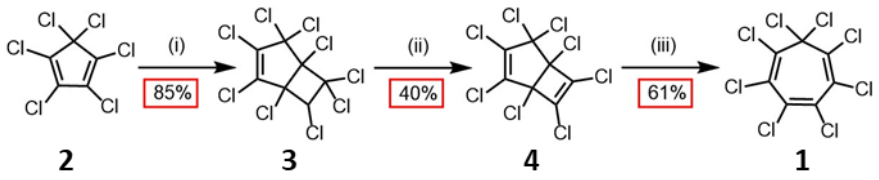

Scheme 4.1: Scheme of the full synthesis of **1**. Reagents and conditions: (i) $AlCl_3$, trichloroethene, 75 °C, 2.5 h; (ii) KOH, MeOH, 40 °C, 30 min; (iii) $AlCl_3$, 150 °C, 15 min.

4.2.2 Friedel-Crafts Reactions

Friedel-Crafts reactions were attempted as a method to acquire equivalents to the aryl-substituted cyclopropenium compounds discussed in Chapter 2, based on the same procedure as those synthesises discussed in Chapter 2, using $AlCl_3$ as a Lewis acid. The first Friedel-Crafts reaction had anisole (**5a**) as the electrophile. Anisole was chosen as a less sterically hindered species to test the reaction upon. 1,2,3-trimethoxybenzene (**5b**) and 1,2,3-tris(*n*-octyloxy)benzene (**5c**) were also tested as Friedel-Crafts electrophiles (Scheme 4.2).

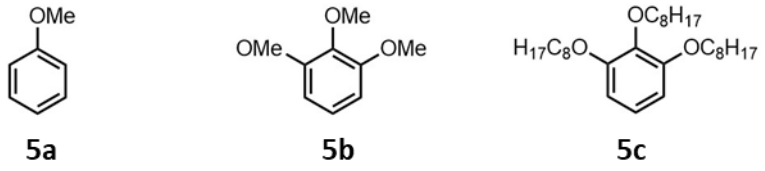

Scheme 4.2: Reagents used as electrophiles for the Friedel-Crafts reactions with **4**.

The bicyclic reagent **4** was used for the Friedel-Crafts reaction for the synthesis of the aryl-substituted tropylium (**6**) in place of **1**, as **3** forms a tropylium species on heating to 150 °C, and so using **3** as the starting material for the Friedel-Crafts reactions rather than **1** reduces the number of steps required for synthesis to isolate the Friedel-Crafts starting materials.

3 was heated to 150 °C to form a tropylium, cooled to 80 °C, and **5a** added in significant excess (Scheme 4.3). Cooling to 50 °C resulted in the reaction halting. Overnight reactions did not show the formation of any product, so the reaction was instead left for seven days.

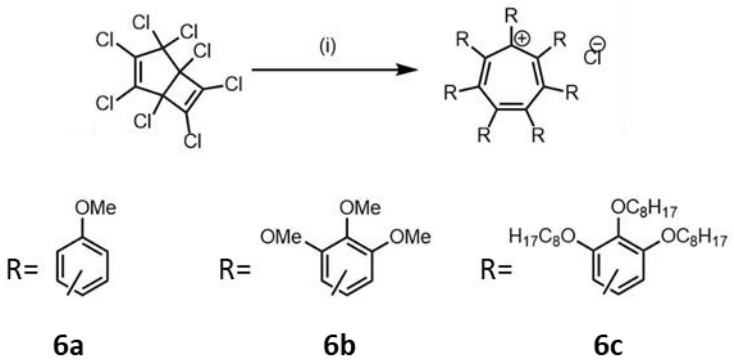

Scheme 4.3: Scheme of the preparation of **6a-c**. Reagents and conditions: (i) 1). $AlCl_3$, 150 °C, 30 min; 2). **5a-c**, 80 °C, 7 days.

The reaction of **5a** and the *in situ* generated tropylium after 7 days showed the appearance of a number of proton resonances in the aromatic region of the ^{1}H NMR spectrum, with the anisole peaks reduced in intensity, though still pronounced in the ^{1}H NMR spectrum. The NMR peaks were attributed to anisole bonded to the central tropylium (Figure 4.1).

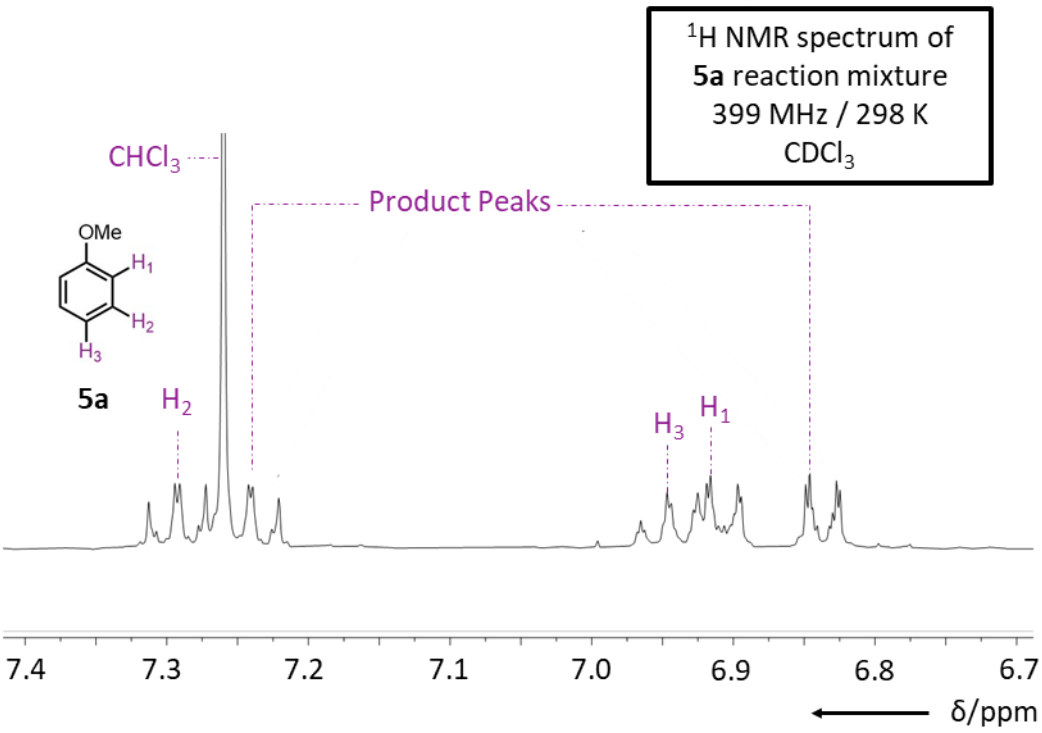

Figure 4.1: ^{1}H NMR spectrum of the reaction of **4** with **5a** after 7 days.

The NMR peaks of the **4** were seen to disappear from the ^{13}C NMR spectrum, and the mass spectrum showed the formation of substituted structures, including a fully substituted structure. However, no product (**6a**) could be isolated.

The same procedure was attempted with **5b** and **5c**, to form pyrogallol-ether substituted tropylium (**6b** and **6c**). For the former, a very slow substitution could be seen over a week from the ^{1}H NMR, but the appearance of a product peak could not be clearly identified from the mass spectra. For the latter no product formed at all, with only the starting material visible after 7 days of the reaction. The lower reactivity of **6b** and **6c** can be explained by the higher steric bulk of the pyrogallol-derived ethers.

The attempted synthesise shows that while **4** can produce an aromatic cation electrophile in the presence of a Lewis acid, the heptachlorotropylium cation is much less reactive than the trichlorocyclopropenium cation in Friedel-Crafts reactions, with higher temperatures and longer reaction times required for any product formation, with a greater scope for the formation of partially substituted species and isomeric mixtures, meaning using these reagents for Friedel-Crafts reactions is more challenging. Part of this low reactivity can be attributed to the heptachlorotropylium being a weaker

electrophile than trichlorocyclopropenium, due to a greater spread of positive charge. The greater steric bulk of substituents around the tropylium would also explain the difficulty of forming the fully substituted product, as the phenyl groups are packed much closer together than on the cyclopropenium equivalent, reducing the reactivity of the ethers. More investigation would be required to make use of heptachlorotropylium for Friedel-Crafts reactions cleanly. A better route to heptaarylcycloheptatriene species might be through the use of Diels-Alder reactions such as those shown in Chapter 1.[9]

4.2.3 Aminotropylium

Much of the work on cyclopropeniums has been around aminocyclopropeniums, with the amine substituents providing additional thermal and electrochemical stability.[6] However, no investigation of amine-substituted tropyliums has performed. Therefore a preliminary superficial study was taken to attempt to synthesise and study a fully amine-substituted tropylium to give a heptaaminotropylium (HAT) cation, using chemistry based on that developed with aminocyclopropenium species. The chosen compound to synthesise was fully diethylamine-substituted tropylium compound (**7**), matching the previously made aminocyclopropenium.[4]

Two different reaction mechanisms were attempted, using of reagent **1**. The first was by using silyl amines, with diethyltrimethylsilylamine used as the source of amine groups (Scheme 4.4),[3] at either RT or 50 ºC for 16 h. The reaction with **1** showed no product at either temperature, with the peaks of the starting material remaining in the ^{1}H and ^{13}C NMR spectra. This showed that the reaction was not viable by this method.

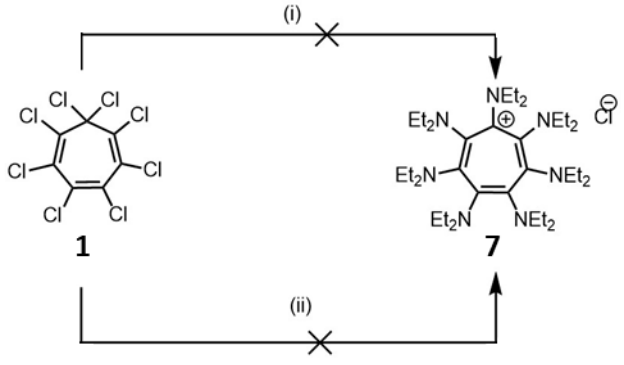

Scheme 4.4: Scheme of two routes for the preparation of **7**. Reagents and conditions: (i) Et_2NSiMe_3, CH_2Cl_2, 50 ºC, 16 h; (ii) 1). $HNEt_2$, NEt_3, CD_3Cl, 0 °C, 1 h; 2). 50 °C, 24 h.

The second attempted procedure was the reaction of **7** with diethylamine in the presence excess base from the triethylamine.[4, 10] The compound was cooled to 0 °C in deuterated chloroform, and diethylamine and triethylamine were added, leaving for 1 h before stirring at RT for 24 h (Scheme 4.4). Unlike for the cyclopropenium synthesis, no gas (HCl) was seen effervescing from the reaction mixture when the amine was added to the octachlorocycloheptatriene at 0 °C.

No reaction occurred at RT, but on heating to 50 °C, a new peak in the carbon spectrum emerged, that corresponded to non-deuterated chloroform, which can be attributed to a hydrogen/deuterium exchange occurring with the deuterated chloroform and the amine base, either directly from the base or through any water present in the chloroform.[11, 12] The product was not formed, as the same peaks were seen with the same procedure without **1** present (Figure 4.2).

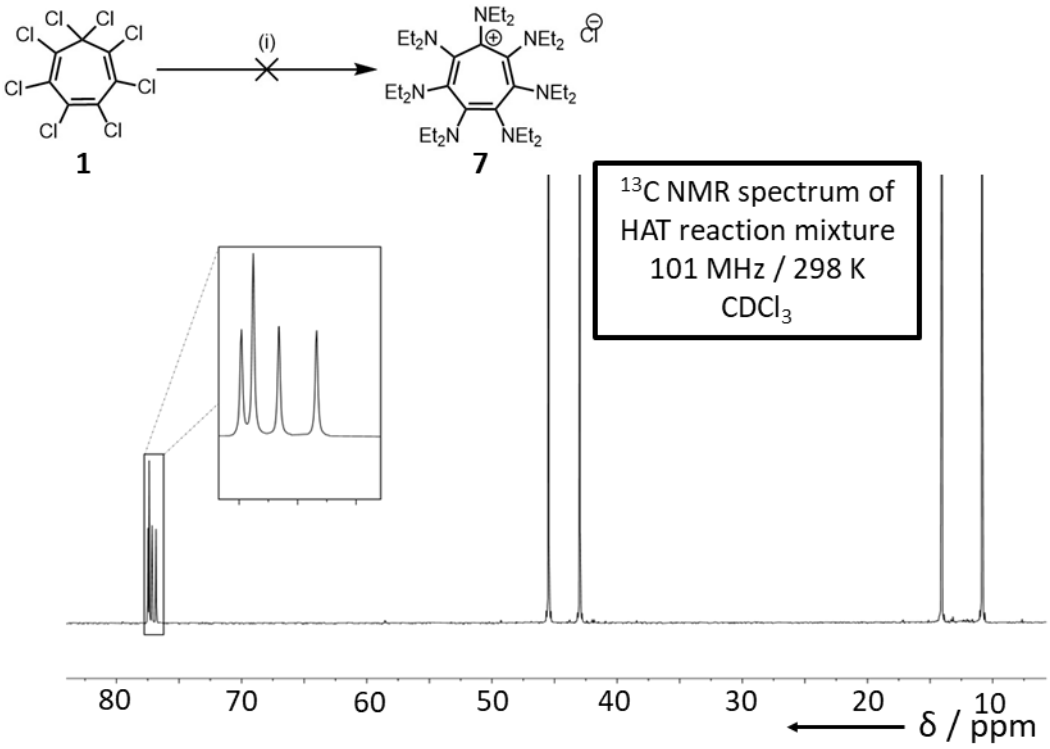

Figure 4.2: ^{13}C NMR spectra of the attempted aminotropylium synthesis, with the scheme of the attempted reaction shown above. Reagents and conditions: (i) 1). $HNEt_2$, NEt_3, CD_3Cl, 0 °C, 1 h; 2). 50 °C, 24 h.

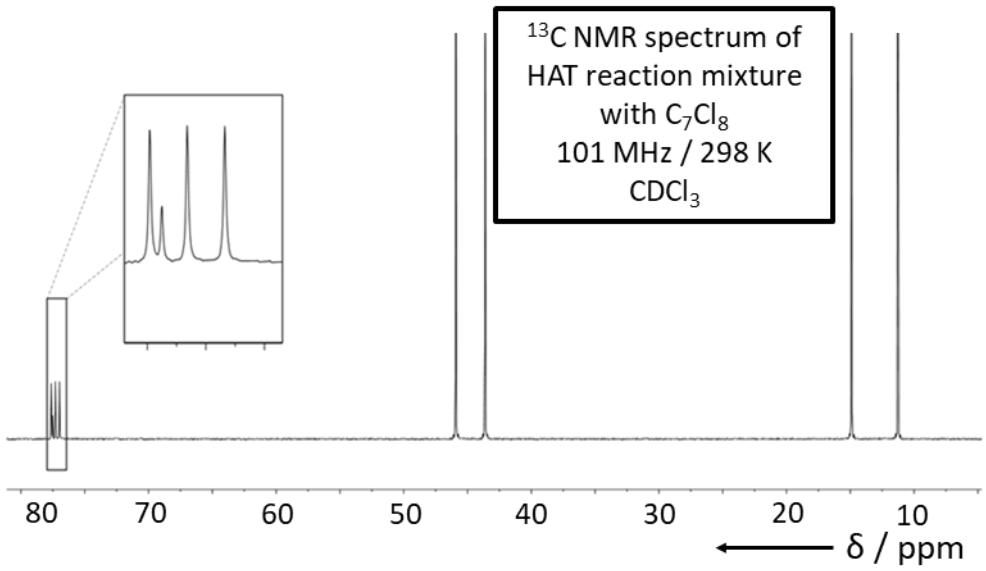

Figure 4.3: ^{13}C NMR spectra of the aminotropylium synthesis reaction conditions without the addition of the octachlorocycloheptatriene.

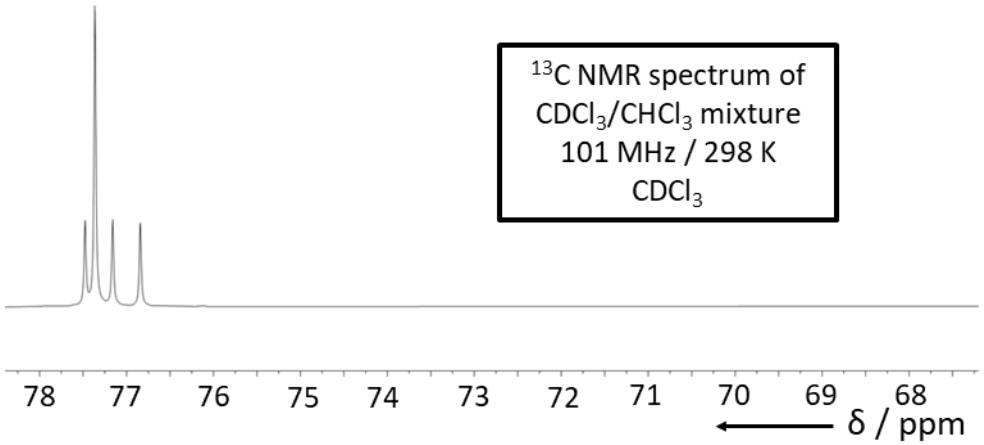

Figure 4.4: ^{13}C NMR spectra of a mixture of deuterated and non-deuterated chloroform (prepared by adding equal parts deuterated and non-deuterated chloroform together).

After removing the amine and solvent under reduced pressure, the remainder was identified as triethylammonium chloride, formed and precipitated during the attempted reaction. Given the triethylammonium chloride was formed even without the addition of octachlorocycloheptatriene to the reaction mixture, the source of chlorine can be seen to be from the chloroform, which also exchanges hydrogen atoms with the diethylamine to form the non-deuterated chloroform (Figure 4.3, which can be

contrasted to a ^{1}H NMR of preprepared mixture of deuterated and non-deuterated chloroform).

The triethylammonium chloride was removed by washing with water. The remainder showed no sign of the starting material, which had degraded over the course of the reaction. This showed that **1** is not stable in the presence of the amines. No product could be seen by performing the reaction in other solvents. Using a solid base, K_2CO_3 or solid supported diisopropylamine, resulted in no reaction occurring, leaving only starting materials in the reaction. The degradation of **1** while heated in the presence of amines means that excess amines are not a reagent that is conducive for the formation of **7**.

The lack of reactivity of **1** for the formation of an aminotropylium with a reaction by silyl amine is notable when compared to cyclopropenium synthesis, which was performed as a comparison to form tri(diamino)cyclopropenium chloride (**8**, Scheme 4.5). The reactions can occur rapidly without heating, with an effervescence of HCl gas occurring quickly on the addition of the silyl amine to the reaction mixture at 0 ºC.[4] The rapid reactivity of the tetrachlorocyclopropene is a major contrast to the lack of reactivity in **1**.

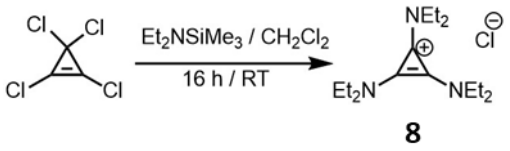

8

Scheme 4.5: Scheme for the synthesis of **8**, as a comparison to 7. Reagents and conditions: (i). Et_2NSiMe_3, CH_2Cl_2, 16 h, RT.

The current limited study has not shown a potential route for the synthesis of a HAT system analogous to TAC synthesis, and shown that HAT cations are more challenging to form than TAC cations. It is possible that a solvent screen or other reaction optimisation could be performed in future work to find conditions to allow for the desired reaction to proceed, enabling **7** to be obtained.

4.3 Conclusion

In summary, the initial study into reactions utilising **1** or **4** has shown that they were unable to be used as an equivalent to tetrachlorocyclopropene for accessing similar chemistry to cyclopropenium with tropylium. A reaction with a Lewis acid can generate a tropylium *in situ* that is able to undertake a Friedel-Crafts reaction, but much more slowly than with the equivalent cyclopropenium, and increasing steric bulk of reagents further reducing the ability to react. Furthermore, fully-substituted tropylium compounds were unable to be isolated using this procedure. **1** appears to be unstable in the reaction conditions for substitution with secondary amines for forming HAT cations, as the starting material could not be isolated after an attempted reaction, and **1** would also not react with silyl amines. This shows that the reactions that are readily accessible for cyclopropenium are much more challenging when applied to tropylium species. The difficulty for tropylium to perform the chemistry that is easily accessible for cyclopropenium highlights the fundamental differences between these two species and shows they cannot be readily compared. However, in either case the work performed in this Chapter represent only superficial studies of potential routes for forming the desired products, with a wider study of different reaction conditions required to determine a method using **1** as a basis for the formation of either desired product. Alternative routes to these compounds with different reagents, such as by Diels Alder reactions, maybe a better route to make these desired compounds.

4.4 Experimental Methods

4.4.1 Synthetic Procedures

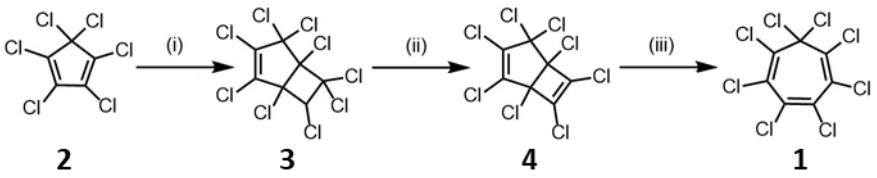

Scheme 4.6: Synthetic route used to prepare **1**. Reagents and conditions: (i) CCl_2CHCl, $AlCl_3$, 75 °C, 2.5 h, 85 %; (ii) KOH, MeOH, 40 °C, 30 min, 40%; (iii) $AlCl_3$, 150 °C, 15 min, 61%.

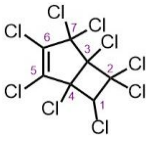

Nonochlorobicyclo[3,2,0]hepta-2-ene (3). 2 (31.0 g, 114 mmol) was mixed with $AlCl_3$ (2.3 g, 17.3 mmol), and then trichloroethene (3.5 g, 2.4 mmol) was added to the mixture while gently stirring over 25 min, over which the temperature was increased steadily to 75 °C from RT by slow heating as the trichloroethene was added over this period. Trichloroethene (11.5 g, 7.9 mmol) was then added to the mixture over 40 min, and the mixture was then left to stir at 75 °C for 90 min. The mixture was then cooled to RT, and the reaction mixture was poured onto ice. A precipitate formed, which was isolated by filtering. The precipitate was then dissolved in hexane (25 mL), dried with $MgSO_4$, filtered and the solvent was then removed under reduced pressure. The product was isolated by flash column chromatography (Teledyne Isco Combiflash Rf+ system, 220 g SiO_2, Hexanes/EtOAc gradient elution [1:0 to 0:1]), and the solvent was then removed under reduced pressure, to isolate the product as a yellow solid (39.1 g, 97.0 mmol, 85% yield). **M. P.**: 78 – 79 °C. **^{1}H NMR (600 MHz, $CDCl_3$)** δ 5.04 (s, 1H, H_1). **^{13}C NMR (151 MHz, $CDCl_3$)** δ 138.0 (C_6), 133.5 (C_5), 91.8, 87.3, 81.1 (C_3), 79.6 (C_7), 70.2 (C_1). **HRMS-ASAP** *m/z* = 364.7616 $[M\text{-}Cl]^+$, calculated for C_7HCl_8 = 364.7586.

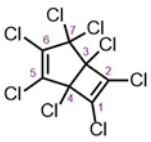

Octochlorobicyclo[3,2,0]hepta-2,6-diene (4). 3 (7.0 g, 17.3 mmol) was added to 50 mL of MeOH and heated to 40 °C. KOH (1.8 g, 32.0 mmol) in MeOH (30 mL) was added dropwise to the mixture over 30 min while stirring. The mixture was then cooled to RT, and water (90 mL) was added to the solution. The solvent was then removed under reduced pressure. The mixture was then purified by flash column chromatography (Teledyne Isco Combiflash Rf+ system, 80

g SiO_2, Hexanes/EtOAc gradient elution [1:0 to 0:1]), giving a colourless liquid. The product was isolated by removing the hexane solvent under reduced pressure and then cooling to -8 °C, which over 14 h, crystallised the product out as a pale yellow solid (2.5 g, 6.9 mmol, 40% yield). **M. P.**: 51 – 53 °C. **^{13}C NMR (101 MHz, $CDCl_3$)** δ 137.6 (chloroalkene-C), 134.4 (chloroalkene-C), 133.6 (chloroalkene-C), 132.4 (chloroalkene-C), 89.2 (chloroalkyl-C), 81.9 (chloroalkyl-C), 78.9 (chloroalkyl-C)**. HRMS-ASAP** *m/z* = 328.7784 $[M\text{-}Cl]^+$, calculated for C_7Cl_7 = 328.7814.

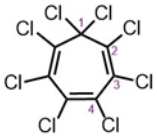

Octachlorocycloheptatriene (1). 4 (0.7 g, 1.9 mmol) and $AlCl_3$ (0.5 g, 3.8 mmol) were added to a microwave vial and heated to 150 °C under N_2 while stirring. The mixture was held at the temperature for 15 min, before cooling to RT. The mixture was added to ice water (20 mL) to give a precipitate, which was then filtered, before washing with water (10 mL). The precipitate was then extracted with hexane (300 mL) in a Soxhlet extraction overnight, dried with $MgSO_4$, filtered and the solvent removed under reduced pressure. The product was recrystallised with hexane (5.0 mL) to isolate the product as pale brown crystals (0.4 g, 1.2 mmol, 61% yield). **M. P.**: 85 – 86 °C. **^{13}C NMR (101 MHz, $CDCl_3$)** δ 134.6 (chloroalkene-C), 134.3 (chloroalkene-C), 129.3 (chloroalkene-C), 84.4 (C_1). **HRMS-ASAP** *m/z* = 330.7785 $[M\text{-}Cl]^+$, calculated for C_7Cl_7 = 330.7785.

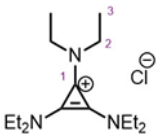

Tri(diethylamino)cyclopropenium chloride (8). Tetrachlorocyclopropene (36 mg, 0.2 mmol) was added to CH_2Cl_2 (10 mL), followed by diethyltrimethylsilylamine (0.1 mL, 0.6 mmol). The mixture was left to stir overnight. The solvent was removed under reduced pressure and the product was then investigated by NMR. **^{1}H NMR (400 MHz, $CDCl_3$) δ** 3.53-3.43 (m, 12H, H_2), 1.32-1.24 (m, 18H, H_3) .**^{13}C NMR (151 MHz, $CDCl_3$) δ** 116.1 (C_1), 47.1 (C_2), 14.3 (C_3).

4.5 References

1. M. Tamm, B. Dreβel, R. Fröhlich, *J. Org. Chem.*, 2000, **65**, 20, 6795
2. A. Balaban, D. Oniciu, A, Katritzky, *Chem. Rev.*, 2004, **104**, 2777.
3. R. Weiss, K. Schloter, *Tetrahedron Lett*., 1975, **16**, 40, 3491.
4. G. Clark, P. Surman, M. Taylor, *J. Chem. Soc. Faraday Trans*., 1995, **91**, 10, 1523.
5. R. Weiss, H. Kölbl, C. Schlierf, *J. Org. Chem.*, 1976, **41**, 13, 2258.
6. J. Bandar, T. Lambert, *Synthesis*, 2013, **45**, 2485.
7. A. Roedig, L. Hörnig, *Eur. J. Org. Chem.*, 1956, **598**, 208.
8. R. West, K. Kusuda, V. Rao, *J. Am. Chem. Soc.*, 1971, **93**, 15, 3627.
9. M. Battiste, *Chemistry and Industry*, 1961, **17**, 550.
10. Z. Yoshida, Y. Tawara, *J. Am. Chem. Soc.*, 1971, **93**, 2573.
11. D. Martin, *J. Inorg. Nucl. Chem.*, 1975, **37**, 9, 1941.
12. J. Hine, R. Peek, B. Oakes, *J. Am. Chem. Soc.* 1954, **76**, 3, 827.

CHAPTER 5

SUMMARY AND OUTLOOK

This thesis highlights the developments made in the field of aromatic carbocations, with particular focus on aromatic carbocations as the centre of mesogen molecules, including the synthesis and study of their phase behaviour and electronic character, all of which was achieved in the period of April 2018 and March 2022. There has been wide study of liquid crystals over the last century, with many different phases being discovered and their applications expanding from focus on display technologies towards use as structural and conductive materials. The use of aromatic carbocations as a part of liquid crystals has been only briefly studied outside of this thesis, with this representing the first study of their potential as electronic materials.

Chapter 2 describes the development of a series of cyclopropenium centred mesogens, forming a series of columnar phases with small halide counter anions. The compounds formed either hexagonal or rectangular columnar phases, depending on the size of the alkyl chains, shorter or longer chains respectively. Changing to methyl groups or larger counter anions resulted in the loss of liquid crystal phases. Switching to a branched chain resulted in the formation of an ionic liquid at room temperature, persisting to below 0 °C. These mesogens have a liquid-like conductivity in both the liquid crystal and solid region for the hexagonal columnar materials, with there being no change in the conductivity with either the phase transition or on changing the alignment. The rectangular columnar materials showed both properties in the liquid crystal phase, with a drop in conductivity and return in anisotropy for the solid phase. This unusual liquid-like conductivity indicated that the counter anions were able to move freely without being defined by the column alignment, with evidence suggesting ions without strong interactions to the cation persisting into the solid phase. Electrostatic potential calculations showed that this may be due to a highly diffuse charge across the entirety of the cation molecule. Attempts to enhance the conductivity of the materials by doping with lithium salts were determined to not be successful in increasing the conductivity of the materials.

The conductive liquid crystals developed in Chapter 2 show unique properties that are not possessed by other conductive liquid crystals, an isotropic conductivity in a columnar phase and phase independence conductivity that results in three phase conductivity. However, the liquid crystals developed do not reach the requirements for the desired application for electrolytes, or other liquid crystal electrolytes that have been attempted previously. The cyclopropeniums reached low conductivities, around four orders of magnitude lower than the best liquid crystal electrolyte materials developed. In addition, the low electrochemical and thermal stability they possess is a major contrast to the high stability of other non-liquid

electrolytes, removing one of the main advantages of mesogen electrolytes, as well as lacking the ability of other ionic mesogens to form stable phases with lithium ion dopants. Improving these areas is a requirement to overcome the two major limitations of these materials.

Chapter 3 describes the development of a series of aminocyclopropenium compounds acting as a continuation of the work in Chapter 2, by attempting to form similar liquid crystals using more stable aminocyclopropenium cores that might give higher conductivities and integrate better with doped salts. A series of aminocyclopropenium compounds were synthesised, and initial studies showed that they had a higher stability than equivalent cyclopropenium compounds. Liquid crystal phases were seen forming for a twelve carbon chained cation with either chloride or tetrafluoroborate anions. Difficulties in isolating the pure compounds in good yields limited the ability to fully study the properties of the compounds.

Chapter 4 discusses the attempts in using cyclopropenium chemistry to make analogue compounds with a tropylium cation as a core of the molecule. Two compounds, octochlorobicyclo[3,2,0]hepta-2,6-diene and octachlorocycloheptatriene, were prepared as the starting materials for these synthesis. A Friedel-Crafts reaction was performed on the octochlorobicyclo[3,2,0]hepta-2,6-diene, using anisole and tri-substituted pyrogallol ether derivatives. The Friedel-Crafts reaction occurred very slowly, and a fully substituted product could not be isolated. The formation of an aminated cation was attempted with octachlorocycloheptatriene and diethyltrimethylsilylamine and diethylamine, neither of which formed the product, with the presence of excess amine instead causing the degradation of the starting material. It was seen that the chemistry used for the cyclopropenium compounds cannot be simply applied to the tropylium compounds.

The work in this thesis demonstrates the potential of cyclopropenium species as cores for liquid crystal materials, with them having an unusual resilience of conductivity against phase change or direction of alignment due to the weak interactions of the ions and counter ions. Further work is needed to study these compounds, and find ways to overcome the issues faced by the cyclopropenium compounds, namely low stability and conductivity, to make use of these materials and their unique properties. The aminocyclopropenium compounds may offer a way to overcome these issues, but methods to isolate these materials in good yields are needed before full study of their electronic properties can be performed. In addition, the study of the stability and effectiveness of these materials as part of energy storage devices must be undertaken to see the potential of these compounds.